Designing an *in vitro* Model of the Bone Marrow Niche using Polyethylene (glycol) Hydrogels and Poly(ethyl acrylate) Surfaces

Sam Donnelly
BSc (Hons), MSc

Submitted in fulfilment of requirements for the degree of Doctor of Philosophy (PhD)

Centre for the Cellular Microenvironment
Institute of Molecular, Cell and Systems Biology
College of Medical, Veterinary and Life Sciences
University of Glasgow
Glasgow
G12 8QQ

September 2020

Abstract

Stem cells are of interest in many research areas due to their ability to self-renew while also undergoing differentiation to regenerate the tissue it occupies (Weiss and Troyer, 2006). Stem cell fate is influenced by many different factors, these include stiffness, cell to cell interactions and secreted factors among others. The cells reside within unique microenvironments referred to as a stem cell niche where these factors are controlled to regulate the maintenance and differentiation of the stem cell population (Ferraro, Celso and Scadden, 2010). One such niche is that found in the bone marrow which hosts populations of haematopoietic stem cells (HSCs), responsible for haematopoiesis, and mesenchymal stem cells (MSCs), important for HSC regulation along with osteogenic, adipogenic and myogenic potential (Yin and Li, 2006; Pinho and Frenette, 2019). In this thesis we show the development of a model, combining both hydrogels and polymer surfaces, for MSC culture to produce a bone marrow like environment *in vitro*.

Poly ethylene(glycol) (PEG) is a bioinert and biocompatible material that can be used to form hydrogels, for 3-dimensional cell culture (Raeber, Lutolf and Hubbell, 2005; Zhu, 2010). Models using hydrogels are becoming increasingly popular due to the control established over the physiochemical properties that are an important part of the *in vivo* ECM such as the water content and stiffness (Tse and Engler, 2010). These gels have also been developed to include bioactive ligands and even full length proteins, that would be found in the ECM, increasing cell interactions with the scaffold (Lutolf and Hubbell, 2005; Trujillo *et al.*, 2020). In this thesis, we have utilised this PEG hydrogel system to produce a 3D scaffold that mimics the properties of the bone marrow stem cell niche. This includes tuning the stiffness of the gels to match that of the bone marrow and the introduction of fibronectin to enhance biological interactions with the gel. The gels were also shown to allow growth factor diffusion and retention an important property of the ECM *in vivo*.

Poly(ethyl acrylate) (PEA) can be used to induce fibrillogenesis, where on contact with the polymer surface the spontaneous formation of fibronectin (FN) networks occurs (Salmerón-Sánchez *et al.*, 2011; Cantini, González-García, *et al.*, 2012; Llopis-Hernández *et al.*, 2013). Formation of these protein networks

exposes various cryptic domains, hidden in the globular formation, along the length of the protein which aid cell adhesion and allow the synergistic presentation of growth factors (Llopis-Hernández *et al.*, 2016). In this thesis we investigate various methodologies, spin coating, plasma polymerisation, UV polymerisation and, surface initiated atomic transfer radical polymerisation, to introduce PEA into our model using different techniques to determine the success of each method. Once a PEA surface was established the interaction with FN was utilised to introduce growth factors into the model relevant to the bone marrow niche, BMP-2 and NGF.

The final model was composed of PEA coated microcarrier polystyrene beads and degradable PEG hydrogels with full length FN incorporated. MSCs seeded onto the PEA beads were successfully encapsulated within the hydrogels and cultured for up to 3 weeks. By combining these two materials, PEG hydrogels and PEA surfaces, we can control physiochemical properties of the model progressing toward a more accurate *in vitro* representation of the bone marrow niche.

Table of Contents

List of Tables

List of Figures

Acknowledgement

Firstly, I would like to give a massive thank you to my supervisors, Professor Matt Dalby and Professor Manuel Salmeron-Sanchez. Matt, it has been lots of ups and downs through the years, but you always believed in me and helped me believe in myself. Manuel, you have always been supportive of the ideas I have come up with and I am a more confident researcher thanks to your guidance. I am so grateful to you both for all the opportunities you have given me through the years and the guidance that got me to this point.

Within my group I would specifically like to mention Sara Trujillo-Muñoz and Mark Sprott without whom this thesis would not be the same or may not exist. Sara, thank you for always helping me with absolutely everything from start to finish, I am eternally grateful and for showing me the wonders of hydrogels. Mark, I want to thank you for all the guidance you gave me in my final year in the lab and I will always be grateful for all the support while writing this.

To all the past and present members of CEMI (CCE and MIME) who have helped me along the way with their endless knowledge and support in the lab. Particularly I would like to mention Carol-Anne Smith, Paula Sweeten, Hannah Donnelly and Oana Dobre though many more have been a part of getting me to this point. I could not have imagined a better group of people to be surrounded with, the memories from the past few years will last a lifetime.

To Emily Cross I cannot thank you enough for just being you, you inspired me to do better and brightened even the darkest days.

To my best friend Lauren, you have always been there to help me through the lows and celebrate with me through the highs, I will forever be grateful to have you in my life.

Lastly, I would like to thank my family- Mum, Emma, Kerry, Gran Stark, Gran and Grandpa Donnelly, and my extended family who have helped me over the years. I am so lucky to have such a wonderful and supportive group of people to call my family I could not have achieved this without you, I hope I have done you all proud.

Author's Declaration

I declare that, except where explicit reference is made to the contribution of others, that this thesis is the result of my own work and has not been submitted for any other degree at the University of Glasgow or any other institution.

Signed:

Date: 19th September 2020

Abbreviations

2D	two-dimensional
3D	three-dimensional
AFM	Atomic force microscopy
ALCAM	Activated leukocyte cell adhesion molecule
BIT	Bovine insulin transferrin BM Bone marrow
BMP	Bone morphogenetic protein
BSA	Bovine serum albumin
CAR	CXCL12-abundant reticular cells
CXCL12	C-X-C motif chemokine 12
DAPI	4’6-diamidino-2-phenylindole
DMEM	Dulbecco’s modified eagle’s medium
DNA	Deoxyribose nucleic acid
EA	Ethyl acrylate
ECM	Extracellular matrix
ELISA	Enzyme-linked immunosorbent assay
FBS	Foetal bovine serum
FN	Fibronectin
FNPEG	Fibronectin based PEG gel
FTIR	Fourier transform infrared spectroscopy
Flt3	Fms-like tyrosine kinase 3 ligand
GF	Growth factor
GFP	Green fluorescent protein
HS	Human serum
HSC	Haematopoietic stem cell
IAA	Iodoacetamide
IF	Immunofluorescence
ICW	In-cell western
IMDM	Iscove’ s modified Dulbecco’ s medium
LT-HSC	Long term - haematopoietic stem cell
MA	Methyl acrylate
MAL	Maleimide
MSC	Mesenchymal stem cell
NGF	Neural growth factor
OCN	Osteocalcin
OPN	Osteopontin
PBS	Phosphate-buffered saline
PDMS	polydimethylsiloxane
PEA	Poly(ethyl acrylate)
PEG	Polyethylene (glycol)
PHSRN	Pro-His-Ser-Arg-Asn amino acid seguence
PMA	Poly(methyl acrylate)
pPEA	Plasma polymerised PEA

PS	Polystyrene
RGD	Arginine, glycine and aspartic acid
RNA	Ribonucleic acid
RT	Room temperature
SCA	Static contact angle
SCF	Stem cell factor
scPEA	Spin coated PEA
SDF1	Stromal cell-derived factor 1
SI-ATRP	Surface initiated - atomic transfer radical polymerisation
ST-HSC	Short term - haematopoietic stem cell
TCEP	Tris(2-carboxyethyl)phosphone hydrochloride
TPO	Thrombopoietin
UV	Ultraviolet
uvPEA	UV polymerised PEA
VCAM1	Vascular cell adhesion molecule 1
WCA	Water contact angle
XPS	X-ray photoelectron spectroscopy

Chapter 1 Introduction

1.1 Stem Cells

A stem cell is defined as a cell that is able to self-renew indefinitely while also being able to differentiate into more specialised cells and has the ability to renew the tissue which it occupies (Weiss and Troyer, 2006). A cell must meet all three of these criteria to be classified as a stem cell. The process of self-renewal occurs through the production of identical daughter cells during cell division and allows the maintenance of a of a stem cell population in an undifferentiated state (Watt and Hogan, 2000). When differentiation occurs progenitor cells may be produced, these are not yet fully committed but are more specialised with a lower capacity for self-renewal (Krause *et al.*, 2001). Stem cells are often characterised by their potential to differentiate, known as cell potency. This is illustrated in Figure 1.1.

In terms of mammalian development these totipotent and pluripotent cells are able to produce the cells to form all three germ layers seen in early embryonic development with totipotent cells also able to form the placenta tissue, amniotic fluid and cord blood (Spinelli, Guillot and De Coppi, 2014). A common test used to determine pluripotency is teratoma formation, this is the cells ability to produce a tumour comprising of cells from all three germ layers (Singh *et al.*, 2016). A cell becomes multipotent once it commits further reducing its potential to a cell lineage within a specific germ layer examples of these are mesenchymal stem cell (MSCs) and haematopoietic stem cells (HSCs) (Spinelli, Guillot and De Coppi, 2014). These are both of mesoderm origin but cannot differentiate into the same cell types. Once cells are further specialised, they are referred to as oligopotent or progenitor cells which have the ability to produce a few specific cell types for example a myeloid progenitor that may produce red blood cells but not white blood cells. It is due to this capacity to produce multiple tissues that multi/pluripotent stem cells are widely studied within biomedical research (Cleton-Jansen, 2015).

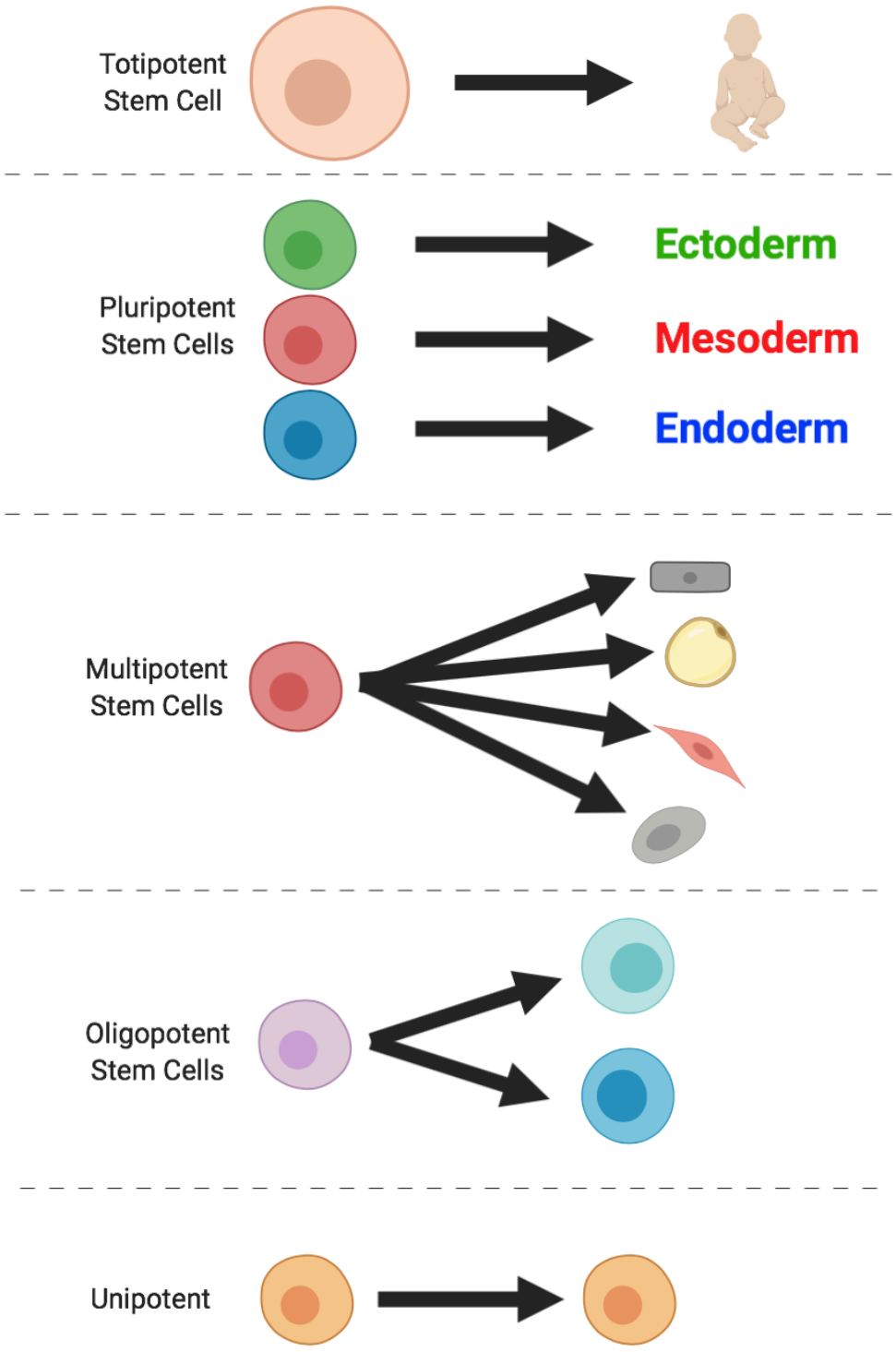

Figure 1.1 Stem Cell potency.
The figure outlines the hierarchy of cell potency and the differentiation ability at each level. Totipotent has the ability to produce an entire organism including the placenta etc, Pluripotent is are able to produce an entire organism, multipotent cells can still give rise to many cell types but are further restricted to a cell lineage within the germ layer, oligopotent can give rise to few specialised cell types and unipotent only has the ability to self-renew. Image created using BioRender.com.

Stem cell fate is not predetermined, there are many different factors that can influence cell differentiation (Guilak *et al.*, 2009; Chen *et al.*, 2016). These factors, illustrated Figure 1.2, together create a unique microenvironment, known as a stem cell niche, which allows the maintenance of a stem cell population along with appropriate differentiation (Ferraro, Celso and Scadden, 2010). Understanding and controlling the effects of each of these factors has a vast potential in biomedical research.

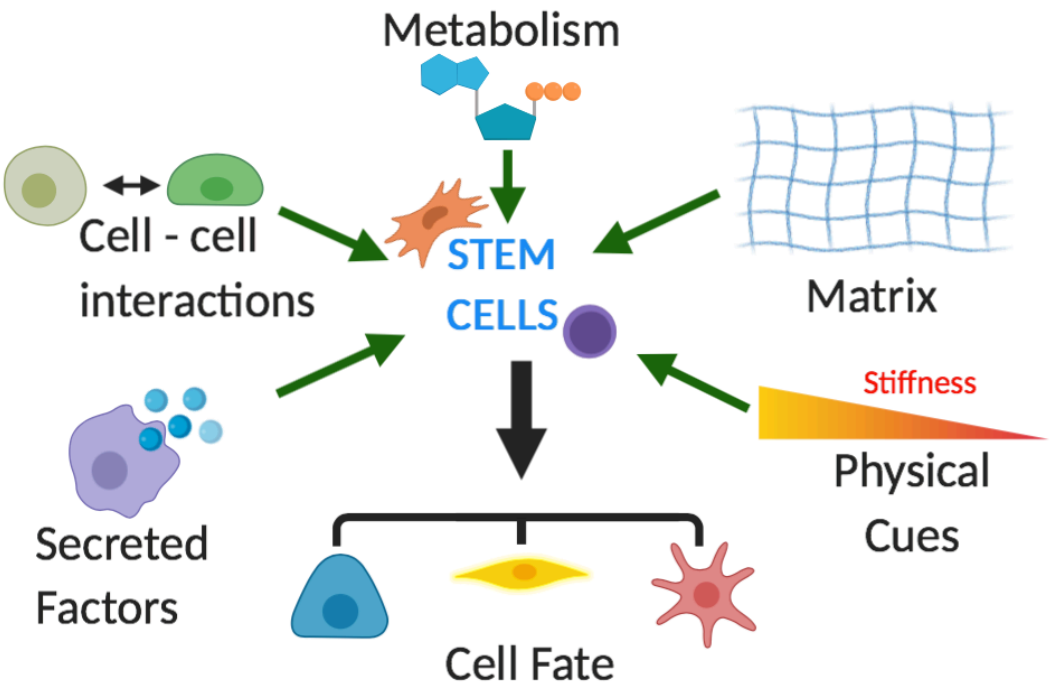

Figure 1.2 Factors influencing stem cell fate.
This diagram highlights the key factors known to have a part in determining cell fate. These include interactions with the extracellular matrix and surrounding cells along with physical cues such as stiffness and viscosity. Cell metabolism and effects from secreted factors can also impact differentiation. Created using BioRender.com.

Previous research has shown that cells can be directed down a specific differentiation pathway through the addition of growth factors into the culture, through changes in surface stiffness and also through topographical changes on culture surfaces (Tsimbouri *et al.*, 2014). Looking at one of these examples, the effect of stiffness has been investigated on inducing differentiation showing that culturing on stiffer materials, of 25-40 kPa, cells can be driven toward osteogenic differentiation whereas a softer culture material, can be used to induce adipogenic differentiation (Discher, Janmey and Wang, 2005; Zhang,

2012; Zhao *et al.*, 2014; Mao, Shin and Mooney, 2016). It has been shown in the literature that differences in the cells ability to form focal adhesions result in differentiation; focal adhesions are how cells adhere to and interact with surrounding materials resulting in the triggering of signal pathways (Trappmann *et al.*, 2012). This is described further in the Integrin binding section. Controlling these factors is a key component of tissue engineering where researchers are attempting to produce the optimal environments including biochemical signals, topographies and mechanical properties for tissue regeneration and *in vitro* modelling (Dalby *et al.*, 2007; Mason, Califano and Reinhart-King, 2012; Mpoyi *et al.*, 2016). However, *in vitro* models generally only consider one or two of the factors that contribute to a stem cell niche making them less representative to what occurs *in vivo*.

1.2 The Bone Marrow Niche

Bone marrow is found within the cancellous bone in marrow filled cavities containing many blood vessels surrounded by bony trabecular struts (Rho, Kuhn-Spearing and Zioupos, 1998). The bone marrow is formed of a protein rich extracellular matrix (ECM) which supports the various cells which reside there and play an important role in stem cell maintenance and regulation. In the literature there are several ECM components which are known to be important within the bone marrow niche with the most abundant being fibronectin, collagen I-XI, tenascin, laminin, thrombospondin and elastin (Klamer and Voermans, 2014; Domingues *et al.*, 2017). Proteoglycans with large glycosaminoglycan side chains are essential for maintaining the structure of the ECM (Klamer and Voermans, 2014). The mechanical properties vary throughout the bone marrow with a stiffnesses from <3 kPa within the soft marrow regions and up to ~40 kPa near the bone surfaces (Choi and Harley, 2017).

The bone marrow is host to two stem cell populations, mesenchymal stem cells (MSCs, also known as mesenchymal stromal cells) and haematopoietic stem cells (HSCs). Along with these stem cells other cell types are found within the bone marrow that contribute to the unique niche microenvironment which contribute to the maintenance and regulation of these stem cells (Pinho and Frenette, 2019). There are two niches that can be identified within the bone marrow these

are known as the endosteal niche and the perivascular niche (Lévesque, Helwani and Winkler, 2010; Morrison and Scadden, 2014) (Figure 1.3).

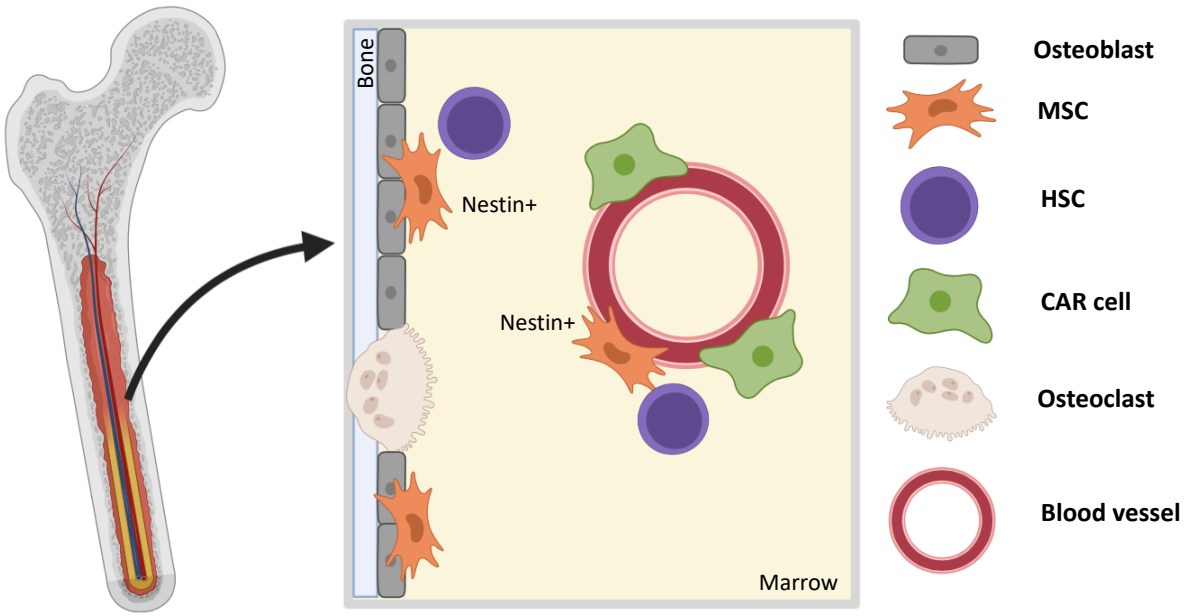

Figure 1.3 The bone marrow niche.
The bone marrow is referred to as containing two distinct stem cell niches, the endosteal niche at the bone interface to the marrow cavity and the perivascular niche found surrounding the vasculature within the marrow. These are both represented in the above figure. Created using BioRender.com.

Both of the niches contribute to maintaining a population of HSCs within the bone marrow for haematopoiesis to take place. As previously mentioned, there are many factors of the niche that contribute to the maintenance and regulation of the stem cell population including the many cell types present in the niche.

1.2.1 Cells in the Niche

Along with the two stem cell types, MSCs and HSCs, there are a diverse range of cell types found within the bone marrow niche (Calvi *et al.*, 2003; Méndez-Ferrer, T. V Michurina, *et al.*, 2010). The endosteal niche contains osteoblastic cells which can influence the niche due to its location at the bone surface to the marrow cavity. Various cytokines, for example stem cell factor (SCF) and Thrombopoietin (TPO) among others, that are secreted by osteoblasts have been associated with the expansion of haematopoietic progenitors (Taichman, Reilly and Emerson, 1996).The perivascular niche, however, is found in contact with

the endothelial cells that vasculature of the marrow is composed of. This is important to the niche as endothelial cells have been shown to secrete cytokines that are important for the regulation of HSCs (Zhang *et al.*, 2003; Kunisaki, Bruns, Scheiermann, Ahmed, Pinho, Zhang, Mizoguchi, Wei, Lucas, Ito, Jessica C Mar, *et al.*, 2013). C-X-C motif chemokine 12 (CXCL12) abundant reticular (CAR) cells, as their name suggests, have been shown to have high expression of CXCL12 and also SCF proteins that are linked to HSC maintenance (Ding and Morrison, 2013).

1.2.2 Mesenchymal Stem Cells

MSCs are one of the two stem cell types found in the bone marrow and are named due to their differentiation potential into cells of mesoderm origin (Caplan, 1991). The differentiation capabilities of MSCs are illustrated in Figure 1.4 below. The bone marrow niche is important for the maintenance and regulation of MSC fate (Shi and Gronthos, 2003). Even as one of the most common used stem cell sources, only 0.001-0.01% of the total cells present in the bone marrow are MSCs (Hanley *et al.*, 2013).

Primitive MSCs can be obtained from umbilical cord blood and cord tissue known as Whartons jelly however sources for these tissues are limited and include foetuses use of which come under ethical debate (Wang *et al.*, 2004; Petrini, 2010). It is therefore easier to isolate MSCs from adult tissues, including the bone marrow and also adipose tissue (Tsai *et al.*, 2004; Kern *et al.*, 2006). The *in vivo* precursors to MSCs were identified as pericytes, a cell type found in vascularised tissues that can display MSC characteristics *in vitro* (Crisan *et al.*, 2008). Due to variations in isolation techniques and source tissues it is important to have a guide for the classification of MSCs. For classification the presence of cell markers CD73, CD90, CD105 and Stro1 with the absence of some others such as CD34, CD45 and more can be used along with the differentiation capabilities

and the ability to adhere to general tissue culture plastic (Dominici *et al.*, 2006; Psaltis *et al.*, 2010).

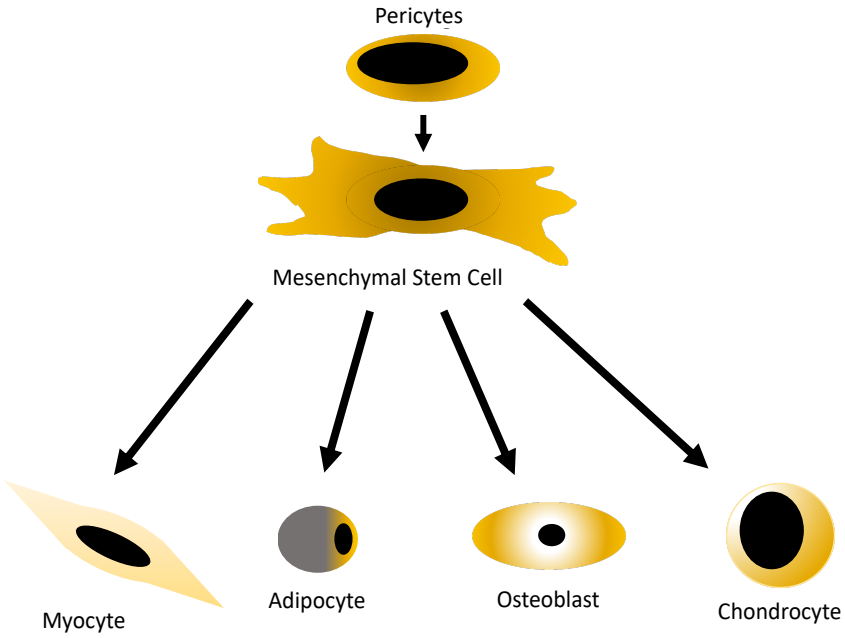

Figure 1.4. The different cell fates of a mesenchymal stem cell.
This figure highlights the differentiation capabilities of mesenchymal stem cells MSCs are formed from perivascular progenitor cells and retain the ability to differentiate into various cell types within the mesoderm germ layer. These include myocytes, adipocyte, osteoblasts and chondrocytes the path which the cell takes will depend on various influencing factors.

Due to their differentiation capabilities MSCs are widely used for research into bone regeneration therapies (Kraus and Kirker-Head, 2006; Jimi *et al.*, 2012; Cheng *et al.*, 2019). Along with being a source of connective tissue cells MSCs play other regulatory roles within the body. These roles include immune response regulation and more specifically to the bone marrow microenvironment the regulation of HSCs (Aggarwal and Pittenger, 2005; Ball *et al.*, 2007). These regulatory functions are controlled by the secretion of a number of cytokines and growth factors by the MSCs, over 100 have been reported in normal conditions (Woon Park *et al.*, 2009). Secreted factors are a key component of the stem cell niche important for regulating the function and differentiation of stem cells (Figure 1.2).

1.2.3 Haematopoietic Stem Cells

During early development HSCs are found in the foetal liver and spleen then in adulthood they are located within the bone marrow (Wang and Wagers, 2011). HSCs can be split into 2 populations within the bone marrow niches, long term renewing (LT HSCs) generally found in the endosteal niche and short term renewing (ST HSCs) in the perivascular niche (Guerrouahen, Al-Hijji and Tabrizi, 2011). LT HSCs maintain the HSC population within the bone marrow while ST HSC are responsible for the production of all our blood cells (Figure 1.5) through a process known as haematopoiesis (Sieburg *et al.*, 2006). This process occurs within the bone marrow niche and can be influenced by various factors within the niche, the mature blood cells produced through haematopoiesis then go on to operate a diverse range of functions such as transport, clotting and immunological roles (Orkin and Zon, 2008). The process of haematopoiesis has to be continuous and dynamic for the maintenance of life day to day and through trauma. The supply of blood cells is dependent on the differentiation of HSCs, despite this continuous vast and important production of cells, they are only present in small numbers comprising of < 0.005% of total cells found in the bone marrow (Kiel *et al.*, 2005; Rodriguez-Fraticelli *et al.*, 2018).

Due to the role HSCs play in the body they are currently used in therapies to treat leukaemia and AIDS (Aversa *et al.*, 2005; DiGiusto *et al.*, 2010). Because of the therapeutic potential for HSCs a lot of research has been carried out on the expansion and culture of these cells *in vitro* (Antonchuk, Sauvageau and Humphries, 2002; Krosl *et al.*, 2003; Zhang *et al.*, 2006). While progress has been made in improving HSC culture and expansion *in vitro*, it is still extremely difficult to expand primitive HSCs which retain their full differentiation capabilities. To help achieve this further studies are focused on mimicking the *in vivo* niche microenvironment through using 3D culture methods and co culture with other cells found in the niche, commonly MSCs (Dellatore, Garcia and Miller, 2008; Sharma, Limaye and Kale, 2012). The ability to expand LT HSC populations *ex vivo* would reduce the demand for donors and allow an increase in transplant treatments using HSCs.

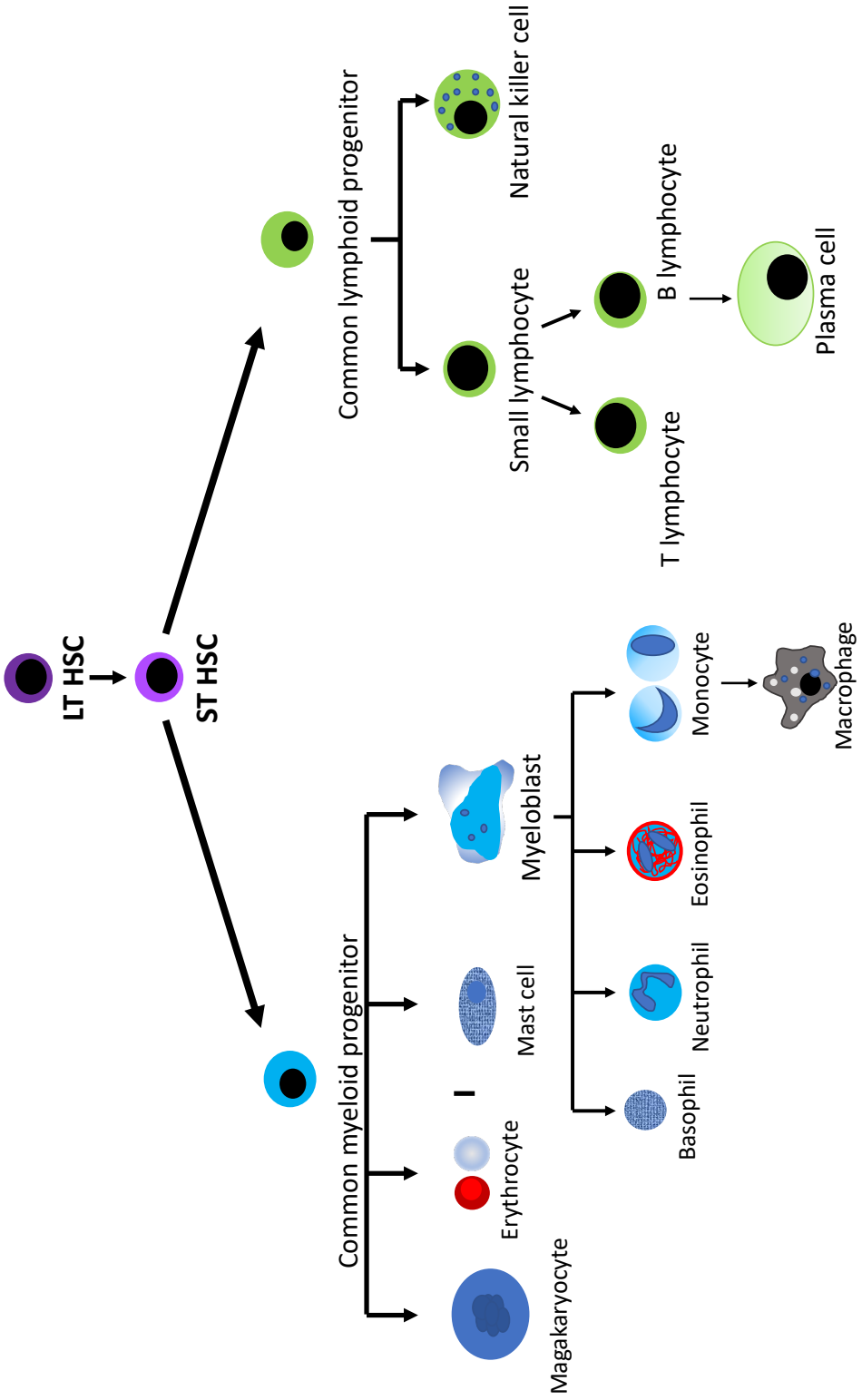

Figure 1.5. The different cell fates of a haematopoietic stem cell.
This figure shows the various cell types that can be produced by differentiating haematopoietic stem cells during haematopoiesis. LT-HSCs will continue maintain the HCS population over time while the ST-HSCs will begin differentiating into the many cell type that form our blood. In the first stage of differentiation the cells commit to either the myeloid or lymphoid lineage. These progenitor cells can then differentiate further down the lineage until they reach a terminal phenotype as seen above.

1.2.4 Cytokines

Cytokines are a family of cell signalling molecules that can be peptides, proteins or glycoproteins and that are important for the regulation of the immune response and cell processes like haematopoiesis (Fossiez *et al.*, 1996; Luster, 1998). Cytokines can also be known more specifically as chemokines if they have chemotactic activities and interleukins if they are produced by and act on leukocytes (Zhang and An, 2009). They can be characterised as either autocrine, paracrine or endocrine dependent on if the cells they act on also secrete them, are nearby or are distant respectively.

The main cytokines associated with the bone marrow niche that influence HSCs are fms like tyrosine kinase 3 (FLT3), stem cell factor (SCF), vascular cell adhesion molecule-1 (VCAM-1), thrombopoietin (TPO), C-X-C motif chemokine 12 (CXCL12 also known as stromal cell-derived factor 1 or SDF1) and osteopontin (OPN). SCF has been shown to cause an increase in HSC self-renewal and is secreted by MSCs, osteoblasts and endothelial cells within the bone marrow (Calvi *et al.*, 2003; Ding *et al.*, 2012). These three cell types also produce CXCL12 (also known as stromal cell derived fact 1 alpha or SDF-1α) which increases HSC retention in the bone marrow and self-renewal (Omatsu *et al.*, 2010; Greenbaum, Y.-M. S. Hsu, *et al.*, 2013). Self-renewal is also increased by TPO which is secreted by osteoblasts within the niche (Qian *et al.*, 2007; Yoshihara *et al.*, 2007). Osteoblasts are also responsible for the secretion of OPN within the niche which maintains population size through preventing apoptosis (Stier *et al.*, 2005). VCAM-1 produced by MSCs and endothelial cells is responsible for regulating HSC homing and adhesion (Avraham *et al.*, 1993; De Ugarte *et al.*, 2003). FLT3 is another cytokine present in the niche which has been shown to be important for regulating the process of haematopoiesis (Lyman and Jacobsen, 1998; Tsapogas *et al.*, 2017). Many of these factors are commonly added to media to supplement the culture of HSCs but this is expensive and also wasteful as during media changes most of the added cytokines are washed away.

1.3 The Extracellular Matrix

The non-cellular component of all tissues is known as the extracellular matrix (ECM) (Frantz, Stewart and Weaver, 2010). The basic elements of the ECM include water, proteins and polysaccharides though the composition is varied in different tissues changing the physiochemical properties; for example in bone the ECM also has a high mineral content, mostly comprised of hydroxyapatite. This non-cellular component also includes growth factors, cytokines and cell adhesion molecules that are secreted by cells and immobilised in the matrix. The ECM provides a complex 3D network which surrounds cells and contributes to regulation of differentiation and viability (Mason, Califano and Reinhart-King, 2012). Along with functioning as a matrix for cells the ECM also; maintains local pH and hydration within tissues; allows for the diffusion of essential nutrients, waste and signalling molecules e.g. cytokines; allows degradation and remodelling after trauma and during development; and makes available receptors for cells and molecules (Mouw, Ou and Weaver, 2014).

The functionality and differentiation of cells is regulated by the ECM through a variety of signals which can be mechanical, chemical or biological. The mechanical properties of the matrix such as stiffness and elasticity can influence cell behaviour, these properties are dictated by the composition of the ECM (Discher, Mooney and Zandstra, 2009; Geiger, Spatz and Bershadsky, 2009). Cell behaviour is also regulated by the ECM through the role it plays in cell adhesion and cell signalling through integrin receptors (Hynes, 2002; Berrier and Yamada, 2007). Factors found within the ECM, most notably the protein fibronectin (FN), have the ability to present biochemical signals, such as growth factors, which can directly control cell function (Martino and Hubbell, 2010; Zhu and Clark, 2014). By presenting biochemical signals which interact with cell-surface receptors, intercellular signal transduction can be induced and gene transduction regulated (Frantz, Stewart and Weaver, 2010). All these properties of the ECM that influence the cells can themselves be changed through the cells ability to remodel the ECM, changing the composition and therefore the effect on the surrounding cells and tissues. Due to the many functions of the ECM maintaining homeostasis is crucial to the preservation of normal tissue function and cell behaviour (Bowers, Banerjee and Baudino, 2010).

1.3.1 Composition of the ECM

Proteins found within the ECM include collagen, FN, elastin, laminin and more. The most abundant of these proteins in mammals is collagen, with 28 different collagen molecules, making up a quarter of the total protein mass (Hynes, 2009). Within the body collagen is mostly located in the skin and bones. The hierarchial structure of collagen fibres contribute to the mechanical properties of the ECM (Brinckmann, 2005). Laminins are glycoproteins that represent a family of sixteen heterotrimeric isoforms (Rhodes and Simons, 2007; Aumailley, 2013). Laminins are mostly found within the basement membrane and although some isoforms can form aggregates, they tend to function as bridges between molecules. Laminins also have been shown to play a role in adhesion and have signalling functions (Gagnoux-Palacios *et al.*, 2001). Elastins are the most abundant ECM protein found within the major arteries, comprising up to 50% of dry weight, though they are also present in other blood vessel and the skin. Elastins are essential due to the elastic properties they introduce to tissues allowing them to return to their original form after deformation. These hydrophobic proteins are essential to blood vessels and other tissues as they have the ability to momentarily stretch (Eble and Niland, 2009).

These proteins are found embedded in the water and polysaccharide element of the ECM which forms a highly hydrated gel-like matrix made up of long linear chains of carbohydrates known as glycosaminoglycans (GAGs). The negative charge of this matrix creates osmotic pressure through the attraction of cations this then leads to a swelling pressure within the matrix which enables it to withstand compressive forces (Mouw, Ou and Weaver, 2014). These GAGs are able to covalently bind to proteins within the ECM producing proteoglycans which have multiple functions within the ECM. Proteoglycans contribute to many of the ECM functions outlined previously such as forming the matrix around cells and regulating the diffusion of molecules. They also have the ability to immobilise secreted molecules this, along with regulation of diffusion, produces a reservoir within the ECM of these molecules. Proteoglycans can also protect against proteolysis, further enhance the presentation of molecules to cell surface receptors and also sterically block protein activity (Frantz, Stewart and Weaver, 2010; Mouw, Ou and Weaver, 2014; Lindahl *et al.*, 2017).

The ECM is dynamic allowing for change in the composition and function over time, an example of this is mammary ECM changes due to reproductive state (Schedin *et al.*, 2004). This dynamic behaviour is essential for the normal function of various tissues though it can also contribute to disease when there is a disruption to the normal ECM (Cox and Erler, 2011). Variations in the composition are driven by the cells and the surrounding microenvironments to produce the ideal environment for the tissue it occupies. It is important to understand the components of the ECM and their various functions within tissues if the role they play in disease is to be investigated.

There are many recent studies which aim to produce *in vitro* models that can mimic *in vivo* conditions including the ECM which will allow research into normal and/or diseased cell behaviour (Romano *et al.*, 2011). It is important to be able to mimic this environment *in vitro* as previous studies have noted that without ECM support cell viability and *in vivo* like phenotype is lost. Studies have shown that through the introduction of ECM proteins to in vitro cultures some of the physical and chemical functions seen *in vivo* can be maintained influencing cell behaviours such as adhesion and spreading (Vandenburgh', Karlisch and Farr, 1988; El-Ghannam, Starr and Jones, 1998). Within *in vitro* models polymer scaffolds and/or hydrogels are commonly used to create a 3D environment acting as an ECM for cells (Han and Gouma, 2006; Tibbitt and Anseth, 2009).

1.4 Fibronectin

FN is a glycoprotein found in the ECM that is essential for embryogenesis and also wound healing. FN consists of two subunits, each approximately 240 kDa in size, that are linked through two disulphide bonds forming a homodimer. Each of these subunits consists of three types of functional domains that repeat along its length, these are; 12 type I, 2 type II and 15 or 17 type III varying between plasma and cellular FN respectively (Zollinger and Smith, 2017). An outline of the FN structure including the organisation of these domains is shown in Figure 1.6 below.

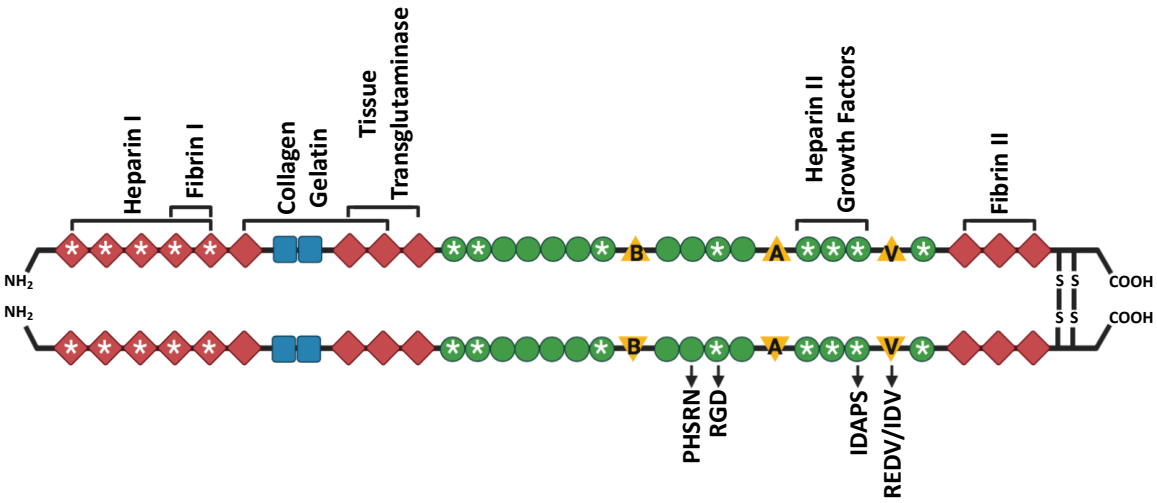

Figure 1.6 Diagrammatic representation of the structure of fibronectin and its domains. This figure outlines the structure of cellular FN, plasma FN lacks the A and B variable domains shown in yellow. The other binding domains are represented by the different units type I domains are red diamonds, type II domains blue squares and type III domains green pentagons. Domains that themselves interact with FN are represented with a white asterix (*). Other key interactions are also denoted within the figure. Adapted from (Pankov and Yamada, 2002) using BioRender.com.

1.4.1 Fibrillogenesis

FN exists naturally in two conformations, globular and fibrillar as shown in Figure 1.7. Plasma FN is soluble and found in the globular conformation circulating the blood where it enhances clotting and healing. The majority of FN, however, is found in the ECM in a fibrillar conformation (Pankov and Yamada, 2002). The fibrillar conformation is achieved through the self-association of FN molecules, when in this fibrillar conformation further organisation occurs leading to the formation of networks, this process is referred to as fibrillogenesis. Within the ECM fibrillogenesis is a cell mediated process which allows cells to produce a FN rich local environment to surround themselves (Hynes, 1999). Cell mediated fibrillogenesis occurs through a single cell binding multiple $\alpha 5\beta 1$ integrins with the RGD and PHSRN domains ($FNIII_{9\text{-}10}$) producing high local concentrations of FN leading to self-association and fibrillogenesis. The conformation of the molecule directly impacts the availability of different functional domains this is due to hidden domains resulting from the folding of the molecule while in a globular conformation.

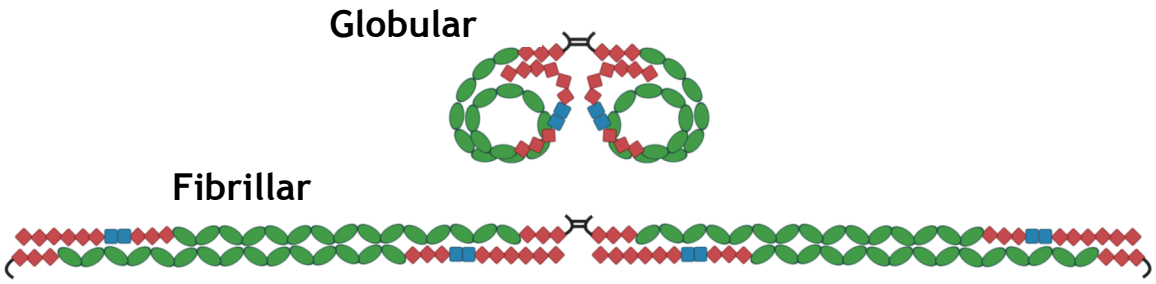

Figure 1.7 Conformation of Fibronectin.
The figure above shows a diagrammatical representation of the two conformations, globular and fibrillar, in which the glycoprotein FN is found naturally within the body. In the fibrillar conformation the FN is able to bind to other FN molecules leading to the formation of a network. Domains are represented in various colours matching those in Figure 1.6. Created using BioRender.com.

Though naturally the process of fibrillogenesis is mediated by cells as previously outlined there are several cell free methods that have been found to induce this process; these can be chemical, physical or material driven (Vartio, 1986; Ulmer, Geiger and Spatz, 2008; Cantini, González-García, *et al.*, 2012). Chemical methods aim to disrupt or to denature FN in the globular conformation leading to self-assembly. Treatment of globular FN using reducing agents for example dithiothreitol (DTT) has been shown to induce non-covalent assembly of FN networks through the decoupling of disulphide stabilised globular domains (Williams *et al.*, 1983). DTT has also shown the ability to induce the intramolecular bonding of FN when used alongside strong oxidants (Vartio, 1986; Sakai, Fujii and Hayashi, 1994). Guanidine is another chemical that has been used as a denaturant in order to drive the formation of FN fibrils through disruption of the FN in the globular conformation (Cantini, González-García, *et al.*, 2012; Llopis-Hernández *et al.*, 2015). Physical methods such as the application of mechanical tension have shown the ability to allow fibrillogenesis through the unfolding of globular FN molecules (Brown, Blunn and Ejim, 1994; Zhong *et al.*, 1998; Ulmer, Geiger and Spatz, 2008). Mechanical disruption has been achieved through extreme differences in hydrophobicity or domain separation of lipid bilayers exposing the cryptic binding domains required for self-assembly through physical elongation (Baneyx and Vogel, 1999; Ulmer, Geiger and Spatz, 2008). Material driven fibrillogenesis has been shown through

use of various materials in the literature including PEA and polyalkyl acrylates (Vanterpool *et al.*, 2014; Bathawab *et al.*, 2016).

1.4.2 Integrin binding

Biochemical and physical cues are used by cells to sense their immediate environment producing signals that can regulate function, differentiation and viability, signal transduction is instigated by cell adhesion receptors or integrins. Integrins are transmembrane proteins with a heterodimeric structure which allow the translation of external cues to intracellular signals through integrin interactions with the ECM and intracellular proteins such as actin (Figure 1.8) (Schwartz, 2010).

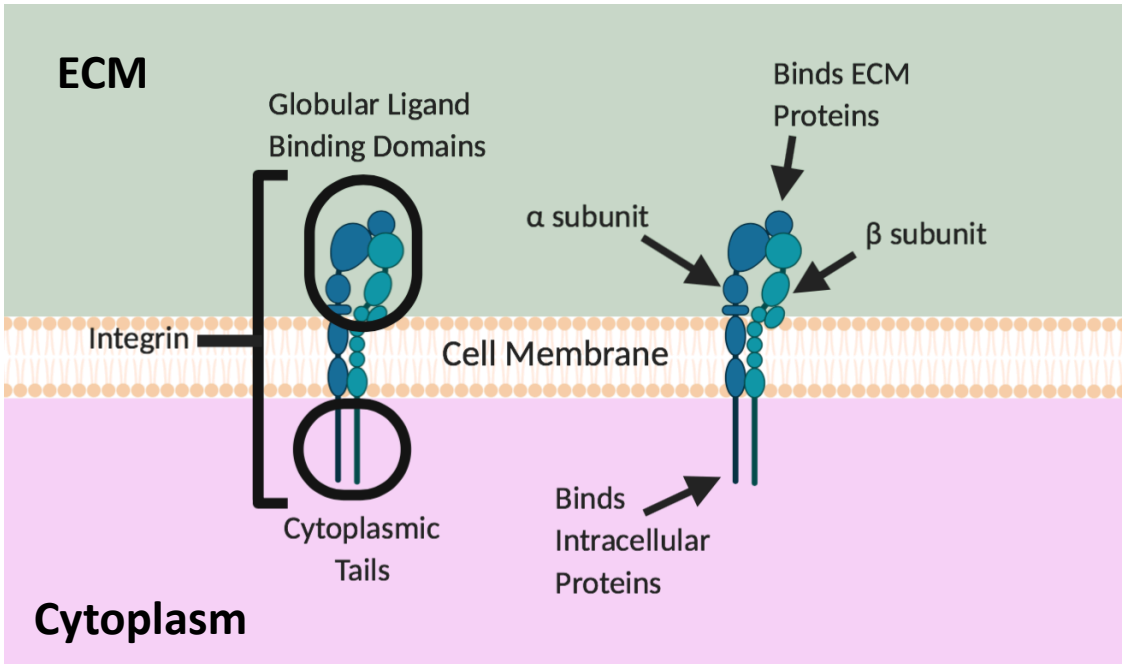

Figure 1.8 The basic structure of an integrin.
The basic regions of integrins are highlighted within the figure above along with binding abilities of different regions with the cytoplasmic tails binding with intracellular proteins and the globular end binding with ECM proteins. The subunits, alpha and beta, are variable changing the binding abilities of different integrins. Intracellular side is pink and extracellular side green. Created using BioRender.com.

When high concentrations of cell binding domains are found clustered, as seen with RGD in a FN network, a build-up of integrins occurs and triggers the formation of structures known as focal adhesions (Takagi and Springer, 2002; Calderwood, 2004). These focal adhesions, formed from clusters of integrins,

link intracellular actin filaments to the extracellular environment. Integrins are responsible for a vast array of specific cellular binding conformations possibly through the different compositions of the α and β glycoproteins from which integrins are formed. Each of these glycoproteins is formed of cytoplasmic tails which bind to intracellular proteins, such as cytoskeletal or signalling proteins, an elongated stalk which is able to traverse the cellular membrane and globular ligand binding domains that interact with components of the ECM (Xiong *et al.*, 2001; Calderwood *et al.*, 2003; Lau *et al.*, 2009).

The ECM protein FN has been shown to possess domains with the sequences that correspond to a multitude of integrin receptor families, such as RGD (Plow *et al.*, 2000). The PHSRN synergy domain at $FNIII_9$ promotes cell binding to the RGD domain located at $FNIII_{10}$ (Figure 1.6) through interactions with the integrin $\alpha5$ subunit although this synergistic binding is not required it does enhance cell binding (Redick *et al.*, 2000). This synergistic interaction between the $\alpha5\beta1$ integrin can only occur when FN is in the fibrillar conformation and the binding sites are exposed (Bachman *et al.*, 2015). This recognition, by $\alpha5\beta1$ integrin, of the RGD and PHSRN domains leads to the mechano-transduction of forces from the ECM into the cell resulting in changes or maintenance of cell phenotype and function.

1.4.3 Growth Factor Binding

Growth factors are proteins involved in cell signalling that can regulate various functions including the proliferation, migration and differentiation of cells (Friedman, 2012). The FN domains $FNIII_{12\text{-}14}$ (Figure 1.6) have been shown to bind and present growth factors within the ECM (Martino and Hubbell, 2010). These growth factor binding domains are found close to the integrin binding RGD domain at $FNIII_{10}$, synergy between these domains has been shown to enhance viability and cellular interactions (Hynes, 2002; Lin *et al.*, 2011; Rodrigues *et al.*, 2013; Donnelly *et al.*, 2018). This is particularly important for certain growth factors, such as vascular endothelial growth factor (VEGF) which requires integrin binding proximal to growth factor binding, like that present on FN, to fully activate the growth factor (Borges, Jan and Ruoslahti, 2000). Growth factor binding occurs through the regions which possess heparin binding domains which many growth factors, for example those in the fibroblast growth factor (FGF)

and transforming growth factor (TGF) families, bind to through their affinity to heparin and heparin sulfate (Pankov and Yamada, 2002; Wijelath *et al.*, 2006; Martino and Hubbell, 2010). This type of growth factor binding to ECM proteins has been shown to facilitate similar signal transduction pathways to integrin binding (Hynes, 2002; Lin *et al.*, 2011).

With this ability of ECM proteins to bind growth factors a reservoir of soluble growth factors can be formed producing local growth factor gradients and allowing controlled release through degradation (Hynes, 2002; Zhu and Clark, 2014). Research has shown that growth factors that are bound are more favourably presented to cells when compared to those in solution (Kuhl and Griffith-Cima, 1996; Llopis-Hernández *et al.*, 2016). Studies have also shown that when growth factors are bound to the ECM and held as solid-phase ligands they can induce cellular signals that differ from those induced by the same growth factor in a soluble state (Mohammadi, Olsen and Goetz, 2005; Zhu and Clark, 2014). Through this binding, it has been shown, prolonged cellular signalling can be achieved in some cases when the growth factors are prevented from being internalised by the cells on contact and instead interact with the cell surface (Platt *et al.*, 2009; Zhu and Clark, 2014).

1.5 Biomaterials

A biomaterial is generally defined as any substance that contacts tissue or biological fluid (Peppas and Langer, 1994; Langer and Tirrell, 2004). The development of biomaterials has allowed further investigation into the biochemical and biophysical cues that influence cell function and behaviour, such as topography and growth factor presence (Discher, Mooney and Zandstra, 2009; Murphy, McDevitt and Engler, 2014; Turner and Dalby, 2014). Biomaterials have been utilised for many research areas including tissue engineering, drug delivery, medical imaging, medical implants, regenerative medicine and *in vitro* modelling (Khandare and Minko, 2006; Mitragotri and Lahann, 2009; O'Brien, 2011; Pradhan *et al.*, 2016). When used for *in vitro* modelling biomaterials are commonly designed to mimic one or more of the properties of the native ECM in which cells are encapsulated to produce an *in vivo* like microenvironment (Anselme, 2000; Engel *et al.*, 2008).

When a biomaterial is similar in architecture, composition and/or other properties to an *in vivo* material they can be described as biomimetic materials (Caliari and Burdick, 2016). Biomaterials used for mimicking hard tissues such as bone are commonly metallic or ceramic materials like titanium or bioactive glass (El-Rashidy *et al.*, 2017; Pobloth *et al.*, 2018). Where the tissue being studied is softer it is more common to use polymer materials to produce scaffolds and/or hydrogels (Berkovitch, Yelin and Seliktar, 2015; Rose *et al.*, 2017; Qian *et al.*, 2018). As suggested biomaterials can be made from a wide range of materials to fulfil a host of different functions such as joint replacement implants, 3D scaffolds for tissue engineering and *in vitro* modelling (Kasemo, 1983; Burdick and Anseth, 2002; Sodunke *et al.*, 2007; Jana, Cooper and Zhang, 2013; Yuan *et al.*, 2014).

1.5.1 Biomaterials in tissue engineering

Biomaterials are commonly used to aid *in vivo* tissue regeneration as cellular or mechanical support scaffolds (O'Brien, 2011). Biomaterials can influence cell adhesion, differentiation and function through mechanical forces, surface topography and biochemical signalling (Mason, Califano and Reinhart-King, 2012; Anderson *et al.*, 2016). Differences in the physical properties of a material, such as stiffness, can change the application for which it can be utilised as a biomaterial, from polymer gels to mimic soft tissues to stiffer polymer scaffolds for use in bone regeneration (Lesný *et al.*, 2002; Kretlow and Mikos, 2007). Biodegradability is another property that is important to consider when choosing a biomaterial. Depending on the application degradability can be beneficial or detrimental to the function; for example, biomaterials used to enhance regeneration need to be biodegradable to allow cell remodelling and eventual removal from the body. However, other uses such as joint replacements require the materials to be non-degradable and maintain their integrity overtime. For *in vitro* modelling biodegradable material can be used to encourage cell mobility and remodelling; though to maintain a long-term model it must not breakdown fully overtime, it can therefore be beneficial to use partially degradable models. As changes in the physical properties can alter the cell response to a material choosing appropriate materials for the application is extremely important.

Modifications to established biomaterials are common to tune the desired properties.

The chemical properties of a biomaterial can be altered to fit the desired application through the addition of biological factors or controlled chemical reactions (Khan, Tanaka and Ahmad, 2015). Interactions between biomaterials and cells can be improved through chemical modifications to alter the surface chemistry of a material which has been shown to modulate these interactions (Curran, Chen and Hunt, 2005, 2006; Benoit *et al.*, 2008; Phillips *et al.*, 2010). Care must be taken when considering surface modifications as it is possible to change surface properties beyond those intended which can negatively impact the biomaterials function. Studies have also shown that changes in topography at a nanoscale level on biomaterial surfaces can influence cell fate (Dalby *et al.*, 2007; Tsimbouri *et al.*, 2014). This occurs through producing differences in cellular adhesion which leads to changes in the biochemical signalling pathways resulting in alterations in the cell phenotype (Dalby, Gadegaard and Oreffo, 2014).

Biomaterials not only interact with cells but can also be used for protein adsorption which can in turn enhance cellular interaction and biological functionality. For example, there are some material surfaces that have the ability to induce fibrillogenesis simply upon the adsorption of FN, this is due to the ability of specific surface chemistries to disrupt the globular conformation, similarly to the other non-cellular methodologies; this is referred to as material driven fibrillogenesis (Salmerón-Sánchez *et al.*, 2011; Cantini, González-García, *et al.*, 2012; Llopis-Hernández *et al.*, 2016). The elongation of FN molecules has been shown to occur when FN is adsorbed onto surfaces which are hydrophilic or negatively charged (Nelea and Kaartinen, 2010). An example of a surface which favours the adsorption of FN in an elongated conformation, leading to the formation of fibrils, is the polymer poly(ethyl acrylate) (PEA) (Salmerón-Sánchez *et al.*, 2011). This process is thought to occur due to interactions between the functional side chains of PEA and hydrophobic regions of the FN molecules, along with physical disruption to the globular conformation resulting from the net negative charge of the polymer ultimately allowing the self-association of the FN producing fibrils (Cantini, González-García, *et al.*, 2012). This phenomenon of

material driven fibrillogenesis can be utilised in the development of biomaterial surfaces to enhance cell interaction.

Cellular adhesion is one of the single most important interactions that must be achieved and understood for a biomaterial to be effective. Adhesion is essential for the regulation and maintenance of cells as well as being an important component of cell communication making it a vital property of biomaterials (Khalili and Ahmad, 2015). The addition of proteins to a material such as the FN network described is known as surface funtionalisation and improves cellular adhesion and interactions with the material surface. However, once adhesion is achieved this then drives signalling pathways, cell function and phenotype it is therefore important to fully understand the cell-material interface. It is due to these interactions that biomaterial have become so popular with a vast potential in various areas of research and future therapies/treatments.

1.5.2 Biomaterials in bone marrow niche models

The bone marrow niche is a growing research topic due to increased interest for stem cell therapies. Many past models produced focussed on the use of a monolayer of stromal cells with HSCs introduced in suspension within the media (Dexter, 1982; Jing *et al.*, 2010). Despite seeing success with the use of biomaterials in 2D cultures to mimic various ECM properties, focus has moved to 3D modelling to better reproduce the *in vivo* environment. A common feature of 3D bone marrow niche models is the use of collagen type I gels which is believed to mimic the elastic properties of the bone marrow (Leisten *et al.*, 2012; Gattazzo, Urciuolo and Bonaldo, 2014). Though gels are popular for producing 3D models other materials have been used to create scaffolds for successful 3D culture of HSCs such as electrospun nanofiber scaffolds (Chua *et al.*, 2007). Also the immobilisation of the ECM protein FN onto nanofiber surfaces has been shown to be effective in enhancing HSC culture (Feng *et al.*, 2006). Many niche models have demonstrated the importance of close proximity of HSCs to MSCs, highlighting the necessity for both cells types to maintain a viable population within the model (Jing *et al.*, 2010). The use of microcarriers allows the encapsulation of MSC into hydrogels alongside HSCs allowing for this desired close proximity, with the microcarriers mimicking the endosteal surface and hydrogels representing the surrounding soft marrow as seen *in vivo* (Figure 1.3).

During *in vitro* culture MSCs begin to differentiate and/or lose the ability to self-renew as they reach a higher passage. As MSCs are an important cell type within the niche, models aim to maintain an undifferentiated HSC supporting phenotype for example nestin positive population (Cook *et al.*, 2012). However, osteoblasts are also important in the niche, secreting various factors that are key to HSC maintenance, therefore some osteogenic differentiation to also produce a population of osteoblasts within models can be beneficial (Lévesque, Helwani and Winkler, 2010). Biomaterials have been used to enhance osteogenic differentiation through immobilising bone morphogenic protein 2 (BMP-2) in close proximity to cell or integrin binding domains to produce synergistic signalling (He, Ma and Jabbari, 2008; Llopis-Hernández *et al.*, 2016). Research in osteogenic differentiation is mainly focussed on bone regeneration but this concept can be used within niche models to produce multiple cell types from a single source.

1.6 Poly (ethyl acrylate)

PEA is a hydrophobic acrylic ester polymer which has been shown to be biostable under *in vivo* conditions such as physiological temperatures. PEA is composed of repeating ethyl acrylate monomer units; properties include a tensile strength of 0.23 MPa and a glass transition temperature of -23 °C. These properties along with the polymer's ability to induce fibrillogenesis give PEA potential in biomedical engineering. The structural formula for PEA is represented in Figure 1.9.

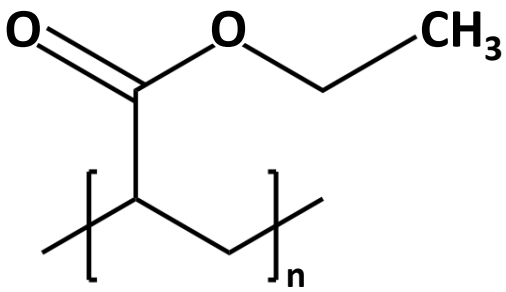

Figure 1.9 Structural formula of Poly (ethyl acrylate).
The figure above shows the structural chemical formula for a single unit of the polymer PEA. The polymer can vary in length and as shown is formed with a hydrocarbon back bone.

1.6.1 PEA and Fibronectin

The interaction between PEA and the ECM protein FN has been utilised for biomedical purposes. This is due to the induction of fibrillogenesis caused by contact with the polymer surface producing FN networks as seen *in vivo* (Salmerón-Sánchez *et al.*, 2011; Cantini, González-García, *et al.*, 2012; Llopis-Hernández *et al.*, 2013; Vanterpool *et al.*, 2014; Sprott *et al.*, 2019). The organisation of FN into networks when coated onto the polymer surface facilitates cellular adhesion and focal adhesion formation. This organisation of FN molecules occurs due to the process of material driven fibrillogenesis induced due to the composition and mobility of the functional groups present in the polymer which promote unfolding. This unfolding of the FN molecules, seen in Figure 1.7, leads to the exposure of various cryptic binding domains allowing cellular and growth factor binding (Bathawab *et al.*, 2016; Llopis-Hernández *et al.*, 2016; Moulisová *et al.*, 2017). This interaction makes PEA a useful material for use in biomedical engineering applications however its use is restricted due to its non-biodegradable nature (Sprott *et al.*, 2019).

Despite being non-biodegradable PEA has been successfully used for *in vivo* tissue regeneration applications by producing thin coatings, in the nanometres, that can be applied to biodegradable substrates allowing eventual removal from the body (Cheng *et al.*, 2019). It is important that these thin coatings must retain the ability to induce fibrillogenesis when in contact with FN while also allowing the degradation of the coated material. Various techniques have been developed to incorporate thin layers of PEA on to surfaces including spin coating, plasma polymerisation and surface initiated atomic transfer radical polymerisation (SI-ATRP) (Llopis-Hernández *et al.*, 2015, 2016; Cheng *et al.*, 2019; Sprott *et al.*, 2019). These techniques have been shown to retain the functionality of PEA providing additional functionality to the underlying material.

This interaction has been utilised for research into critical bone defect regeneration by our group showing that by using plasma polymerisation to treat decellularised bone chips with PEA, the favourable presentation of growth factors, BMP-2 in this study, by FN networks allows for use of an ultra-low dose when compared to previous studies while still promoting bone regeneration

(Cheng *et al.*, 2019). Studies have also shown that control over the FN conformation, and therefore the activity, can allow manipulation of the phenotype of various cell types through changes in adhesion (Donnelly *et al.*, 2018). Primarily having been used for bone regeneration studies PEA also has potential in other biomedical engineering applications and research. Developing the coating techniques and exploring other ways to utilise this polymer-protein interaction could aid understanding of *in vivo* processes and development of new treatments.

1.7 Hydrogels

A hydrogel is a material which consists of a solid hydrophilic network with the ability to immobilise water, this gives it a continuous solid and liquid phase (Ahmed, 2015). The network is commonly made up of polymer chains held together by covalent bonds or self-assembled aggregated fibres held together by non-covalent intermolecular forces. Hydrogels are becoming more popular as a biomaterial that can be used for applications such as wound dressings, implants, drug delivery systems and tissue scaffolds (Fu and Kao, 2011). These materials create a 3-dimensional (3D) scaffold (Figure 1.10) that can be used for culturing cells in a 3D network as opposed to 2D culture methods.

3D culture methods are becoming particularly important as research is pushing toward animal free research models which require accurate *in vitro* culture conditions. Hydrogels have various properties which make them good for use in tissue engineering including high water content, biocompatibility, mass transport of oxygen, nutrients and waste products, and the ability to control mechanical and/or chemical properties of the gels (Khetan and Burdick, 2009; Hoffman, 2012; Caliari and Burdick, 2016). Hydrogels can be classified based on their crosslinking method, electrical properties, physical characteristics or their origin from natural or synthetic sources.

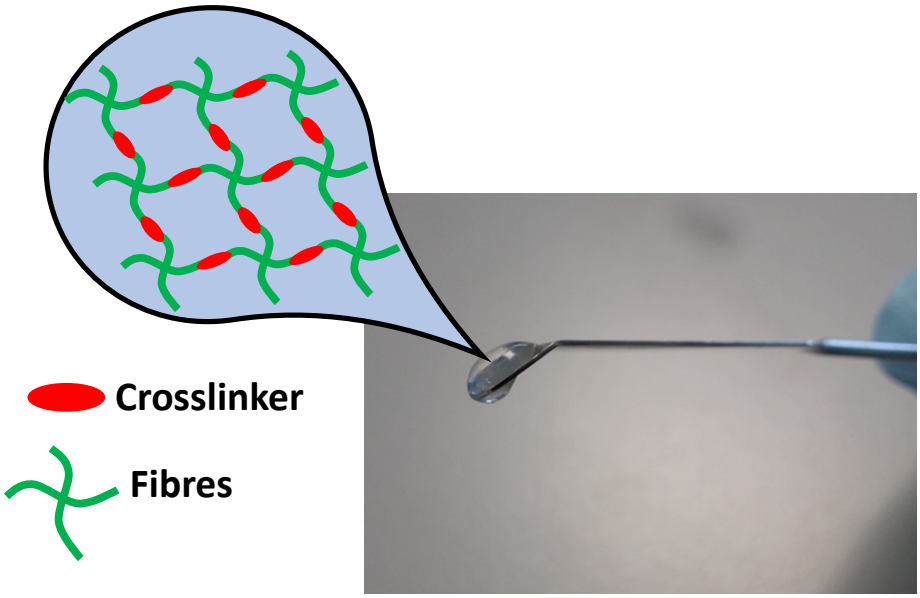

Figure 1.10. A hydrogel with a diagrammatic representation of the network of fibres. The figure above shows a PEG based hydrogel (Photo) with a diagrammatic representation of the internal structure produced, this comprises of a network of 4-arm PEG molecules joined using crosslinker molecules.

1.7.1 Properties of Hydrogels

Hydrogels can be used in 3D systems to produce microenvironments for cells with specific mechanical properties. These include stiffness, material stiffening or softening which can be controlled through modulation of the linear elasticity, viscoelasticity and spatiotemporal properties of the hydrogel (Huebsch *et al.*, 2010; Chaudhuri *et al.*, 2015, 2016; Doyle *et al.*, 2015). Cells cultured within hydrogels respond to their surrounding stiffness with changes in morphology, spreading, migration and differentiation (Boontheekul *et al.*, 2007; Her *et al.*, 2013; Charras and Sahai, 2014). One study showed that by encapsulating MSCs within alginate gels produced over a wide range of stiffnesses (2.5 - 110 kPa) that lower stiffnesses could result in adipogenesis (2.5 – 5 kPa) whereas osteogenesis occurred in higher stiffness gels (11 – 30 kPa) (Huebsch *et al.*, 2010). Hydrogel stiffness can be controlled through the modulation of polymer molecular weight, polymer concentration or the crosslinker density. In order to receive signals from their surroundings cells must be able to attach to the hydrogel matrix. It is therefore essential that the cells are able to adhere:

studies have shown that the introduction of peptides into gels allows for cell adhesion (Burdick and Anseth, 2002; Zhu *et al.*, 2009).

Most hydrogels, like soft tissues, are viscoelastic which makes them ideal for mimicking the *in vivo* microenvironment of soft tissues. Viscoelastic materials are defined as materials which show both viscous and elastic properties, viscous properties are shown through the viscosity or loss modulus of a material while the elasticity is characterised through stiffness or the storage modulus. Various studies have shown the importance of the viscoelastic properties of the microenvironment on cell spreading, proliferation and differentiation (Chaudhuri *et al.*, 2015, 2016). Similar to the stiffness the viscoelastic properties can also be controlled through hydrogel composition, component concentration, molecular weight and crosslinking.

Degradation properties have been utilised within biomedical engineering for drug delivery systems and control of cell motility. Degradation *in vivo* is essential for the maintenance of tissue homeostasis and in the remodelling of the ECM (Page-McCaw, Ewald and Werb, 2007). Cells can remodel their microenvironment through the secretion of proteases that target enzyme sensitive macromolecules within the ECM. Through the feedback cells receive from this remodelled environment degradation influences the cells behaviour. Degradation is therefore an important factor to consider when choosing the appropriate hydrogel for your application and it is essential to ensure any by products produced during degradation are biocompatible. Hydrogels used for *in vivo* applications may benefit from higher degradability which matches the degradation properties to the native tissues. For *in vitro* modelling however, if the model is to maintained long term a non-degradable hydrogel would be more beneficial. Degradation of hydrogels can vary depending on the source material, crosslinking and the environmental conditions. Degradability of hydrogels can be controlled by introducing enzyme sensitive peptides as degradable crosslinkers into non-degradible PEG-based hydrogels (Phelps *et al.*, 2012).

1.7.2 Naturally Derived Hydrogels

Natural hydrogels can also be described as promoting hydrogels, this is due to the biological components of these gels promoting cellular functions as the

matrix interacts directly with the cells (Tibbitt and Anseth, 2009). Materials from both animal and plant sources can be used to develop natural hydrogels. Decellularised ECM is a common naturally derived hydrogel which has been obtained from many tissue sources including the heart, blood vessels and diaphragm (Ott *et al.*, 2008; Quint *et al.*, 2011; Gubareva *et al.*, 2016; Yu *et al.*, 2016). The use of decellularization benefits from the maintenance of architecture and composition from the origin tissue (Yu *et al.*, 2016). Using decellularized tissues have produced promising results but have issues with batch to batch variation which is common in naturally derived materials. The ability to produce this material is also donor dependent which is not a consistent reliable source.

Hydrogels can also be produced from individual components of natural tissues such as proteins or polysaccharides. Protein based hydrogels can be produced from a single component or a mixture examples include collagen, gelatin, elastin and fibrin (Nakatsu *et al.*, 2003; Mason *et al.*, 2013; Stratesteffen *et al.*, 2017). These materials are widely used in bioengineering due to their biocompatibility, bioactivity, structure and formation in physiological conditions. These gels again suffer from batch to batch variation as well as a lack of tunability and uncontrollable degradation. Polysaccharide based hydrogels include alginate, chitosan and hyaluronic acid which are suitable for biological use due to their biocompatibility and formation in mild conditions (Rowley and Mooney, 2002; Jana, Cooper and Zhang, 2013; Jha *et al.*, 2016). A benefit to polysaccharide based hydrogels over protein based it that they are usually less immunogenic along with better control over physical properties. However, unlike protein based gels they have to be modified to increase bioactivity as they lack adhesion ligands and are not biodegradable (Rowley and Mooney, 2002; Jha *et al.*, 2016).

1.7.3 Synthetic Hydrogels

Synthetic hydrogels are also decribed as permissive hydrogels as, unlike naturally derived hydrogels, the matrix itself does not interact with or influence the cells (Tibbitt and Anseth, 2009). Synthetic polymer hydrogels are formed from bioinert monomers or macromers that can be crosslinked through various synthetic chemical reactions. Examples of synthetic hydrogels include poly(ethylene glycol), poly(acrylamide) and poly(vinyl alcohol) amongst others

(Nuttelman *et al.*, 2001; Tse and Engler, 2010; Cruz-Acuña *et al.*, 2017). The most notable advantage of the use of synthetic hydrogels over those that are naturally derived is the lack of a batch to batch variation. This is possibly through finely controlled composition and chemistries during fabrication which also allows for custom modifications to alter properties allowing tunability during formation. As synthetic hydrogels are bioinert and non-degradable modifications can be made to introduce degradable peptides and bioactive molecules while retaining control over what is present to influence cells or surrounding tissues (Raeber, Lutolf and Hubbell, 2005; Guvendiren and Burdick, 2013; Kyburz and Anseth, 2015). By using bioinert hydrogels and introducing bioactive components, non-specific cell adhesion and protein adsorption can be prevented allowing more control of the system and understanding of cell behaviour.

1.7.4 Poly (ethylene glycol)

PEG is formed of a repeating monomer unit, ethylene glycol, and is a compound which is soluble in aqueous media. The molecular weight of PEG can vary depending of its use and the properties required from the resulting gel. The hydrophilic properties of PEG help to produce structural and physiochemical properties similar to those of the ECM (Krsko and Libera, 2005). These hydrophilic properties along with a relatively low dispersity index (1.01 – 1.1), allowing control over physiochemical properties, make PEG a useful material in biomedical engineering applications (Pfister and Morbidelli, 2014).

PEG is a commonly used synthetic hydrogel which has been shown to be biocompatible and bioinert (Krsko and Libera, 2005). PEG gels are commonly used to produce 3D microenvironments for studying cell behaviour due to their tuneable properties (Lutolf and Hubbell, 2005; Raeber, Lutolf and Hubbell, 2005). PEG can be modified through the addition of different functional groups, for example maleimide, acrylate, thiol, norbornene or amine, allowing for variations in gelation methods such as ionic, covalent or physical gelation (Phelps *et al.*, 2012; Roberts and Bryant, 2013). Hydrogels which are formed chemically through covalent bonds generally present a relatively stable structure. One of the properties that make PEG compatible for biological applications, specifically the encapsulation of cells, is the biocompatible

crosslinking methods that can be used such as the Michael-type addition reaction (Figure 1.11) which occurs instantly in mild physiological conditions when the components of the reaction are mixed (Zhu, 2010).

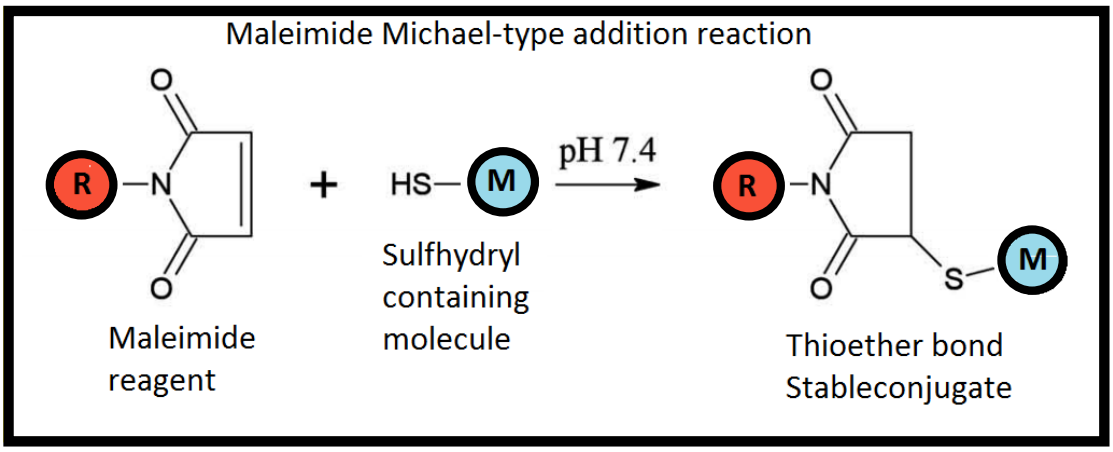

Figure 1.11 Maleimide Michael-type addition reaction
The figure shows the reaction that occurs when a molecule with the maleimide group reacts with a sulfhydryl containing molecule. It is common that these would be modified PEG molecules to include the maleimide and sulfhydryl groups.

Covalent crosslinking can occur through photopolymerisation where gelation is initiated in the presence of UV light, due to the speed of the crosslinking this method is suitable for encapsulating cells (Zhu *et al.*, 2009). Another method for covalent crosslinking is the use of two or more functional components which contain complementary reactive groups. There is no need for an initiator in this type of reaction as it occurs upon mixing of the multiple components through a chemical reaction such as the Michael-type addition reaction (Fu and Kao, 2011). These methods are broadly used in research using PEG hydrogels though other methods have been developed.

Research using PEG hydrogels has shown the inclusion of degradable components and other bioactive molecules. PEG hydrogels are commonly functionalised with the incorporation of RGD and IKVAV, peptides responsible for cell adhesion *in vivo*. This leads to increased interaction between cells and the hydrogel network better mimicking the ECM enhancing cell viability and function (Benoit and Anseth, 2005; Weber *et al.*, 2007; Salinas and Anseth, 2008; Lin and Anseth, 2009). PEG hydrogels have been used for both *in vitro* and *in vivo* research and have shown tunability in their stiffness and swelling properties (Rizzi and Hubbell, 2005; Rizzi *et al.*, 2006). PEG which has been functionalised with

maleimide produce a fast reaction with thiol groups through a Michael-type addition reaction that occurs at physiological pH (Phelps *et al.*, 2012). PEG gels have also been shown to possess the capacity to incorporate a whole protein through crosslinking to the PEG backbone further increasing bioactivity potential (Almany and Seliktar, 2005). PEG hydrogels are already widely used in the world of biomedical engineering but continue to have potential through its tuneable and modifiable nature.

1.8 Aims and Objectives

The aim of this thesis was to engineer an *in vitro* model that mimics the *in vivo* bone marrow niche. Hydrogels, used to create a 3D environment for the cells, were engineered to incorporate the ECM protein FN to encourage cellular interactions with the gel. FN was used due to its abundance within the bone marrow niche; also, its various domains allow interactions with cells and other secreted molecules. The gels were investigated to show they could successfully mimic key features of the ECM such as the diffusion of essential molecules. The model was designed to mimic stiffness characteristics of the soft bone marrow, <3 kPa, through tuning the properties of the PEG hydrogels to match the softer marrow tissue and the addition of microbeads which represent the *in vivo* endosteal surface. The stiffer surface of the microbeads was developed for the adherence of MSCs in the model, while the gel would provide a 3D network to encapsulate HSCs.

These surfaces were developed to introduce PEA into the model, this was to allow greater control over the MSC behaviour and phenotype through the introduction of growth factors. Various methods were assessed to find the most effective way to introduce PEA to the microbeads including plasma polymerisation, UV polymerisation and SI-ATRP. Various techniques were used to investigate the success of each method and further to look at the interaction with FN to allow the tethering of growth factors.

NGF and BMP-2 were investigated to assess the maintenance of an MSC phenotype which release cytokines known to be important in the bone marrow niche for the maintenance of a LT HSC population. BMP-2 was used due to the importance of osteogenic cells within the endosteal niche and NGF has been

linked to the perivascular niche. There were 2 models developed initially with a more 2D approach to help assess the system and a final 3D model to be carried forward for HSC culture (Figure 1.12). The 2D model is similar to those used by our group in the past (Sweeten, 2019; Donnelly, 2020) where cells were seeded onto a PEA coated coverslip followed by the introduction of a gel on top. Alternatively, in the final model, maintaining a more 3D environment, cells were seeded onto microcarrier beads which were then encapsulated into the gels.

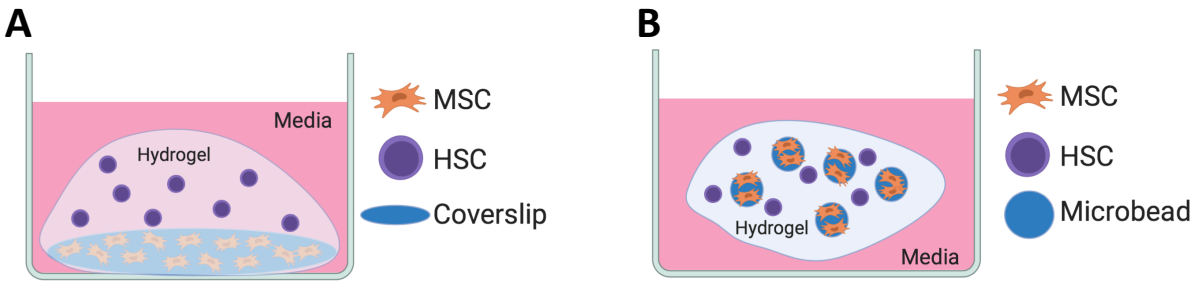

Figure 1.12 Proposed set up for final niche models.
The figure shows the two proposed models for introducing a PEA surface to the niche models. A - shows the use of a PEA coated coverslip onto which MSCs could be seeded with HSCs encapsulated in the PEG hydrogel formed on top. B - shows the use of PEA coated microbeads that can be encapsulated within the gel.

Chapter 2 General Materials and Methods

2.1 Materials

The following materials were used to complete the work outlined in this thesis.

Table 2.1 List of reagents used in gel formation.

Reagent	Product	Provider	Further Information
4-arm PEG-Maleimide	4arm-PEG-MAL-20K-5g	LaysanBio	PEGMAL, 20 kDa
SH-PEG-SH	PSB-613	Creative PEGworks	PEGdiSH, 2 kDa
Fibronectin	663	YoProteins	Human, from plasma
VPM peptide	Custom synthesised	GensScript	GCRDVPMSMRGGDRCG

Table 2.2 List of reagents used in microbead preparation for cell culture.

Reagent	Product	Provider	Further Information
BMP-2	H4791-10	Sigma	Human
NGF	256-GF-100	R&D	Human
Fibronectin	F2006-2	Sigma	Human, from plasma
Microbeads	3772	Corning	Untreated polystyrene microcarriers

Table 2.3 List of cells and cell culture reagents.

Reagent	Product	Provider	Further Information
Pericytes		Patients	Primary cells
MSCs		Patients	Primary cells

Dulbecco's Modified Eagle's Medium	41965-039	Gibco	DMEM
Iscove's Modified Dulbecco's Medium	12440-061	Gibco	IMDM
Penicillin/Streptomycin	15140-122	Gibco	P/S
Foetal Bovine Serum	10500-064	Gibco	FBS
Human Serum	H4522-100	Sigma	HS
Bovine Insulin Transferrin		StemCell Technologies	BIT

Table 2.4 List of kits.

Reagent	Product	Provider	Further Information
DyLight 488 NHS Ester	46402	ThermoFisher	
ELISA kit Reagent Diluent	DY995	R&D	
ELISA kit Substrate	DY999	R&D	
ELISA kit Stop Solution	DY994	R&D	
LIVE/DEAD® kit Calcein-AM	C3099	ThermoFisher	
LIVE/DEAD® kit Ethidium homodimer-1	E1169	ThermoFisher	
BMP2 DuoSet ELISA kit	DY355-05	R&D	
NGF DuoSet ELISA kit	DY256-05	R&D	
Human CXCL12/SDF-1 alpha Quantikine ELISA Kit	DSA00	R&D	
Human Thrombopoietin Quantikine ELISA Kit	DTP00B	R&D	

Table 2.5 List of antibodies and other reagents for immunostaining or in cell western.

Reagent	Product	Provider	Further Information
Phalloidin Rhodamine			1:200
Phalloidin 488			1:200
Cy3 anti mouse	315-165-003	Jackson ImmunoResearch	1:200
Cy3 532 anti rabbit	711-165-152	Jackson ImmunoResearch	1:200
Osteocalcin antibody (anti mouse)	73464	SantaCruz	1:100
Osteopontin antibody (anti mouse)	21742	SantaCruz	1:100
Nestin antibody (anti mouse)	23927	SantaCruz	1:100
Stro1 antibody (anti mouse)	47733	SantaCruz	1:50
SCF antibody (anti rabbit)	20935	Cell Signaling Technologies	1:50
Alcam antbody (anti rabbit)			1:100
Alexa 488 donkey anti mouse			1:400
CellTag 700		LI-COR	1:500
IRDye conjugated goat anti-mouse		LI-COR	1:800
IRDye conjugated goat anti-rabbit		LI-COR	1:800
Odyssey blocking buffer		LI-COR	

Tween20		Sigma	
Formaldehyde		Fisher Scientific	
Bovine serum albumin		Sigma	BSA
Vectashield mounting medium with DAPI		Vectorlabs	

Table 2.6 List of all other reagents and material used.

Reagent	Product	Provider	Further Information
Anhydrous Dimethyl Sulfoxide	276855	Sigma	DMSO
D_2O			
Dulbecco's phosphate buffer solution	14190-094	Gibco	DPBS
Collagenase D	11088858001	Sigma	
Iodoacetamide	I1149-5G	Sigma	IAA
Dialysis tubes	MWCO 10 kDa	ThermoFisher	Mini-A-Lyzer
Optimal cutting temperature compound	361603E	VWR	OCT
Rain-X	80199200	Rain-X	
Tris(2-carboxethyl)phosphine hydrochloride	75259-5G	Sigma	TCEP
Trypan blue	T8154	Sigma	
Trypsin-EDTA	T4049-100ML	Sigma	0.25%
Urea	U5378	Sigma	
Hexane		Sigma	anhydrous

α-Bromoisobutyryl bromide		Sigma	BIBB
Pyridine		Sigma	Py anhydrous
Chloroform			
Copper(I) Bromide		Sigma	CuBr
Tris (2-pyridylmethyl) amine		Sigma	TPMA
Sodium BiSulfite			NaHSO3
Toluene			
Ethyl Acrylate Monomer		Sigma	EA
Benzoin		Sigma	
Benzophenone		Sigma	BPO

2.2 Methods

The following section outlines some of the general methods used throughout the thesis. Methods which are more specialised to particular chapters are found within the chapter methods (Sections 3.2, 4.2 and 5.2).

2.2.1 Cell Culture

Culture conditions

MSCs were isolated from patient bone marrow samples within our lab and selected to be Stro1+. Cells were used at a maximum of passage 3 for all experiments discussed in this work. Cells were grown to confluency, within a T75 tissue culture flask, in DMEM with 10% FBS, 2% antibiotics (streptomycin and penicillin), 1% sodium pyruvate and 1% non-essential amino acids (100x concentrated). For experimental work once seeded in hydrogels or on coverslips cells were in DMEM with 2% human serum 2% antibiotics (streptomycin and

penicillin), 1% sodium pyruvate and 1% non-essential amino acids (100x concentrated).

Pericytes were adipose derived and supplied in cryovials from the University of Edinburgh. Cells were used at passage 4 for cell viability experiments. Cells were cultured in DMEM with 10% FBS, 2% antibiotics (streptomycin and penicillin), 1% sodium pyruvate and 1% non essential amino acids (100x concentrated).

Bone marrow HSCs were obtained from CalTag MedSystems in cryovials. Cells were used before passage 3 for viability experiments within the model. Cells were cultured in IMDM+BIT media with the addition of a cytokine mix containing SCF (10 ng/mL), TPO (5 ng/mL) and Flt3 (10 g/mL).

Cell Seeding

Specific seeding densities vary and are stated for individual experiments throughout the thesis. For experiments seeding cells (MSCs or Pericytes) directly into gels the cells were introduced to the solution before mixing with crosslinker to allow encapsulation of cells during gelation. When working in 2D MSCs were seeded and left to attach overnight before the introduction of a gel over the top. For experiments including the microcarrier beads cells were placed in an Eppendorf tube with the beads and allowed time to attach, mixing every 15 minutes to prevent the clumping of beads for 1 hour. This bead/cell mixture was then added to the gels as mentioned above before the addition of crosslinker allowing encapsulation at the point of gelation.

2.2.2 Cell Staining

Viability assays

To carry out viability tests cells were seeded at various densities in differing culture conditions which are stated throughout the results.

To test viability of the cells in different culture conditions a LIVE/DEAD® kit was used with calcein-AM and ethidium homodimer-1 stains to show live and dead cells respectively. All media was removed from the culture with care taken not

to aspirate any hydrogels where cells were encapsulated within hydrogels. Samples were washed twice with PBS to ensure media was completely removed. A solution with 4 μM ethidium homodimer-1 and 2 μM calcein AM was made up with PBS. The solution was added to each of the samples ensuring full coverage, the samples were then incubated at 37 °C for 15 minutes. After incubation the staining solution was removed, and samples washed twice with PBS. Samples were then left in PBS to prevent drying during imaging which was done immediately after staining.

Imaging was carried out using a ZEISS AxioObserver Z.1 with a 10X objective using DsRed (Red) channel for dead cells and GFP (Green) channel for live. The resulting images were then analysed using ImageJ software to count the live and dead cells allowing the calculation of the viable percentage of cells in each. For each image each channel was filtered using the gaussian blur filter with the sigma ball radius set at two followed by counting object through the find maxima process, those on edges were excluded from all counts. The viability was then calculated as a percentage of total cell number (Equation 1).

Equation 1 Calculation for the viability (%)

$$\boldsymbol{Viability}\ (\%) = \left(\frac{\boldsymbol{Live_{cells}}}{\boldsymbol{Cell\ Number_{Total}}}\right) * \mathbf{100}$$

Immunostaining

Immunostaining was carried out in MCSs after three weeks culture in the final 3D model. Before staining at the end of 3 weeks culture cells were fixed in a formaldehyde solution (10 mL formaldehyde + 90 mL PBS + 2 g sucrose) for 15 minutes.

Before staining all gels were transferred to a fresh 48 well plate removing the surrounding media. Primary antibody was added at the appropriate dilution (following protocol) and incubated overnight at 4 °C protected from the light. The primary antibody was then removed and samples washed 3 times for 5 minutes in wash buffer (PBS with 0.5% Tween20) on a plate shaker. After the final wash buffer was removed the secondary antibody was added along with phalloidin, again diluted according to protocol, the plate was then incubated at

37 °C for 1 hour protected from the light. After incubation washing was repeated. Samples were then transferred to glass bottom petri dishes and coated with VECTASHIELD® mounting medium with DAPI and wrapped in foil to protect from light until imaging.

Imaging was performed on a spinning disc confocal microscope. Z stacks were gathered to image the microbeads embedded within the hydrogels. These were then analysed using ImageJ software by quantifying the fluorescence for the marker of interest normalised to DAPI nuclear stain.

In Cell Western

In cell western (ICW) was used to analyse cells in the 2D set up. Before staining at the end of 3 weeks culture cells were fixed in a formaldehyde fixative solution (10 mL formaldehyde + 90 mL PBS + 2 g sucrose) for 15 minutes. Cells were then permeabilised in permeabilising buffer (10.3 g sucrose + 0.292 g NaCl + 0.006 g $MgCl_2$ + 0.476 g Hepes + 100 mL PBS at pH 7.2 + 0.5 mL Triton X-100) for 4 minutes at 4 °C. Perm buffer was then removed and to block further permeabilising a solution of PBS with 1% milk protein was added and left to block on a shaker for 1 and a half hours.

After cells were fixed and permeabilised primary antibody for the marker of interest was added and incubated overnight at room temperature. Primary antibody was removed after incubation and plate washed 5 times with wash buffer for 5 mins on a plate shaker. After removal of the final wash buffer the secondary antibody solution with CellTag700 was added and incubated for 1 hour on a plate shaker protected from the light. After incubation and plate washed 5 time with wash buffer for 5 min on a plate shaker. After removal of the final wash buffer plates were stored at 4 °C protected from the light and imaged once completely dry. Samples were then scanned using a LI-COR Odyssey Sa scanner in the 800 nm and 700 nm channels with measurements taken as fluorescent units. The final readings were normalised using CellTag700 control readings.

2.2.3 Surface Modifications

Various surface modifications were used to incorporate PEA surfaces into the models. Methods to analyse these surfaces are described in Chapter 4.

Spin coating

2D experiments were carried out on 12 mm glass coverslips coated in PEA using a spin coating method. First glass coverslips were cleaned by placing in 100% ethanol and sonicating for 30 minutes, ethanol was drained, and then the coverslips were rinsed with more ethanol to ensure the removal of any dirt. Once complete, coverslips were transferred to a glass petri dish and placed in the oven until fully dried. Coverslips were then prepared for coating.

Bulk polymers PEA and poly (methyl)acrylate (PMA) were previously prepared, within our lab, from monomer solutions via radical polymerisation with 1% benzoin photoinitiator. These bulk polymers were dissolved in toluene to form solutions that could be used for coating at 4% w/v for PEA and 6% w/v for PMA. Coverslips could then be placed on the spin coater (Brewer science, USA), held in place by a vacuum, and 100 μl of polymer solution added to the centre. Coating took place at 3000 rpm over 30 seconds with an acceleration of 3000 rpm s^{-1}. Once coated excess toluene was removed by placing in a vacuum oven for 2 hours at 60 °C. Before use in cell culture coverslips were sterilised under UV for 30 minutes.

Spin coating was not an option for coating the polystyrene microbeads for the 3D model but was used for coating coverslips in a layer of polystyrene in order to assess other coating techniques success on polystyrene. The process outlined above was followed using a solution of polystyrene in toluene.

Plasma Polymerisation

For 3D cell work polystyrene microbeads were coated in PEA through plasma polymerisation. Microbeads were weighed and placed into a glass petri dish ensuring that they could be spread in a single layer within the dish. This was then placed into the plasma chamber (Figure 2.1) and underwent an air plasma

cycle for 5 minutes. The monomer vessel was then attached at the inlet and monomer plasma polymerisation carried out for 15 minutes at a power of 50 W and pressure maintained between 0.2 – 0.25 mbar.

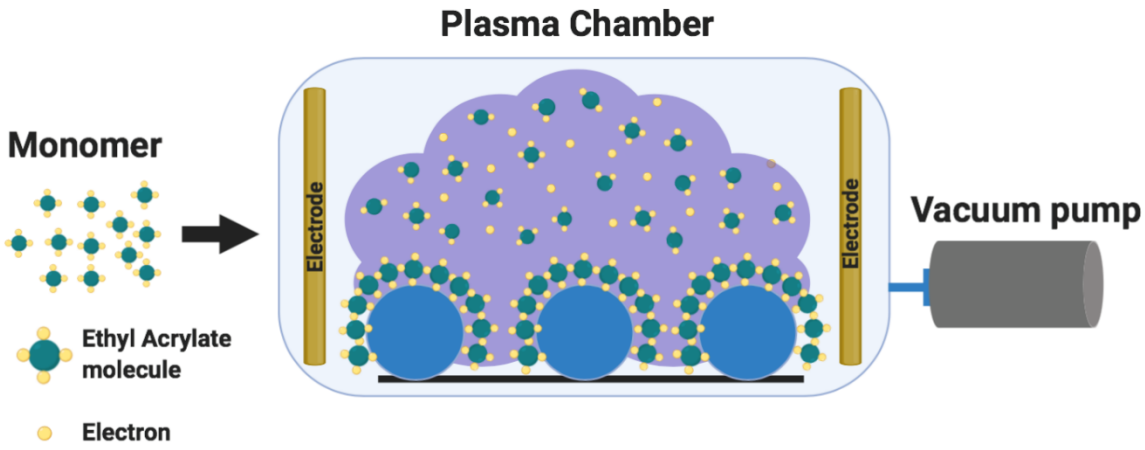

Figure 2.1 Diagram of the basic components of a plasma chamber.
The figure illustrates the basic components of the chamber including the vacuum pump outlet and monomer inlet. The plasma is represented as a purple cloud and is initiated by copper electrode which are situated on the outside of the chamber.

After coating and the chamber was evacuated of any excess monomer the microbeads were removed from the chamber. Before any cell culture beads were sterilised under UV for 30 minutes.

Fibronectin and growth factor adsorption

Coverslips coated in polymer were placed on parafilm within a cell culture hood to maintain sterility. FN, from human plasma, was adsorbed in solution during a 1 hour incubation at room temperature at a concentration of 20 μg/mL. Excess solution was removed, and coverslips were washed twice with PBS. Growth factors, BMP-2 and neural growth factor (NGF), were then co-adsorbed for 2 hours at room temperature each at a concentration of 25 ng/mL. This was followed by 2 washes with PBS, coverslips were then transferred to a 24 well plate ready for use covered in PBS.

Microbeads coated in PEA were placed in an Eppendorf for adsorption of FN and growth factors using a similar protocol as above. Timings and concentrations were kept consistent with those used to coat coverslips though for removal of solutions and washing the Eppendorf was spun down and liquid carefully

removed through pipetting. One additional wash step was introduced to ensure removal of FN and growth factor solutions. Once treated microbeads were stored in PBS until use.

UV Polymerisation

Polystyrene pellets were used in place of microbeads, for ease of handling and characterising, to investigate the success of UV polymerisation on a polystyrene surface. Glass coverslips coated in polystyrene via spin coating were also coated for certain analysis techniques.

Pellets were placed into glass test tubes and 10 % benzophenone (BPO) in ethanol was added to cover the samples. Coverslips were placed in a glass petri dish and BPO solution added as a droplet onto the surface. The samples were then placed in a UV box and irradiated for 20 minutes with UV light. After this any excess BPO solution was removed from the samples and they were washed twice in ethanol. The samples were then covered in a 5, 10 or 20% monomer solution produced from ethyl acrylate monomer and ethanol. Samples were returned to the UV box and irradiated for 30 minutes with UV light. Excess monomer solution was then removed, and samples washed twice with ethanol. Samples vacuum dried at 60 °C for 2 days to ensure removal of all monomer. Samples were then ready to be analysed. Due to the danger of working with monomer solutions all work was carried out in a fume hood with the appropriate personal protective equipment.

Surface Initiated – Atomic Transfer Radical Polymerisation

SI-ATRP was carried out in two stages: bromination (initiator immobilisation) and polymerisation. Before beginning the polystyrene pellets were cleaned by placing in 100% ethanol and sonicating for 5 minutes, ethanol was drained, and then the pellets were rinsed with 70% ethanol to ensure the removal of any dirt. Once completed, pellets were transferred to a glass petri dish and placed in the oven until fully dried. Each process was carried out in separate reaction vessels like that shown in Figure 2.2. Polystyrene pellets were used in place of microbeads, for ease of handling and characterising, to investigate the success

of SI-ATRP on a polystyrene surface. Glass coverslips coated in polystyrene via spin coating were also coated for certain analysis techniques.

Figure 2.2 Reaction vessel used during SI-ATRP.
The above experimental set up was used for bromination of samples, reaction is occurring when photo was taken hence the cloudy appearance of the reaction vessel. A similar set up is used for the polymerisation of the samples. The reaction vessel has 3 necks and is clamped to form a vacuum seal, the vessel is connected to a condenser and dropper side arms. Reaction vessels were placed within a glass water bath on a magnetic stirrer bench heater allowing control of temperature and agitation during reaction. A Soxhlet can be seen on the righthand edge of the photo, this is used for washing samples after treatment. This was set up with a boiling vessel and glass boiling beads along with a collection Soxhlet tube and a Teflon sieve.

For bromination the samples were placed in the bottom of the reaction vessel which was then fully sealed and degassed with oxygen free nitrogen gas. The reaction vessel was degassed held under a nitrogen atmosphere through the reaction. Anhydrous hexane and α-Bromoisobutyryl bromide (BIBB) were added to one of the side arms and degassed before being added to reaction vessel to

cover the samples. Pyridine was then added to the second side arm, degassed and added dropwise into the reaction vessel. The final ratio of reactants was 10:1:0.4 hexane: BIBB: pyridine. The reaction temperature was maintained at 0 °C in an ice bath for 2 hours. After this point the reaction was left at room temperature for 6 or 24 hours, 2 time points were used to asses effectiveness of each, the nitrogen flow was maintained throughout the entire reaction. Once finished the samples were removed from the reaction vessel and washed with a deionised water and methanol solution 2:1 in a Soxhlet for at least 72 hours before vacuum drying.

A second reaction vessel was set up for the polymerisation step with Copper (I) Bromide (CuBr) and Tris(2-pyridylmethyl)amine (TPMA) placed at the bottom of the reaction vessel. The brominated samples were then transferred into the reaction vessel. The vessel was fully sealed and degassed producing a nitrogen atmosphere as in the previous step again this was maintained throughout the reaction. Ethyl acrylate and methanol were then added to the side arm after degassing this solution was then added to the reaction vessel submerging the samples. An ascorbic acid solution in methanol was then introduced dropwise over a period of at least 1 and up to 4 hours. The final ratio for reactants was 96:0.005:1:0.4 for EA: CuBr: TPMA: AsAc. After 4 hours the polymerisation was stopped through flooding the reaction vessel with oxygen. Samples were then washed following the same procedure described for bromination.

2.2.4 Hydrogel formation

All PEG hydrogels were formed using the Michael-type addition reaction at physiological temperature and pH unless otherwise stated. The basic process of gelation is shown in Figure 2.3 for gels that do not contain FN the first 3 steps are not required and hydrogels were formed by simply mixing a solution of 4-arm PEGMAL with a crosslinker solution. FN could be incorporated into the gels through the process of PEGylation described in the next section; fibronectin PEGylation. The crosslinker was always added last at a molar ration of 1:1 between maleimide : thiol to achieve full crosslinking. The crosslinker used was either non degradable PEG dithiol (PEGSH) or a custom protease degradable peptide chain, GCRDVPMSMRGGDRCG (VPM) with cysteine groups at either end. Cells and other additives such as growth factors could be mixed with the protein

solution to be encapsulated within the gel during gelation. Gelation occurs instantly and gels were incubated for 30 minutes at 37 °C to ensure gelation was complete. The final volume of the hydrogels unless otherwise stated were 50 μL.

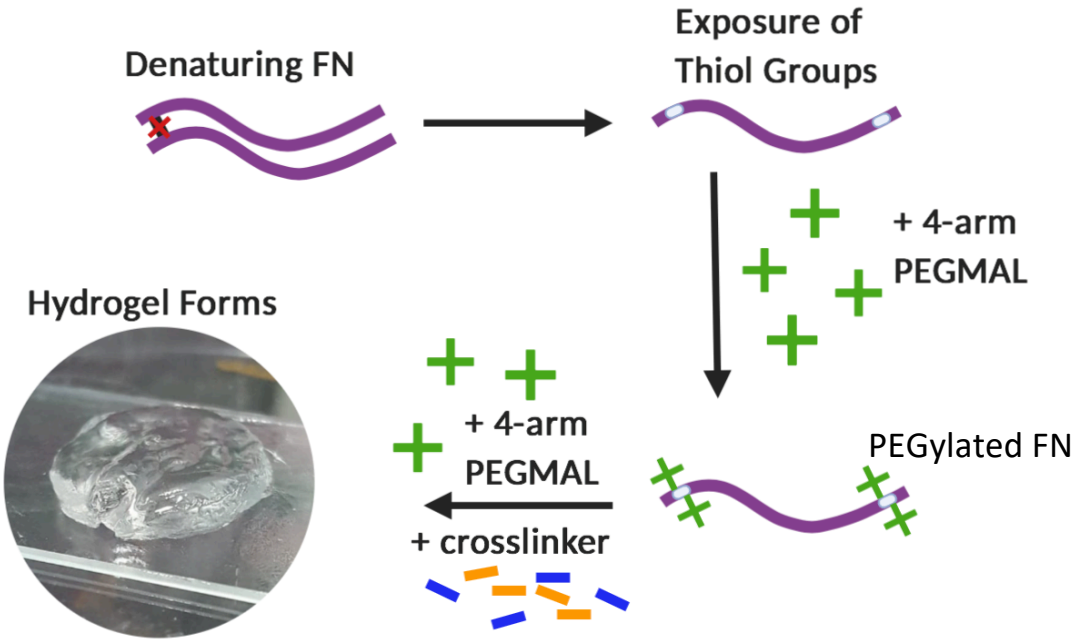

Figure 2.3 Schematic diagram of the process of gel formation.
The figure shows the basic steps to gel formation including the PEGylation of FN and showing a final gel formed through this method. The crosslinker added could be PEG dithiol, VPM or a mixture for the two.

Fibronectin PEGylation

Fibronectin was incorporated into the hydrogels through the process of PEGylation, binding 4-arm PEG-Maleimide molecules onto the FN. This process was created by our group through modification of a procedure used by Seliktar's group (Almany and Seliktar, 2005; Trujillo *et al.*, 2019). Initially FN was denatured incubating for 15 minutes at room temperature in a denaturing buffer with 8 M urea, 5 mM TCEP and PBS at a pH of 7.4. 4-arm PEGMAL was then added to the denatured FN solution at a molar ration of 4:1 (PEGMAL : FN) and incubated at room temperature for 30 minutes. This reaction was stopped by increasing the pH slightly to pH 8.5 with 1 M NaOH. Any unreacted cysteines were then blocked by alkylation, 14 mM of iodoacetamide was added to the mixture and incubated for 2 hours at room temperature. After alkylation the solution was dialysed against PBS for 1 hour at room temperature. Nine volumes

of cold 100% ethanol was added to the protein solution, mixed and incubated at -20 °C overnight. After incubation the solution was centrifuged at 15000 g for 15 minutes at 4 °C. The supernatant was carefully discarded and the pellet washed with cold 90% ethanol before centrifuging for 5 minutes at 15000 g and 4 °C. Supernatant was again discarded and the pellets dried. The resulting pellets were dissolved in 8 M urea producing a protein concentration of 2.5 mg/mL. This was again dialysed against PBS for 1 hour at room temperature. The final dialysed protein was then placed into aliquots and stored at -20 °C until use.

Hydrogel Formulations

The formulation of the gels was varied for different experiments to assess the effects on gel properties and cell viability. The various formulations are outlined in the tables below (Table 2.7 and Table 2.8). Unless stated these are the formulations used to form all the hydrogels used for this work.

Table 2.7 Amount of PEGMAL in hydrogels used.

FNPEG hydrogels	3% FNPEG	5% FNPEG	10% FNPEG
PEGylated FN (mg/mL)	1	1	1
PEGMAL (mg/mL)	30	50	100
PEG only hydrogels	3% PEG	5% PEG	10% PEG
PEGylated FN (mg/mL)	-	-	-
PEGMAL (mg/mL)	30	50	100

Table 2.8 Amount of crosslinker used in degradable vs non degradable hydrogels.

Hydrogels	Non degradable	Degradable
PEGSH (mg/mL)	8.2	6.1

VPM (mg/mL)	0	2.1

2.2.5 Growth factor tagging

Growth factors (NGF, Flt3, TPO, SCF and CXCL12) were fluorescently tagged with an amino reactive dye (DyLight 488 NHS Ester) following the protocol provided. In summary, the growth factor underwent a buffer exchange against 0.05 M sodium borate at pH 8.5 using dialysis membrane tubes (Mini-A-Lyzer, COMW 10kDa, ThermoFisher) for 2 hours at room temperature. The dye was then added to the solution, calculated according to the protocol, and left to react for 1 hour at room temperature protected from the light. Any non-reacted dye was removed through dialysis against PBS for 3 hours exchanging the PBS after every hour. The final product was aliquoted and stored at -20°C until required. These could then be used to investigate growth factor release and diffusion.

2.2.6 Statistical analysis

All statistical analysis mentioned in this work was carried out using GraphPad Prism 6 software. Differences seen amongst data sets are represented by p-values which are represented by Asterix meaning the following; * $p < 0.05$, ** $p < 0.01$, *** $p < 0.005$ and **** $p < 0.001$. Graphs produced to represent data are produce from 3 repeats and show the mean +/- standard deviation (SD) unless stated otherwise. The test used to analyse each data set is stated along with the results due to variations in sample number and the normal distribution of data. D'Agostino-Pearson Normality test was used to determine the distribution of the data and the appropriate test chosen depending on the result. For normally distributed data ANOVA with Tukey multiple comparison test or T-test were used to compare data sets. Kruskal-Wallis test was used when the sample number was too low to determine normal distribution or data did not fit normal distribution.

Chapter 3 Hydrogels

3.1 Introduction

Hydrogels are defined as materials that have both a solid and liquid phase, a gel is formed when the liquid phase is immobilised within a network of fibres (Cacopardo *et al.*, 2019). A technique used to measure the mechanical properties of soft materials such as hydrogels is rheology. Through rheology we are able to measure both the solid and liquid phase of a material and gain information such as stiffness, viscosity and strength (Yan and Pochan, 2010). Rheology can also be used along with nuclear magnetic resonance (NMR) to assess the gelation kinetics (Figure 3.1) of hydrogels. NMR measures the molecular assembly while rheology can measure the structural assembly that occurs when the fibres that are produced entangle and immobilise water forming a hydrogel (Raghavan *et al.*, 1996; Escuder, LLusar and Miravet, 2006).

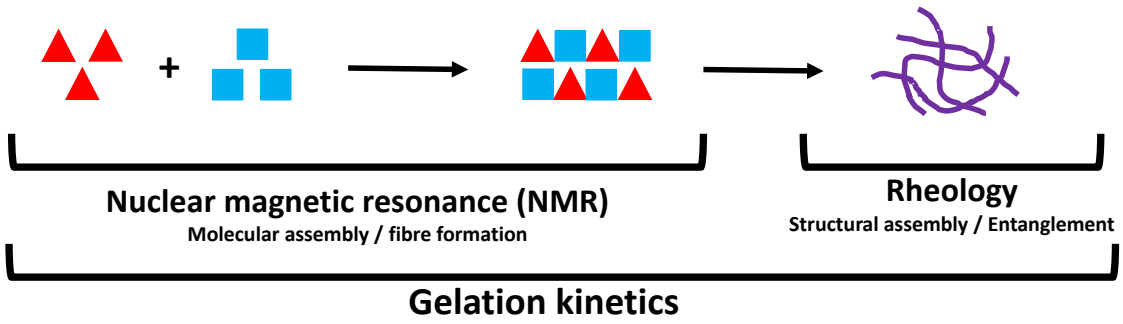

Figure 3.1. Methods to determine gelation kinetics.
This figure is a diagrammatical representation for how Rheology and NMR can be used to measure the stages of gelation.

Rheology is a technique which can be used to measure the storage modulus (G′) and the loss modulus (G″) which represent the solid and liquid phases of a material respectively. These can be measured under a controlled strain and/or frequency applied through a geometry which either sits in contact with the surface or within the gel. As the geometry oscillates applying a set strain and/or frequency the gel deforms and recovers, information is gathered on how the gel reacts to the oscillations allowing the rheometer to determine values for G′ and G″ along with other properties. There are many different geometries including

parallel plates and vane & cup, which have been used to gather the results discussed later in this chapter, among others. Each geometry comes with different limitations and advantages therefore the specific geometry used can be chosen depending on the material that is to be measured.

Parallel plate geometry can be used for measuring the properties of hydrogels, this method involves a stationary lower plate and an adjustable upper plate that can vary in size, which rotates according to the test being performed (Figure 3.2). Advantages of parallel plate geometries include the variability of the upper plate, volume of gel required is lower than using vane & cup. This can influence the cost of an experiment and the use of sandblasted plates to avoid slipping, which can occur when the plate moves without moving the gel (Mezger, 2006). Despite this, slipping can still be a disadvantage to the parallel plate geometry if the material itself is particularly slippery. Another disadvantage is the specific size and formation of the material. The ideal sample fills the gap between the plates without spilling out or not meeting the sides, which may cause some inaccuracies, and is flat on the top for contact with the upper plate. Lastly, transferring the sample to the lower plate can be problematic depending on the sample being measured.

Vane & cup geometry has also been used in previous studies to measure the properties of hydrogels (Draper *et al.*, 2015; Akhtar *et al.*, 2018). This involves a stationary cup that can be inserted into the base of the rheometer with a vane that can be lowered into this cup before rotating according to the test required (Figure 3.2). By lowering the vane into the cup, it is immersed in the sample removing the need for a specific shape and a flat surface to the sample giving this geometry an advantage over the parallel plate. Other advantages include the use of a removable cup in which the sample can be formed therefore allowing the sample to be placed in the rheometer without the need to remove it reducing the chances of disruption and slipping (Mezger, 2006). Again, slipping can still be a problem while using vane & cup and can be further avoided by sanding the inside of the cup to increase roughness. The biggest disadvantage is the volume of material required as the vane has to be fully immersed in order to get an accurate measurement, this is mostly a problem when measuring expensive materials. Choosing the best geometry will be dependent on the

material being measured, in particular looking at if it is easy to produce flat gels within a mould and the expense of the materials used.

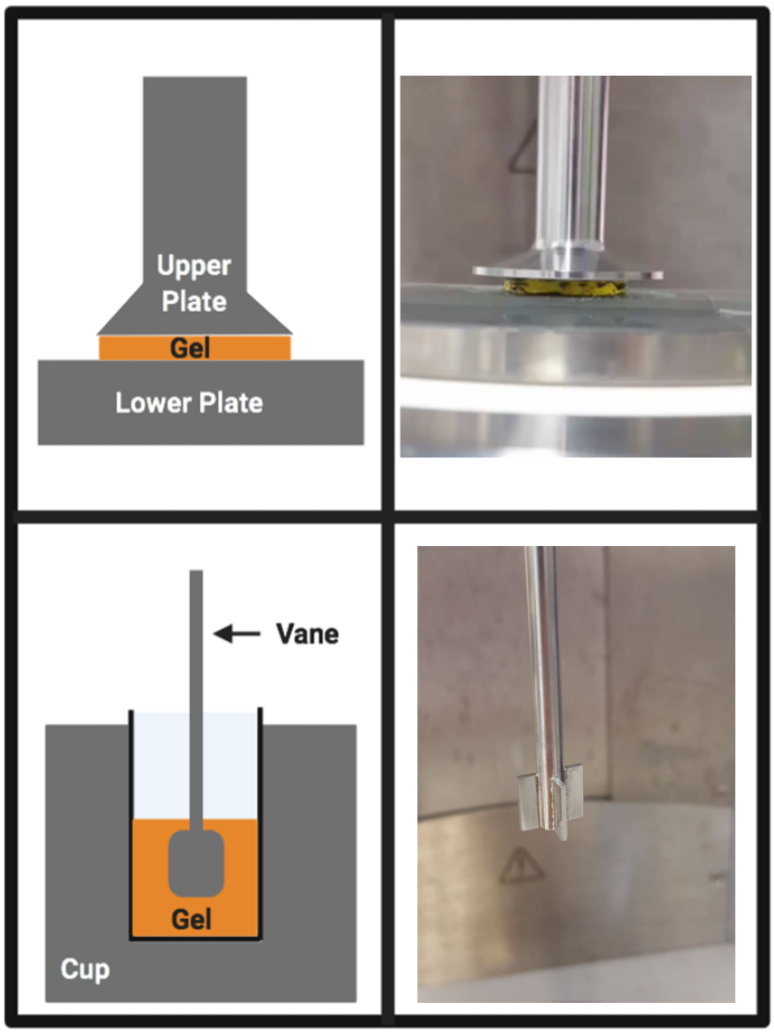

Figure 3.2. Rheology geometries: parallel plate vs vane & cup.
Figure shows a schematic drawing of the parallel plate geometry (top left) and the vane & cup geometry (bottom left) and pictures of the instruments used with parallel plates (top right) and a vane (bottom right).

As previously mentioned, another technique that can be used when looking at the characteristics of hydrogels is nuclear magnetic resonance (NMR). NMR works through applying an external magnetic field which aligns the spin of the nuclei that are in their lower energy state. A radio frequency is applied (Figure 3.3) that is able to shift the nuclei to their higher energy state where the spin is opposite to that of the external magnetic field. The energy gap between the two states corresponds to the frequency and can be used to analyse the molecules

present. There are different nuclei that can be used for NMR analysis the most common being proton or ^{1}H NMR (Zia *et al.*, 2019).

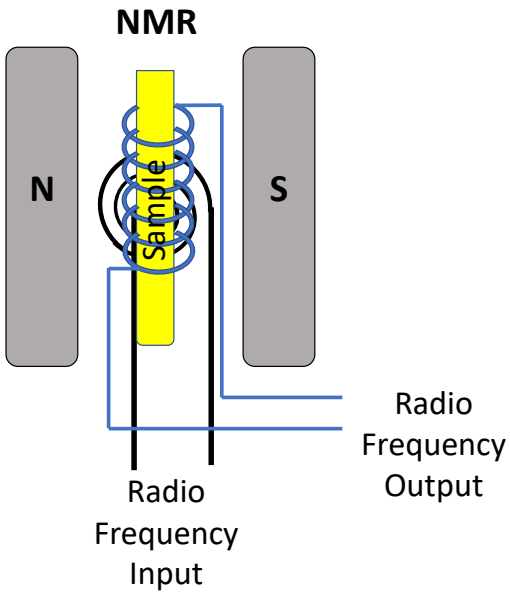

Figure 3.3. Basic set up for nuclear magnetic resonance.
This figure shows a schematic drawing of the basic structure of an NMR machine, N and S represent the magnet defining north and south respectively.

Through NMR the molecular composition of a solution can be quantified. This can be used for determining the purity of a known sample or discovering the content of unknown samples. This can also allow gelation to be observed as larger molecules greater than approximately 25 kDa are invisible to standard NMR (Foster, McElroy and Amero, 2007). Due to this, the gelator peaks seen in NMR reduce in size as the chains forming become too large to detect. By taking measurements over a period of time this method is able to show the ratio of assembled versus unassembled gelator (Hirst *et al.*, 2008). Through comparing this over time the kinetics of network formation are able to be shown (Rhoner et al 2015).

For hydrogels used in cell *in vitro*/ *in vivo* models, it is important to know the mechanical properties of the network as this can have an influence on cell behaviour. The aim of the work in this chapter was to measure the properties of the PEG hydrogel matrix to be used to create the *in vitro* niche model in order

to show tunability helping to understand what cells encapsulated in the system will experience. By using tuneable hydrogels to mimic *in vivo* properties of the bone marrow we can better understand how changes influence the cells within this environment.

3.2 Methods

3.2.1 Nuclear Magnetic Resonance (NMR)

NMR was used to study the formation of PEG hydrogels at a molecular level, this was done for gels formed at pH 4.5 and pH 3.5, gels at pH 7.4 formed instantly and could not be measured. The 1H NMR spectra were recorded using a Bruker Avance III 500 MHz spectrometer with the temperature internally controlled. Samples were run in D_2O (deuterated water) with DCL (deuterium chloride) to reduce the pH and ethanol (2 µL/mL) added as an internal standard. For the kinetic measurements, ethanol was added to 1 mL of each solution, PEG dithiol and PEGMAL in an NMR tube. Each of these solutions were measured alone in order to record a standard measurement prior to mixing (i.e. a time zero measurement). After the standard measurement was obtained, the two solutions were mixed into a new NMR tube and inserted into the spectrometer. Due to the experimental limitations, there was a time delay of around 5 minutes from mixing of the two samples to the first sample acquisition. Spectra were recorded every 5 minutes until change in the gelators' proton peaks were no longer detectable. This took around 5 hours depending on the sample. Examples of the spectra obtained of the proton environments are shown in Figure 3.4.

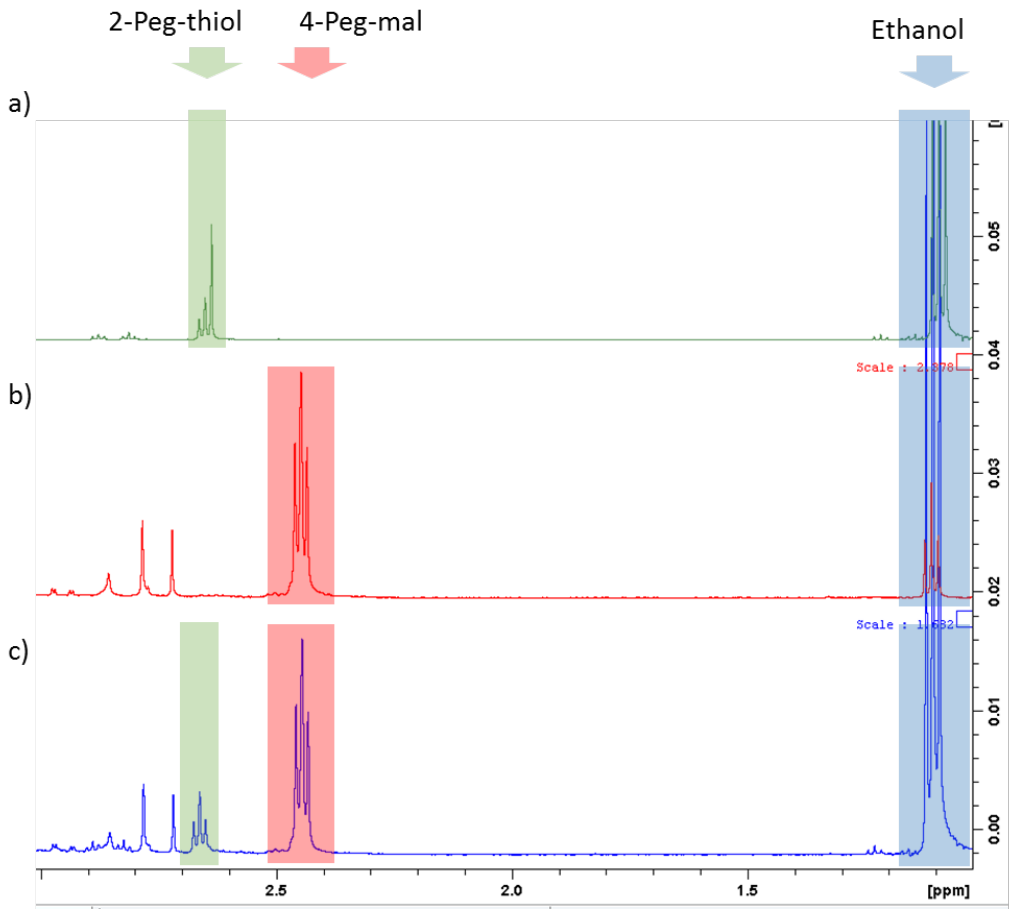

Figure 3.4. Example of a ^{1}H NMR spectra.
Figure shows a ^{1}H NMR spectra recorded of a) PEG dithiol b) PEGMAL and c) both PEG dithiol and PEGMAL. The methyl groups from the ethanol standard against which peaks of PEG dithiol and PEGMAL are integrated are just over 1 ppm. The proton environments labelled PEG dithiol was used to determine the percentage assembly over time.

The proton environments identified for PEG dithiol (highlighted green in Figure 3.4) were used to determine the percentage assembly overtime as the peaks were reduced during gelation. Once there was no more change in the peaks observed this was assumed to be full molecular assembly and the data collected was normalised with respect to this.

3.2.2 Rheology

To form gels for rheology, first a custom cylindrical mould was created using polydimethylsiloxane (PDMS) with an inner diameter of 16 mm and 2 mm thick. Moulds were fixed to a glass slide using vacuum grease producing an airtight seal between the mould and the slide, this prevents the gels solution from leaking during gelation. Hydrochloric acid (HCl) was added to PBS to produce a low pH solution, pH 3.5, slowing the gelation to compare the properties with those

formed at pH 7.4 (unaltered PBS). The pH value was lowered to slow the gelation reaction in order to produce a gel with a flat upper surface, which is advantageous for the parallel plate methodology. Due to difficulty moving the gels from the slide to the rheometer plate, the glass slides were placed on to the rheometer plate for measuring, held in place with adhesive tape, and then the moulds removed once the gel was in place.

Parallel plate measurements were carried out using a 25 mm sandblasted plate with a constant height of 2.8 mm set for each of the samples and a normal force set at 0 N. All the gels analysed through this methodology were 5% PEG (exact composition seen in Table 3.1) with a total volume of 350 µL (before any swelling). For swollen conditions, 200 µL PBS was placed on top of the gels overnight and any excess that was left was removed before measurements were taken. For unswollen measurements, gels were stored in petri dishes that contained water soaked tissue below the slides to prevent any evaporation before measuring. For the time sweep measurements the solution was added to the rheometer as liquid straight after being mixed and left to form a gel while measurements were carried out.

Table 3.1. PEG concentration in 3, 5 and 10% hydrogels.

PEG gel condition	PEGMAL (mg/mL)	PEG dithiol (mg/mL)
3% PEG	23.5	4.8
5% PEG	40	8.2
10% PEG	83	16

For the vane & cup rheology, a cup base was fitted on the rheometer that allowed a Sterilin sample vial to be used and a measuring vane. A volume of 2 mL of gel was required in order to fully immerse the vane. To form these, PEGMAL and PEG dithiol solution were added directly into a Sterilin vial

producing gels instantly. The vial containing the gel was placed directly into the rheometer cup and held in place by blue tac to prevent any movement during the experiment. Gels were produced with different concentrations of PEG; 3%, 5% and 10% in order to assess the effect on gel stiffness.

Rheological measurements were all carried out using the same Anton Parr 301 rheometer. A frequency sweep was carried out at a strain of 10% and a frequency of 1 – 100 rad/s. Strain sweep tests were all performed at an angular frequency of 10 rad/s and a strain of 0.1 – 5000 %. Time sweeps were measured with an angular frequency of 10 rad/s with a strain of 0.5 % taking a reading every 30 seconds. All experiments were performed at 25 °C. Data was analysed using Origin software to produce graphs. Further analysis was used to calculate the Young's modulus using Equation 3.1 where E is the Young's modulus, G^* is the complex modulus and υ is the Poisson's ratio (Lee, Zhang and Ryu, 2018).

$$G^* = \frac{E}{2(1+v)}$$

Equation 3.1 Determining Young's modulus.
The above equation was rearranged in order to calculate a Young's modulus for the gels using rheological data.

In order to calculate the Young's modulus data for the G^* was taken from the linear viscoelastic region of the graph highlighted in Figure 3.5. Poisson's ratio is assumed to be 0.5 for hydrogels (Anseth, Bowman and Brannon-Peppas, 1996). These could then be used to find the Young's modulus for each gel. From the rheology data we can also determine the strength of the gel through its breaking point (Figure 3.5).

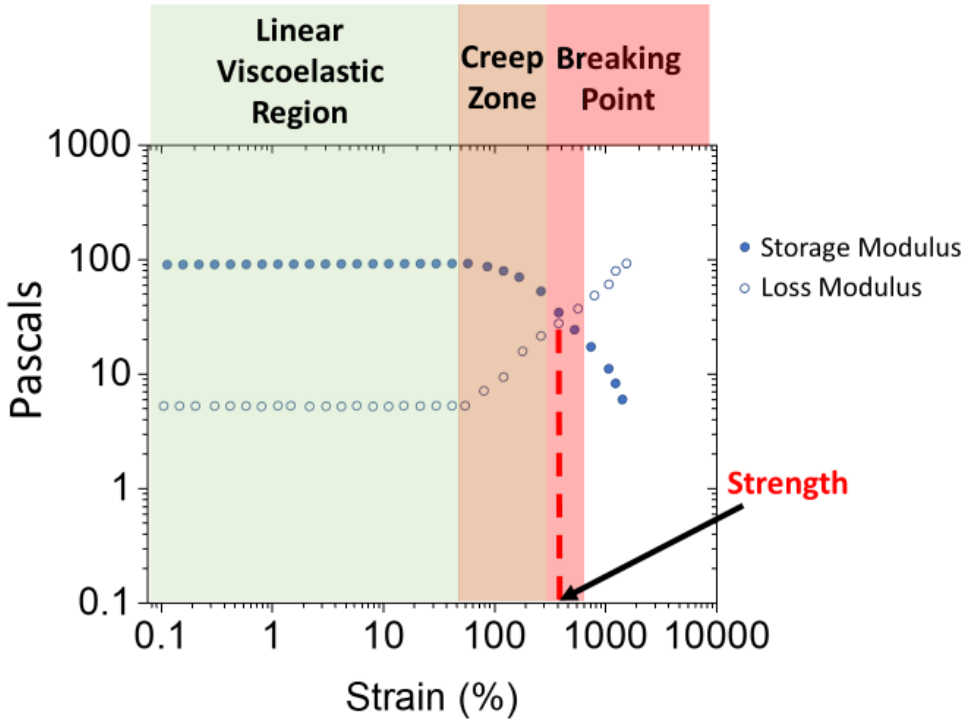

Figure 3.5 Example of a graph produced through rheology.
This figure highlights the different areas seen on a rheology graph with linear viscoelastic region (green), the creep zone (yellow) and the breaking point (red). The breaking point is used to determine the strength of a gel while storage modulus can be used to determine the stiffness of the gels.

3.2.3 Swelling

The swelling of several gel compositions was assessed, these included differing amounts of PEGMAL (3 %, 5 % and 10 % (w/V) Table 3.1) and differing VPM crosslinker content (Table 3.2). Only 5 % PEG gels were included in condition containing VPM.

Table 3.2. VPM : PEG dithiol ratio in hydrogels.

Gel condition	VPM (mg/mL)	PEG dithiol (mg/mL)
0 VPM	0	8.2
0.25 VPM	2.05	6.15
1 VPM	8.2	0

All gels were formed in the end of a 1 mL syringe before being transferred to an Eppendorf tube for weighing. The gels were then swollen for ~24 hours in excess PBS. After swelling PBS was removed and the gels were weighed once again. The gels were then freeze dried to remove any remaining solution overnight for approximately 16 hours before a final weighing. This was then used to compare to the theoretical dry weight which was calculated from stock solution concentration and volume required.

3.2.4 Cell viability

Cell culture is carried out as described in chapter 2 (2.2.1).

To produce the data shown below 3 biological replicates were analysed for each condition with multiple images taken to get an average viability for each sample. This was done through image J and is explained in general methods chapter 2 (2.2.2).

3.3 Results

3.3.1 The effect of frequency on stiffness

In order to determine the parameters of the rheological tests it was important to first ensure that the frequency chosen did not influence the results. This is due to some materials undergoing changes to their properties when different frequencies are applied for example frequency hardening where the G′ increase with increasing frequencies. To do this, a frequency sweep was run, showing no significant change in G′ over a wide range of frequencies (Figure 3.6). Given these results the gels were determined to be frequency independent meaning the properties do not change under different frequencies. A frequency of 10 rad/s was chosen to carry out measurements through strain and time sweeps.

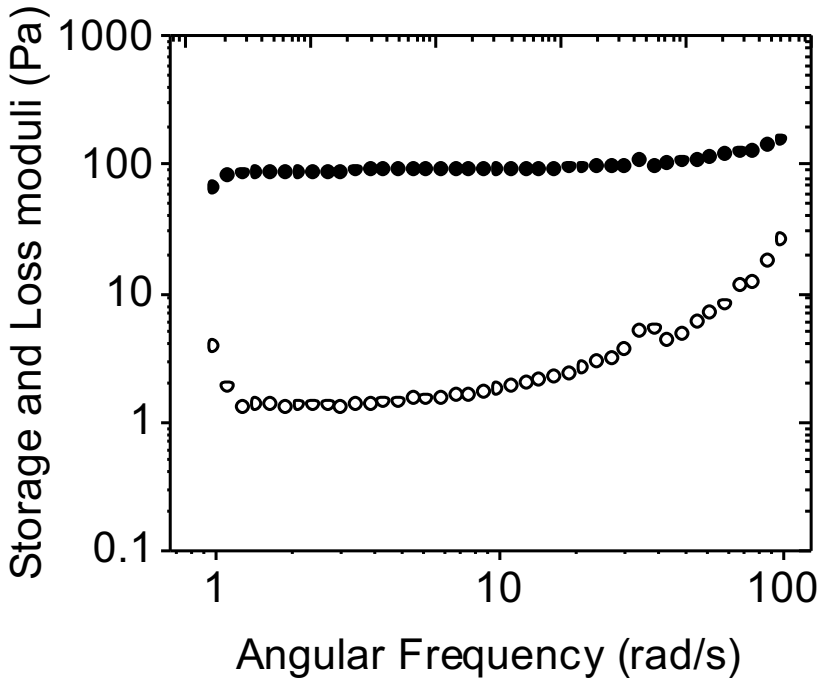

Figure 3.6 Frequency effect on stiffness
This figure shows the G′ (solid) and G″ (hollow) over a range of frequencies at a consistent strain. The G′ stays consistent throughout varying frequencies suggesting that the gel is frequency independent.

3.3.2 The effect of pH on gelation and stiffness

When preparing gels for parallel plate rheology it was difficult to produce the flat upper surface required to get the most accurate readings. This was due to the speed of the Michael-type addition reaction where gel is formed instantly as the solutions are mixed (in cystine free media or PBS) which is good for encapsulating cells. This, as shown in Figure 3.7, produces a gel with a very uneven surface or in some case where the solution didn't mix properly when added the gels were completely misshapen.

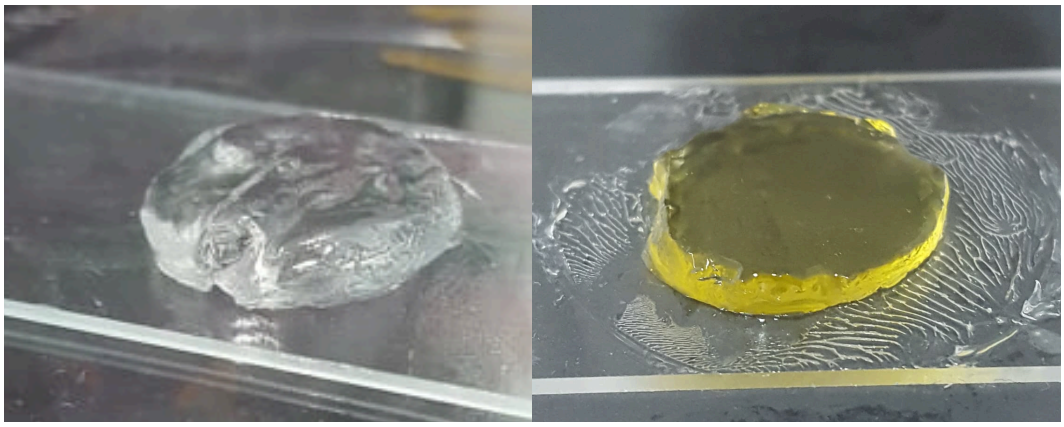

Figure 3.7. PEG gels formed at pH 7.4 vs pH 3.5.
This figure shows the ability to create a flat gel (right) when lowering the pH of the reaction while at higher pH an uneven gel surface is created (left).

In order to overcome this problem, the pH of the gelator solutions were lowered under the assumption this would alter the reaction taking place and allow slower gelation. The ability to slow the reaction through changing the pH allowed the production of gels with a flat surface (Figure 3.7) ideal for using a parallel plate geometry on the rheometer. This was investigated using NMR to see the effect on the molecular assembly of the gels and time sweep rheology to see the effect on structural assembly. These results can be seen in Figure 3.8, the dashed lines were added to highlight correlation between the end of molecular assembly and beginning of structural assembly of the network. It is at the point of full molecular assembly that a network able to immobilise water begins to form creating a hydrogel.

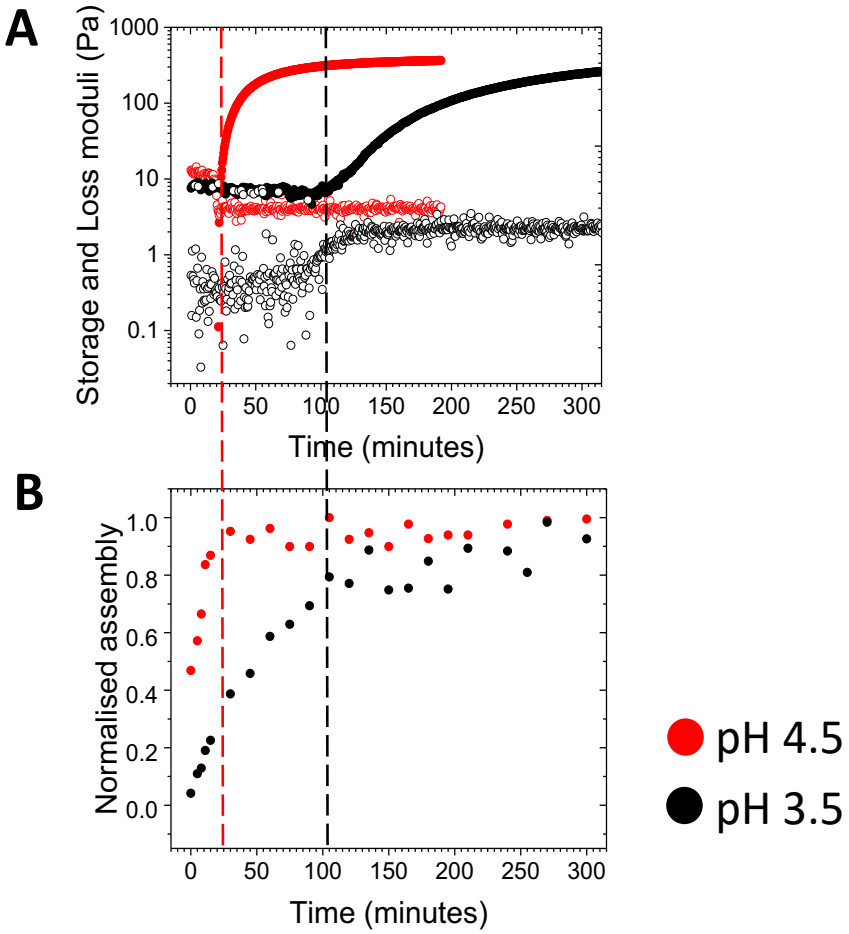

Figure 3.8. Assembly of hydrogels overtime shown through NMR and Rheology. Figure showing the assembly of PEG hydrogels as a function of time through ^{1}H NMR (B) and rheology using a time sweep (A) at pH 3.5 (black) and pH 4.5 (red). For the rheological data the storage modulus is represented by the solid circles while the loss modulus is represented through the hollow circles.

However, after testing it was shown that this slower gelation caused the production of softer gels (Figure 3.9) compared to those produced at pH 7.4. The softer gels, with a Young's modulus ~ 150 Pa, did not represent those used for the final cell model and therefore slowing the reaction could not be used as a method for creating flat gels to carry out rheology.

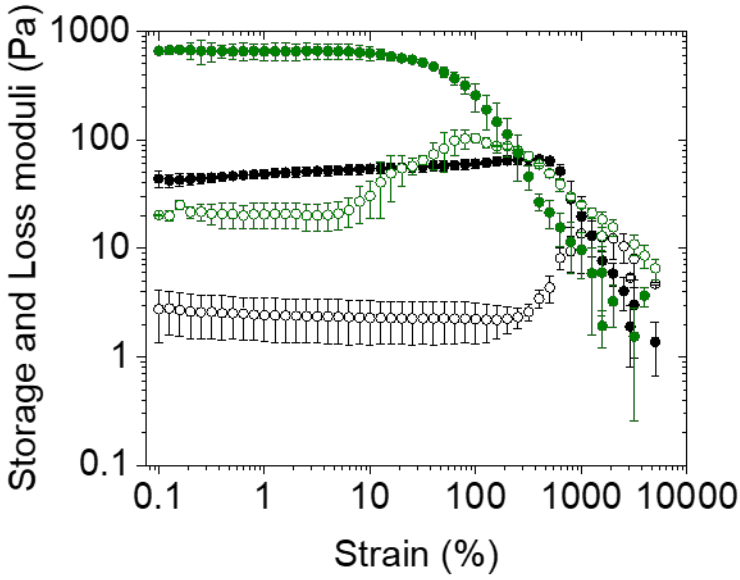

Figure 3.9. Rheology pH 3.5 vs pH 7.4
Figure showing the storage and loss modulus measurements for 5% PEG hydrogels at pH 7.4 (Green) and pH 3.5 (Black) using parallel plate rheology. Showing the mean n=3 +/- SD.

Due to the uneven surface produced by the faster reaction (Figure 3.7) that occurs at pH 7.4 a vane and cup geometry was used for further rheological measurements. As the vane is fully submerged in the gel as measurements are taken this technique is not influenced by the uneven surface. Results for the two different geometries were compared to assess if the uneven surface would have an influence on the stiffness measured, these are shown in Figure 3.10 below.

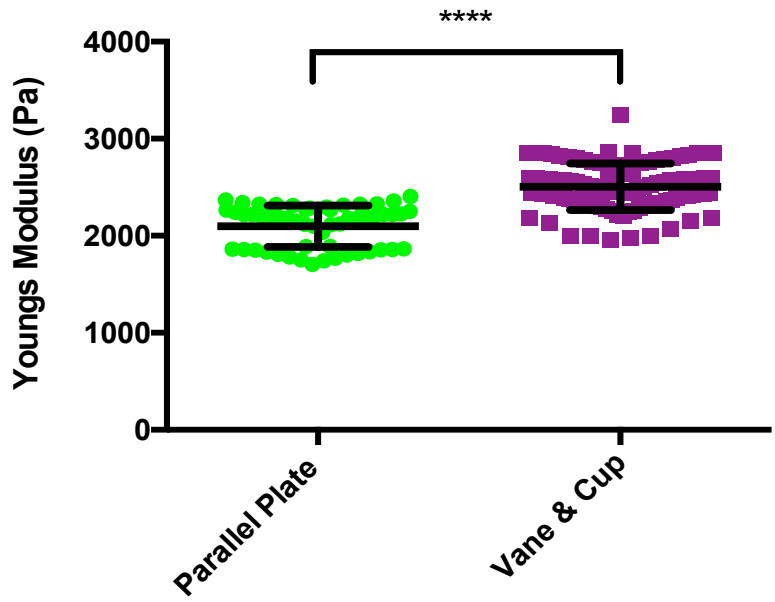

Figure 3.10. Parallel plate vs vane & cup rheology at pH 7.4.
This figure shows that there is a significant difference between these techniques when comparing the same gels **** $p < 0.0001$ using Kruskal-Wallis in prism software. Graph shows mean +/- SD along with individual readings.

A significant difference was seen between the Young's modulus calculated for each technique. The Young's modulus for the vane & cup was significantly higher than that for parallel plates with means of 2505 Pa and 2098 Pa respectively. To get results comparable to those seen in cell culture conditions gels must be produced at pH 7.4 as a change in pH and therefore the rate of reaction significantly reduces the stiffness. The vane & cup technique is thought to be more accurate for these measurements as it cannot be influenced by the uneven surface. Due to these two factors the vane and cup technique was used for all further rheological measurements.

3.3.3 Concentration of PEG effect on stiffness

The concentration of PEG within the gels was altered between 3, 5 and 10% weight/volume (Table 3.1) to assess the effect on gel stiffness. The G′ and G″ of the gels was measured through rheology using a vane & cup geometry showing an increase in the G′ with the increase in PEG concentration along with the small scale of any deviations between repeated gels suggesting a level of reproducibility in the formation of the gels for each condition (Figure 3.11A). The storage modulus measurements, within the viscoelastic region, at a strain of

10% were extracted and plotted against percentage PEG showing a positive linear relationship (Figure 3.11B). This linear relationship shows the tuneability of stiffness in a PEG system and should allow gels to be made at a required stiffness. A significant difference was seen between the Young's modulus of all the gel conditions (Figure 3.11C). With a mean stiffness of 4433Pa, 2505Pa and 934Pa for gels of 10, 5 and 3 % gels respectively.

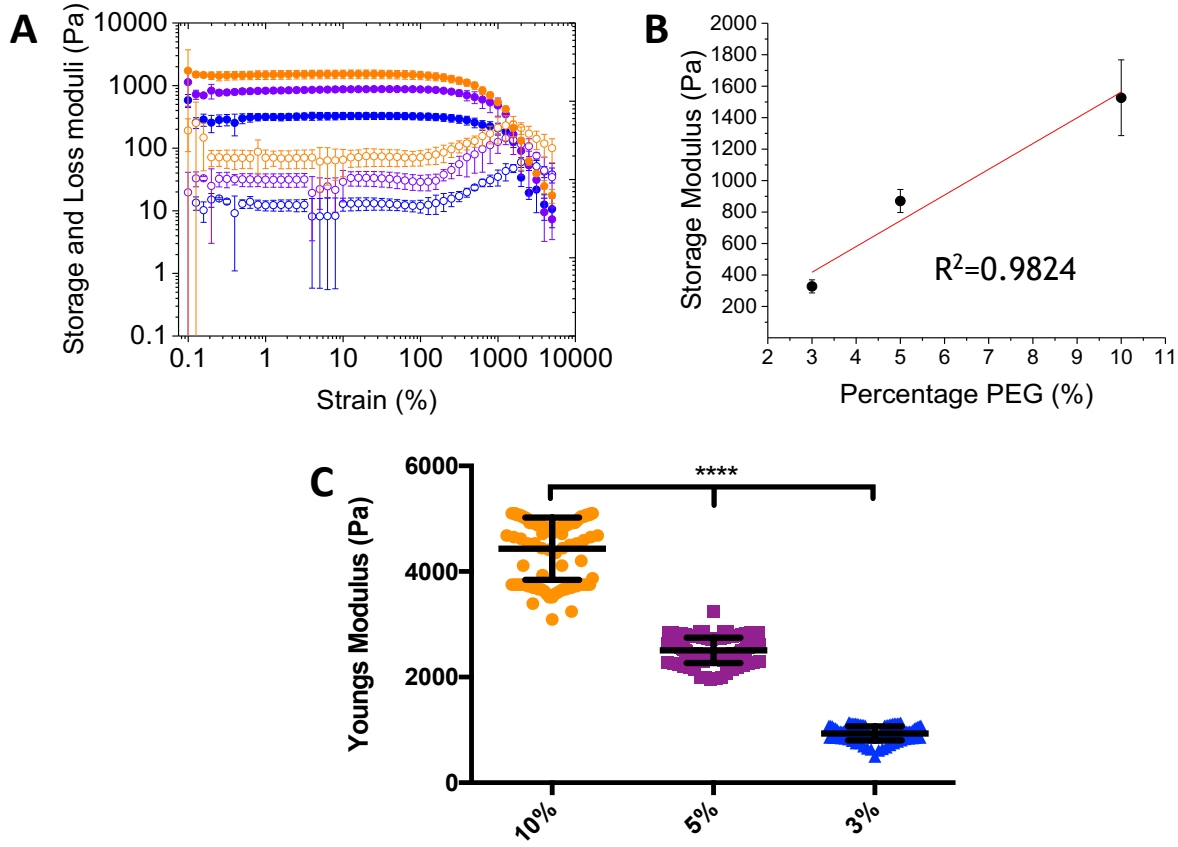

Figure 3.11. The effect of PEG concentration on stiffness.
This figure shows 3% w/v (blue), 5% w/v (purple) and 10% w/v (orange) gels measured through rheology n=3 (A) and the storage modulus of each at 10% strain to highlight the relationship between this and PEG % w/v. The Young's modulus calculated from the rheology data within the viscoelastic region (C) shows a significant different between all gel conditions using a Kruskal-Wallis statistical test in prism software where **** is $p \leq 0.0001$.

3.3.4 Swelling Behaviour

The swelling assay (3.2.3) revealed no significant differences in the gel swelling for varying VPM % (Figure 3.12). This is important to show that the addition of the degradable crosslinker (VPM) is not changing the ability for the gel to hold water. This was not the case when comparing the amount of PEG in the gels where a significant difference was seen between the 3% PEG gels and the 10%

PEG gels with swelling varying from ~50% to ~150% relative to initial gel mass. The 5% PEG gels showed no significant differences between the other 2 conditions (Figure 3.12). This shows that the volume of swelling is varied by the amount of PEG in the gel.

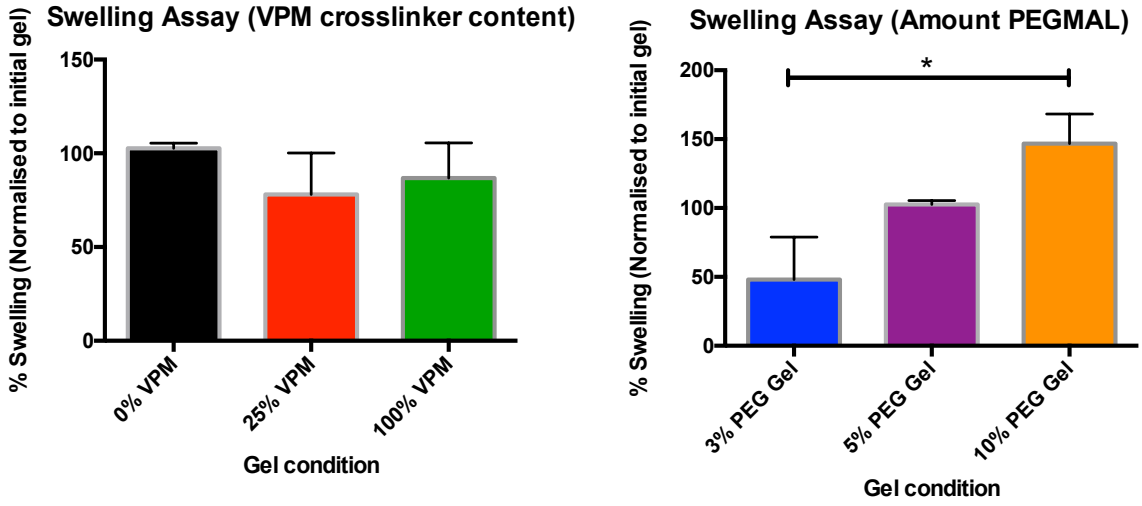

Figure 3.12. Swelling behaviour of gels.
Figure shows the percentage of swelling at ~24 hours with differing VPM crosslinker content and the percentage swelling with various PEG concentrations. Both are normalised to the initial gel mass with n=3 +/- SD. *p ≤ 0.05 Kruskal Wallis multiple comparison test carried out on all data within graphs.

No significant difference was found between any of the calculated theoretical dry mass and the experimental dry mass for any of the gel conditions. Though not significantly different the experimental weight was higher in every case (Table 3.3) than the theoretical, this is thought to be due to some inefficiency in the drying.

Table 3.3. Experimental vs theoretical dry mass of gels with varying PEG volumes.

Gel Condition	Experimental Dry Mass (mg)	Theoretical Dry Mass (mg)
3% PEG	1.60 ± 0.1	1.42
5% PEG	2.57 ± 0.29	2.41
10% PEG	5.03 ± 0.23	4.95

If used as a model where cells are encapsulated into the gels during gelation, they will experience any changes in the properties that occur over the gelation period. This includes any changes in stiffness that occur during swelling of the gels after gelation. The differences in swollen and unswollen gels were also assessed by rheology using parallel plates. These results are shown in Figure 3.13. Effect of swelling on the stiffness of gels. Here, we saw that for tests carried out at pH 3.5 a change in the storage modulus was observed between the swollen gels and the unswollen gels increasing as the gels are swollen. However, using gels at pH 7.4 the storage modulus was consistent for both swollen and unswollen conditions.

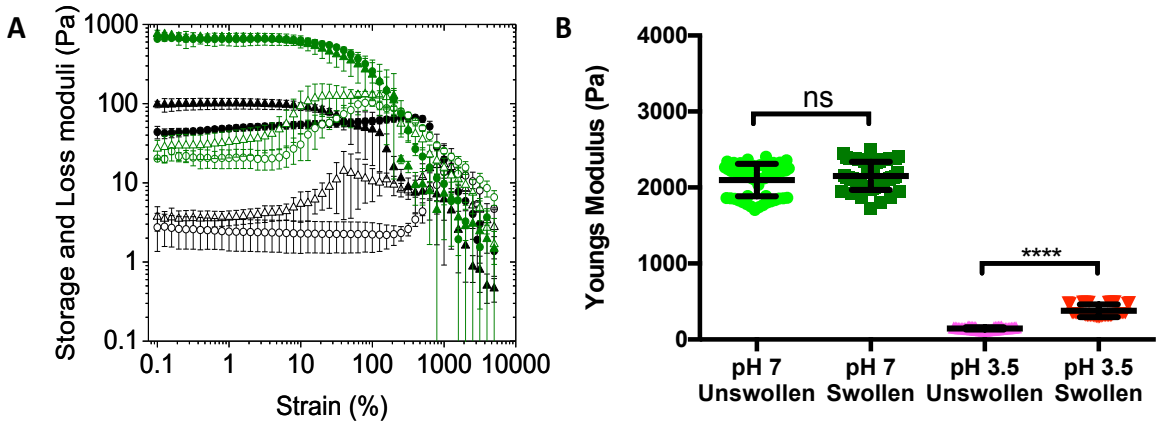

Figure 3.13. Effect of swelling on the stiffness of gels.
This figure shows the rheology measurements for swollen and unswollen gels at pH 7.4 and pH 3.5 n=3 +/- SD (A) and the Young's modulus (B) calculated from measurements within the viscoelastic region showing mean +/- SD ****p < 0.0001 using Kruskal-Wallis test.

3.3.5 Viability of Cells in Gels

With the final goal for the gels to be used for an *in vitro* bone marrow niche model, cells were introduced to the gels under various conditions. Two cell types were used: pericytes and MSCs. Pericytes were investigated here to determine if they would be a more viable cell type for this model, as precursor cells for MSCs they would have the same capabilities within the model as MSCs. Pericytes were seeded in gels with and without the ECM protein FN to investigate if the presence of the protein influences cell viability (Figure 3.14). Once quantified it was found that due to the high variability no significant

difference was seen in the viability between gels with and without FN, though it is notable that while some gels without FN had good cells numbers there were some with no viable cells at all. The average viability for the 2 conditions was also notably different with the presence of FN showing an average of 65% while with no FN the average was 46%.

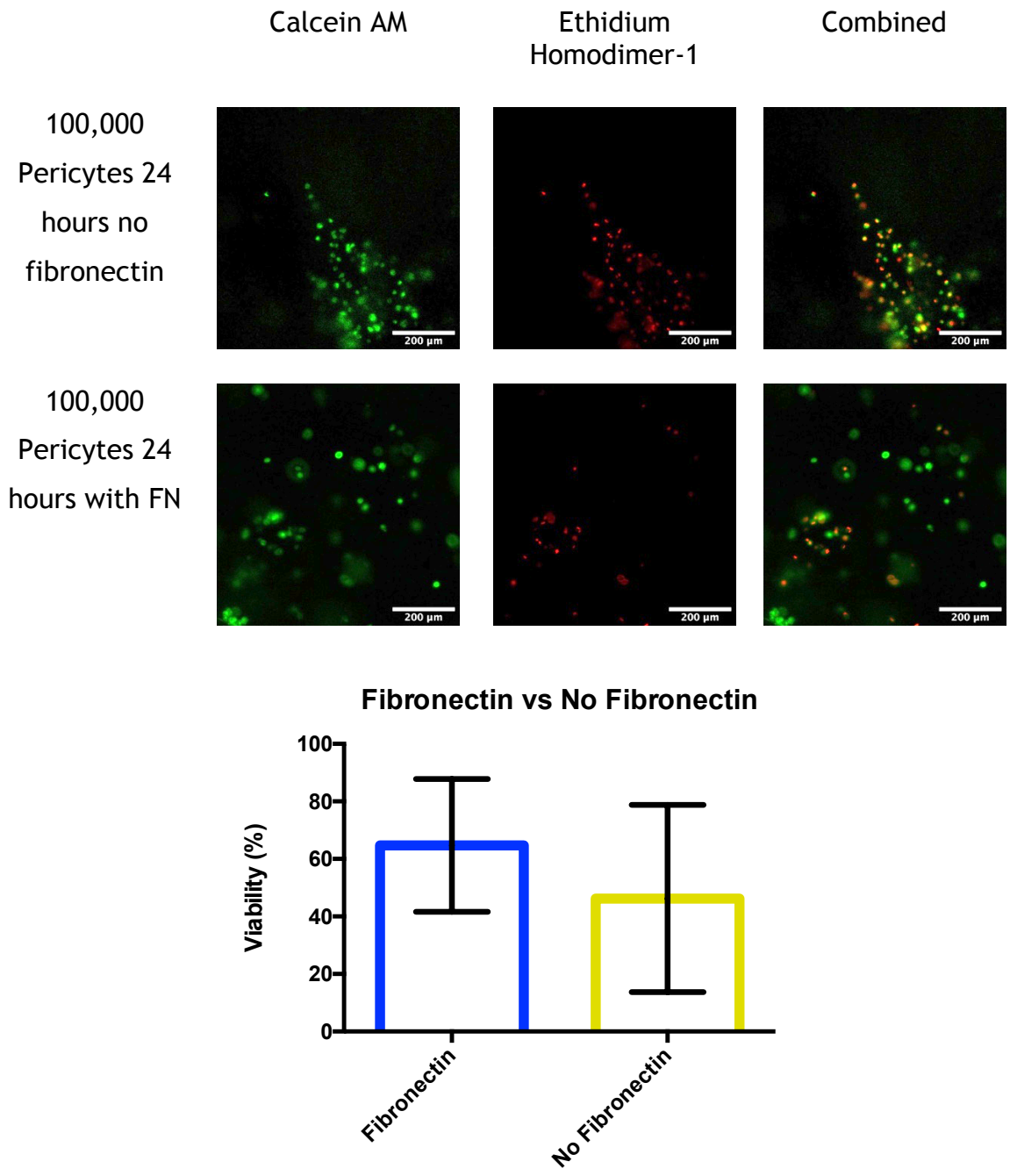

Figure 3.14. Effect of FN pericyte viability in gels.
This figure shows examples of the images acquired while investigating the effect of FN within the gels on cell viability. The graph shows mean +/- SD viability quantified from the images gathered from 3 biological replicates and analysed using image J. A no significant difference is observed between the conditions determined by Kruskal-Wallis using prism software.

A reduction in seeding density was investigated along with a longer time point to see if the cells would start to recover over time (Figure 3.15). Again, the average viability was low with the longer time point showing a drop in viability though not statistically significant. For the lower seeding, a density of 50,000 cells/gel was used. The viability increased to 50% compared to 40% viability obtained for the higher density seeding of 100,000 cells/gel. However, 50% viability was considered too low to carry out further experiments on this model.

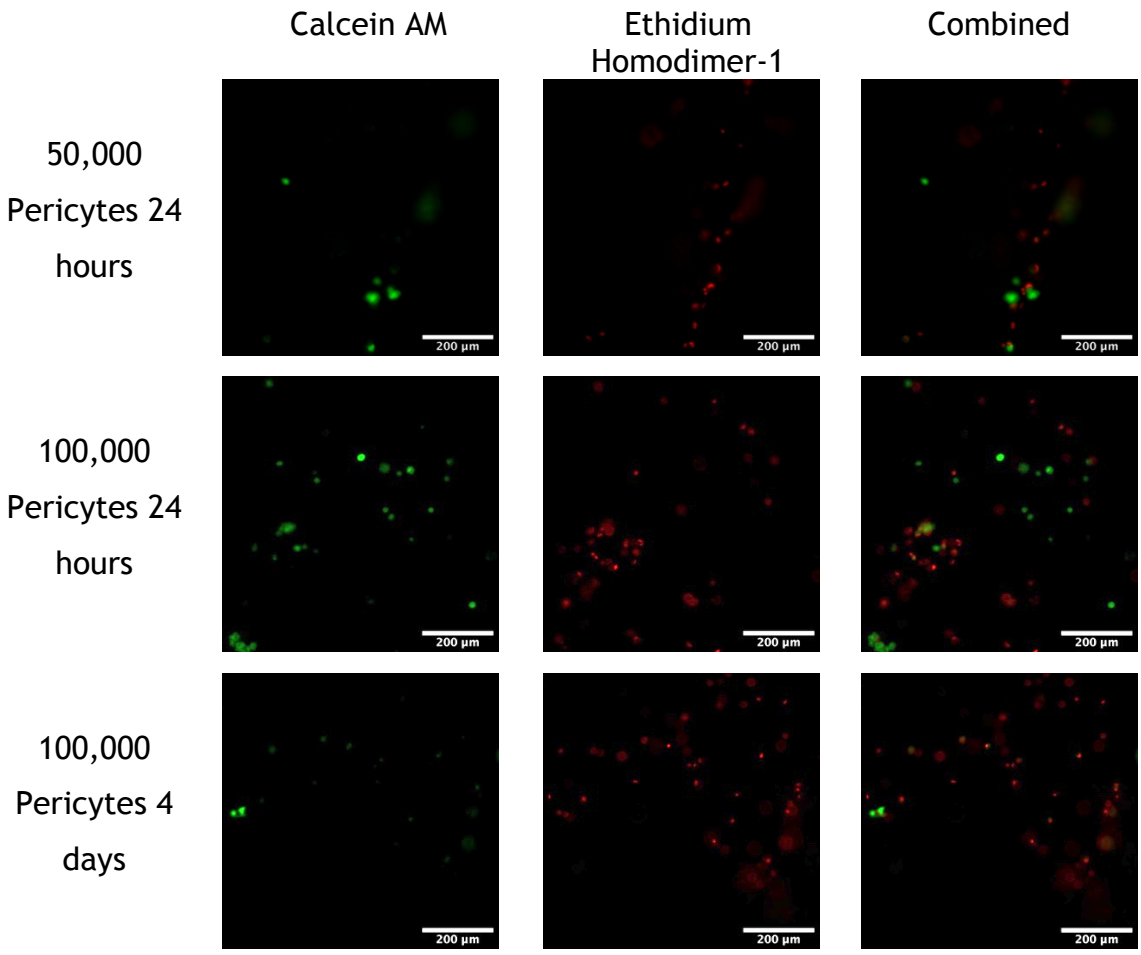

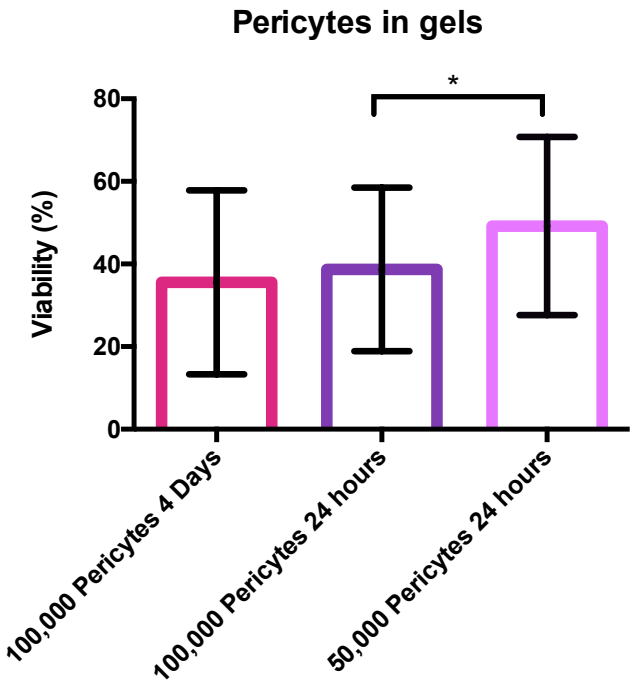

Figure 3.15. Live dead results for pericytes in gels
This figure shows example images taken for each condition covered looking at pericytes in 5% PEG gels with FN. The graph shows mean +/- SD viability quantified from the images gathered from 3 biological replicates and analysed using image J. A significant difference is observed 50,000 and 100,000 cells at 24 hours some of the conditions where *$p \leq 0.05$.

For MSCs seeded in gels at 20,000, 50,000 and 100,000 cells/gel no significant difference was observed at a 24 hour timepoint (Figure 3.16). Though observing a higher average viability than seen with pericytes, the viability was still far below that desired for a functional model.

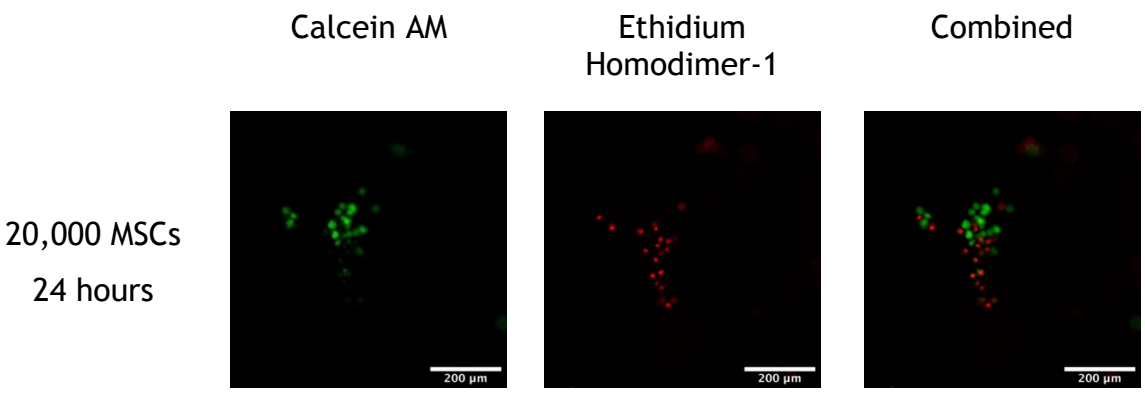

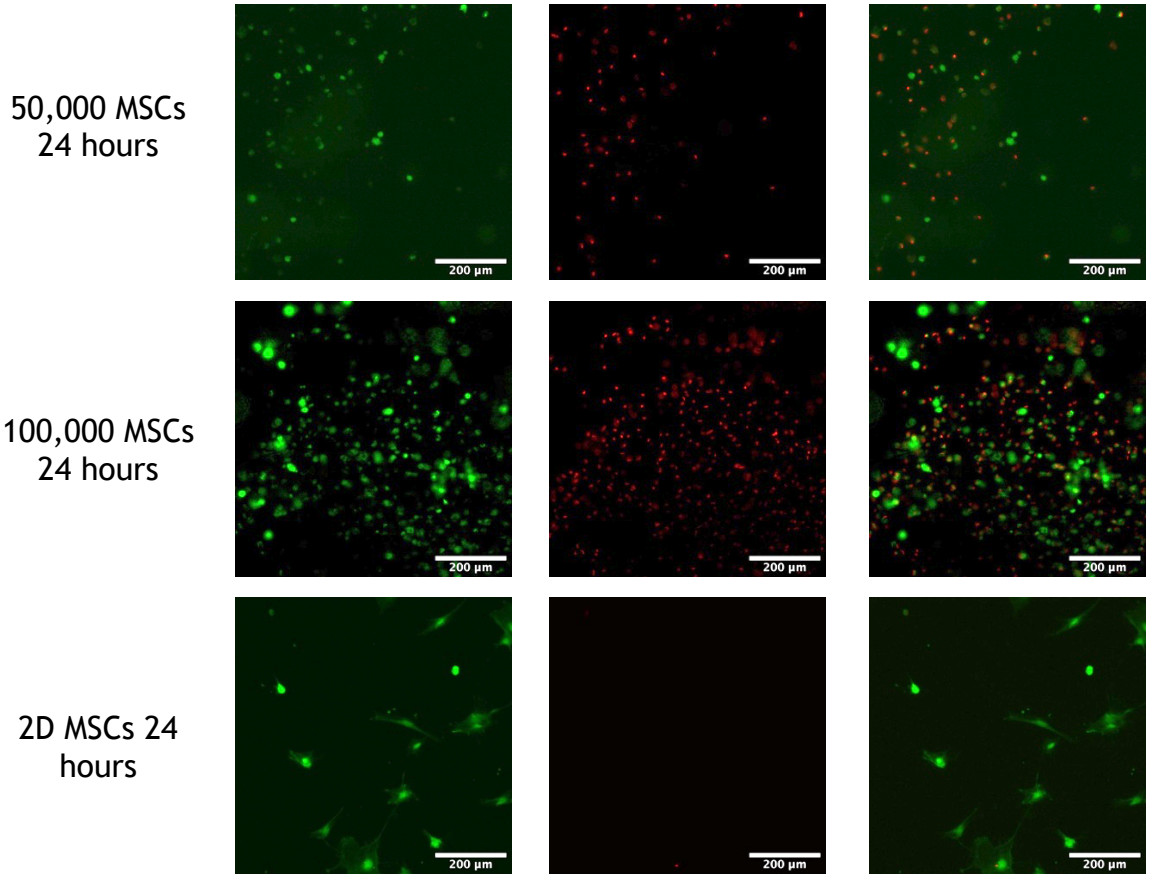

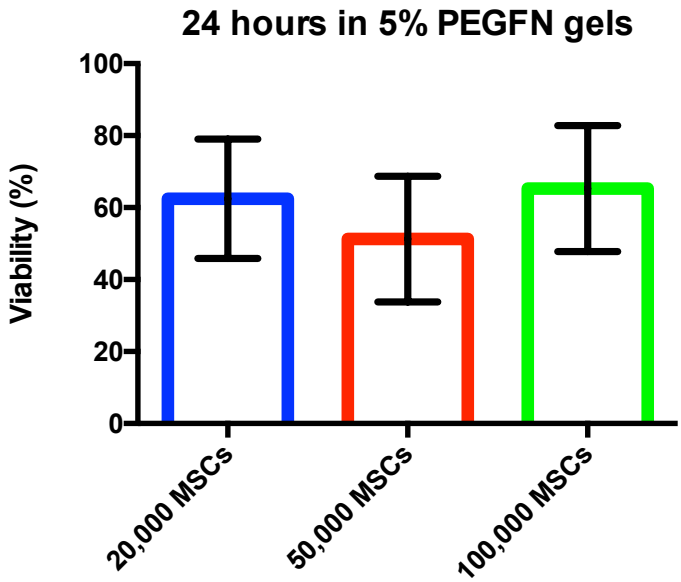

Figure 3.16. Live dead results for MSCs in gels (24 hours)
This figure shows examples of the images acquired while investigating the effect of MSC seeding density on cell viability in the gels over 24 hours. The graph shows mean +/- SD viability quantified from the images gathered from 3 biological replicates and analysed using image J. A no significant difference is observed between the conditions determined by Kruskal-Wallis using prism software.

At the 7 day time point again there was no significant difference to the 3 seeding densities tested for MSCs (Figure 3.17). With the average viability dropping compared to those seen at 24 hours showing no recovery of the cells over time.

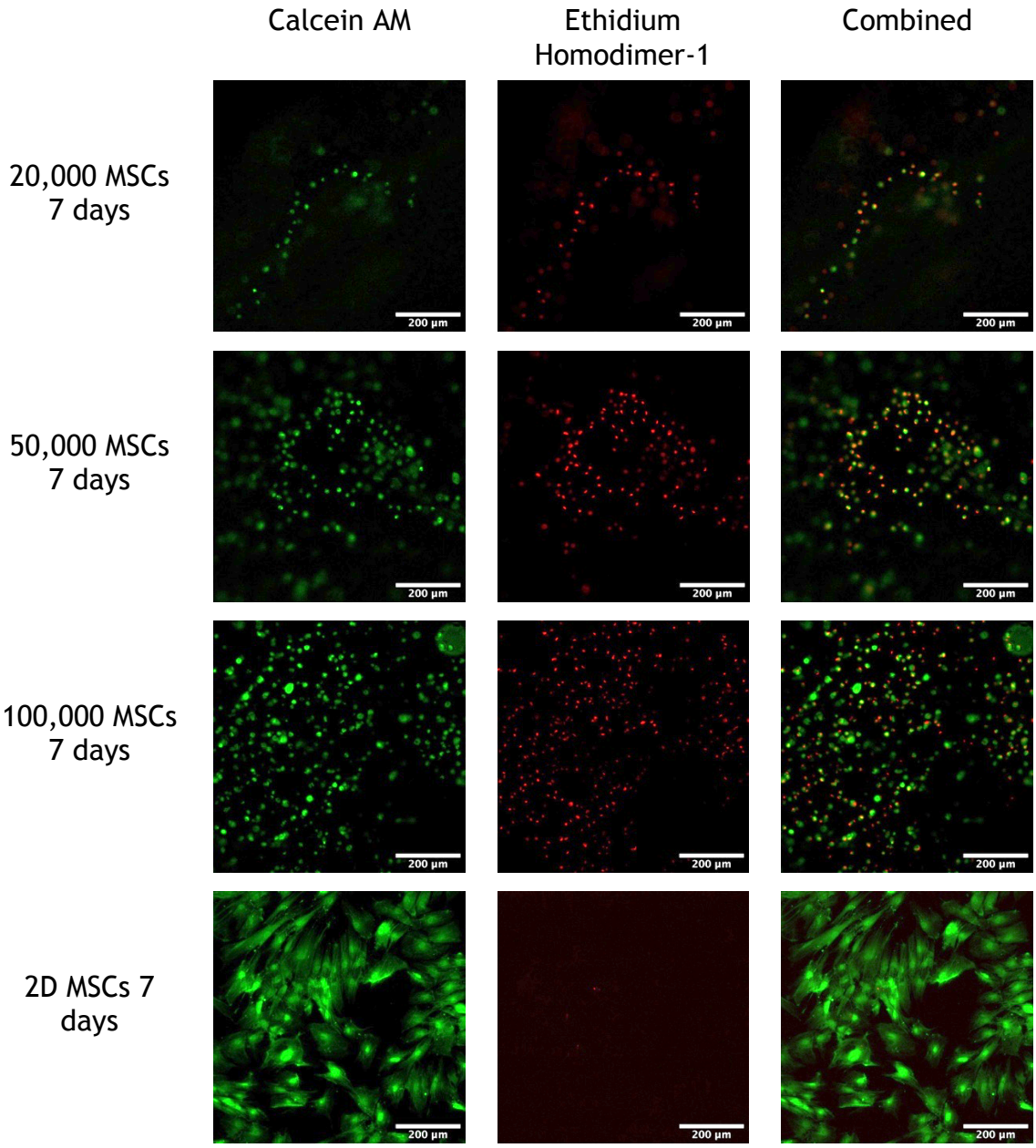

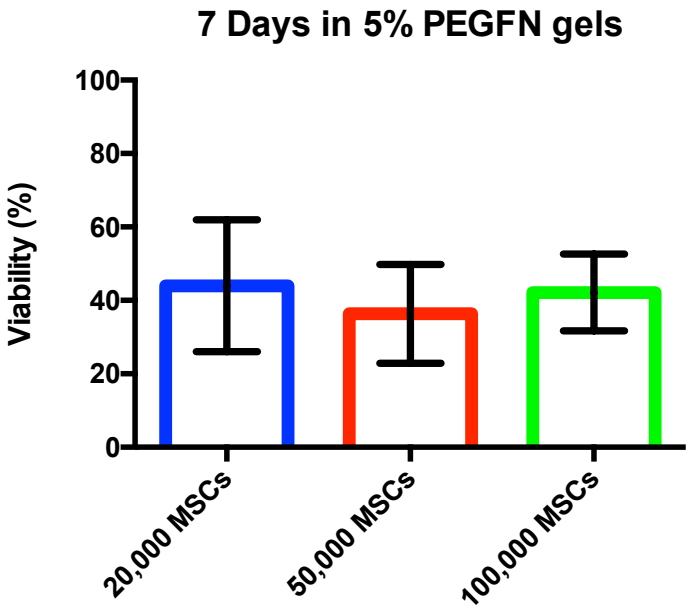

Figure 3.17. Live dead results for MSCs in gels (7 days).
This figure shows examples of the images acquired while investigating the effect of MSC seeding density on cell viability in the gels over 24 hours. The graph shows mean +/- SD viability quantified from the images gathered from 3 biological replicates and analysed using image J. A no significant difference is observed between the conditions determined by Kruskal-Wallis using prism software.

When investigating the gelation temperature effects on viability no statistical significance was shown between those where cells were combined with the pre-gelation mixture and gelled at room temperature and those gelled at 37°C (Figure 3.18). The average viability for room temperature gelation was higher though the results were more variable with more spread maximum and minimum observed for this condition.

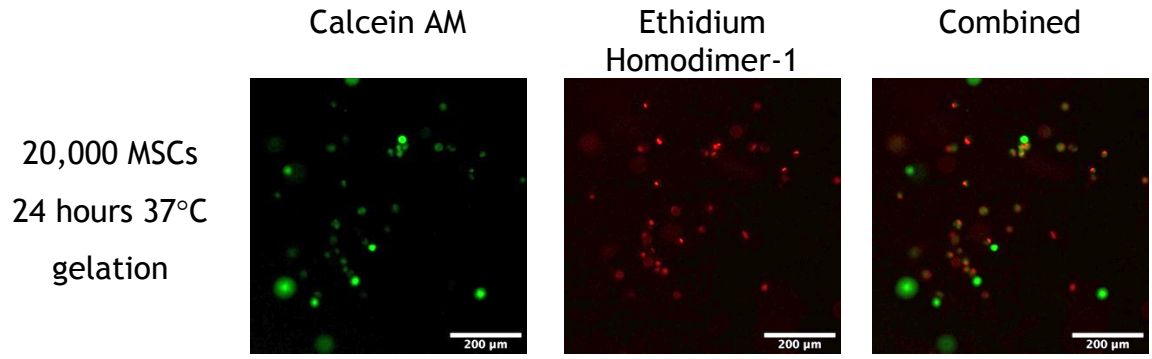

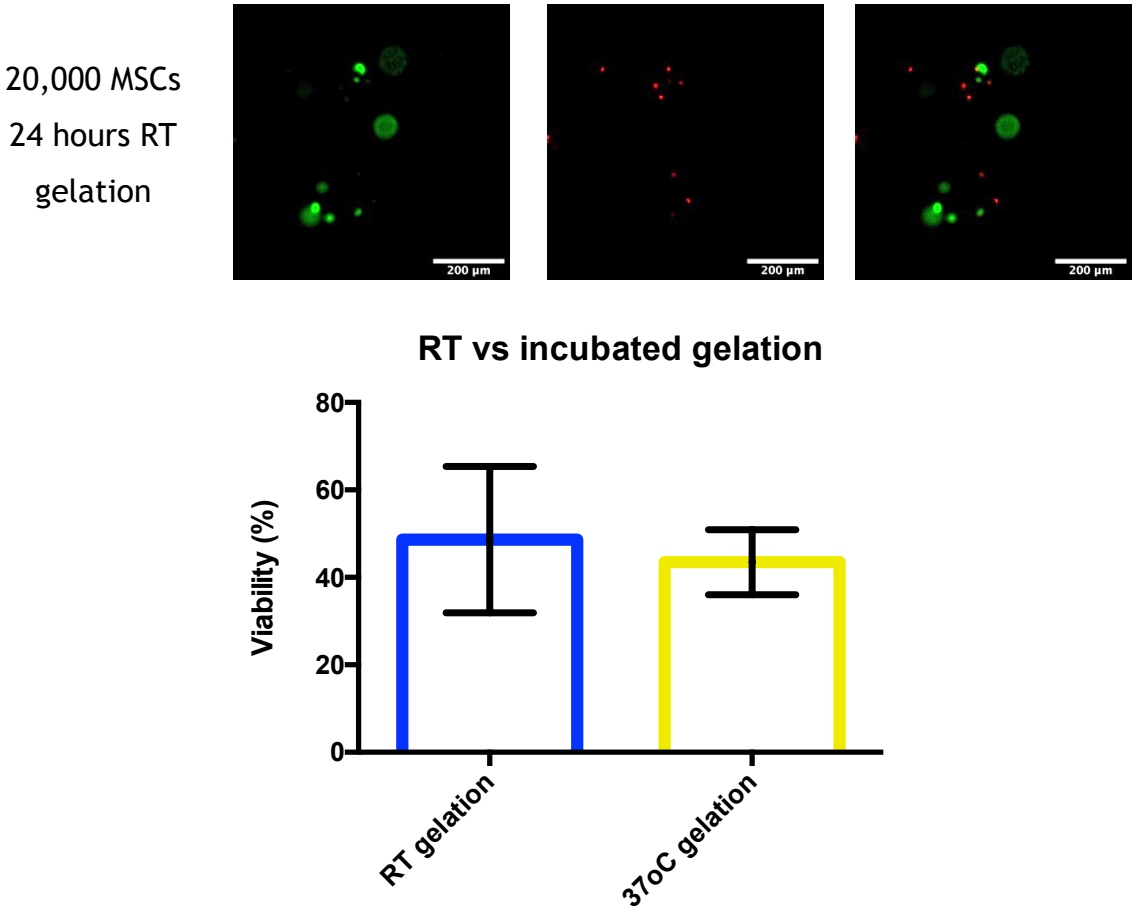

Figure 3.18. MSC viability during room temperature gelation vs 37°C gelation.
This figure shows examples of the images acquired while investigating the effect of incubated gelation on the cell viability. The graph shows mean +/- SD viability quantified from the images gathered from 3 biological replicates and analysed using image J. A no significant difference is observed between the conditions determined by Kruskal-Wallis using prism software.

2D controls that were run alongside experiments to ensure that the cells were not influenced by any other factors other than the gels can be seen in Figure 3.16 and Figure 3.17, though not shown on the graph, viability for these controls was >98%.

3.4 Discussion

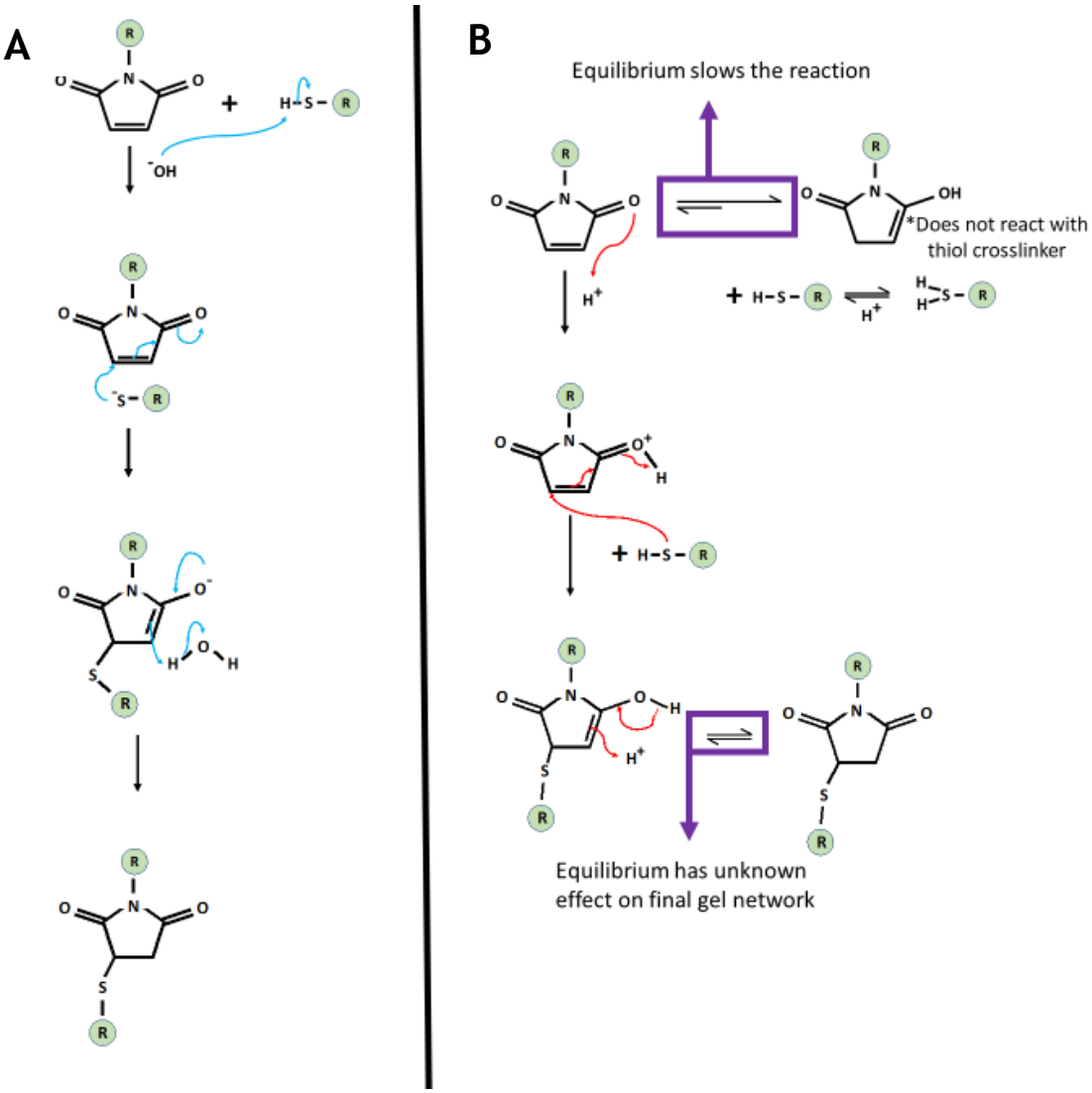

Figure 3.19 Michael addition of 4-arm PEGMAL and PEG dithiol at physiological and acidic pH.
Reaction pathway with curly arrow annotation of the Michael addition of 4-arm PEGMAL with PEG dithiol at physiological pH (A) and an acidic pH (B). At an acidic pH the presence of the enol version of 4-arm PEGMAL and the protonated version of PEG dithiol inhibits the Michael addition, slowing the rate of reaction.

The ability to slow gelation using pH is due to a change in the chemical reaction. At physiological pH, gelation occurs instantly through a Michael type addition reaction; this is ideal for forming gels for a cell based model (Rizzi and Hubbell, 2005; Nair *et al.*, 2014). At physiological pH the maleimide group is in its keto form, when the pH is lowered an equilibrium is created between the keto maleimide and its enol tautomer. The enol tautomer is unreactive to the thiol group found on the PEG dithiol. An equilibrium is also formed between the PEG

dithiol and its protonated version which is unreactive to the 4-arm PEGMAL, this only occurs at an acidic pH (Figure 3.19). Through rheology and NMR (Figure 3.8) we can see that the reaction is slowed down on a molecular level when the pH of the gelator solution is lowered. We can also see through rheology that the changing of the pH and therefore the rate of the reaction alters the final stiffness of the gel (Figure 3.9). From this we can conclude when working with a PEG system similar to that outlined here, the pH must not be altered from that appropriate for the work planned. Changes in pH have previously been noted to change the rate of thiol reaction, however these reports did not cover changes outside the physiological range and the effect on the physical characteristics (Rizzi and Hubbell, 2005; Fu and Kao, 2011; Nair *et al.*, 2014).

In Figure 3.10 there was a significant difference observed in the stiffness when comparing the geometry used when measuring fast forming gels (pH 7.4) with an uneven surface. The parallel plate can be influenced by an uneven contact with the gel as this causes uneven forces to be applied creating inaccuracies in the calculation performed by the rheometer. As the vane & cup geometry does not contact the surface of the gels with the measuring surface but rather takes measurements from within the gel the uneven surface has no influence on the measurements, therefore these can be assumed to be more accurate. This led to the conclusion that for gels that form quickly and produce uneven surfaces the vane & cup geometry should be utilised over parallel plates where possible.

It is important to have a system with tuneable properties if we wish to mimic different tissues of the body or diseased tissues using comparable models. An example for this is the increase in stiffness commonly seen with cancerous or precancerous tissues compared to the healthy tissue (Huang and Ingber, 2005; Plodinec *et al.*, 2012). I have shown that the PEG gels I am using for my model can have varying stiffness dependent on the amount of PEG in the gel's composition. Figure 3.11 shows a range in stiffness between ~1kPa - ~4.5kPa for gels of 3 – 10% PEG though it is notable that this range could be extended. As my model is aimed at the bone marrow niche I did not investigate outside this range and chose to work with 5% PEG gels which lie within the range of the bone marrow seen in literature which is said to be <3kPa (Choi and Harley, 2017). It is

also shown in the figure that there is a positive linear relationship between the storage modulus and the amount of PEG.

Through changes in the amount of PEG changes in swelling properties were also observed (Figure 3.12). A higher PEG concentration leads to a higher percentage of swelling suggesting that increasing the PEG content gives the gels a higher capacity to hold water. It is important to understand the swelling properties of the gels as any cells within the gel will experience this and the volume of the final gel will differ. If the volume of the final gel differs this may have to be taken into account for calculating the seeding density of cells in the model or the concentration of any additional factors. Understanding swelling allows the model to be kept consistent and comparable. Swelling has not posed a problem or a benefit to this model though knowing the properties have allowed accurate cell density and growth factor concentration calculations. While looking at the inclusion of a degradable crosslinker (VPM) there was no significant effect shown on the swelling ability of the gels (Figure 3.12). It is important to consider degradability when looking at cell models as it allows them to remodel and create their own matrix (Anderson *et al.*, 2011; Madl *et al.*, 2017). Therefore, for the final model 25% of the crosslinker used to form the gels was VPM allowing degradability as shown previously in our group (Trujillo *et al.*, 2020).

As the aim of the project is to produce a bone marrow niche like model *in vitro* for investigating cell behaviour in normal and diseased states focus moved to seeding cells within the PEG gels. For initial cell work the focus was on ensuring that healthy cells could survive within the gels this was done by looking at basic live/dead staining. Cell types chosen for the initial cell work were pericytes, a progenitor cell to MSCs and fully formed MSCs as these are a key component to the bone marrow niche and one of the two stem cell types that reside there (Crisan, Yap, Casteilla, C. W. Chen, *et al.*, 2008; Frenette *et al.*, 2013; Morrison and Scadden, 2014). The model was unable to support cells as results for both cell types within the gels showed poor viability, up to ~50% and ~65% respectively, over various time points (Figure 3.15 & Figure 3.16). Due to pericytes showing a lower average viability than MSCs the latter was chosen to continue investigating the viability within the gels. Many different conditions were considered including cell density, removal of FN and the gelation

temperature but showed no significant increases for the viability (Figure 3.14, Figure 3.15, Figure 3.16, Figure 3.17 & Figure 3.18). The average viability over the conditions tested varied from ~35 – 70% with large variation within the same conditions; poor viability has been seen in the literature and was overcome through the introduction of peptide sequences to functionalise the gels (Benoit, Durney and Anseth, 2007; Salinas and Anseth, 2008).

Due to the low viability observed when cells were seeded within the gels a new model had to be considered in order to continue. Examining the differences observed in the cell morphology where cells in 2D culture are spread flat adhered to the surface of the tissue culture vessel while those in the gel are small and rounded. This suggested that the inability to adhere and spread within the soft gels may be a reason behind the low viability. The low stiffness of the gels though it well represents the bone marrow stiffness it does not represent the stiffer surface of the endosteum one of the locations where MSCs are found within the marrow cavity. For these two reasons the model was altered to test seeding cells under gels showing a much higher consistent viability up to 100% viable cells (Figure 4.12). By introducing this surface an opportunity arose to include surface modifications to the model opening up new possibilities for the model.

Chapter 4 Surface Modification

4.1 Introduction

Polystyrene (PS) is a versatile synthetic polymer with various uses in both commercial and medical applications which range from packing materials to tissue culture plastics. PS is manufactured through addition polymerisation of styrene monomers, producing a polymer comprising of carbon and hydrogen molecules in an aromatic ring formation on a hydrocarbon backbone (Figure 4.1). PS is commonly used as the base material to manufacture tissue culture plastics due to its availability, modification potential, biocompatibility and bioinert nature. Various treatments have been developed to enhance cell-material interactions when PS is employed in more refined cellular systems (Lerman *et al.*, 2018). The most frequently utilised of these treatments is oxygen plasma which changes the surface properties by incorporating negatively charged ions onto the surface, increasing hydrophobicity and improving cellular surface interactions (Ramsey *et al.*, 1984). Notably, this surface modification technique is utilised to produce commercially available tissue culture plastics and enhance cellular adhesion for culture (Lerman *et al.*, 2018).

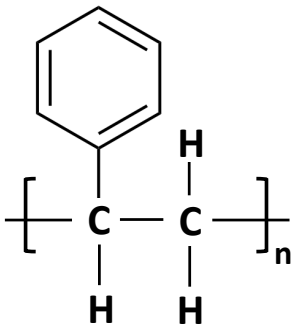

Figure 4.1 Chemical structure of PS.
The figure shows a representation of one monomer unit of PS.

Within the field of biomedical engineering surface modifications are commonly implemented in order to aid cellular interactions and function and are often refined so as to maintain favourable bulk characteristics of the base polymer. These can be as simple as an energetic plasma activation treatment on PS to more complex alterations in surface chemistries to influence, induce or drive

more complex biological functions. Many methodologies have been developed to achieve the appropriate changes to a material to fulfil a specific role each with their own benefits and issues (Schwalm, 2007; Sprott *et al.*, 2019). For example, within our group several methodologies (as will be detailed below) have been developed for the incorporation of Poly (Ethyl Acrylate) (PEA) onto several bulk surfaces, providing novel biological interactions to these materials.

For 2D surfaces such as coverslips, spin coating has been utilised as a technique for producing a polymer coating (Llopis-Hernández *et al.*, 2013). Through spin coating a thin layer of polymer can be produced on the surface of the coverslip. However, this technique is not feasible for coating small materials (smaller than the head of the spin coater, ~ 0.5 cm) and/or 3D structures such as the microbeads (Corning) proposed for use within this model. PS microbeads (PSm) were chosen to create a surface for MSCs to adhere to, their small size (125 µm to 212 µm) make them easy to encapsulate within the gel while the shape allows cells to adhere over the entire surface, they were also commercially available sterilised for cell culture. Due to the limitations of spin coating other methods were therefore considered and assessed to find the best option for incorporating PEA onto the PSm.

Plasma polymerisation, via high electrical monomer stimulation, has been shown to coat both the external and penetrate the internal surfaces of scaffolds (Cantini, Rico, *et al.*, 2012; Llopis-Hernández *et al.*, 2016). This technique has previously been used with success to coat decellularised bone fragments for a study on regenerating critical sized bone defects by utilising the relationship between PEA, FN and growth factors (Cheng *et al.*, 2019). These studies have shown the ability to create a coating of PEA on the material surface while retaining the functionality of the polymer, maintaining the ability to influence FN conformation on the material surfaces. These studies also highlight the potential to use plasma PEA coatings for use on osteogenic regenerative implants. Despite this there are still disadvantages to modifying surfaces via plasma polymerisation. It has to be considered that due to the handling process the section of the sample resting on the base of the chamber will be unreachable resulting in a section of the material remaining untreated.

Due to the potential issues with plasma PEA, chemical surface modification techniques were also investigated. Surface Initiated Atomic Transfer Radical Polymerisation (SI-ATRP) is a widely used technique for the development of materials used for various biomedical applications (Matyjaszewski *et al.*, 2007). The process allows control over properties such as functionality and the macromolecular structure which are important when designing materials for biomedical purposes (Siegwart, Oh and Matyjaszewski, 2012). SI-ATRP works through the addition of polymer brushes onto a base polymer backbone adding functionality. This is achieved through the immobilisation of an initiator molecule onto the base polymer which subsequently reacts with the addition of a transition metal catalyst creating a free radical and an oxidised transition metal. On the introduction of a monomer polymerisation is triggered by the presence of the free radicals and this newly formed polymer chain is bound to the base polymer surface in place of the initiator molecule (Matyjaszewski and Xia, 2001; Matyjaszewski *et al.*, 2007).

SI-ATRP has previously been utilised to incorporate PEA onto poly l-lactic acid (PLLA) surfaces, promoting the formation of fibronectin networks and subsequently enhancing cellular adhesion and differentiation on these surfaces (Sprott *et al.*, 2019). PS has been used in SI-ATRP systems, however these studies predominantly use the process to graft PS onto other base materials (Jeyaprakash *et al.*, 2002; Morandi, Heath and Thielemans, 2009; Kumar *et al.*, 2016) rather than modifying a PS base with another polymer. However, utilising this system we aim to incorporate functional PEA brushes onto PS surfaces, chemically bound to the base polymer in a homogenous coverage. The more complex process of SI-ATRP compared to plasma treatment also introduces higher likelihood of unwanted damage to the base polymer due to the chemicals required and the heat produced through the reaction.

Another chemical based method which is used to modify surfaces is UV polymerisation or light controlled radical polymerisation. UV polymerisation is commonly used in biomedical applications for initiating crosslinking to produce hydrogels (Mellott, Searcy and Pishko, 2001) but can also be used as a surface modification technique (Chen, Zhong and Johnson, 2016). For the process to work a photoinitiator is required, this acts similarly to the initiator in the SI-

ATRP process and is introduced to the base material in the initial stage of the process. Once incorporated within the surface this then reacts under UV irradiation producing free radicals that trigger the polymerisation of monomer present in the surrounding solution. The benzoyl group is known to be a powerful initiating species making benzophenone (BPO) a good candidate as a photoinitiator (Decker, 1996). BPO has been commonly utilised for surface modifications as well as bulk polymerisation of various polymers including methyl methacrylate (MMA) and PEA (Achilias and Sideridou, 2002; Lozano Picazo *et al.*, 2015). In light driven polymerisation, parameters such as the duration of UV treatment and monomer concentration allows control of the resulting polymer chain length (Chen, Zhong and Johnson, 2016). Additionally, coverage or patterning can be modulated by defining the UV exposure areas this can also be viewed as a disadvantage when working with 3D structures as areas may be inaccessible to the light source. All these factors along with the simplicity of the process make UV polymerisation a good candidate for our surface modification.

The aim of the work outlined in the following chapter was to find the most effective and efficient way to coat PSm in PEA. Various methodologies were chosen from established surface modifications techniques available and assessed by evaluating the chemical, topographical and biological variations within certain parameters. This aimed to establish which technique would provide the best coverage and functionality of PEA and therefore be optimal for use within the niche model.

4.2 Methods

The methods for surface modifications investigated in this chapter SI-ATRP, UV polymerisation, plasma polymerisation and spin coating are described in Chapter 2 (2.2.3). For ease of handling and to better assess any damage caused by the process's polystyrene pellets (PSp) were used, rather than microbeads (PSm) due to the larger size for SI-STRP and UV treatments. These PSp were also dissolved in toluene (12% w/v) and spin coated onto surfaces for flat 2D analysis used for atomic force microscopy (AFM) and water contact angle (WCA). These 2D samples allowed for comparison of PS surface modification to previous studies.

4.2.1 Imaging FN networks

AFM was used to visualise the surface coating and the formation of FN nanonetworks. FN protein was adsorbed onto the surface of PEA coated coverslips for 10 minutes at room temperature at a concentration of 20 μg/mL. AFM was used in AC mode (Nanowizard-3 Bioscience AFM, JPK) to obtain height images of the PEA samples both with and without FN adsorbed. The cantilevers had a resonance frequency of 75 kHz and a force constant of 3 N m^{-1} (MPP-21120, Bruker). Images were processed using JPKSPM data processing software, utilising a polynomial filter to normalize images.

FN (Sigma) tagged using DyLight 488 NHS Ester (ThermoFisher) following the manufacturers protocol was used to confirm FN adsorption on PEA coated PSm and a control spin coated PEA glass coverslip. These were then imaged at 40x magnification on a ZEISS AxioObserver Z.1. This could not image specific networks but could confirm successful adsorption of FN.

4.2.2 Water Contact Angle

WCA measurements were taken using a Theta Optical Tensiometer (Biolin Scientific, Sweden) for all surface modification methods and controls. These were taken as 3 measurements at different locations on each sample with 3 samples for each condition. Static contact angles were measured by dropping 3 μL of deionised water onto the sample, contact angles were then recorded by

the tensiometer. Angles that were greater than 90° indicate a hydrophobic surface while angles less than 90° show a hydrophilic surface (Figure 4.2).

Figure 4.2 Diagram of WCA on hydrophobic vs hydrophilic surfaces
This shows how the tensiometer measures the contact angle produced by the water droplet on the material surface.

4.2.3 Fourier-Transform Infrared Spectroscopy

Fourier-Transform Infrared Spectroscopy (FTIR) was performed to characterise the bulk chemical composition of samples before and after surface modifications. Initial blank scans were taken to correct for air conditions and any background signals produced. Surface scrapings were taken from samples and scanned between the range of 650 – 4000 cm^{-1} using an Agilent Cray 630 spectrometer. The resulting data was then analysed using GraphPad Prism to highlight any changes created through the surface modification process.

4.2.4 X-ray photoelectron spectroscopy

X-ray photoelectron spectroscopy (XPS) was used to define the chemical composition of the top ≤ 10 nm of the of sample surfaces. All XPS analysis was performed on a NEXSA spectrometer (ThermoFisher Scientific) using a micro-focused monochromatic Al X-ray source (19.2 W) over an area of ~100 μm. Each sample was analysed at 3 points or in the case of the PSm due to their small size 3 individual beads were measured. XPS data collection was performed at the EPSRC national facility for XPS (‘Harwell XPS’), operated by Cardiff University and UCL, under contract No. PR16195. Survey scans were recorded at pass energies of 200 eV while high resolution scans were recorded for oxygen, carbon, nitrogen and bromine at 50 eV. The resulting spectra were analysed, and curve fitting performed using CasaXPS version 2.3.16 (Casa Software Ltd).

4.2.5 Cell viability on surfaces

Cell viability testing was carried out with cells seeded in a 24-well plate and left overnight to adhere in media with 2% human serum. Non degradable 5% PEG hydrogels (2.2.4) were then formed on top of the cells. Viability was tested at 1, 2 and 3 week time points, controls were performed alongside with no gels included.

Cell viability was also carried out on PSm that were encapsulated into 25% degradable 5% PEG hydrogels. The cells were imaged at 1 and 2 weeks but viability was not quantified due to the difficulty with the 3D structure of the beads. Confocal imaging was carried out using a Zeiss Observer Z1 spinning disc confocal microscope, equipped with a Yokogawa CSU-X1 filter wheel and spinning disc unit and a Photometrics Evolve 512 delta EM-CCD camera to better visualise the cells on the beads confirming adherence and spreading.

4.3 Results

Various techniques were used to investigate the efficiency of several surface modification methodologies as possible approaches for coating PSm.

4.3.1 Water contact angle

WCA was measured on coverslips that were coated in PS, through spin coating, to match the base material of the PSm. The results were used to show any changes in the hydrophobicity and thus surface chemistry from treatment through any changes in the contact angle. Spin coated PS and spin coated PEA samples were included as controls to observe changes in the hydrophobicity produced through each methodology.

Spin coated PEA (scPEA) was observed to be significantly more hydrophilic than spin coated PS, however no difference was observed between either of these conditions and plasma treated PS samples (Figure 4.3 A). This may imply that while PEA is present on these surfaces, as suggested by the drop in contact angle, the coverage is not homogenous and certain areas may retain the hydrophobicity of PS or that the plasma treatment results in variation from bulk PEA characteristics. For UV polymerisation (Figure 4.3 B) both BPO treated and BPO + PEA treated (uvPEA) conditions showed no significant change in the mean WCA from that of scPS although these samples did present slightly lower contact angles more similar to those seen for scPEA. A significant difference was seen between scPEA and SI-ATRP (Figure 4.3 C) and the final contact angle was similar to that of the scPS suggesting that the surface may not have been altered in the desired way. These results suggest that both plasma polymerisation and UV polymerisation changed the surface chemistry of the samples to one more similar to PEA. For SI-ATRP, however, the treatment did not appear to have changed the surface chemistry and remains similar to the PS. Though WCA can be used to imply certain changes in the surface chemistry it cannot definitively confirm or deny the presence of PEA.

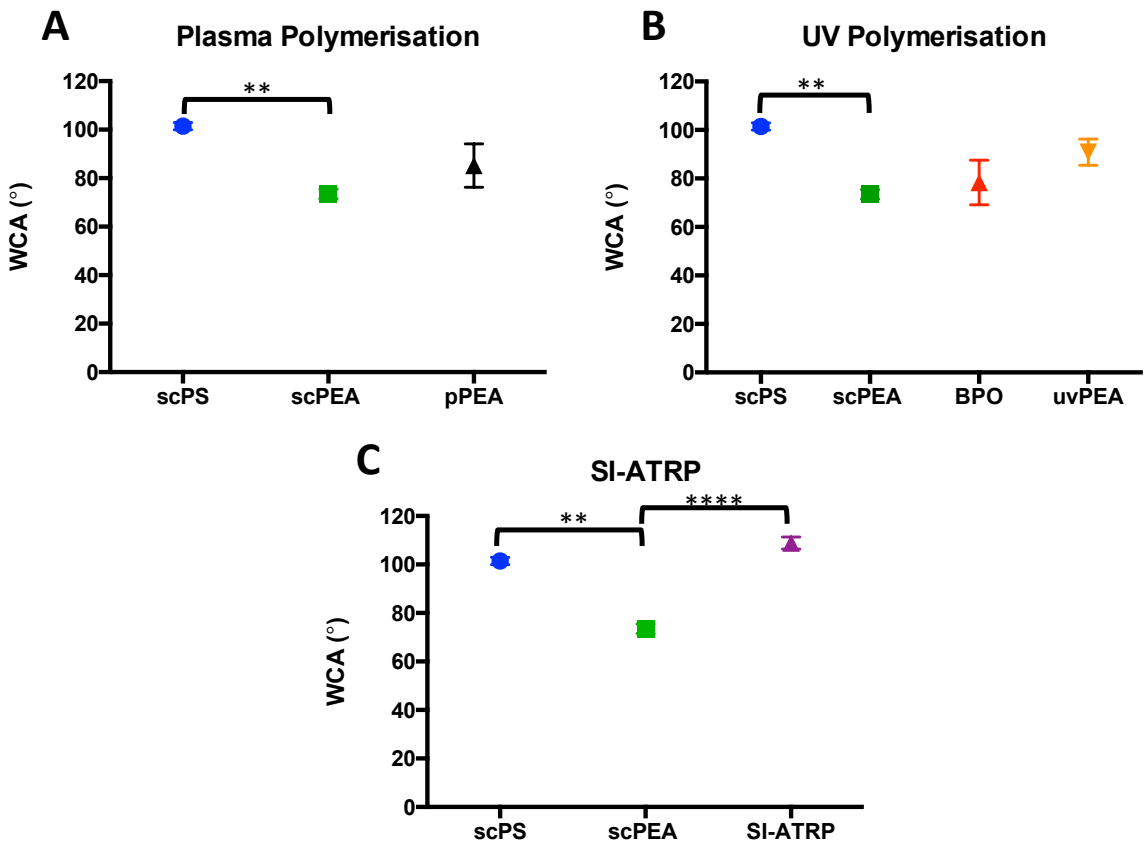

Figure 4.3 Water contact angle characterisation.
Graphs show the static water contact angle characterisation of the various surface modifications used to incorporate PEA. No difference was observed between pPEA or uvPEA and scPEA. A difference was seen between bPEA and scPEA control. All 3 graphs show the mean +/- SD statistical differences shown through Kruskal-Wallis test where p** > 0.01 and p**** >0.0001.

4.3.2 FTIR

FTIR was used as a way to assess the bulk composition of each treated sample, plasma treated (pPEA), UV treated (uvPEA) and SI-ATRP (bPEA) along with untreated PSp, PSm and bulk PEA for comparison. The full spectra were measured from 650 cm^{-1} to 4000 cm^{-1} and analysed for any changes from the base material composition. As FTIR measures the bulk composition of the material scanned, the base material will also appear in the spectra though visible changes can show modifications have occurred. For pPEA and uvPEA there were no obvious changes in the scans when compared to their respective PS base materials, PSm for plasma and PSp for UV (Figure 4.4). The lack of changes seen for these samples is likely due to the thin layer produced through these techniques being masked by the volume of the base material. The PEA control

shows a clear peak at approximately 1700 cm^{-1} which is related to the C=O bonds in the polymer.

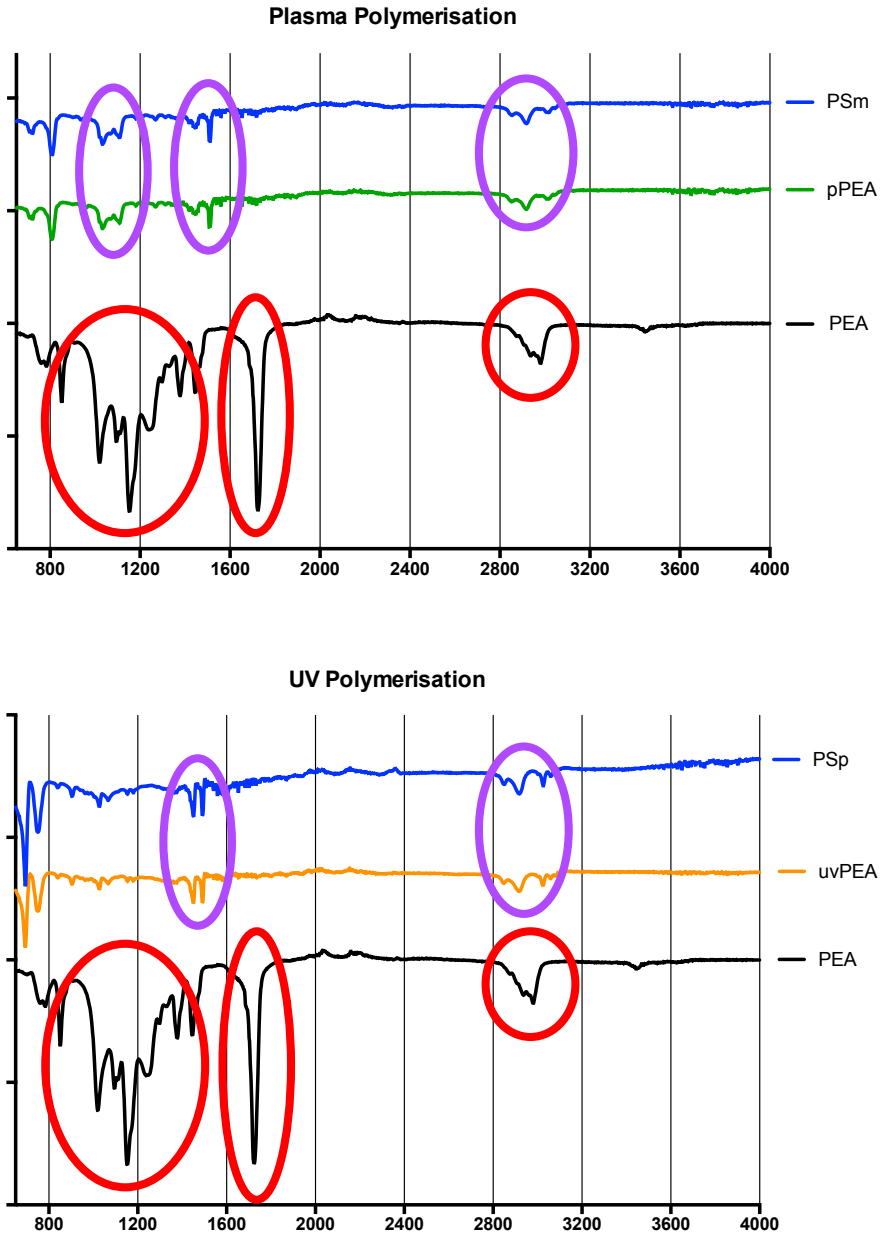

Figure 4.4 Full FTIR spectra for plasma and UV polymerised samples.
Spectra are shown between 650 cm^{-1} and 4000 cm^{-1} for plasma polymerisation (top) and UV polymerisation (bottom). The most obvious differences (red) or similarities (Purple) observed are circled within the spectra. Both Plasma and UV polymerisation maintain a spectrum that matches that of the PS base materials rather than that of the PEA control.

For SI-ATRP treated samples the full spectra from 650 cm^{-1} to 4000 cm^{-1} (Figure 4.5) was analysed more closely with a focus between 650 cm^{-1} and 1550 cm^{-1} with the changes that coincide with the PEA spectra outlined in Figure 4.6. A

large peak appears in the bPEA sample spectrum at ~800 cm^{-1} which can be associated to the peak seen in PEA at ~790 cm^{-1} as they are both in the range of peaks associated with C-H bonding, this peak was not present in either the PSp or the brominated spectra (Figure 4.6 A). Also within this section we see the peak at ~ 680 cm^{-1} increase in size for the brominated sample in comparison to the PSp, this region is associated C-Br bonding, this increase could be an indication of the introduction of C-Br bonds. The peak highlighted at ~1025 cm^{-1} is sharp in the PEA spectra and broad in the bPEA spectra associated with a carbonyl group, another peak is noted ~1090 cm^{-1} this can be associated with C-O bonding (Figure 4.6 B). These are again not present in the PSp or brominated spectra suggesting the addition of these binding regions through SI-ATRP treatment. Another peak appeared within the bPEA spectrum that was seen in the PEA spectrum but was completely absent from the others at ~1260 cm^{-1} this region is associated with C-O bonding (Figure 4.6 C). Two peaks are also noted to have increased in size on the brominated spectrum compared to PSp again suggesting that this reaction did produce changes to the base material. These peaks seen at 1450 cm^{-1} and 1490 cm^{-1} are within regions associated with C-H bonding.

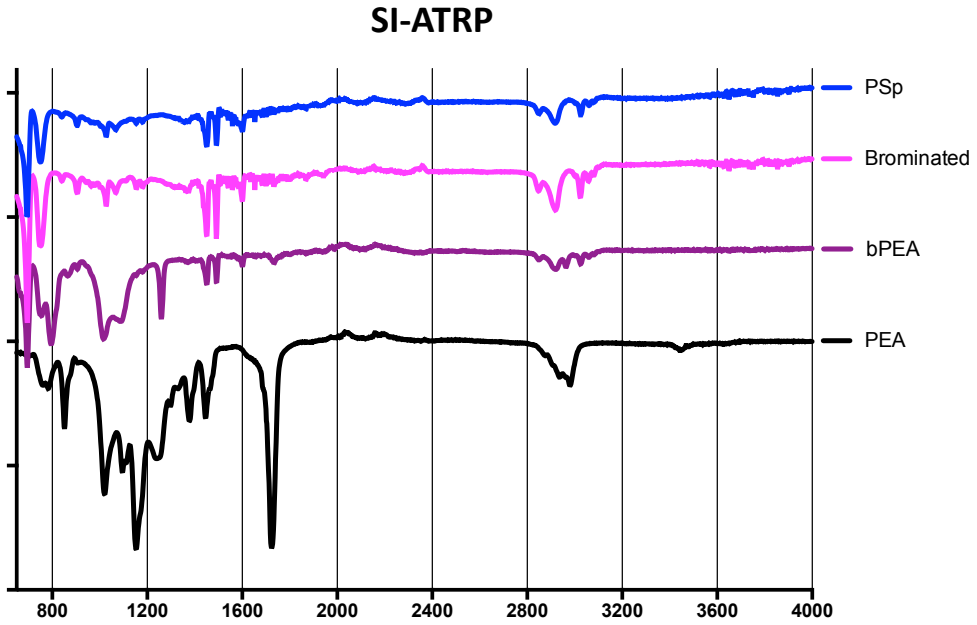

Figure 4.5. Overview of full FTIR spectra for SI-ATRP treatment process including bromination stage.
There are some clear changes in the spectra between the PSp base and bPEA though the spectrum still varies from that of PEA control. The brominated sample spectrum appears generally unchanged from the PSp in this overview spectra.

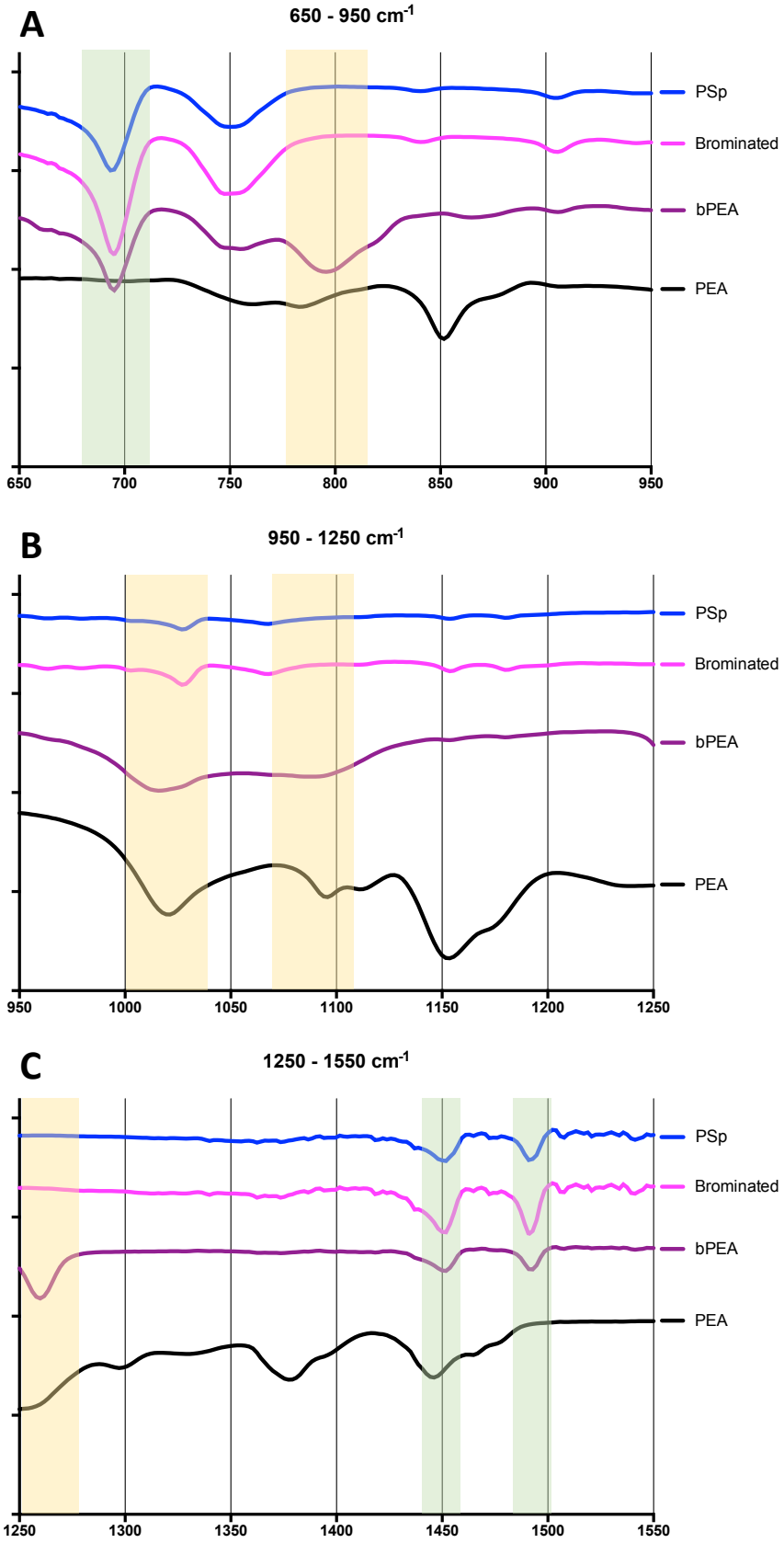

Figure 4.6 Focussed FTIR Spectra for SI-ATRP samples.
The figure shows select parts of the spectra which show changes caused by the process of SI-ATRP. A PSp control and bulk PEA were used as a comparison between a brominated sample and a sample that was fully treated with the SI-ATRP protocol (bPEA). Changes in bPEA spectra are highlighted in yellow with changes in brominated spectra highlighted in green, including changes in peak size.

Changes in the FTIR spectra confirm that the surface chemistry of the PS has been altered through the SI-ATRP process. The most obvious modification to the samples appears to take place in the final stage of the process as more changes appear in the fully treated spectra. Though brominating the samples does cause changes to the spectra indicating that the chemical addition of the bromine based initiator has occurred. Despite no indication of surface changes through the WCA results, FTIR data suggests that chemical changes have occurred to the samples. Though FTIR peaks can be associated with particular chemistries further analysis was carried out with XPS to definitively confirm the presence of PEA on the sample surfaces.

4.3.3 XPS

XPS was used to analyse the surface chemical composition of the samples to verify if the changes occurring through treatment were the result of a PEA coating on the sample surfaces. The scans have been fitted with peaks that relate to different binding conformations of the specified atoms. The specific binding points of PEA are annotated in Figure 4.7 for the carbon and oxygen scans. For carbon scans; 1 defines the C-C bonding, while 2 represents an ester bond C-O, 3 the carboxyl group O-C=O and 4 represents tertiary carbon bonds.

XPS spectra showed significant changes in the profiles between PSm and PEA allowing easy comparison with pPEA sample to assess the success of the treatment and introduction of PEA (Figure 4.7). The carbon binding composition, as shown from the C1s scans for pPEA matched that seen for the PEA control scan with the introduction of a peak between 290 – 288 eV which is not seen in the PSm sample and represents the carboxyl group annotated as 3 within the PEA formula. An increase in peak height in line with PEA scan compared to PSm is seen at ~286 – 284 eV showing the introduction of ester groups and tertiary carbon bonds and a similar ratio between these and secondary carbon bonds as seen within PEA scan. Within the oxygen scans the peak seen at ~533 eV, annotated 2 in the PEA O1 scan, representing the C-O-C bond is present in both pPEA and PSm scans. The second oxygen peak showing the C=O bonding is found between 531.5 – 532 eV, the notable change between the PSm control, pPEA and

PEA scans is the ratio between C-O-C : C=O PSm has the smallest ratio this increases in pPEA and is highest in PEA. Due to the obvious shift of the carbon and oxygen spectra of the pPEA from that of PSm to those resembling more PEA we are able to confirm the successful PEA coating through use of plasma polymerisation.

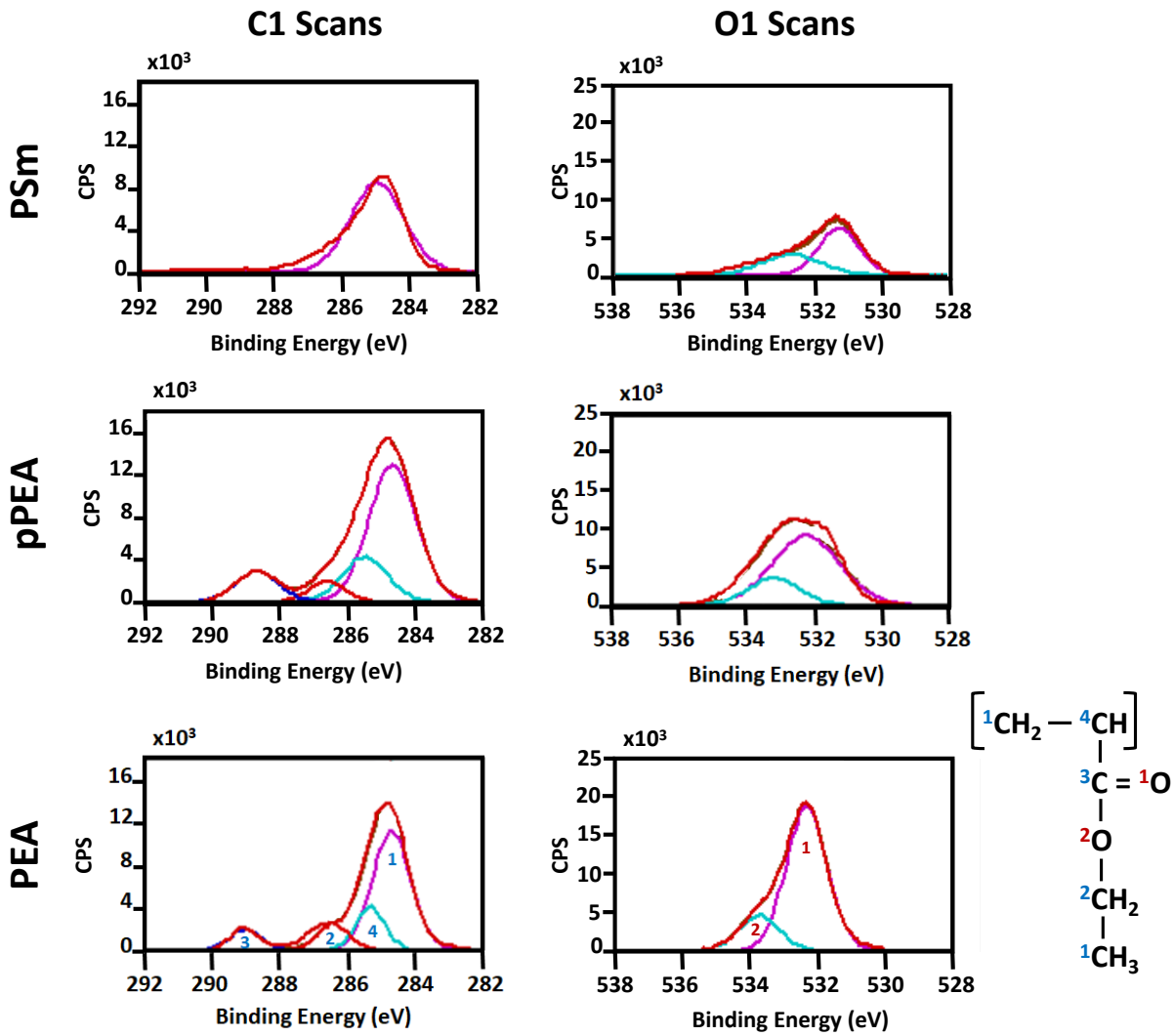

Figure 4.7 XPS for plasma coated microbeads.
Figure shows the carbon and oxygen scans for PEA, polystyrene microbeads (PSm) and PEA plasma coated microbeads (pPEA). The chemical formula for PEA is outlined in the top right for the figure annotated to match the components with the peaks present in the scans (blue for carbon, red for oxygen). The peaks as seen on the PEA spectra left to right for carbon are; peak 3 carboxyl group (dark blue), peak 2 ester bond (red), peak 4 carbon-carbon backbone with sidechain (light blue) and peak 3 carbon-carbon backbone without sidechain (pink). The peaks as seen on the PEA spectra left to right for oxygen are; peak 2 ester bond (light blue) and peak 1 carboxyl group (pink).

XPS was performed to investigate the chemical changes caused by UV polymerisation (Figure 4.8) with PEA and PSp controls along with a sample

treated only with the photoinitiator BPO and the final samples treated in 5% EA solution or 20% EA solution. There is a clear difference between the scans for PEA and the PSp allowing easy comparison with other samples to assess the success of the treatment and introduction of PEA. BPO scans for carbon and oxygen are almost unchanged from the PSp except for the loss of the peak seen on the carbon scan at 292 eV, this is an Auger peak produced by the presence of the aromatic ring on the PS, its absence suggests masking or loss of this ring. 5% EA treatment carbon scans show the introduction of carboxyl and ester peaks present in PEA sidechains but absent from PSp confirming the successful addition of PEA to the surface. The Auger peak seen at 292 eV is seen in this scan as in the PSp suggesting that the PEA present is not thick enough to fully mask the underlying base material in the scan.

A second oxygen peak is present at ~534 eV which is absent for PSp but seen on PEA representing C-O-C bonding further confirming the presence of PEA in the scan. For the treatment with 20% EA, like with 5%, there is and introduction of carboxyl and ester peaks, at ~289 eV and ~286.5 eV respectively, consistent with those seen in the PEA scans while being absent from PSp. The absence of the Auger peak at 292 eV is also noted indicating that this treatment potentially creates a thicker coating of PEA able to mask the base material fully compared to the 5% EA treatment. For treatment with 20% EA, when compared to the 5% EA, there is an obvious increase in the peaks on both the oxygen and carbon scans with the exception of the peak at 292 eV on the carbon scan which is absent on this sample and the peak between 285-286 eV which appears slightly reduced for this condition compared to 5% EA.

When comparing to the PSp and PEA scans it can be concluded that PEA is present on the surface of the samples. It is clear upon comparing the spectra for 5% and 20% EA that the higher concentration of EA solution used in the process increases the PEA on the surface of the samples. Also, the absence of the peak at 292 eV shows less or none of the base polystyrene is being recorded in the scan suggesting a thicker layer of PEA beyond the scan range (≤10 nm).

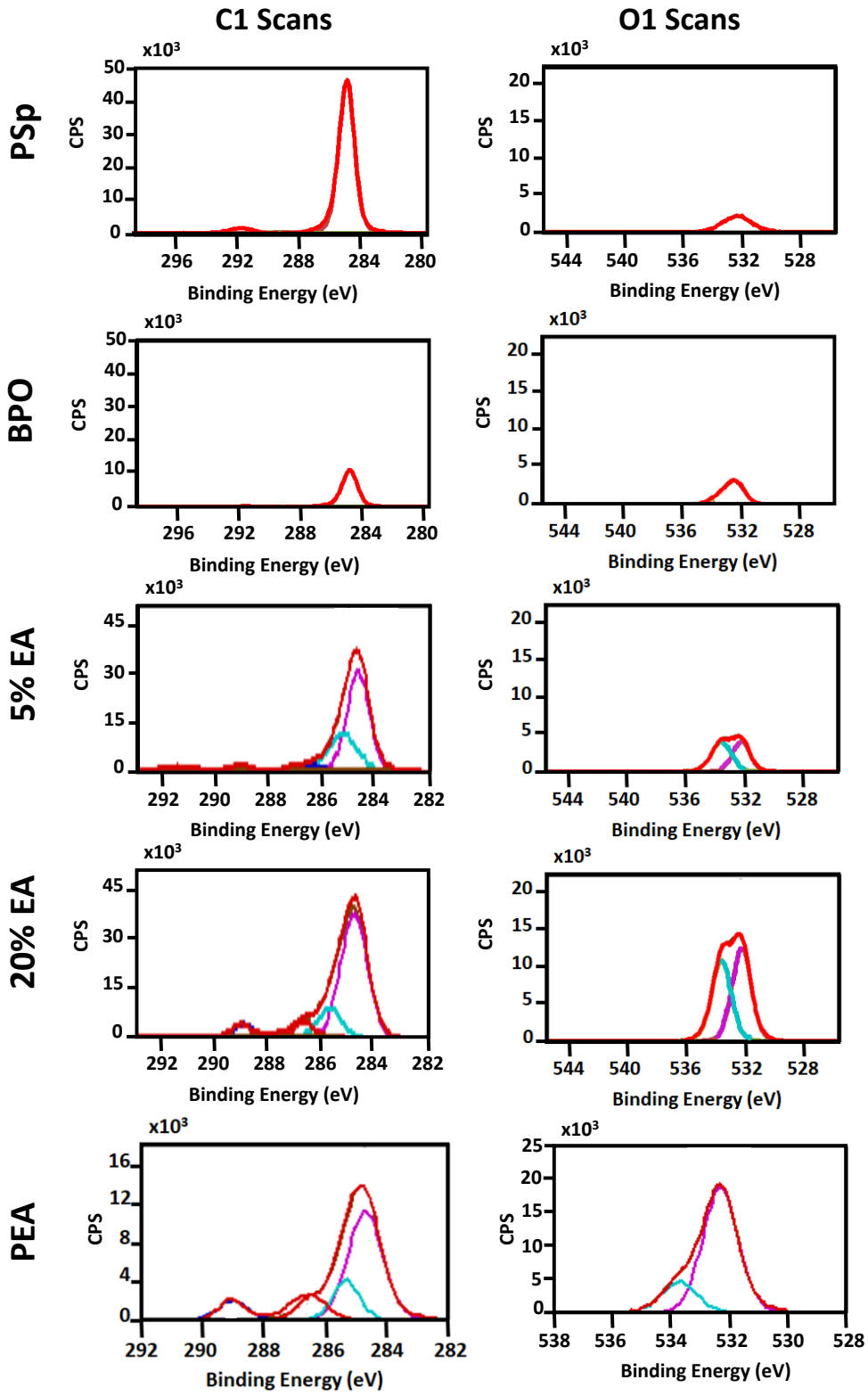

Figure 4.8 XPS for UV polymerised polystyrene.
The figure shows the XPS carbon, oxygen and nitrogen scans for PEA and PSp controls polymerisation with 5% and 20% EA as well as the BPO initiator stage of the polymerisation. It should be noted that PEA is on a different scale to the other samples but still represents the binding composition. Auger peaks are labelled while all other peaks related to the binding composition of the surfaces are described in main text. The peaks are as described in Figure 4.7.

XPS results for SI-ATRP (Figure 4.9) were less conclusive than those for plasma and UV polymerisation. There is an introduction of peaks on the bromine (Br3D) scans for the brominated samples confirming the successful introduction of the bromine-based initiator onto the surface. The bromine peaks present in the fully treated samples suggest that the subsequent polymerisation was unsuccessful, and the initiator did not react as planned. For oxygen scans of bPEA, samples are similar to the PEA control while the brominated sample was consistent with the PSm control, suggesting that while the polymerisation was not obviously successful some chemical modification did take place. For the carbon scan, however, brominated and bPEA samples were observed to have similar spectra to that of PSp with the exception of the loss of the Auger peak representing the aromatic ring. This indicates that there were some changes occurring with polymerisation particularly from the oxygen scans though not to the extent that would be required for sufficient introduction of PEA.

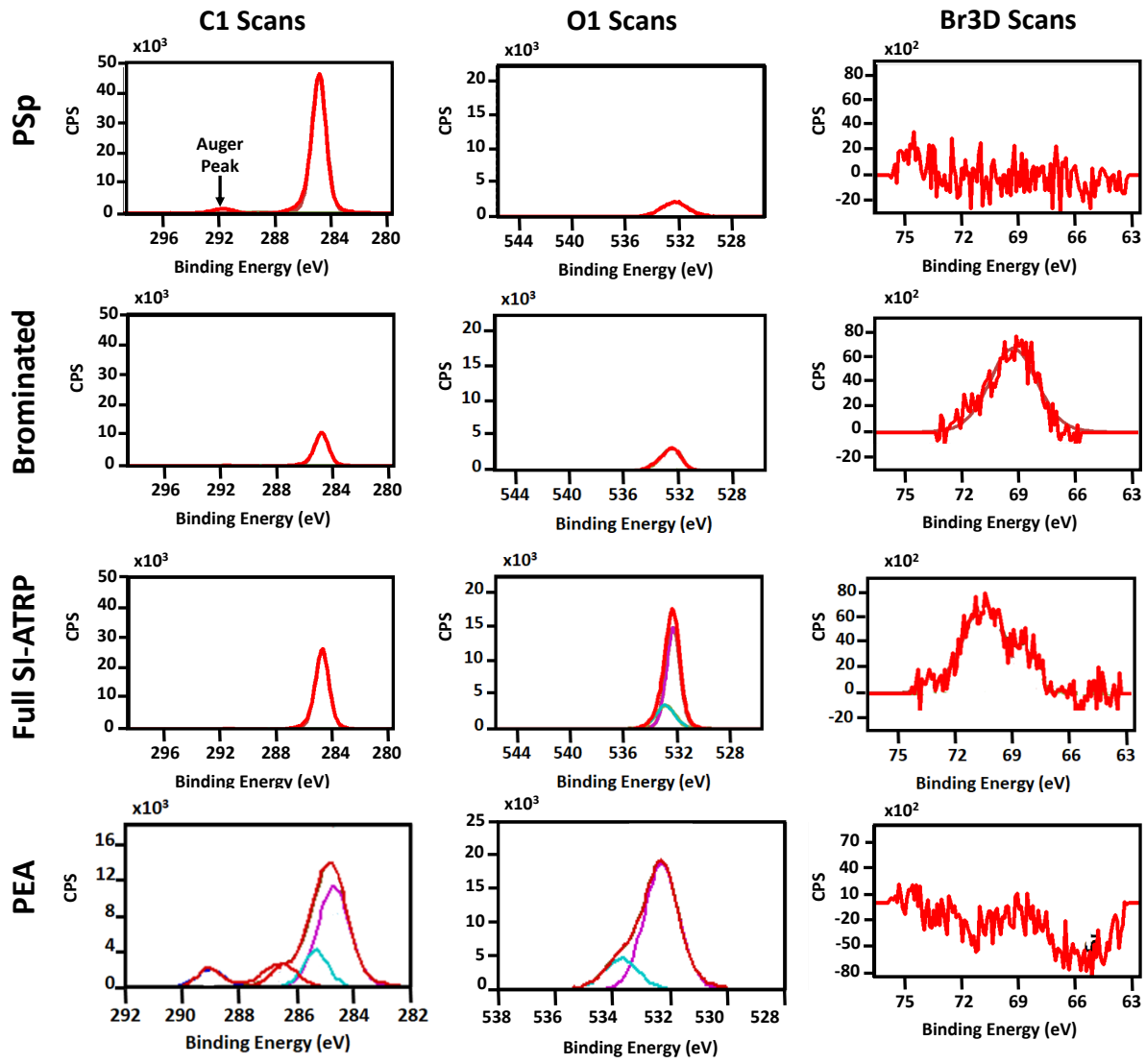

Figure 4.9 XPS for SI-ATRP treated polystyrene.
The figure shows the XPS carbon, oxygen and bromine scans for PEA and PS control samples along with samples taken at the bromination stage and samples that have undergone the full SI-ATRP protocol (bPEA). Auger peaks are labelled while all other peaks related to the binding composition of the surfaces are described in main text. Peaks are as described in Figure 4.7.

4.3.4 FN Networks

AFM was used to confirm the presence of FN networks through imaging surfaces at the nanoscale on PEA surfaces created through various methodologies; spin coating, plasma polymerisation and UV polymerisation. SI-ATRP samples were not used for AFM imaging due to the XPS results showing insufficient polymerisation. The images below (Figure 4.10) show height scans with the colour scale shown on the right of each image. FN networks were visualised in all three samples though the organisation of the network varied depending on the

methodology used to incorporate PEA. Similarities are seen in the network produced through spin coating and plasma treatment with dense FN networks seen on both surfaces, though pPEA appeared denser. This was different to the sparser and more spread network which appeared on the UV polymerised samples. The height measured on each of the images varied with uvPEA showing fibres at 4 times the height of scPEA and pPEA. Though they appear different FN networks can be confirmed on all PEA surfaces showing the maintenance of polymer functionality after each process.

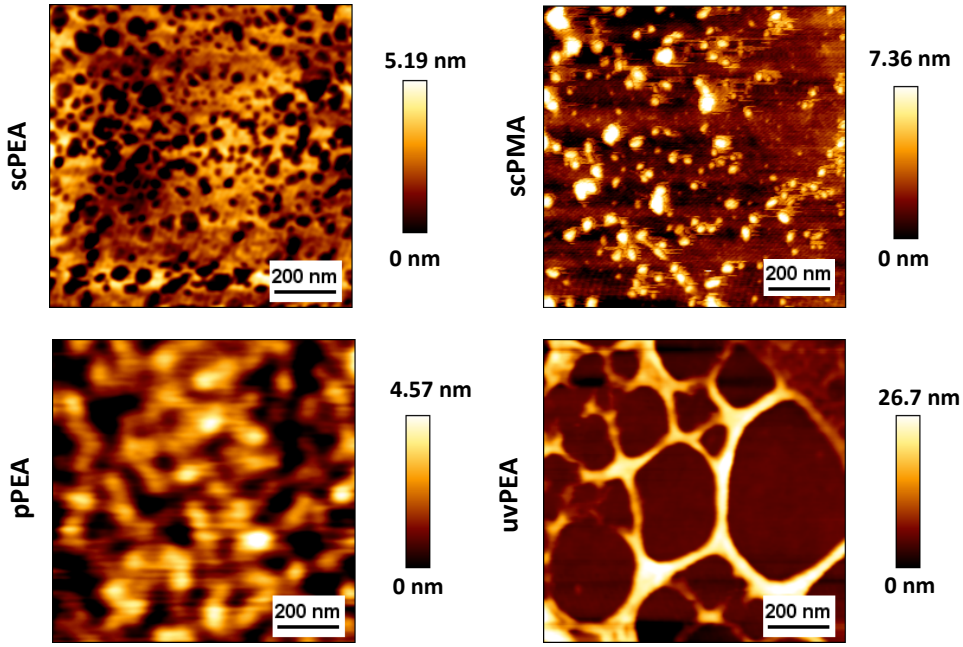

Figure 4.10 AFM images of FN networks on PEA surfaces.
Figure shows 1 x 1 μm height images produced using AFM to visualise FN networks on PEA surfaces produced through either spin coating (top), UV polymerisation (bottom right) or plasma polymerisation (bottom left). Scale bar shows 200 nm on each image and colour scale varies for each. The scPMA sample was used as a control to show FN in the globular formation as a comparison to the network shown on scPEA. All PEA coatings produce a FN network though each network has variations in the fibre height/ width.

Due to the difficulty of imaging the PSm resulting from their small size and curvature AFM could not be used and so fluorescence microscopy was used to confirm FN adsorption. Figure 4.11 shows confirmation that FN could be adsorbed onto the pPEA coated PSm. A control, scPEA, coverslip was used for comparison, it is clear from observation that FN is present in both samples. Uncoated PSm were also tested for FN adsorption, a small amount of FN was thought to be present due to areas of slightly higher fluorescence however, this

was difficult to define compared to that seen on pPEA and scPEA due to higher background autofluorescence of the beads.

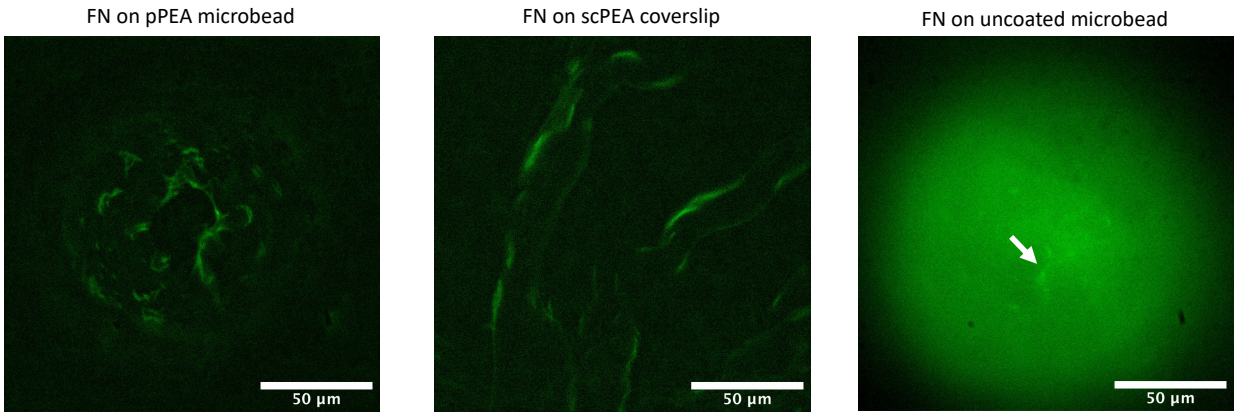

Figure 4.11 Fluorescently tagged FN on PEA surfaces.
The figure shows images of DyLight 488 fluorescently tagged FN which has been adsorbed onto PEA plasma (pPEA) coated microbeads, PEA spin coated (scPEA) coverslips and an uncoated PS microbead. Arrow used to indicate area of higher fluorescence on uncoated microbeads assumed to be FN.

4.3.5 Cells on Surfaces

In chapter 3 it was shown that encapsulating cells directly into PEG hydrogels resulted in low viability, a lack of cell spreading was observed in these conditions. Due to these results the model was altered to include a surface for the cells to adhere and spread. After assessing various methods for introducing a PEA surface to the model cell work was continued with pPEA coated microbeads or scPEA coverslips. Live dead staining was carried out to test the viability for cells seeded on a scPEA coverslips with gels, 5% PEG 25% VPM degradable crosslinker, formed on top (Figure 4.12). The mean viability after 1 week of culture sat at 88% rising to 89% after 3 weeks, no statistical differences were found between these time points showing a maintenance of cell viability over long term culture. A slight dip in viability was observed at week 2 with the mean dropping to 77%, this is still above that seen when cells were encapsulated within the gels and with the recovery at week 3 did not cause concern.

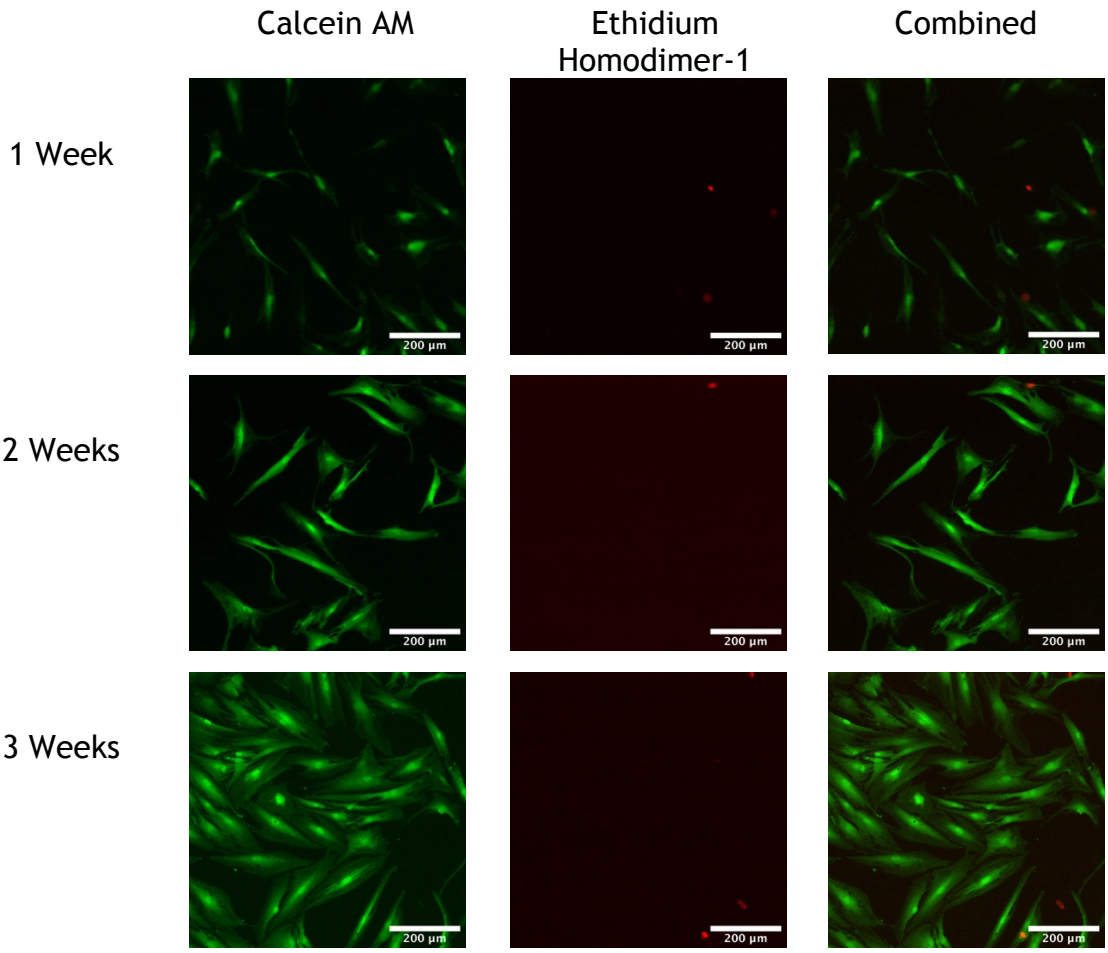

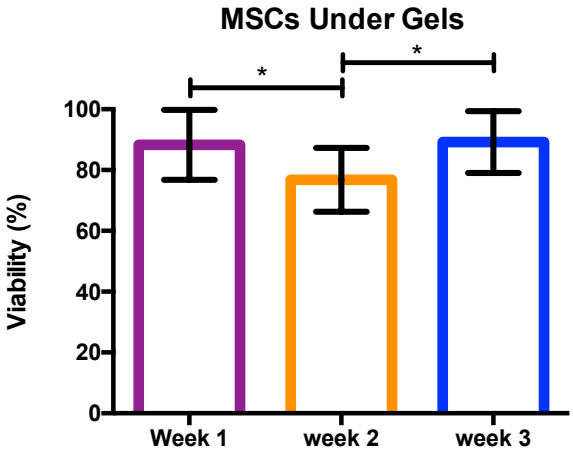

Figure 4.12 Live dead results for MSCs under gels.
This figure shows example images taken for each time point covered looking at MSCs seeded under 5% PEG hydrogels. The graph shows mean +/- SD, viability quantified from the images gathered from 3 biological replicates and analysed using image J. A significant difference is observed between the viability at week two compared to week one and three where *$p \leq 0.05$. The shows good viability for cells seeded below gels on a PEA coated coverslip.

Live dead staining was also carried out on cells which had been seeded onto pPEA treated microbeads with FN adsorbed and encapsulated into gels. Images collected from this could not be quantified accurately, due to the curvature of the beads it was difficult to focus and define cells. The images could, however, be assessed qualitatively. Cells were present at both time points with far less dead staining visible compared to live staining at each position (Figure 4.13). The increased viability appeared to follow the same trend as seen for coverslips at the same time points suggesting that the introduction of a stiffer surface within the gel improved cell viability allowing the maintenance of a cell population in the gels over time.

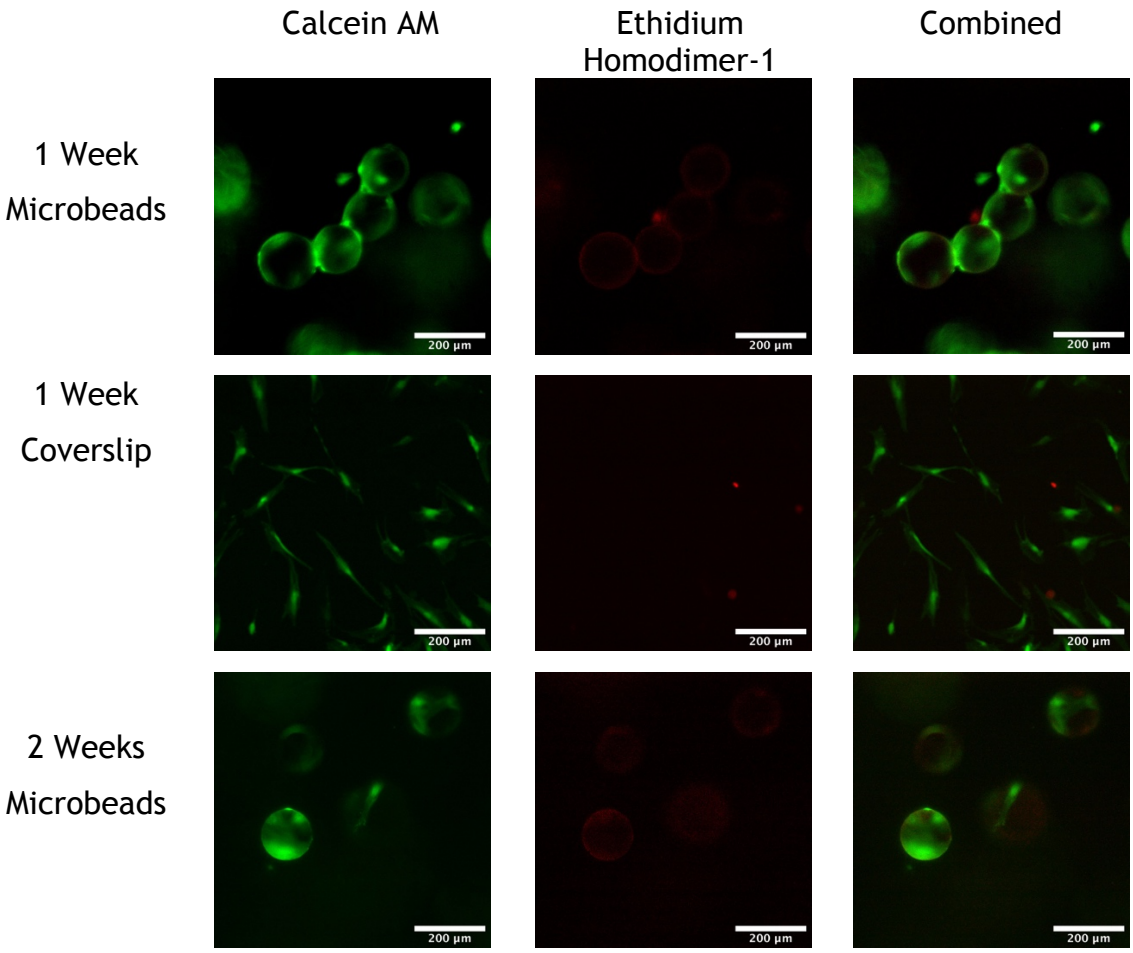

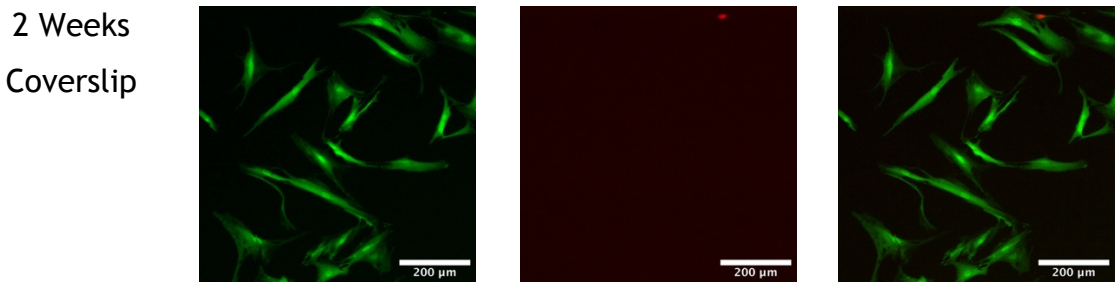

Figure 4.13 Live dead staining for MSCs on beads within gels.
The figure shows example images taken of MSCs which have been seeded onto microbeads and encapsulated into degradable 5% PEG hydrogels after live / dead staining. This shows that the cells remained comparatively viable when seeded onto the beads and encapsulated within the gels as when seeded under gels onto coverslips.

Due to the difficulty experienced in imaging with the 3D nature of the microbeads within the gels confocal imaging was used to observe the cells more clearly. Cells were stained for actin to highlight cell spreading and DAPI to highlight the nuclei of individual cells. Four conditions, PEGFN gels with or without GFs (BMP-2 and NGF) and PEG gels with or without GFs, were used and cultured for 3 weeks before staining, all gels were 5% PEG gels with 25% VPM degradable crosslinker. Figure 4.14 shows images selected from the z stacks that show various features observed. A slight sprouting from the bead was observed in gels containing FN where GFs were also present on the beads. PEGFN gels without the presence of GFs show how cells appear to have the ability to adhere between 2 beads holding them together. In the PEG gel with GFs the nuclei appear clumped together while actin staining shows the cells spreading over the whole bead. In the final condition of PEG without GFs a section of the bead appears to be avoided by the cells this may be the section of the bead that would be uncoated during plasma treatment therefore making it less favourable for cell adhesion compared to surrounding areas.

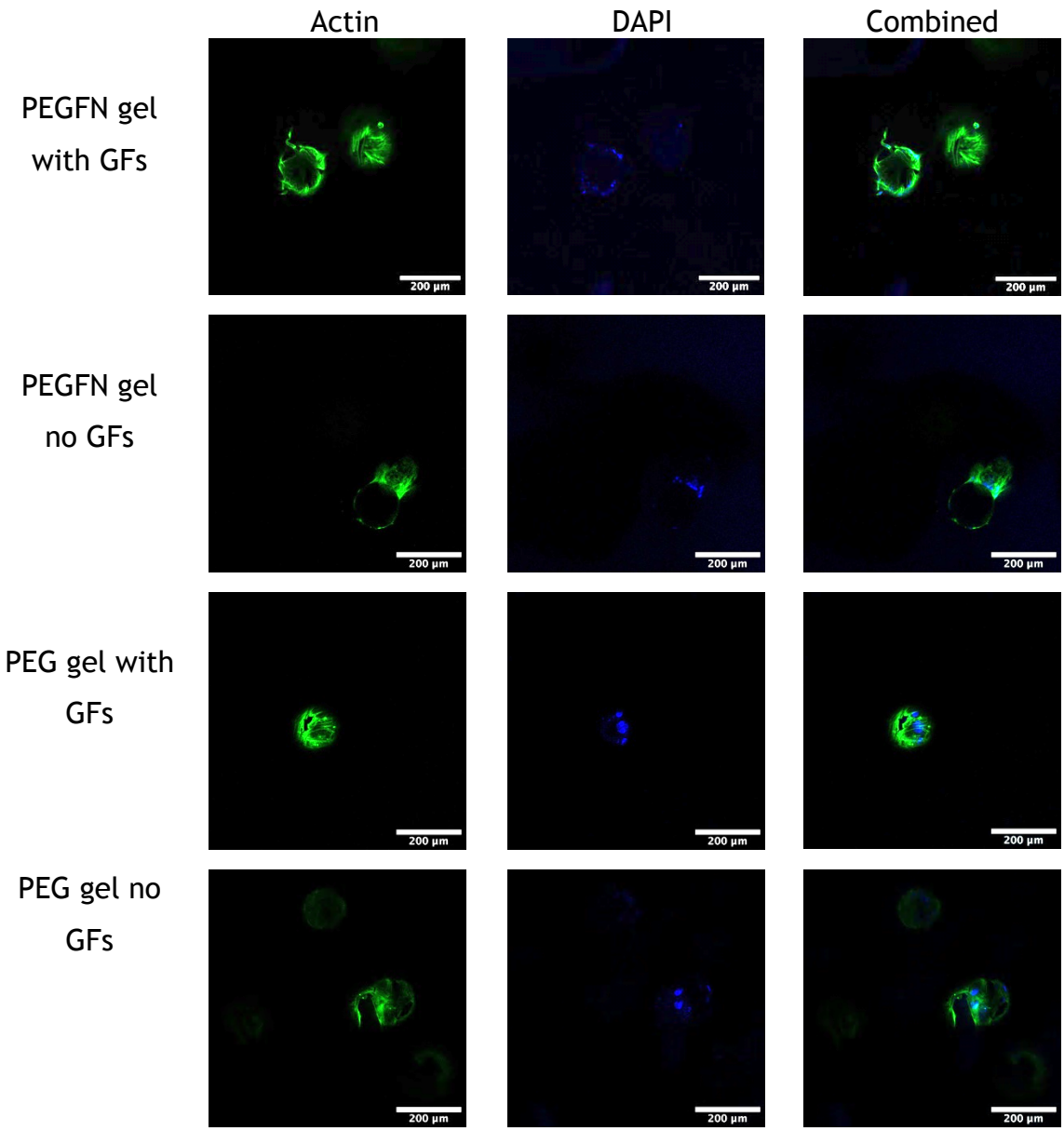

Figure 4.14 Confocal images of MSCs on beads after 3 weeks culture.
The images above show Actin (green) and DAPI (blue) staining of cells adhered onto microbeads coated in FN and in some conditions (with GF) containing BMP-2 + NGF. These were encapsulating into 25% degradable PEG or PEGFN hydrogels.

4.4 Discussion

Due to the low cell viability observed when cells were encapsulated directly into the PEG hydrogels a stiffer surface was introduced to the model, the development of this surface has been outlined in this chapter. The introduction of a surface allowed for the inclusion of another polymer, PEA, providing additional functionality and control to the final model. Microcarrier beads (corning) were chosen to be encapsulated within the gels to allow cell adhesion while retaining the advantages of the cells being held within the gel. In this chapter we investigated the effectiveness of various surface modification techniques on incorporating PEA on to a PS surface representing the base material of the microbeads. The incorporation of PEA is favourable for the model due to the relationship with the ECM protein FN (Salmerón-Sánchez *et al.*, 2011; Cantini, González-García, *et al.*, 2012). The relationship with FN inducing the formation of protein networks leads to improved cellular adhesion and provides a means to incorporate and allow solid-phase presentation of growth factors enhancing cellular interactions and control within the model (Llopis-Hernández *et al.*, 2016).

The various surface modification techniques included spin coating, plasma polymerisation and SI-ATRP which were previously established for use with PEA (Llopis-Hernández *et al.*, 2016; Cheng *et al.*, 2018; Sprott *et al.*, 2019). Spin coating was only viable for use on flat surfaces, for example coverslips, due to this limiting factor spin coated PEA was only used for comparison with WCA, to show PEA networks using AFM and for cell viability quantification. A decrease in hydrophobicity was shown in the WCA results between scPS and scPEA on a glass coverslip using the spin coating technique with scPEA showing similar results to previously published data (Guerra *et al.*, 2010; Alba-Perez *et al.*, 2020). Spin coated PEA was then used to compare to the other modification techniques looking for similar trends in WCA with the introduction of PEA. Both plasma treated and UV polymerised samples showed no significant difference to the scPEA this corresponded to results seen in the literature for pPEA surfaces (Alba-Perez *et al.*, 2020). These results suggested a similar surface chemistry though this could not be used to definitively confirm the presence of PEA. This change in hydrophobicity with the introduction of PEA also has the potential to improve cellular attachment as it has been shown in the literature that hydrophilic

surfaces promote enhanced cellular adhesion (Chuah *et al.*, 2015). SI-ATRP however, saw a statistically significant difference when compared to scPEA and no notable difference when compared to the scPS. This suggests that after treatment the surface either remains unchanged or maintains the hydrophobic properties of the PS base material. It should be noted that damage occurred on samples treated via SI-ATRP resulting in swelling of treated PSp and peeling of scPS from the glass coverslips which could also influence WCA results.

FTIR was carried out to measure the bulk composition of samples after the various treatments and compared to untreated samples as well as bulk PEA. No changes were observed between the untreated PS and the treated samples for pPEA and uvPEA. It has been noted in literature that XPS should be chosen over FTIR when investigating surface modifications that effect the material on a nanometer level due to the technique reading the bulk material (Morent *et al.*, 2008). This is thought to be why no changes were seen in the plasma and uv treated samples, the layer of PEA produced through plasma treatment has been shown to be in the nm range, ~ 34 nm (Cheng *et al.*, 2019; Alba-Perez *et al.*, 2020). Therefore, it can be assumed with the FTIR results that the layer produced by UV polymerisation is also within a nm range, this could be confirmed through further characterisation such as a scratch test. For SI-ATRP samples, we were able to see changes in the FTIR spectra when compared to the PSp untreated sample. These confirmed changes in the surface chemistry had occurred through the treatment. However, much like WCA, these could not be used to definitively confirm PEA presence only that chemical modification had occurred. After confirmation of changes on all samples, through either WCA or FTIR results, they were all sent for XPS analysis to determine if the modifications had resulted in a PEA layer on the surface.

XPS measures the top ~10 nm of a sample (Mather, 2009) and was used to determine the presence of PEA on a sample after treatment. The results confirmed the presence of PEA on plasma treated microbeads and UV treated polystyrene pellets (Figure 4.7 & Figure 4.8), showing spectra that were almost identical to control PEA and modified from bulk PS samples. Plasma treatment has been previously shown to successfully coat PEA onto various base materials (Cantini, Rico, *et al.*, 2012; Cheng *et al.*, 2019; Alba-Perez *et al.*, 2020), the

results in this chapter confirmed that the treatment was successful in incorporating PEA onto the PS microbeads. XPS results for SI-ATRP were less conclusive, though there were changes the spectra did not definitively represent PEA on the surface concluding that this technique would need further optimization if it were to be used. Though the XPS scans confirmed the success of bromination through presence of a bromine peaks, the lack of definitive PEA polymerisation is possibly due to low initiator activity. This could be improved through the introduction of a further step to create more active initiation points at the bromination stage. If continued the process would also be altered to minimise chemical damage to the base polystyrene which underwent some swelling with the current method. On optimisation of this protocol samples would then have to be tested for degradation, mechanical properties and functionality to assess if it could be a better method to the current plasma treatment. Due to the success of the other techniques SI-ATRP was not developed past this point though it has potential for future modification.

After the confirmation of successful incorporation of PEA through plasma treatment and UV polymerisation the functionality of the polymer was tested. As previously mentioned, PEA induces the formation of FN nanonetworks due to its unique chemistry (Cantini, González-García, *et al.*, 2012; Llopis-Hernández *et al.*, 2016). AFM imaging was used to ensure that the PEA surfaces produced through each technique retained the ability to drive formation of these FN nanonetworks as seen on spin coated samples. Results revealed the formation of networks on spin coated, plasma polymerised and UV polymerised PEA surfaces when FN was introduced. Networks observed on plasma polymerised samples were denser than those seen on spin coated samples, this corresponds to previous results in the literature (Cheng *et al.*, 2019; Alba-Perez *et al.*, 2020). Networks seen on UV polymerised surfaces appeared sparser with an increase in fibril height compared to those seen on plasma and spin coated samples. This is likely due to UV polymerisation producing polymer brushes rather than simply coating the surface, as with pPEA and scPEA, as it is similar to the networks observed in a previous study which introduced PEA brushes through SI-ATRP (Sprott *et al.*, 2019).

Though UV treatment was shown to be successful and a viable method for coating 3D materials further investigation would be required to refine the method for ideal PEA coverage. As was shown in the XPS results changing the volume of monomer in the solution used for polymerisation resulted in an increase in the polymer detected on the surface (Figure 4.8). Factors like this as well as the mechanical properties would have to be tested further to develop the method to the point of use. Other properties of the surface would have to be investigated like the degradation over time and FN functionality when adsorbed onto the surface for example using *in vitro* analysis to assess the availability of the various binding domains. This method has lots of potential for future use in creating PEA surfaces for cell studies but was not developed further due to the optimisation required and established method of plasma polymerisation.

Plasma polymerisation was chosen as the technique to coat the microbeads for continuing to develop the *in vitro* model. This is due to the established success of plasma polymerisation shown in previous *in vitro* and *in vivo* studies (Cheng *et al.*, 2019; Alba-Perez *et al.*, 2020) alongside the positive results obtained for PS outlined in this chapter. Plasma polymerisation was successful in coating the chosen microbeads showing the ability to coat 3D materials while maintaining the ability to adsorb FN. The lack of any obvious chemical alterations from the bulk characterisation technique FT-IR through plasma polymerisation may be regarded as a positive result. XPS showed definitive PEA chemical composition this shows that plasma polymerisation while successfully able to incorporate PEA onto the PSm does not induce significant chemical alterations. Fluorescently tagged FN was used to confirm adsorption of FN on pPEA coated microbeads as this could not be imaged through AFM due to the curvature. Though networks could not be visualised by this method FN could be confirmed on the surface and it was hypothesised that networks would therefore form as on the 2D surface used for AFM.

Table 4.1 Summary of the results from each technique.

	Spin coating	Plasma	UV	SI-ATRP
WCA	scPEA more hydrophilic than scPS	pPEA more hydrophilic than scPS	uvPEA more hydrophilic than scPS	Similar to contact angle for scPS
FT-IR	No FT-IR performed for these samples	No changes observed through FT-IR	No changes observed through FT-IR	Changes in FT-IR confirm chemical modification
XPS	No XPS performed for these samples	XPS confirms presence of PEA	XPS confirms presence of PEA	XPS not consistent with presence of PEA
AFM	AFM confirms presence of FN networks	AFM confirms presence of FN networks	AFM confirms presence of FN networks	No AFM performed on these samples

The inclusion of pPEA treated microbeads and scPEA coverslips was observed to increase cell viability (Figure 4.12 & Figure 4.13). This resolved the previous issue of low viability seen when cells were seeded directly into the gels suggesting this was caused by a lack of cell adhesion within the gels. The higher viability quantified in the new system allowed for adaptation of the final model into two possible set-ups. Firstly, a model that had been utilised with a collagen gel previously within our lab (currently unpublished data) where cells are seeded onto PEA coated coverslips with the gel introduced on top (Figure 4.15 A). This would be used switching out the collagen gel for the PEG gels investigated in this work, collagen gels were replaced due to difficulty in full controlling biologically sourced gels as discussed previously (1.7.2). Secondly a model where the stiffer surface would be introduced within the gel through the encapsulation of

microcarrier beads on which cells could be seeded prior to encapsulation (Figure 4.15 B).

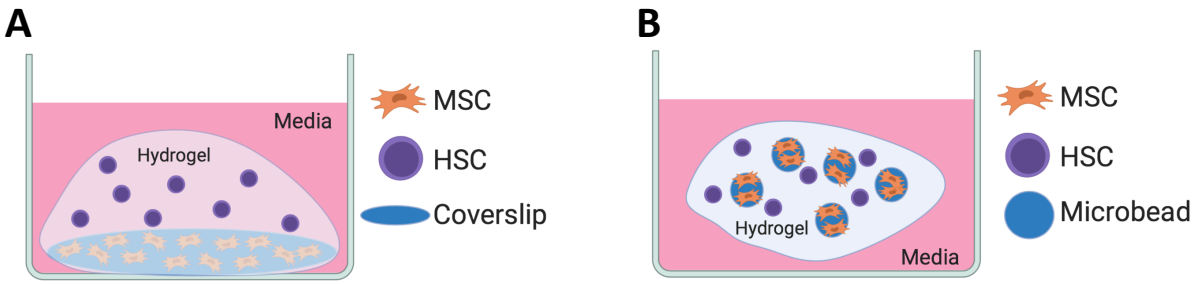

Figure 4.15 Proposed set up for final niche models.
The figure shows the two proposed models for introducing a PEA surface to the niche models. A shows the use of a PEA coated coverslip onto which MSCs could be seeded with HSCs encapsulated in the PEG hydrogel formed on top. B shows the use of PEA coated microbeads that can be encapsulated within the gel.

In conclusion, this chapter has outlined the development of surface modification techniques to introduce a PEA coating onto PS microbeads. This was carried out to achieve similar functionality observed in previous 2D systems, such as seeding cells on spin coated PEA with gels formed on top, in a 3D model. Successful PEA coatings were achieved using plasma polymerisation and UV polymerisation, due to its previous optimisation plasma was continued for *in vitro* studies. Cells were shown to adhere to these surfaces with improved viability over cells encapsulated straight into gels. FN has been show to adhere to beads and is assumed to form networks as shown using 2D samples.

Chapter 5 The Model

5.1 Introduction

In vitro modelling is commonly used following tissue engineering principles to investigate cell behaviour under controlled conditions such as drug treatments (Baguley and Marshall, 2004). *In vitro* modelling has become more popular driven by the easier use of techniques for cell analysis but also the ethics and public opinion that surround the use of *in vivo* animal modelling (Ashrafian, Ahmed and Athanasiou, 2010). This has led to the development of many *in vitro* modelling techniques aimed to mimic the *in vivo* conditions including the use of co-cultures and materials such as hydrogels.

A major difference between early *in vitro* modelling and *in vivo* conditions was the 2D nature of most tissue culture techniques. One way in which this has been overcome is the use of hydrogels to introduce a 3D matrix that can mimic the ECM (Tibbitt and Anseth, 2009; Geckil *et al.*, 2010). Collagen gels are commonly used when producing bone marrow niche models as they have been shown to enhance osteogenic differentiation and mimic the elastic properties of the bone marrow (Schneider *et al.*, 2010; Metzger *et al.*, 2014). Collagen gels, however, due to their biological source have a batch to batch variation that can influence experimental results when used in a model. To overcome this, synthetic gels are becoming increasingly popular for *in vitro* modelling, such as PEG (Burdick and Anseth, 2002). The use of synthetic gels over biologically sourced gels allows more control and understanding of the influencing factors within a model.

An important function of the ECM is to allow the diffusion of essential nutrients, signalling molecules and waste (Mouw, Ou and Weaver, 2014). This is a central property to consider when developing an *in vitro* model, so that essential molecules and influencing factors introduced to the culture such as growth factors or drugs can reach the cells. Another factor to consider is the ability of the ECM to immobilise secreted molecules within the matrix creating a reservoir effect which can surround the cells with signalling molecules influencing behaviour (Frantz, Stewart and Weaver, 2010).

The use of co-cultures allows cell types found within the same tissue and that interact *in vivo*, to have the same interactions *in vitro*, maintaining biological cues. An example is the use of a stromal layer when culturing HSCs to mimic the cells within in the bone marrow. This technique has been shown to successfully induce the maintenance and proliferation of a HSC population *in vitro* (Dexter, 1982; Leisten *et al.*, 2012).

MSCs, particularly those which are found to be nestin positive, have been shown to be important within the bone marrow niche due to their expression of HSC maintenance factors and are commonly used within niche models (Méndez-Ferrer, T. V. Michurina, *et al.*, 2010; Pinho *et al.*, 2013). Along with nestin, Stro-1 positive MSCs have also been shown to support HSCs and is important to consider within niche modelling (Kolf, Cho and Tuan, 2007). ALCAM is another MSC marker that can show the maintenance of the MSC phenotype in culture (Nakamura *et al.*, 2010). It is important to be able to define the maintenance of an MSC population for long term culture of the model as differentiation may occur resulting in the depletion of these cells.

Though the maintenance of an MSC population is favourable within a bone marrow niche model, some differentiation, particularly osteogenic, can be beneficial due to the role of osteoblasts within the niche. Osteoblasts have been shown to produce HSC maintenance factors such as IL-6, SCF, and CXCL-12 and have been well characterised for their key role in supporting HSCs within the endosteal niche (Calvi *et al.*, 2003; Nakamura *et al.*, 2010). Due to this expression of HSC maintenance factors, some osteogenic differentiation within the MSC population can be desirable for niche models. This can be investigated looking at the expression of osteocalcin (OCN) and osteopontin (OPN) which are expressed during the stages of osteogenic differentiation (Yang *et al.*, 2014).

There are many proteins that have been linked to roles in HSC maintenance, one which has been well characterised is SCF (Calvi *et al.*, 2003; De Ugarte *et al.*, 2003; Ding *et al.*, 2012).When introduced to *in vitro* HSC cultures, SCF has been shown to increase self-renewal and maintenance of the HSC population (Ema *et al.*, 2000; Walasek, van Os and de Haan, 2012). It has been shown that HSCs become less sensitive to SCF as they mature despite expressing the same number of receptors, making it important that the cells within a niche model excrete a

high enough level to influence the HSCs (Zhang and Lodish, 2008). VCAM-1 is another protein well characterised as a HSC maintenance factor, which is important for the co-localisation of HSCs to MSCs and osteoblasts (Kopp *et al.*, 2005). This is key within a niche model as closer localisation to MSCs and/or osteoblasts will expose the HSCs to factors secreted by those cells.

The aims of this chapter were to assess the hydrogels ability to mimic the ECM in allowing the diffusion of soluble proteins throughout the matrix and the retention of proteins relevant to the bone marrow niche. To assess the MSC phenotype within the final model looking to maintain a stem-like, nestin and Stro-1 positive, MSC population while inducing some osteogenic differentiation shown through OCN and OPN expression along with the expression of HSC maintenance factors SCF and VCAM-1.

5.2 Methods

Cell culture, ICW, immunostaining, GF tagging and material preparation is described in the general methods Chapter 2 (2.2.1, 2.2.2 and 2.2.5).

5.2.1 Growth Factor Diffusion and Release

Diffusion

Hydrogels were produced as described in section 2.2.4 with conditions PEG only, PEGFN and PEGFN with VPM, n=3 for each condition. The gels were then swollen overnight in PBS. After swelling the gels were placed in a solution of PBS containing 5 μg/mL of 488 tagged NGF (2.2.5) and left for 24 hours protected from the light and incubated at 37 °C. The gels were then removed from the solution, quickly rinsed with fresh PBS to wash excess GF solution from the outside and mounted on glass bottom petri dishes with VECTASHIELD mounting media to prevent drying during imaging. Imaging was carried out using confocal microscopy on a Zeiss LSM 880 at 10X magnification (Figure 5.1). Z-steps were taken through the gel comprising of 42 images each with an interval of 5 μm between each image in the Z plane. Images were then analysed using ImageJ software, where fluorescence was quantified by measuring the integrated density for the different regions of the gel to investigate the efficiency of diffusion. The quantified data was then analysed using GraphPad Prism software.

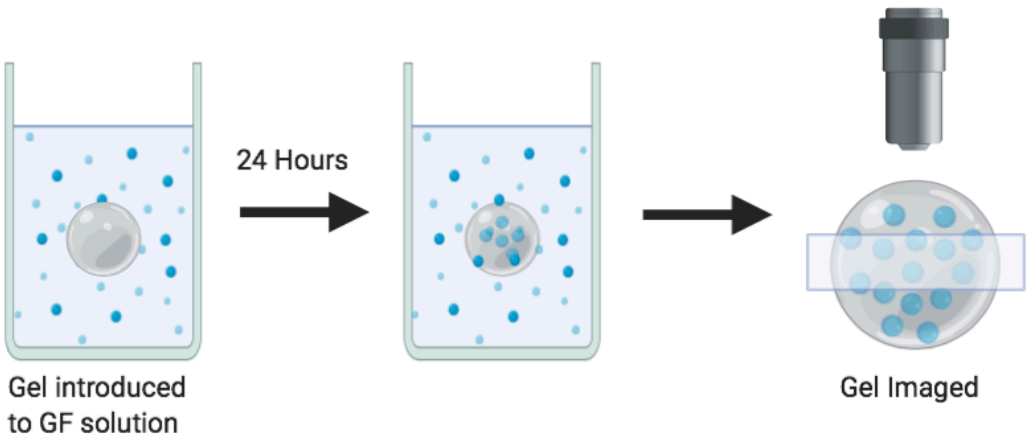

Figure 5.1 Schematic of the diffusion assay method.

PEG hydrogels were added to a tagged GF solution and left for 24 hours to allow diffusion. These were then imaged throughout the width of the gel from one edge to the other using confocal microscopy. Created using BioRender.com.

Release

Release assays were carried out for SCF, Flt-3, CXCL12 and TPO that had been tagged with Dylight 488 dye (2.2.5). A standard curve was produced using 8 solutions starting from 10 μg/mL halving the concentration at each point with the final solution being blank. Hydrogels were prepared (2.2.4) with PEG only, PEGFN and PEGFN with VPM conditions, n=3 for each condition. 488 tagged cytokines were incorporated into the gels at a final concentration of 10 μg/mL before gelation. Gels were protected from the light from the point of adding the tagged cytokines. After gelation was complete gels were transferred into PBS and incubated at 37 °C. PBS was removed at each time point, 3 hours, 6 hours, 24 hours and 48 hours and replaced with fresh PBS. The PBS removed at each time point was used to measure fluorescence using a plate reader (BIOTEK) with Ex/EM wavelength set at 493/518 nm (Figure 5.2). Analysis of collected data was carried out using GraphPad Prism software.

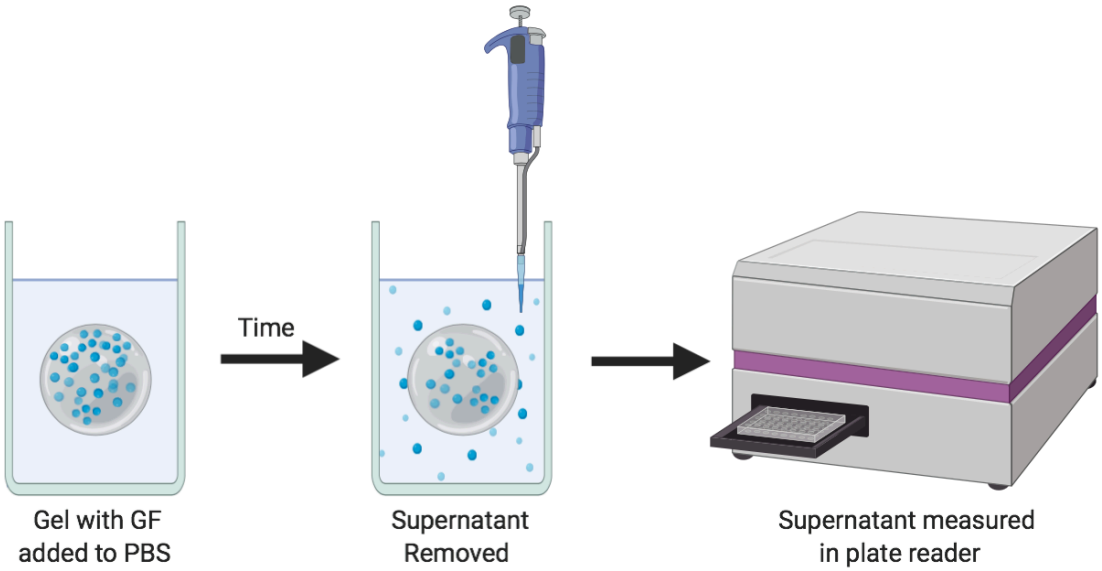

Figure 5.2. Schematic of the release assay method.
Gels loaded with tagged GFs are placed into PBS then after set time points the supernatant is removed and the fluorescence measured using a plate reader to show the release over time. Created using BioRender.com.

5.2.2 PCR

RNA extraction

Cells had to be extracted from gels before RNA extraction could be carried out. The gels were first digested using collagenase D at 2.5 mg/mL with pipetting used to encourage the breakdown of the gel every 30 minutes for 1.5 hours. A cell strainer with 80 µm diameter pores was then used to remove the microbeads and undigested gel from the mix. The mixture was then centrifuged to remove collagenase and produce a cell pellet. RNA was then extracted using a MinElute spin column following the Qiagen RNAeasy micro kit protocol, DNase was used to degrade and remove any DNA from the samples. Once extracted RNA volume and purity was measured using a nanodrop, this was then used to calculate total RNA.

qPCR

Reverse transcription was then carried out using a Qiagen Quantitect reverse transcription kit following the protocol provided to produce the cDNA. This can be summarized in 2 steps, first the elimination of genomic DNA followed by the reverse transcription forming the cDNA which can then be used to carry out qPCR. PCR was carried out using the QuantiFast SYBR Green PCR kit (Qiagen) using appropriate forward and reverse primers (Table 5.1) for the genes of choice following the kit protocol. The final samples were analysed by real time-PCR using a 7500 real time PCR system (ThermoFisher). Due to a low RNA yield only 3 genes, GapDH, nestin and ALCAM, could be analysed and only 3 ng of RNA was used per sample.

Table 5.1 Forward and reverse primer sequences for markers investigated using PCR.

Marker	Forward Sequence	Reverse Sequence
GapDH	TCAAGGCTGAGAACGGGAA	TGGGTGGCAGTGATGGCA
Nestin	GAGGTGGCCACGTACAGG	AAGCTGAGGGAAGTCTTGGA

ALCAM	ACGATGAGGCAGACGAGATAAGT	CAGCAAGGAGGAGACCAACAAC

5.2.3 Confocal imaging

MSCs were seeded onto microbeads (2.2.1) before being encapsulated into 5% PEG (with and without FN) gels with 25% VPM various conditions were; gels with FN with and without growth factors (BMP2 and NGF) on the microbeads and gels without FN with and without growth factors on the microbeads. All the gels were 50 μL in volume 5% PEG with 25% VPM and all microbeads were coated in PEA via plasma polymerisation with FN adsorbed. Once gelation was complete gels were transferred to a 48 well plate and cultured for 3 weeks. Gel formation and cell seeding methods are found in general methods Chapter 2.

After 3 weeks of culture, gels were then fixed and stained for actin, nuclei and the marker of interest using monoclonal antibodies (Table 2.5) ready to be imaged using confocal microscopy. Confocal imaging was carried out on a Zeiss observer Z1 spinning disc confocal microscope. For each condition three beads were captured producing a z stack to image the entire bead with a gap of 2 μm between each slice. Actin was stained using Phalloidin 488, nuclei using DAPI and the marker of interest using Cy3 stain. Once acquired, these stacks were analysed using ImageJ software. To quantify the presence of the marker of interest the integrated density was measured, and an average taken for the whole stack for the DAPI and Cy3 images this allowed the results to be normalised to the nuclei staining.

5.3 Results

5.3.1 Diffusion Assays

Diffusion assays were carried out in order to investigate the ability of soluble molecules to enter the different gels. Images were gathered and quantified to show that molecules are able to diffuse through to the centre of all gel conditions. For the PEG only condition (Figure 5.3) a statistically significant difference was found between the edge of the gel and the points within the gel. This lower presence of NGF at the edge is thought to be down to the diffusion

gradient changing more readily at the edge of the gel with the molecules flowing in and out to reach an equilibrium with the outside conditions, perhaps some diffusing out during the short wash step. Images within the gels centre show that the tagged GFs were able to diffuse through the entirety of the gel as desired.

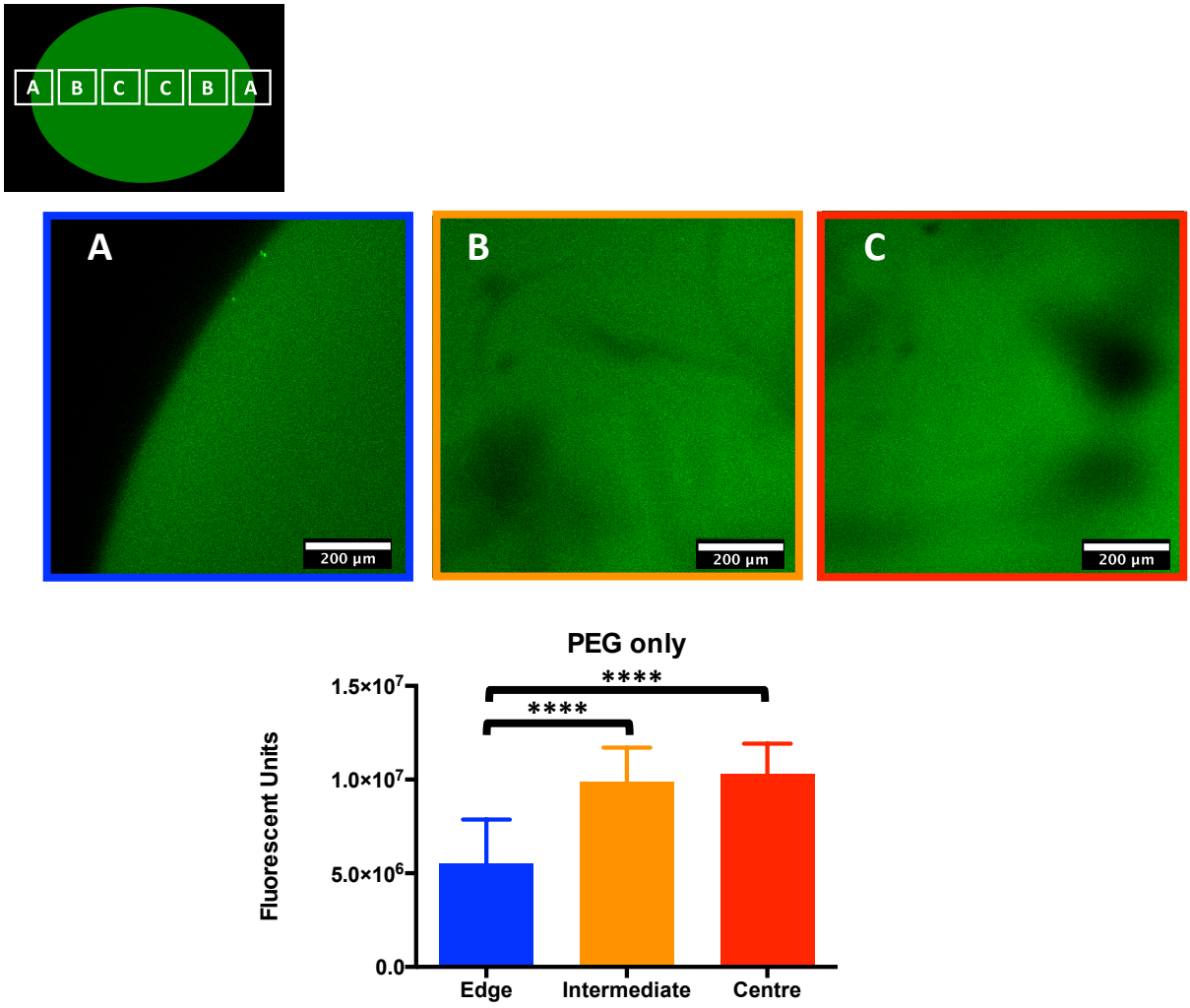

Figure 5.3 Diffusion in PEG only hydrogel.
Images represent stacks taken throughout the gel (outlined in top left diagram) these were then analysed to produce the graph shown. Images from points A represented the edge, points B the intermediate section and points C the centre of the gels. Kruskal-Wallis statistical test was used to find statistical differences between the fluorescence at the various positions in the gel where p**** ≤ 0.0001. This result indicates that GFs can move into the PEG only gels successfully.

For the PEGFN condition (Figure 5.4) the images again showed complete diffusion through to the centre of the gel. When looking at the different areas of the gel, no notable differences were observed suggesting an equilibrium was reached within the gel. When comparing to the PEG only results the lack of a drop at the edge of the gel may be a result of some GF binding onto the FN

which is present becoming part of the solid phase of the hydrogel and/or suggests slower diffusion of the growth factor. Therefore, the diffusion gradient introduced by the quick wash did not cause a drop in the GF concentration at the edge in this condition before imaging suggesting the hydrogel is actively retaining the GF slowing the diffusion.

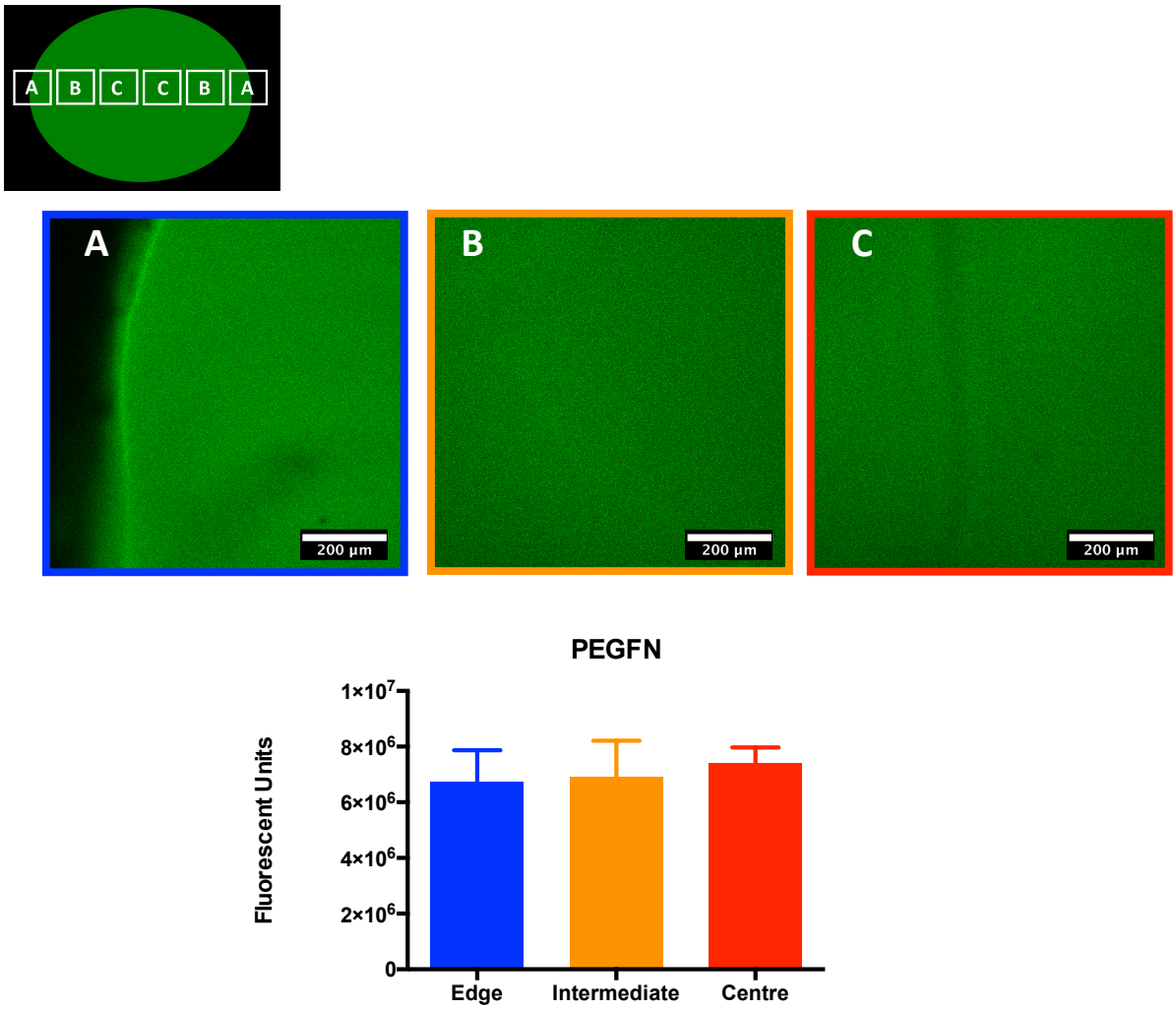

Figure 5.4 Diffusion in a PEGFN hydrogel.
Images represent stacks taken throughout the gel (outlined in top left diagram) these were then analysed to produce the graph shown. Images from points A represented the edge, points B the intermediate section and points C the centre of the gels. No statistical difference was observed between the various positions in the gel. This result indicates that GFs can move into the PEGFN gels successfully.

For the condition containing degradable crosslinker, 25% VPM PEGFN (Figure 5.5), it was again seen that the GF was able to diffuse to the centre of the gel. Difference seen between the GF measured in the centre compared to the other points in the gel were found to be statistically significant, this is likely the result

of slower diffusion through the gel possibly a result of smaller pore size from crosslinker differences. The difference noted between the edge and the other points is again thought to be due to the wash step or increased diffusion back out due to the increased gradient found at the edge position.

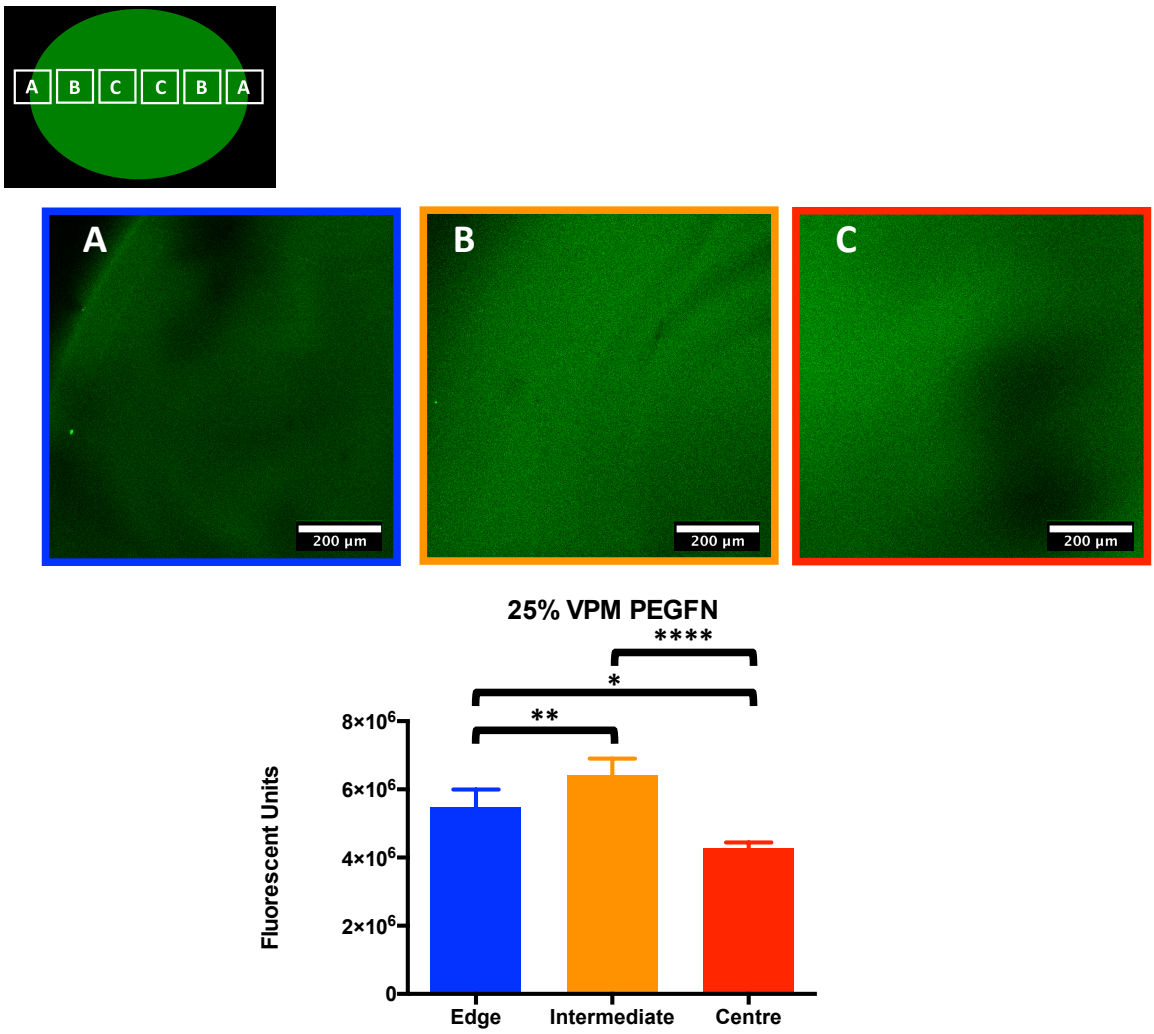

Figure 5.5 Diffusion in a 25% VPM PEGFN hydrogel.
Images represent stacks taken throughout the gel (outlined in top left diagram) these were then analysed to produce the graph shown. Images from points A represented the edge, points B the intermediate section and points C the centre of the gels. Kruskal-Wallis statistical test was used to find statistical differences between the fluorescence at the various positions in the gel where $p^* \leq 0.05$, $p^{**} \leq 0.01$ and $p^{****} \leq 0.0001$. This result indicates that GFs can move into the 25% VPM PEGFN gels successfully.

All 3 gel conditions showed the ability for the tagged NGF to diffuse through to the centre of the gels despite differences observed in each condition. This allows the assumption that molecules could readily diffuse through the gels over time as required.

5.3.2 Release Assays

Release assays were carried out focussing on GFs that are commonly used to supplement the media when culturing HSCs: CXCL12, Flt-3, SCF and TPO. The release over time is shown in Figure 5.6 and shows that for all growth factors the release plateaus after 6 hours. The majority of the release occurs in the first 3 hours shown by the sharp increase seen in all the graphs. The plateau after 6 hours suggests that no/very little GF is released after this time point implying the gels have the ability to retain the remaining GF.

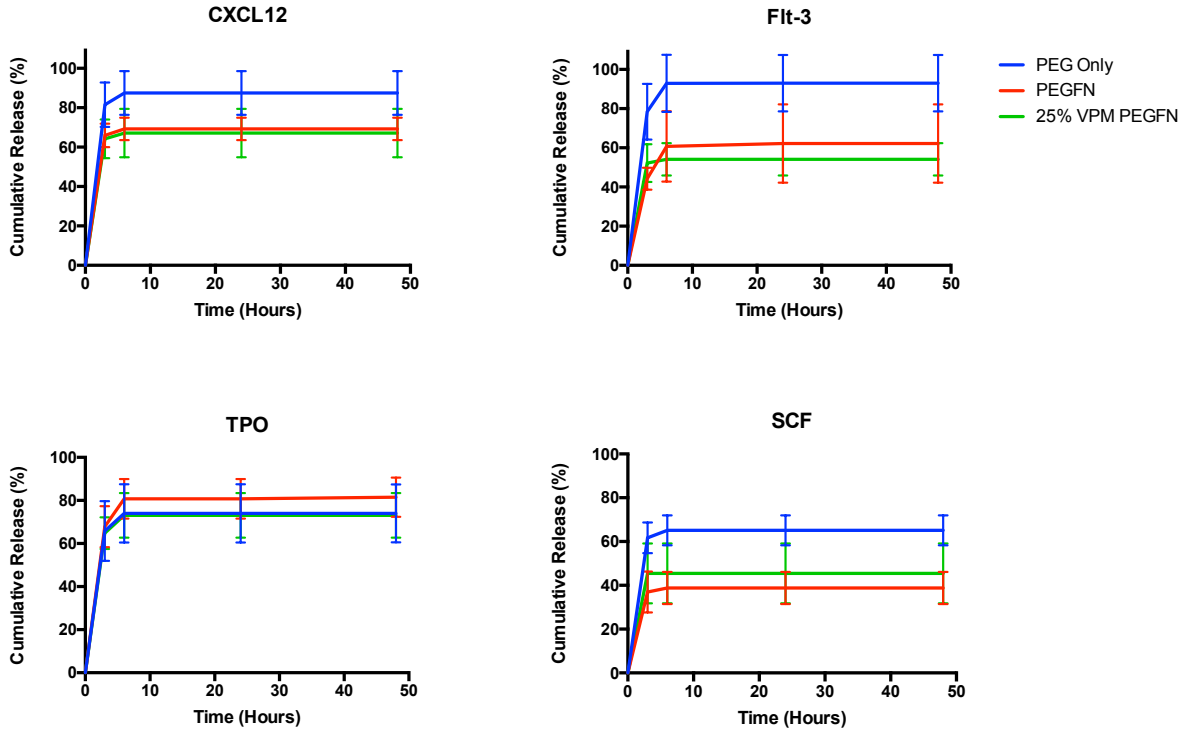

Figure 5.6 Growth factor release profiles over time.
The graphs above show the release of GFs from different gel conditions overtime. The graph shows the mean release at each time point with error bars representing +/- SD. In less than 10 hours the gels reach maximum release in all conditions.

Excluding TPO the general trend of the graphs shows that the inclusion of FN into the gels reduces GF release over time. This would suggest that some of the GF may be binding to the FN present. Focusing on the end points the GF retention was calculated after 48 hours (Figure 5.7). For CXCL12, Flt-3 and SCF PEGFN hydrogels were able to retain more GF than PEG only while release for TPO was similar for all gels. For CXCL12 after 48 hours the retention within

PEGFN gels and 25% VPM PEGFN was higher when compared to PEG only gels with means of 30.8%, 32.8% and 12.5% respectively. However, only PEGFN was found to be statistically significant due to the spread of the data. Release of Flt-3 revealed the same trend with the mean values for each condition. PEG only has the highest release with a mean retention of 7.0% and 25% VPM PEGFN gels showing the lowest release retaining 45.9%, this difference was statistically significant. PEGFN was also lower than PEG only with a mean of 37.8% though it was not statically significant. For SCF the mean retention for all conditions increased compared to the other growth factors. However, the trend of PEG only showing the lowest retention was maintained. A mean retention of 34.9% seen for PEG only compared to 61.2%, statistically significant, and 54.6% for PEGFN and 25% VPM PEGFN conditions respectively. TPO does not follow this pattern of PEG only retaining the lowest percentage of GF with PEG FN showing the highest release with a mean retention of 18.5% compared to the very similar means of 26.0% and 26.9% seen for PEG only and 25% VPM PEGFN conditions.

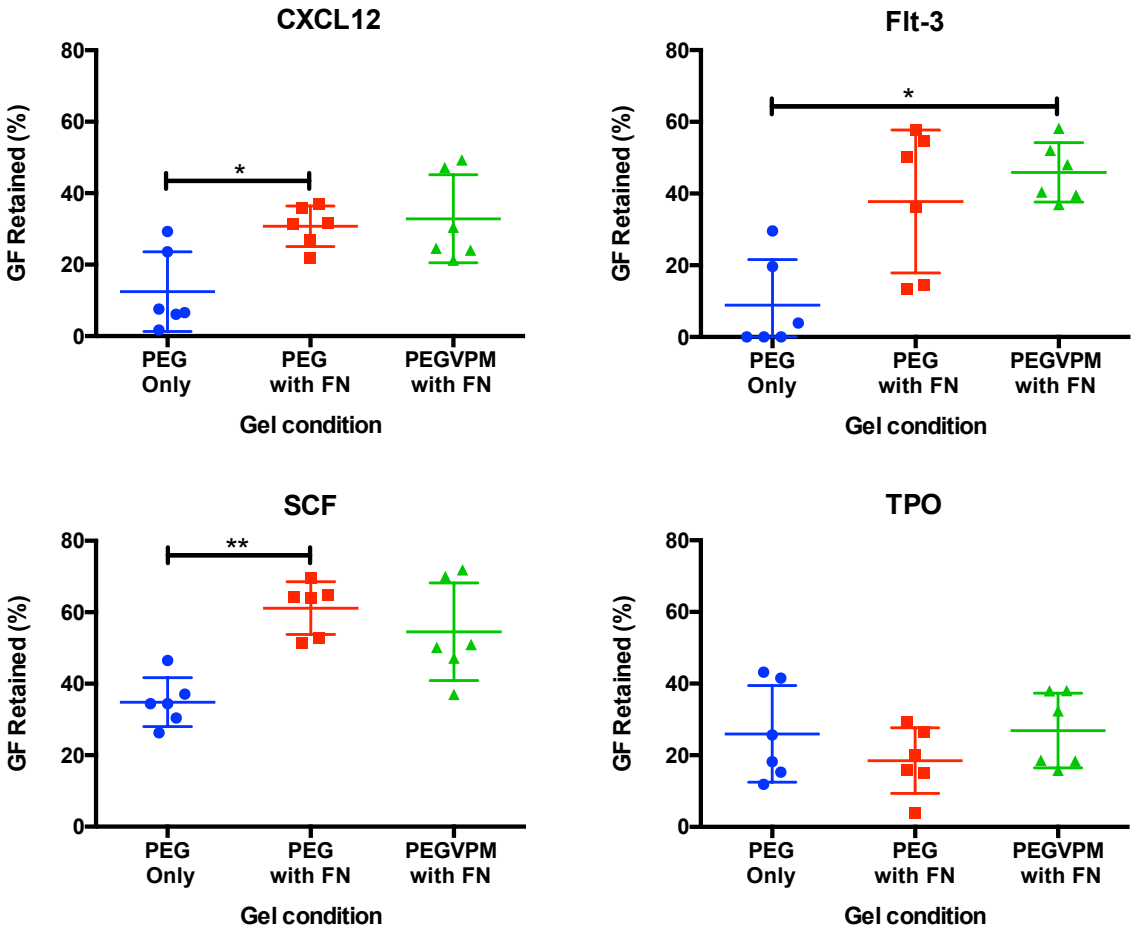

Figure 5.7 Total retained GFs in hydrogels after 48 hours.

The graphs above show the total retained GFs calculated after a 48 hour time period. Graphs show the mean +/- SD where n = 6 for each condition. Kruskal-Wallis statistical test was carried out where $p^* \leq 0.05$ and $p^{**} \leq 0.01$.

5.3.3 In cell western

In cell western was carried out to assess changes in cell phenotype when cultured on different surfaces under a 5% non-degradable PEG hydrogel (Figure 5.8). Data was normalised to the CellTag 700 stain and represented as a fold change to a glass control. Three other conditions were investigated; glass with FN, PEA spin-coated glass with FN and, PEA spin coated glass with FN and GFs (BMP-2 and NGF). Markers were selected to look at stemness, HCS maintenance and osteogenic differentiation.

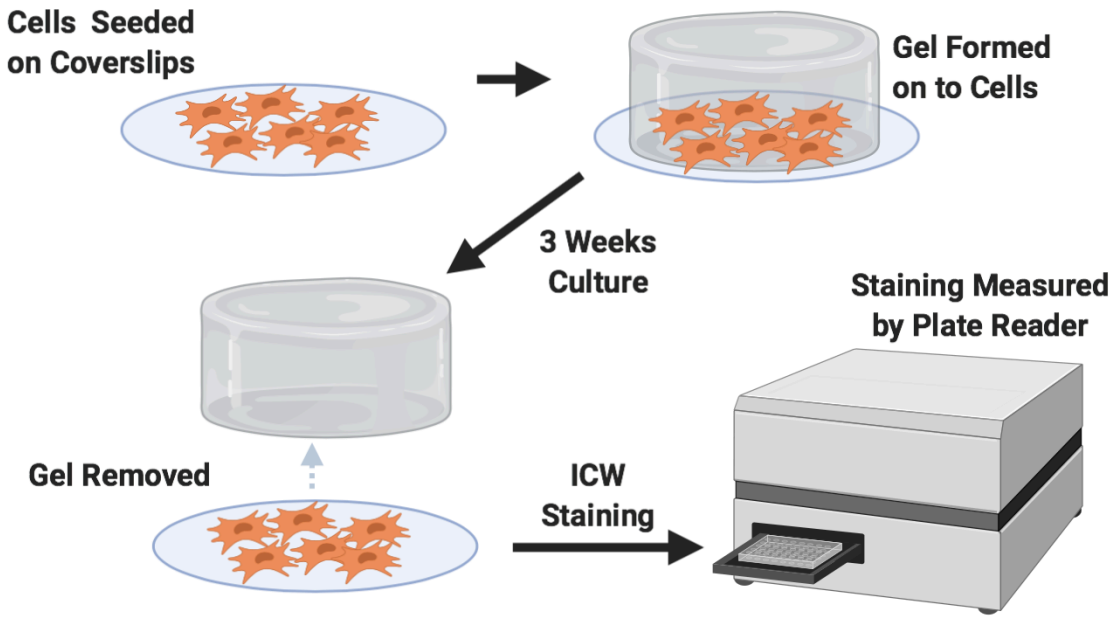

Figure 5.8 Concept figure for ICW set up.
Outlined above is the set up for ICW experiments. Cells are seeded onto glass coverslips with and without a PEA coating all with FN absorbed with and without GFs depending on the condition required. Gels are then formed on top of the adhered cells followed by 3 weeks culture. Gels are then removed prior to ICW staining, protocol outlined in methods, and finally staining is measured using a plate reader. Figure created using BioRender.com.

The markers investigated to show changes in stem cell marker expression were Stro-1, nestin and ALCAM (Figure 5.9). Stro-1 and ALCAM both follow the trend of the lowest expression in the condition with GFs present, and highest expression in the glass with FN. For nestin however, an increase in expression was observed in the condition containing GFs compared to the others with PEA with FN showing the lowest mean. Despite these observations there was no statistical

significance in the differences observed, though this does not suggest an increase in the stem phenotype, it also shows no loss of the phenotype in these conditions compared to glass with FN.

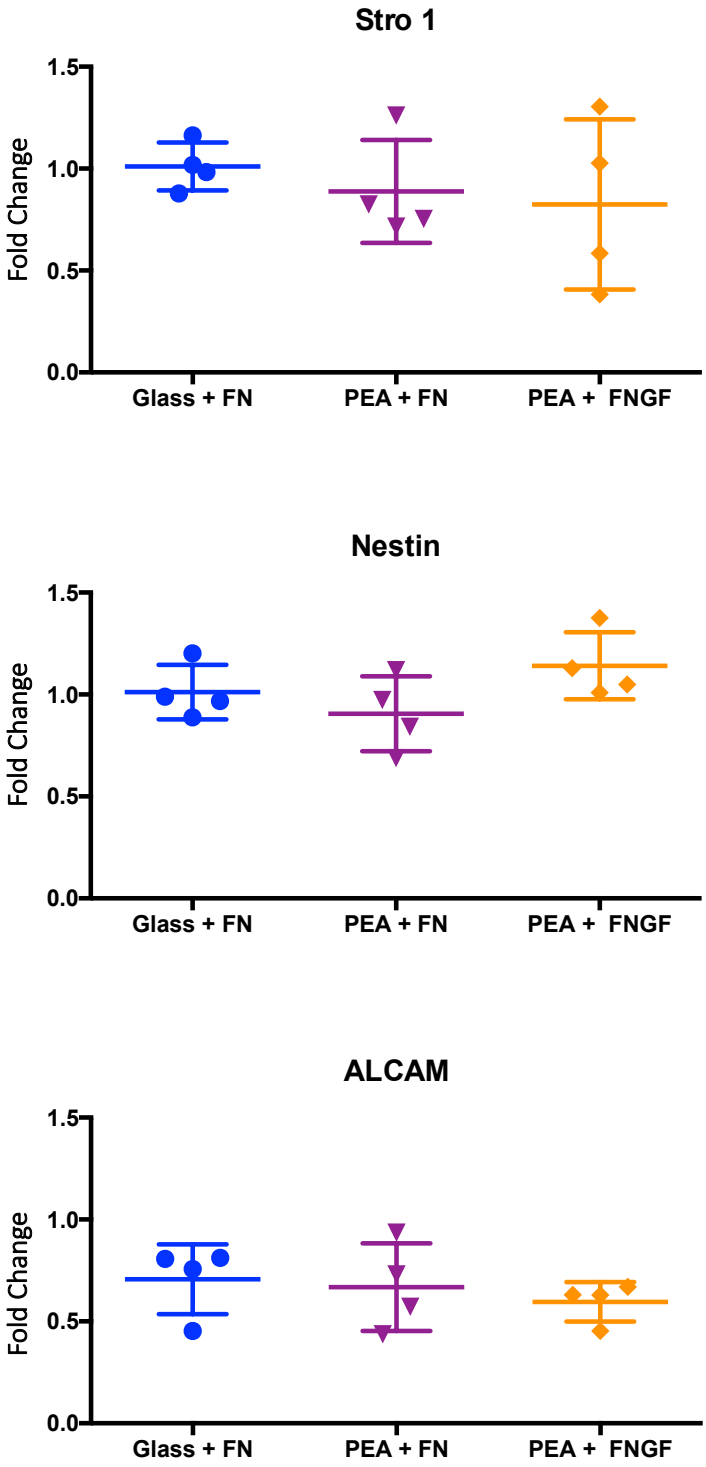

Figure 5.9 In cell western results for MSC stem markers.
Graphs show the expression of MSC stem markers represented as a fold change to the expression on a glass surface. Bars represent the mean values +/- SD with n = 4. Statistical analysis was carried out using the Kruskal-Wallis test with no significant differences found for any markers.

VCAM-1 and SCF were used as markers to represent HSC maintenance phenotype from the MSCs (Figure 5.10). VCAM-1 showed almost no change for any condition all maintaining similar expression to glass as seen by means sitting ~1. A higher variance in the data was observed for SCF particularly for PEA with FN and GF. Again, none of the differences observed in these conditions were found to be statistically significant. Though this shows no increase in HSC maintenance phenotype it also shows no loss of this phenotype in the new conditions.

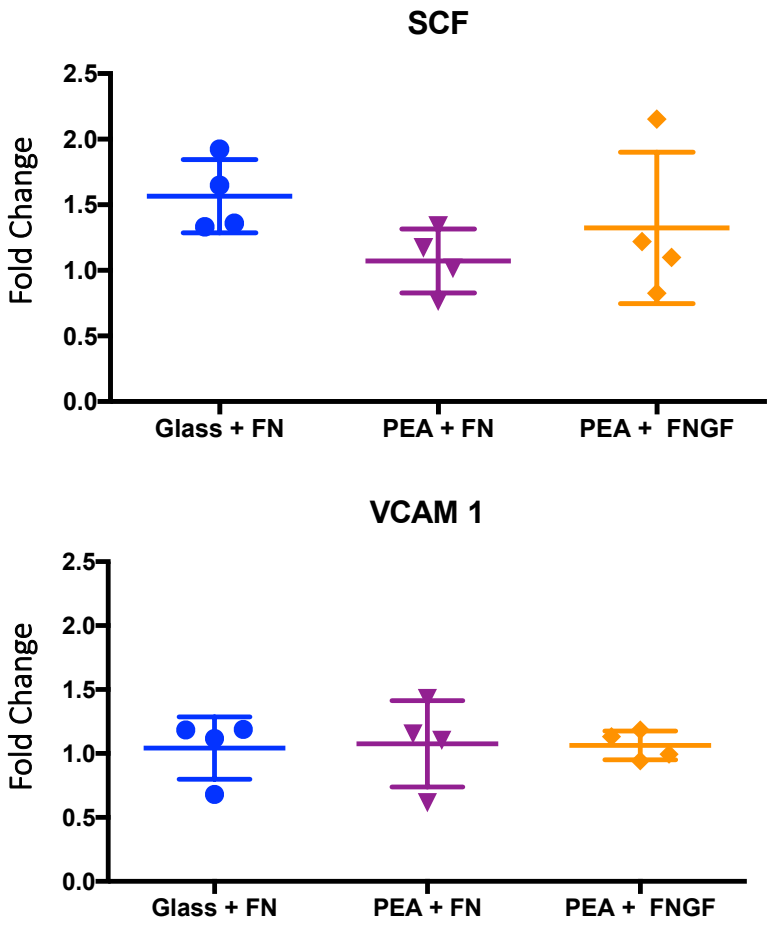

Figure 5.10 In cell western results for HSC maintenance markers.
Graphs show the expression of HSC maintenance markers represented as a fold change to the expression on a glass surface. Bars represent the mean values +/- SD with n = 4. Statistical analysis was carried out using the Kruskal-Wallis test with no significant differences found for any markers.

To assess changes caused by osteogenic differentiation, OCN and OPN were both investigated (Figure 5.11). Both markers saw the lowest expression in the condition with the GFs present which was unexpected as the presence of BMP-2 should induce some differentiation. If looked at as a fold change to glass OPN

showed an increase in expression while OCN showed a general decrease. Like the other markers no statistically significant differences were found suggesting no change in osteogenic potential through the different conditions.

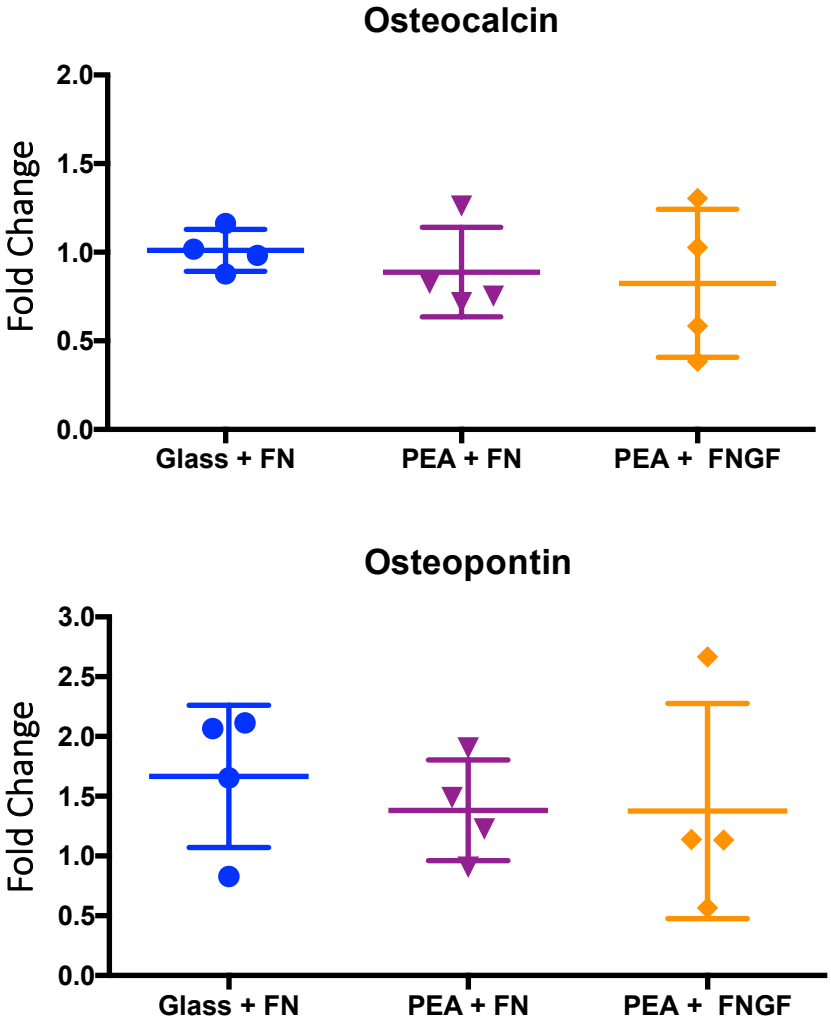

Figure 5.11 In cell western results for osteogenic markers.
Graphs show the expression of osteogenic markers represented as a fold change to the expression on a glass surface. Bars represent the mean values +/- SD with n = 4. Statistical analysis was carried out using the Kruskal-Wallis test with no significant differences found for any markers.

The HSC maintenance and osteogenic markers were also assessed without gels present to observe if the addition of the gel on top influenced the cell phenotype with regard to these markers (Figure 5.12). This data was gathered for cells cultured on PEA coated coverslips with both FN and GFs adsorbed with results normalised using cellTag 700. For osteogenic markers, OCN and OPN the

presence of the gel appears to reduce the expression of the marker in comparison to no gel with OCN showing a statistically significant difference in the conditions. For VCAM-1 and SCF the trend appears the opposite with the mean expression with a gel revealed as higher than without a gel though the difference was not found to be significantly different. These trends specifically the difference seen in osteocalcin suggest that gel presence may inhibit osteogenic differentiation of MSCs and further work would have to be carried out to investigate the potential increase in HSC maintenance capabilities.

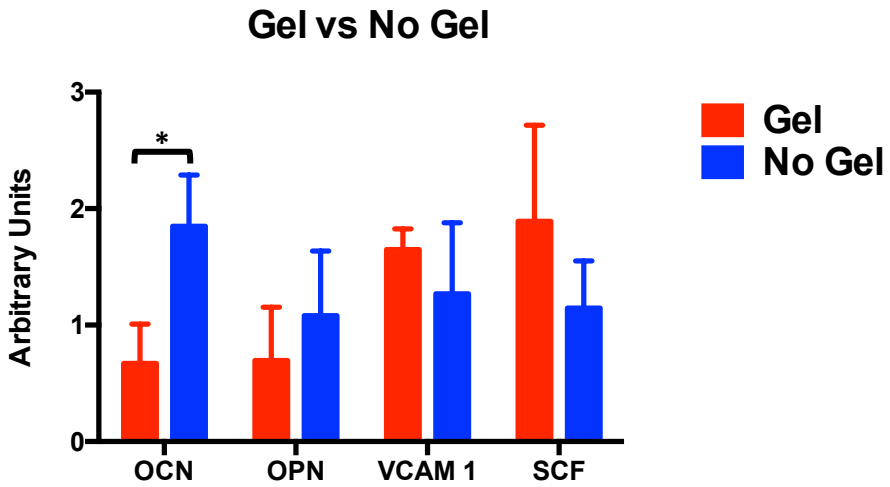

Figure 5.12. Comparing marker expression with and without gel presence.
In cell western results were used to compare differences in marker expression with and without the presence of a PEG hydrogel. A Mann-Whitney test was used to compare conditions with and without the gel for each marker. Bars represent the mean +/- SD with n = 4 for each, P* ≤ 0.05.

5.3.4 PCR

PCR was used for the 3D model with the microbeads to back up the data seen through In-cell Western for the 2D model with the spin coated coverslips. Unfortunately, due to difficulty and a low RNA yield, only 2 genes could be investigated. Nestin and ALCAM were chosen to assess the maintenance of a stem-like phenotype in the various conditions; PEGFN gels with GFs, PEGFN gels no GFs and PEG only gels with GFs normalised to the expression in PEG only gels without GFs (Figure 5.13). All gels were 5% PEG with 25% VPM.

For nestin the PEG only gel with GFs and the PEGFN gel with GFs showed little change from the control condition (PEG only without GFs). However, the PEGFN

gel without GFs saw an increase in nestin expression. Due to the wide spread of the data, there was no statistical significance found. ALCAM data showed a similar trend with PEGFN with GFs showing the biggest change to the control but again with a widespread in the data. Due to the wide variation no conclusion was drawn from this data.

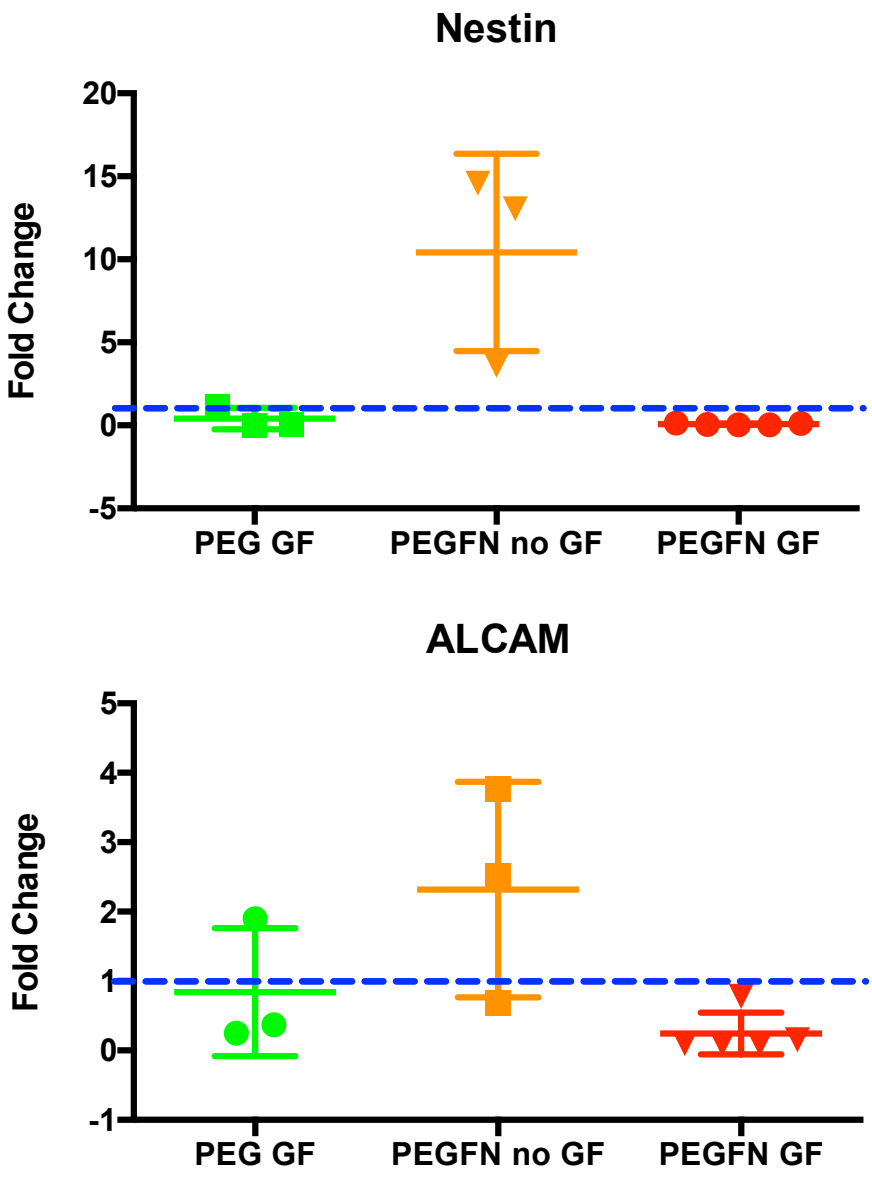

Figure 5.13 PCR results for nestin and ALCAM.
The graphs above represent the PCR data for nestin and ALCAM genes in MSCs cultured for 3 weeks within PEG hydrogels. The data is shown as fold change to the control PEG only gel with no GFs present (represented by the blue line). Graph shows the mean +/- SD with variation in sample number due to RNA yield.

The lack of RNA at the start of the process is likely to have impacted the overall success of the PCR process. No firm conclusions could be drawn from this data

and further work would have to be carried out to refine the RNA extraction to achieve a more efficient yield. If able to extract more RNA this technique could be further utilised to analyse the model but was not possible at this time.

5.3.5 Confocal

Due to difficulty with attaining RNA to carry out reliable PCR, immunostaining was used to visualise the cells on the microbeads within the 3D model. Staining for some relevant markers to the bone marrow niche: nestin, Stro-1 and SCF. Samples were stained after 3 weeks in culture with 4 different conditions: PEG only gel no GFs, PEG only gel with GFs, PEGFN gel no GFs and PEGFN gel with GFs, all gels were 5% PEG with 25% VPM.

Nestin was present in all conditions though no changes were observed over the different conditions (Figure 5.14). With the quantification of the image fluorescence higher mean was found for the conditions with PEGFN gels vs PEG gels however, this appeared to be a result of general variance and showed no statistical significance. The PEG gel with no GFs had the lowest average nestin staining, though still showed no statistically significant differences to the others.

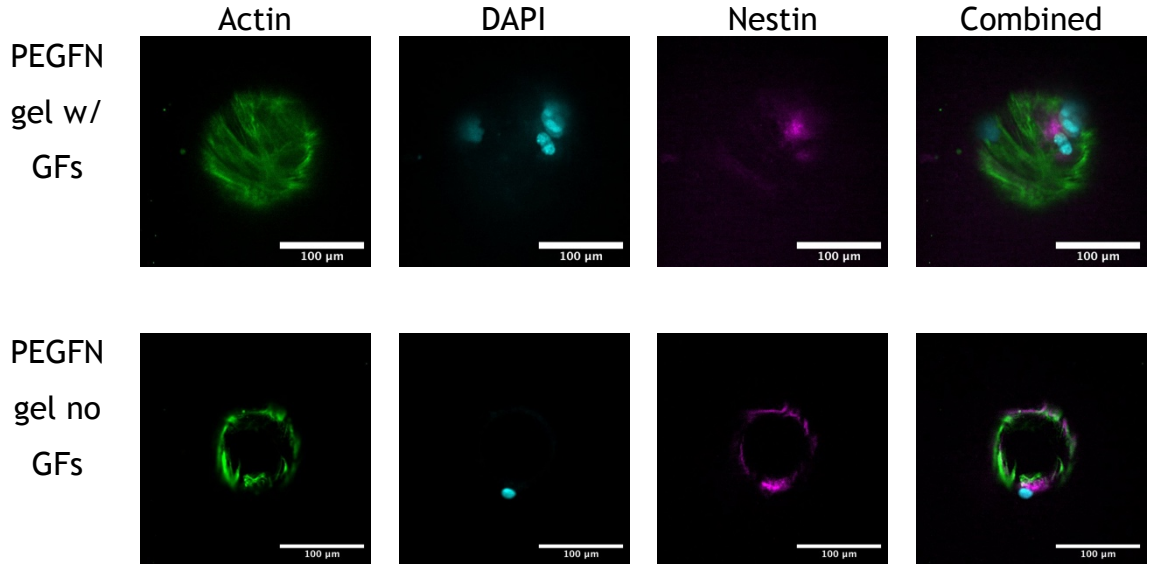

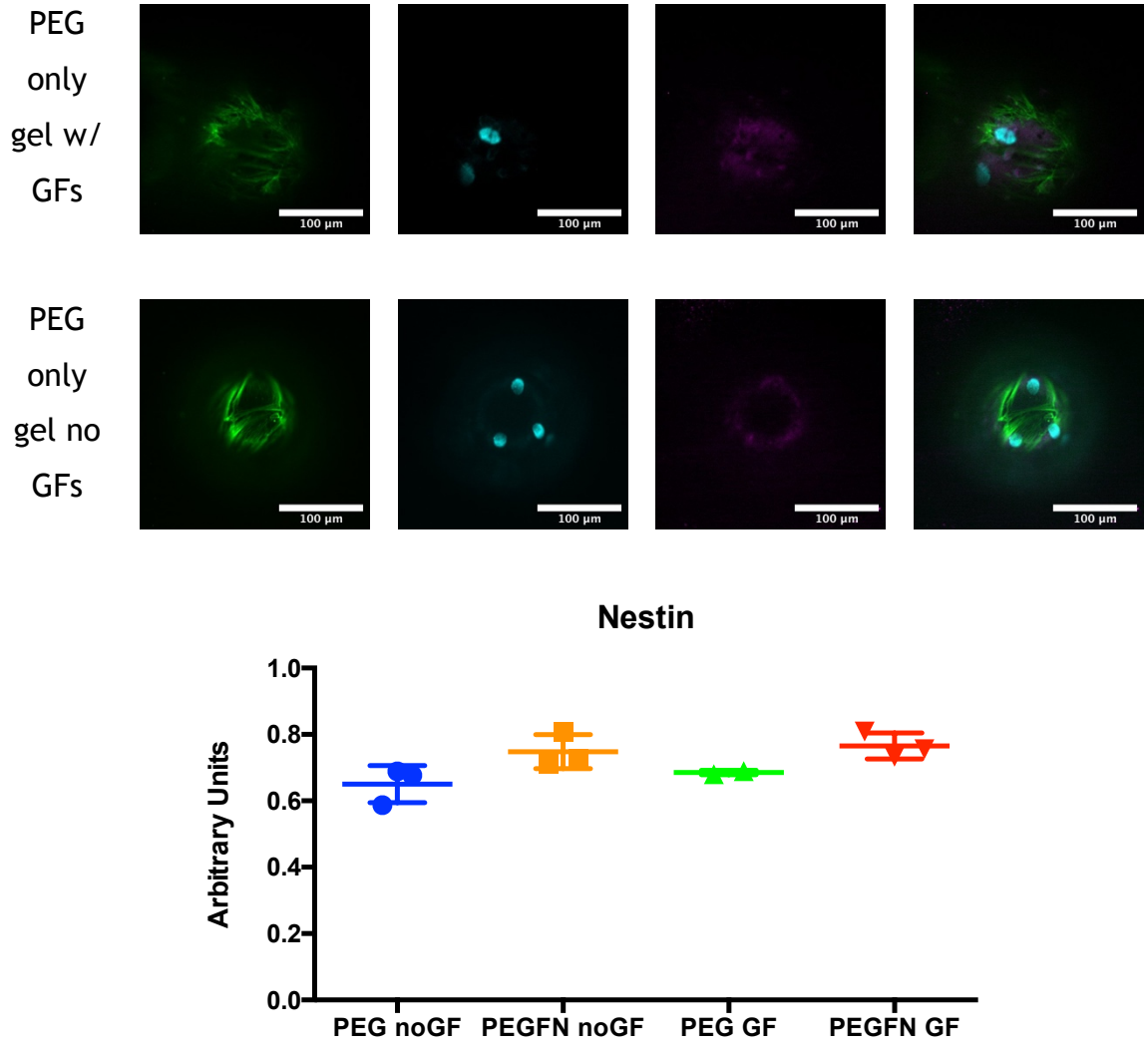

Figure 5.14 Nestin confocal images and quantified results.
Images show a selected point through one of the stacks obtained to best represent what was observed. Actin, DAPI and nestin staining of MSCs seeded on microbeads within 5% PEG 25% VPM hydrogels for each condition. Graphs shows the quantified results normalised to the DAPI nuclei staining for each condition. Bars represent the mean +/- SD with n=3 for each condition except PEG w/ GFs when n=2 Tukey test was carried showing no significant differences within the data.

Stro-1 (Figure 5.15) staining was, like nestin, lowest in the PEG gel with no GFs. Conditions with PEGFN gels had the highest average staining though PEG gels with GFs was very similar to PEGFN gels with no GFs. The highest average staining for Stro-1 was seen in the PEGFN gels with GFs which was found to be statistically significant versus all other conditions. Suggesting the addition of FN along with GFs to the PEG gels may increase the maintenance of the stem-like phenotype.

Actin DAPI Stro1 Combined

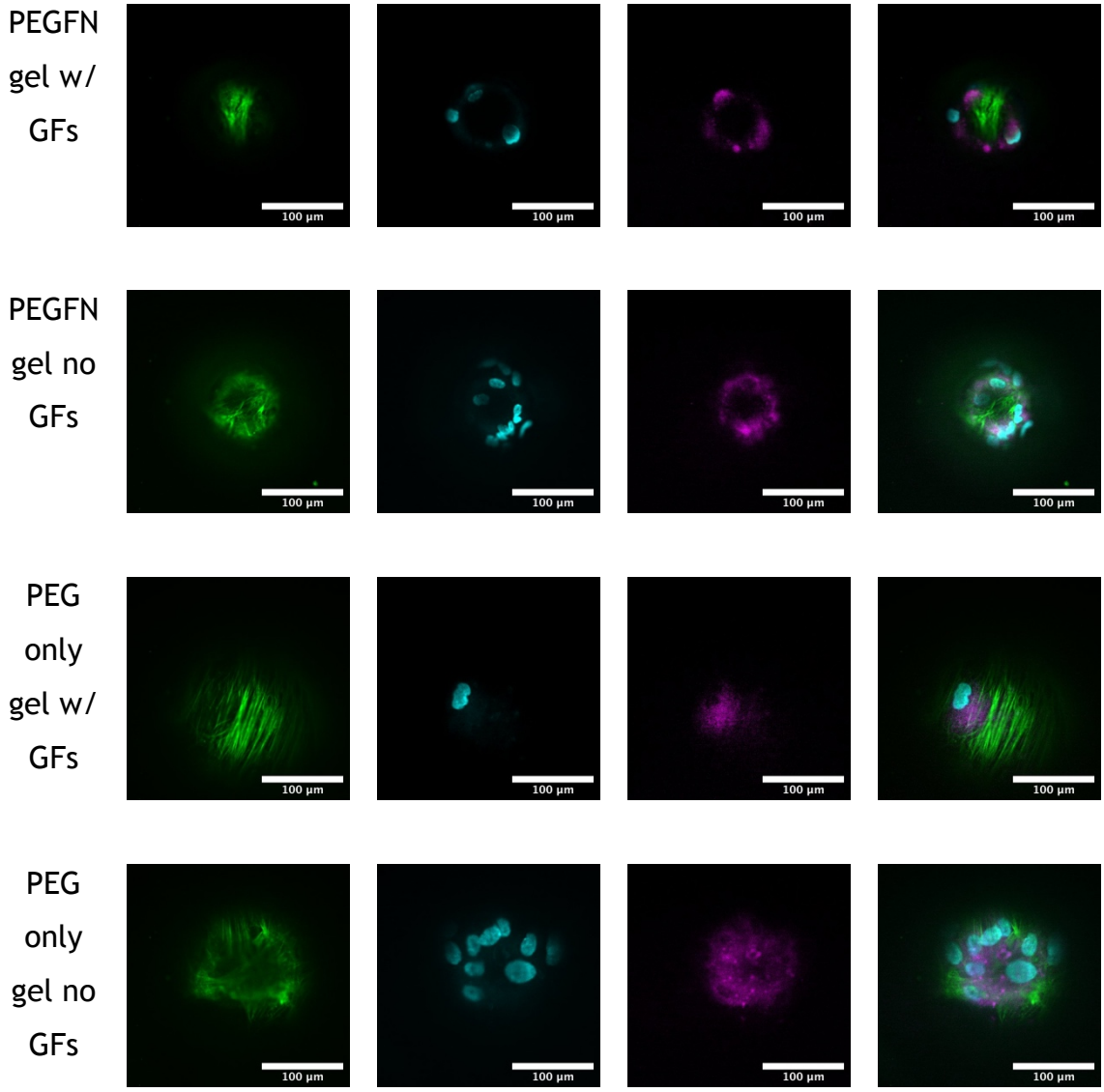

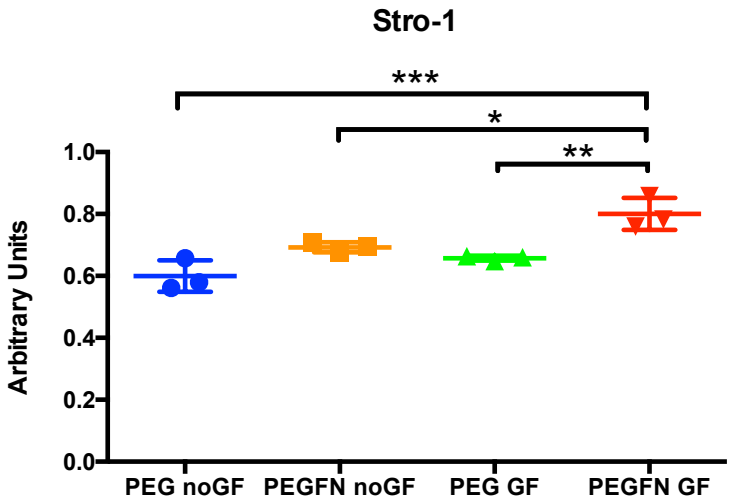

Figure 5.15 Stro-1 confocal images and quantified results.
Images show a selected point through one of the stacks obtained to best represent what was observed. Actin, DAPI and Stro-1 staining of MSCs seeded on microbeads within 5% PEG 25% VPM hydrogels for each condition. Graphs shows the quantified results normalised to the DAPI nuclei staining for each condition. Bars represent the mean +/- SD with n=3 where p* ≤ 0.05 p** ≤

0.01 and p*** ≤ 0.001. Tukey test was carried showing significant differences within the data between PEGFN with GFs and all other conditions.

The staining assessed presence membrane bound SCF, though soluble SCF is also likely present within the model. SCF (Figure 5.16) did not follow the same trend seen for nestin and Stro-1 with conditions containing GFs, PEG gels with GFs and PEGFN gels with GFs, showing the highest average staining. Like the other markers PEG gels with no GFs showed the lowest average staining of all the conditions for SCF. Data for SCF revealed notable differences between conditions containing GFs and the PEG without GFs condition.

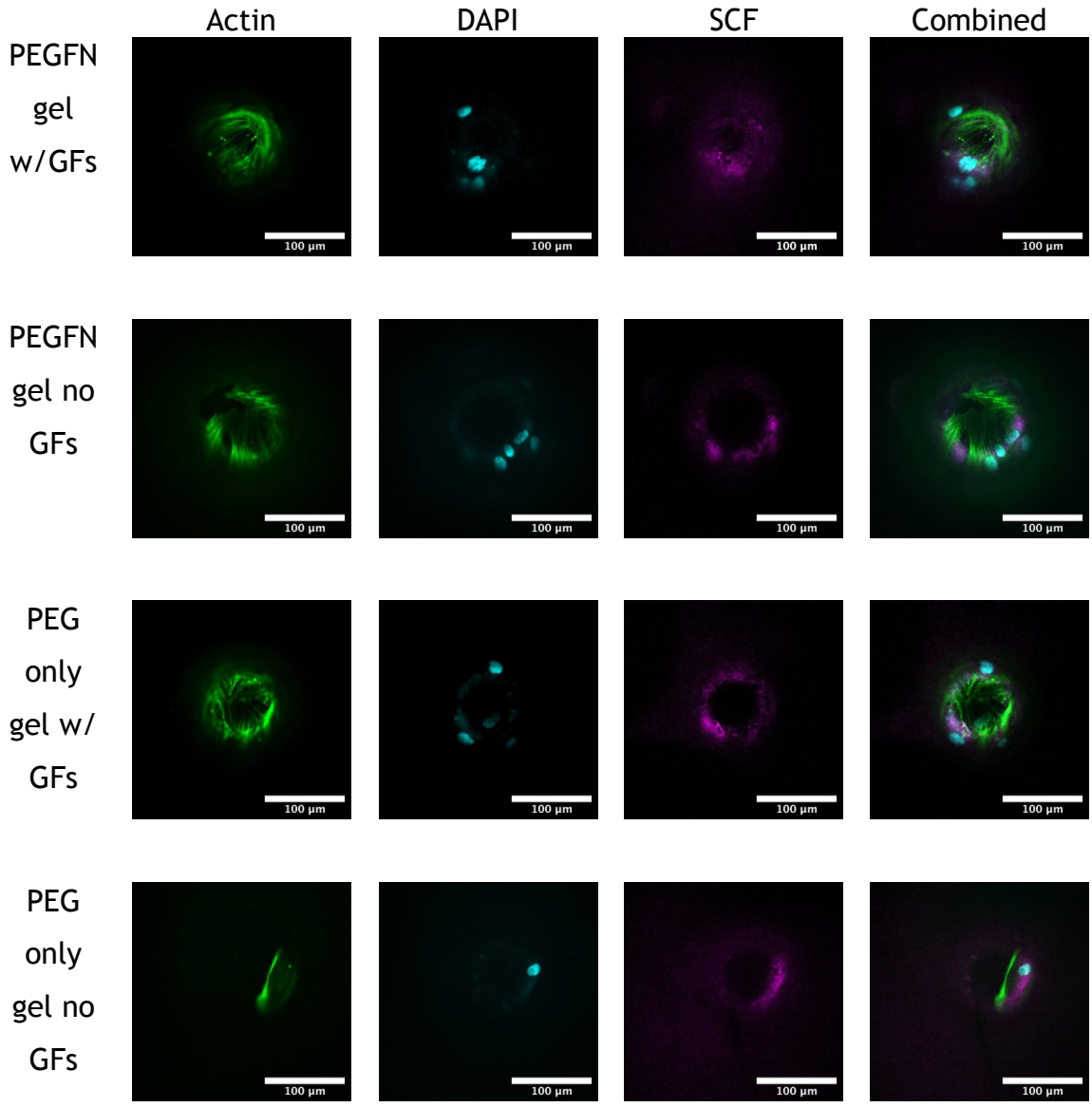

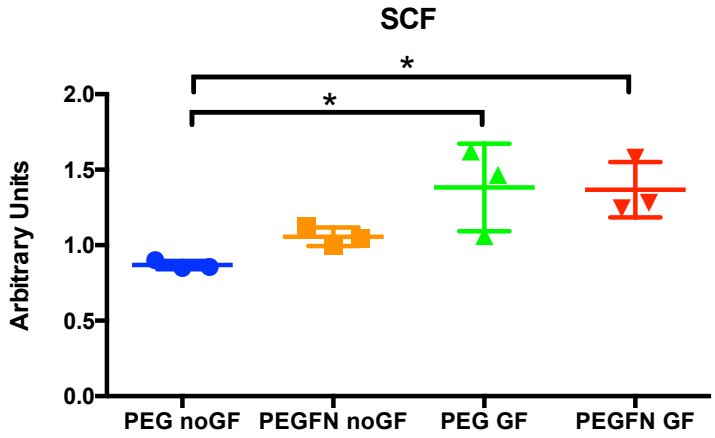

Figure 5.16 SCF confocal imaging and quantified results.
Images show a selected point through one of the stacks obtained to best represent what was observed. Actin, DAPI and SCF staining of MSCs seeded on microbeads within 5% PEG 25% VPM hydrogels for each condition. Graphs shows the quantified results normalised to the DAPI nuclei staining for each condition. Bars represent the mean +/- SD with n=3 where $p^* \leq 0.05$. Tukey test was carried showing significant differences within the data between PEG without GF and both conditions including GFs.

5.4 Discussion

Within the final model we put together the components developed in the previous chapters to mimic the various components of the bone marrow niche. The PEG hydrogel tuned to the stiffness of the bone marrow was used to produce a 3D matrix around the cells that could mimic the functions of the ECM *in vivo*. This included the ability to allow diffusion through the matrix allowing the movement of waste, essential nutrients and soluble molecules (Mouw, Ou and Weaver, 2014). Figure 5.3, Figure 5.4 and Figure 5.5 all show the ability for soluble proteins to diffuse through the entire gel for 3 different gel formulations. Though differences were observed in the ability to reach an equilibrium within the gels there were no concerns that essential diffusion would be obstructed by the gel matrix. The release assays shown by Figure 5.6 and Figure 5.7 also support the conclusion that diffusion through the gel is possible as they show the ability of GFs to leave the gels into the surrounding supernatant.

Release assays were carried out using CXCL12, Flt-3, SCF and TPO to investigate the ability for the matrix to retain signalling molecules to surround the cells. These specific GFs were chosen due to their roles within the bone marrow niche *in vivo* and common addition to media when culturing HSCs (Calvi *et al.*, 2003; Yoshihara *et al.*, 2007; Greenbaum, Y. M. S. Hsu, *et al.*, 2013; Sugimura *et al.*, 2017; Tsapogas *et al.*, 2017). The release profiles over time (Figure 5.6) showed that any molecule not trapped within the matrix would diffuse out within the first 6 hours after which no further release was recorded up to 48 hours. The total cumulative release calculated after the 48 hour time point, varies for each GF though a general pattern does emerge (Figure 5.7). With the exception of TPO the highest release is seen in the PEG only gels vs those containing FN, possibly due to a lack of FN affinity. CXCL12 was of particular interest as it not only is known to be produced by MSCs within the niche and to influence HSC maintenance but also have a known affinity to FN binding (Pelletier *et al.*, 2000; Ding and Morrison, 2013). With Flt-3 and SCF following the same trend it could suggest some interaction between FN and these GFs. In the literature we see a similar outcome when looking at VEGF, which has a known affinity to FN binding,

release from PEG vs PEGFN hydrogels (Trujillo *et al.*, 2019). This study also showed that introducing VPM could have an influence on the release which supports the results produced in this chapter where we see a general reduction in the mean between PEGFN vs 25% VPM PEGFN gels. It has been shown in the literature that the introduction of VPM causes a reduction in pore size compared to using dithiol which could explain what is observed in the release and diffusion assays when VPM is present (Weaver *et al.*, 2018).

The second material component in the model is the PEA coated surface, either a coverslip or microbead, which was incorporated as a surface for MSCs to adhere and allowing the incorporation of GFs. Previous research completed by colleagues in our research group found that the addition of BMP-2 and NGF produced the best HSC supporting phenotype. BMP-2 was included to induce some osteogenic differentiation of the MSCs as osteoblast cells are important in HSC regulation and NGF due to nestin positive MSCs being linked to peripheral nerves and control within the niche (Lucas *et al.*, 2011).

The use of NGF was to support the maintenance of naïve MSC population which was investigated looking at MSC stem markers like nestin, Stro-1 and ALCAM using ICW (Figure 5.9). Results showed that, with the inclusion of growth factors, an increase in nestin expression is observed compared to the other conditions, with an upregulation to glass. For other MSC markers however, no change in expression was observed when GFs were included. Phenotype control within the model is still difficult and would require further assessment and optimisation to make definitive conclusions. With nestin positive MSCs being noted as particularly important within the niche (Méndez-Ferrer, T. V Michurina, *et al.*, 2010; Pinho *et al.*, 2013) the slight increase in nestin with GFs present could be further investigated using other techniques such as PCR or flow cytometry in order to draw further conclusions. For culture in the 3D based model with the microbeads encapsulated within the gels with MSCs, immunostaining was carried out to determine the maintenance of a nestin and Stro-1 positive population of cells after 3 weeks. Figure 5.14 shows the presence of nestin in all conditions allowing the conclusion that MSCs remain nestin positive after 3 weeks in culture though there are no differences observed between the different conditions. Stro-1 (Figure 5.15) similarly, is observed in all conditions suggesting cells are

maintained in a naïve state with PEGFN gels with GFs present showing a significant increase in Stro-1 presence compared to other conditions. The use of other techniques to confirm this data and further analyse the cell phenotype should be considered before concluding these results, a method to extract cells more efficiently would allow this to be done more easily.

BMP-2 is a GF known to induce osteogenic differentiation of MSCs (Knippenberg *et al.*, 2006). With osteoblasts playing such an important role in the bone marrow niche in the regulation of HSCs and production of HSC maintenance factors (Nakamura *et al.*, 2010) it is favourable that osteogenic differentiation occurs within the model while maintaining a population of naive MSCs. Figure 5.11 showed a down regulation of OCN expression in both PEA with FN and PEA with FN and GF conditions compared to glass after 3 weeks culture. For OPN however, there is an up regulation in all conditions compared to glass though the GF condition still does not appear to enhance the osteogenic capabilities. Despite BPM-2 not showing the effect expected further analysis should be carried out to assess any effect on osteogenesis as these markers are up-regulated at different stages of differentiation that could influence these results (Yang *et al.*, 2014). The lack of an increase in these markers may also be explained by an inhibition to osteogenesis brought on by the presence of the gel, this is suggested by the results shown in Figure 5.12. A possible cause for this reduced osteogenic commitment could be the production of a hypoxic culture environment created by the gel. It has been shown in the literature that hypoxic culture can reduce osteogenic differentiation in bone marrow derived MSCs (D'Ippolito *et al.*, 2006; Fehrer *et al.*, 2007) and also that hydrogels can be used to create a hypoxic environment (Park and Park, 2016). Again, future analysis with PCR or flow cytometry would be beneficial looking at more genes associated with the differentiation process before drawing a final conclusion to this data.

Finally the expression of HSCs maintenance markers, VCAM-1 and SCF, was investigated using ICW (Figure 5.10) due to their known roles in the HSC niche (Calvi *et al.*, 2003; Kopp *et al.*, 2005). SCF can be found in a membrane bound or soluble state, the presence of membrane bound SCF has been shown to influence HSCs (Driessen, Johnston and Nilsson, 2003; Takagi *et al.*, 2012). Little to no

differences were observed in VCAM-1 expression through all conditions and with respect to glass. SCF on the other hand showed an upregulation of all conditions compared to glass though the condition with the GFs present showed the smallest increase. When comparing this to the same condition with no gel however, the presence of the gel appears to increase the expression of both HSC maintenance markers with SCF showing the largest increase (Figure 5.12). Techniques such as PCR and/ or flow cytometry could be utilised for further phenotyping using this 2D based model with the coverslips due to the ease of removing cells compared to the 3D model. Immunostaining was used to observe and quantify the presence of SCF when MSCs were cultured on the microbeads within the gels (Figure 5.16). The results showed a significant increase in the volume of SCF staining within the conditions containing GFs this indicates that these conditions would be more favourable to host an HSC population. Continuing work with immunostaining could further characterise the cells or if the cells are able to be removed from gels efficiently techniques such as PCR and flow cytometry could be used to more accurately assess the phenotype.

In conclusion, this chapter has outlined some of the biological interactions and effects of the model. Diffusion and release assays show the ability of the hydrogel to act like the ECM allowing movement of molecules while also creating a reservoir of influencing factors around the cells. Cell characterisation shows a general reduction in osteogenic differentiation in the presence of hydrogels which could be resultant of the creation of a hypoxic culture environment. Generally, cells appeared to retain stemness and HSC maintenance markers though further work would have to be carried out to fully characterise the MSCs within the model.

Chapter 6 General Discussion

6.1 Discussion

The overall aim of this project was to develop an *in vitro* model, for the culture of stem cells, able to mimic the *in vivo* environment of the bone marrow niche. The work presented in this thesis shows the tuning of PEG hydrogels simulating the stiffness that has been previously recorded for the bone marrow. We have also demonstrated the ability of these gels to reproduce ECM functionalities, such as allowing diffusion and retention of soluble molecules, that can act as influencing factors, within the matrix, mediated by the inclusion of FN within the gels. This model was further developed with the inclusion of solid polymeric surfaces within the gels to facilitate MSC cultures. With the inclusion and surface modification of polystyrene microbeads, we have then shown the potential of UV polymerisation to be used as a technique to coat materials in PEA for cell studies and the successful use of plasma polymerisation to coat polystyrene microcarrier beads for cell culture. We demonstrated the ability of PEA coatings produced through UV and plasma polymerisation to induce fibrillogenesis when FN is introduced to the surface. The work also demonstrated the ability for the system to sustain MSCs for long term culture. This was in aim of producing a system that is able to induce *in vivo* like cell behaviour within an *in vitro* model.

In vitro modelling has become an important method used in research to further understand cell behaviour in both diseased and healthy tissues. The use of *in vitro* models allows control over the cellular environment leading to a better understanding of influencing factors as found *in situ*(Arantes-Rodrigues *et al.*, 2013). A disadvantage, however, is that cells when cultured *in vitro* may not behave as they do *in vivo*, potentially due to a variety of differences in mechanical, biological or chemical factors, it is therefore important to mimic the *in vivo* environment of the cells as closely as possible during development of *in vitro* models. Recent studies have utilised hydrogels, as an *in vitro* equivalent to the ECM, reproducing selected mechanical and biological cues within models, (Tibbitt and Anseth, 2009) as has been done in this work. The ECM, as summarised in chapter 1, is the non-cellular component of tissues and provides various functions for the cells, including support through a 3D matrix (Frantz, Stewart and Weaver, 2010). It is known that the stiffness of the cells

environment can influence their behaviour (Discher, Janmey and Wang, 2005) it is therefore important to use a model with the appropriate mechanical properties for the tissue being studied. In this work the model was developed to mimic the bone marrow niche. Therefore, the stiffness was tuned to fall within the known range of bone marrow stiffness, generally <3 kPa (Choi and Harley, 2017). This was performed through investigating how gel composition and gelation conditions could influence the resulting bulk properties of the gel measured using rheology. Changing the concentration of PEG within the gels was shown to influence the stiffness of the gels with a positive linear relationship found between the storage modulus and the concentration of PEG in gels up to 10% w/v. This allowed us to choose a composition which would produce gels with the appropriate stiffness to mimic the bone marrow, in this instance 5% PEG gels were chosen with an average Young's modulus of 2.5 kPa. Altering the starting pH also resulted in changes to the final stiffness of the formed gels with lower pH starting solutions producing softer gels.

Though the bulk stiffness of the bone marrow is found to sit at <3 kPa (Choi and Harley, 2017) it has also been found to be heterogenous ranging between 0.25 to 24.7 kPa throughout the marrow (Jansen *et al.*, 2015). Microcarrier cell culture beads were introduced to our model providing localised points of higher stiffness allowing cellular adhesion within the gel and improved cell viability. The surface introduced by the microcarrier beads allowed for further development of the model through the use of PEA surfaces. As previously described PEA interacts with the ECM protein FN and induces fibrillogenesis producing protein networks on the polymer surface (Cantini, Rico, *et al.*, 2012). FN, when in this fibrillar conformation, compared to the soluble globular conformation, allows the exposure of various binding sites improving cellular adhesion and allowing the tethering of GFs (Llopis-Hernández *et al.*, 2016). In this work various methodologies; plasma polymerisation, UV polymerisation and SI-ATRP, were investigated to find the most effective way to coat polystyrene, the base material of our microcarrier beads, with PEA. SI-ATRP was unsuccessful at coating polystyrene samples, producing insufficient chemical modification to confirm the presence of PEA, however with optimisation the process has potential to be an effective modification method. UV polymerisation and plasma polymerisation were both found to successfully produce a PEA surface on

polystyrene samples, as shown by XPS analysis. Further analysis also revealed the presence of FN networks on surfaces coated via these methodologies, confirming the functionality of the polymer coating. As an established method in both *in vitro* and *in vivo* studies plasma polymerisation was taken forward for use in cell work where microcarrier beads are used.

Another important aspect of the ECM is the diffusion of essential/ signalling molecules and waste through the matrix (Mouw, Ou and Weaver, 2014). There are various cytokines secreted by cells *in vivo* that have been shown to play key roles within the bone marrow niche such as; FLT-3 ligand, SCF, TPO, OPN, VCAM-1 and CXCL-12 (Calvi *et al.*, 2003; De Ugarte *et al.*, 2003; Stier *et al.*, 2005; Qian *et al.*, 2007; Greenbaum, Y.-M. S. Hsu, *et al.*, 2013; Tsapogas *et al.*, 2017).It is important that the hydrogels used *in vitro* mimics the ECMs ability to retain these molecules and even immobilise them within the matrix (Powers, McLeskey and Wellstein, 2000; Zhu and Clark, 2014). Within this work we have shown that the PEG hydrogels used allow diffusion of molecules through the entirety of the gels. Release assays carried out also showed the ability for the hydrogels to retain some of these molecules known to be important in the bone marrow niche particularly in gels with FN incorporated. Therefore, this model was confirmed to be able to simulate the ECMs ability to both allow diffusion of and facilitate the solid state presentation of cytokines.

The bone marrow niche is of particular interest in the field of regenerative medicine as it is home to two populations of stem cells, MSCs and HSCs, which give rise to bone, cartilage, fat, muscle (MSCs) and blood cells (HSCs) (Méndez-Ferrer, T. V Michurina, *et al.*, 2010). This unique environment is able to maintain a naïve population of stem cells while differentiation continues to sustain mature cell types. A successful *in vitro* niche model would give rise to vast research and therapeutic potential such as; pharmaceutical screening, disease modelling and cell sourcing. MSCs seeded within the model developed in this thesis were shown to survive long term culture, of up to 3 weeks, after encapsulation. The phenotype was assessed to investigate the maintenance of a naïve population within the model with emphasis on HSC maintenance phenotype. After 3 weeks MSCs were shown to be nestin positive, which is related to expression of HSC maintenance markers and linked to a naïve

phenotype (Méndez-Ferrer, T. V Michurina, *et al.*, 2010; Kunisaki, Bruns, Scheiermann, Ahmed, Pinho, Zhang, Mizoguchi, Wei, Lucas, Ito, Jessica C. Mar, *et al.*, 2013; Pinho *et al.*, 2013), though further investigation is required to fully determine the MSC phenotype within the model. It was also found that the introduction of the hydrogel reduced osteogenic commitment of MSCs, even in the presence of BMP-2, which is thought to potentially be due to a hypoxic environment within the gel.

6.2 Summary of Key Findings

- PEG hydrogels can be tuned to match the stiffness of the bone marrow through changes in PEG concentration, higher PEG concentrations produce stiffer hydrogels. Lowering the pH slows the rate of gelation resulting in the production of softer gels, slowed gelation likely produces more homogenous gels.

- Soluble proteins can diffuse fully through the PEG hydrogels. PEG hydrogels can retain certain growth factors creating a reservoir of influencing factors for cells like the ECM *in vivo*. This growth factor retention is likely influenced by the inclusion of the ECM protein FN within the hydrogels

- UV polymerisation can successfully produce a PEA surface on a PS base material. The PEA layer produced through UV polymerisation has the ability to induce protein networks when FN is introduced.

- Plasma polymerisation can be used to coat PS microcarrier beads in PEA suitable for cell culture.

- MSCs are viable after encapsulation within the PEG hydrogels for long term culture (3 weeks) when seeded on to PEA coated PSm. MSCs are still Nestin positive after 3 weeks culture. PEG hydrogels appear to inhibit osteogenic differentiation even in the presence of BMP-2.

6.3 Recommendations for Future Work

The following section outlines future work that may be considered taking the model forward.

The PEG hydrogels are now well established and characterised for use in tissue models. However, a few further characterisations may be beneficial. It may be beneficial to assess the ability of the gels to induce a hypoxic environment which is thought to be important in maintaining stem cell quiescence (Mohyeldin, Garzón-Muvdi and Quiñones-Hinojosa, 2010).The range of PEG volumes assessed may be increased to determine if the linear relationship observed between 3% - 10% PEG gels and storage modulus continues or plateaus at higher volumes. Rheological characterisation should be carried out with the inclusion of FN and microcarrier beads within the gels in order to investigate any effects these have on the final bulk properties. Finally, it may be helpful to investigate any changes in stiffness over time when using the gels for long term culture. Though degradation studies have been carried out on these gels in previous research no study specifically looks at changes in stiffness over an extended period (Trujillo *et al.*, 2020). This would improve the validity of the model over longer time points and potentially provide new avenues of study with higher degrees of stiffness.

There is potential for further work to be carried out on the method of surface modification used to introduce PEA to the surfaces with UV polymerisation and SI-ATRP. SI-ATRP has been shown to successfully introduce PEA onto PLLA surfaces (Sprott *et al.*, 2019) but was unsuccessful when used on our polystyrene surfaces. Optimisation of the method would likely involve including a step to produce more active initialisation points from the bromination step. If optimisation was successful further testing into degradation, mechanical properties and functionality would have to be carried out to determine if this would be a more effective method than plasma polymerisation. UV polymerisation successfully produced a layer of PEA on the polystyrene surface though similar validation would have to be carried out as with SI-ATRP. Additionally, cellular cytotoxicity should also be investigated to confirm that the chemical treatment of the surfaces with BPO and ethyl acrylate monomer do not negatively impact the cells.

In order to determine the success of the model for mimicking the bone marrow niche cell phenotyping would have to be continued. The inclusion of HSCs into the model along with MSCs would determine if the co-culture is able to maintain a LT-HSC population over time. Optimising a technique to successfully remove the cells from the system would allow the utilisation of techniques like PCR and flow cytometry to determine cell phenotype. The final model may also be optimised through tuning stiffness, changing GFs and cell types included in the system to mimic other tissues.

List of References

Achilias, D. S. and Sideridou, I. (2002) 'STUDY OF THE EFFECT OF TWO BPO/AMINE INITIATION SYSTEMS ON THE FREE-RADICAL POLYMERIZATION OF MMA USED IN DENTAL RESINS AND BONE CEMENTS', *Journal of Macromolecular Science, Part A*, 39(12), pp. 1435–1450. doi: 10.1081/MA-120016045.

Aggarwal, S. and Pittenger, M. F. (2005) 'Human mesenchymal stem cells modulate allogeneic immune cell responses', *Blood*, 105(4), pp. 1815–1822. doi: 10.1182/blood-2004-04-1559.

Ahmed, E. M. (2015) 'Hydrogel: Preparation, characterization, and applications: A review', *Journal of Advanced Research*. doi: 10.1016/j.jare.2013.07.006.

Akhtar, R. *et al.* (2018) 'Oscillatory nanoindentation of highly compliant hydrogels: A critical comparative analysis with rheometry', *Journal of Materials Research*, 33(8), pp. 873–883. doi: 10.1557/jmr.2018.62.

Almany, L. and Seliktar, D. (2005) 'Biosynthetic hydrogel scaffolds made from fibrinogen and polyethylene glycol for 3D cell cultures', *Biomaterials*, 26(15), pp. 2467–2477. doi: 10.1016/j.biomaterials.2004.06.047.

Anderson, H. J. *et al.* (2016) 'Mesenchymal stem cell fate: Applying biomaterials for control of stem cell behavior', *Frontiers in Bioengineering and Biotechnology*, 4(MAY), pp. 1–14. doi: 10.3389/fbioe.2016.00038.

Anderson, S. B. *et al.* (2011) 'The performance of human mesenchymal stem cells encapsulated in cell-degradable polymer-peptide hydrogels', *Biomaterials*. Elsevier Ltd, 32(14), pp. 3564–3574. doi: 10.1016/j.biomaterials.2011.01.064.

Anselme, K. (2000) 'Osteoblast adhesion on biomaterials', *Biomaterials*, 21(7), pp. 667–681. doi: 10.1016/S0142-9612(99)00242-2.

Anseth, K. S., Bowman, C. N. and Brannon-Peppas, L. (1996) 'Mechanical properties of hydrogels and their experimental determination', *Biomaterials*. doi: 10.1016/0142-9612(96)87644-7.

Antonchuk, J., Sauvageau, G. and Humphries, R. K. (2002) 'HOXB4-induced expansion of adult hematopoietic stem cells ex vivo', *Cell*, 109(1), pp. 39–45. doi: 10.1016/S0092-8674(02)00697-9.

Arantes-Rodrigues, R. *et al.* (2013) 'In Vitro and In Vivo experimental models as tools to investigate the efficacy of antineoplastic drugs on urinary bladder cancer', *Anticancer Research*, 33(4), pp. 1273–1296.

Ashrafian, H., Ahmed, K. and Athanasiou, T. (2010) 'The ethics of animal research', *Key Topics in Surgical Research and Methodology*, pp. 229–235. doi: 10.1007/978-3-540-71915-1_18.

Aumailley, M. (2013) 'The laminin family', *Cell Adhesion & Migration*, 7(1), pp. 48–55. doi: 10.4161/cam.22826.

Aversa, F. *et al.* (2005) 'Full haplotype-mismatched hematopoietic stem-cell transplantation: A phase II study in patients with acute leukemia at high risk of relapse', *Journal of Clinical Oncology*, 23(15), pp. 3447–3454. doi: 10.1200/JCO.2005.09.117.

Avraham, H. *et al.* (1993) 'Characterization of adhesive interactions between human endothelial cells and megakaryocytes', *Journal of Clinical Investigation*, 91(6), pp. 2378–2384. doi: 10.1172/JCI116470.

Bachman, H. *et al.* (2015) 'Utilizing Fibronectin Integrin-Binding Specificity to Control Cellular Responses', *Advances in Wound Care*, 4(8), pp. 501–511. doi: 10.1089/wound.2014.0621.

Baguley, B. C. and Marshall, E. S. (2004) 'In vitro modelling of human tumour behaviour in drug discovery programmes', *European Journal of Cancer*, 40(6), pp. 794–801. doi: 10.1016/j.ejca.2003.12.019.

Ball, L. M. *et al.* (2007) 'Cotransplantation of ex vivo-expanded mesenchymal stem cells accelerates lymphocyte recovery and may reduce the risk of graft failure in haploidentical hematopoietic stem-cell transplantation', *Blood*, 110(7), pp. 2764–2767. doi: 10.1182/blood-2007-04-087056.

Baneyx, G. and Vogel, V. (1999) 'Self-assembly of fibronectin into fibrillar networks underneath dipalmitoyl phosphatidylcholine monolayers: Role of lipid matrix and tensile forces', *Proceedings of the National Academy of Sciences of the United States of America*, 96(22), pp. 12518–12523. doi: 10.1073/pnas.96.22.12518.

Bathawab, F. *et al.* (2016) 'Lateral Chain Length in Polyalkyl Acrylates Determines the Mobility of Fibronectin at the Cell/Material Interface', *Langmuir*, 32(3), pp. 800–809. doi: 10.1021/acs.langmuir.5b03259.

Benoit, D. S. W. *et al.* (2008) 'Small functional groups for controlled differentiation of hydrogel-encapsulated human mesenchymal stem cells', *Nature Materials*. doi: 10.1038/nmat2269.

Benoit, D. S. W. and Anseth, K. S. (2005) 'The effect on osteoblast function of colocalized RGD and PHSRN epitopes on PEG surfaces', *Biomaterials*, 26(25), pp. 5209–5220. doi: 10.1016/j.biomaterials.2005.01.045.

Benoit, D. S. W., Durney, A. R. and Anseth, K. S. (2007) 'The effect of heparin-functionalized PEG hydrogels on three-dimensional human mesenchymal stem cell osteogenic differentiation', *Biomaterials*, 28(1), pp. 66–77. doi: 10.1016/j.biomaterials.2006.08.033.

Berkovitch, Y., Yelin, D. and Seliktar, D. (2015) 'Photo-patterning PEG-based hydrogels for neuronal engineering', *European Polymer Journal*. Elsevier Ltd, 72, pp. 473–483. doi: 10.1016/j.eurpolymj.2015.07.014.

Berrier, A. L. and Yamada, K. M. (2007) 'Cell-matrix adhesion', *Journal of Cellular Physiology*, 213(3), pp. 565–573. doi: 10.1002/jcp.21237.

Boontheekul, T. *et al.* (2007) 'Regulating myoblast phenotype through controlled gel stiffness and degradation', *Tissue Engineering*, 13(7), pp. 1431–1442. doi: 10.1089/ten.2006.0356.

Borges, E., Jan, Y. and Ruoslahti, E. (2000) 'Platelet-derived growth factor receptor ß and vascular endothelial growth factor receptor 2 bind to the ß 3

integrin through its extracellular domain', *Journal of Biological Chemistry*, 275(51), pp. 39867–39873. doi: 10.1074/jbc.M007040200.

Bowers, S. L. K., Banerjee, I. and Baudino, T. A. (2010) 'The extracellular matrix: At the center of it all', *Journal of Molecular and Cellular Cardiology*. Elsevier Ltd, 48(3), pp. 474–482. doi: 10.1016/j.yjmcc.2009.08.024.

Brinckmann, J. (2005) 'Collagens at a glance', *Topics in Current Chemistry*, 247, pp. 1–6. doi: 10.1007/b103817.

Brown, R. A., Blunn, G. W. and Ejim, O. S. (1994) 'Preparation of orientated fibrous mats from fibronectin: composition and stability', *Biomaterials*, 15(6), pp. 457–464. doi: 10.1016/0142-9612(94)90225-9.

Burdick, J. A. and Anseth, K. S. (2002) 'Photoencapsulation of osteoblasts in injectable RGD-modified PEG hydrogels for bone tissue engineering', *Biomaterials*, 23(22), pp. 4315–4323. doi: 10.1016/S0142-9612(02)00176-X.

Cacopardo, L. *et al.* (2019) 'Engineering hydrogel viscoelasticity', *Journal of the Mechanical Behavior of Biomedical Materials*. Elsevier Ltd, 89(May 2018), pp. 162–167. doi: 10.1016/j.jmbbm.2018.09.031.

Calderwood, D. A. *et al.* (2003) 'Integrin ß cytoplasmic domain interactions with phosphotyrosine-binding domains: A structural prototype for diversity in integrin signaling', *Proceedings of the National Academy of Sciences of the United States of America*, 100(5), pp. 2272–2277. doi: 10.1073/pnas.262791999.

Calderwood, D. A. (2004) 'Integrin activation', *Journal of Cell Science*, 117(5), pp. 657–666. doi: 10.1242/jcs.01014.

Caliari, S. R. and Burdick, J. A. (2016) 'A practical guide to hydrogels for cell culture', *Nature Methods*. Nature Publishing Group, 13(5), pp. 405–414. doi: 10.1038/nmeth.3839.

Calvi, L. M. *et al.* (2003) 'Osteoblastic cells regulate the haematopoietic stem cell niche', *Nature*, 425(6960), pp. 841–846. doi: 10.1038/nature02041.1.

Cantini, M., Rico, P., *et al.* (2012) 'Controlled wettability, same chemistry: Biological activity of plasma-polymerized coatings', *Soft Matter*, 8(20), pp. 5575–5584. doi: 10.1039/c2sm25413a.

Cantini, M., González-García, C., *et al.* (2012) 'Material-Driven Fibronectin Fibrillogenesis', in, pp. 471–496. doi: 10.1021/bk-2012-1120.ch022.

Caplan, A. I. (1991) 'Mesenchymal Stem Cells', *Journal of Orthopaedic Research*, 9(5), pp. 641–650. doi: doi.org/10.1002/jor.1100090504.

Charras, G. and Sahai, E. (2014) 'Physical influences of the extracellular environment on cell migration', *Nature Reviews Molecular Cell Biology*. Nature Publishing Group, 15(12), pp. 813–824. doi: 10.1038/nrm3897.

Chaudhuri, O. *et al.* (2015) 'Substrate stress relaxation regulates cell spreading', *Nature Communications*. Nature Publishing Group, 6, pp. 1–7. doi: 10.1038/ncomms7365.

Chaudhuri, O. *et al.* (2016) 'stem cell fate and activity', 15(March). doi: 10.1038/NMAT4489.

Chen, M., Zhong, M. and Johnson, J. A. (2016) 'Light-Controlled Radical Polymerization: Mechanisms, Methods, and Applications', *Chemical Reviews*, 116(17), pp. 10167–10211. doi: 10.1021/acs.chemrev.5b00671.

Chen, Q. *et al.* (2016) 'Fate decision of mesenchymal stem cells: Adipocytes or osteoblasts?', *Cell Death and Differentiation*, 23(7), pp. 1128–1139. doi: 10.1038/cdd.2015.168.

Cheng, Z. A. *et al.* (2019) 'Nanoscale Coatings for Ultralow Dose BMP-2-Driven Regeneration of Critical-Sized Bone Defects', *Advanced Science*, 6(2). doi: 10.1002/advs.201800361.

Choi, J. S. and Harley, B. A. C. (2017) 'Marrow-inspired matrix cues rapidly affect early fate decisions of hematopoietic stem and progenitor cells', *Science Advances*, 3(1). doi: 10.1126/sciadv.1600455.

Chua, K.-N. *et al.* (2007) 'Functional nanofiber scaffolds with different spacers modulate adhesion and expansion of cryopreserved umbilical cord blood hematopoietic stem/progenitor cells', *Experimental Hematology*, 35(5), pp. 771–781. doi: 10.1016/j.exphem.2007.02.002.

Cleton-Jansen, A.-M. (2015) 'Role of mesenchymal stem cells in bone cancer; initiation, propagation and metastasis', in *Bone Cancer*. Second Edi. Elsevier, pp. 73–82. doi: 10.1016/B978-0-12-416721-6.00007-8.

Cook, M. M. *et al.* (2012) 'Micromarrows-three-dimensional coculture of hematopoietic stem cells and mesenchymal stromal cells', *Tissue Engineering - Part C: Methods*, 18(5), pp. 319–328. doi: 10.1089/ten.tec.2011.0159.

Cox, T. R. and Erler, J. T. (2011) 'Remodeling and homeostasis of the extracellular matrix: Implications for fibrotic diseases and cancer', *DMM Disease Models and Mechanisms*, 4(2), pp. 165–178. doi: 10.1242/dmm.004077.

Crisan, M., Yap, S., Casteilla, L., Chen, C.-W., *et al.* (2008) 'A Perivascular Origin for Mesenchymal Stem Cells in Multiple Human Organs', *Cell Stem Cell*, 3(3), pp. 301–313. doi: 10.1016/j.stem.2008.07.003.

Crisan, M., Yap, S., Casteilla, L., Chen, C. W., *et al.* (2008) 'A Perivascular Origin for Mesenchymal Stem Cells in Multiple Human Organs', *Cell Stem Cell*, 3(3), pp. 301–313. doi: 10.1016/j.stem.2008.07.003.

Cruz-Acuña, R. *et al.* (2017) 'Synthetic hydrogels for human intestinal organoid generation and colonic wound repair', *Nature Cell Biology*, 19(11), pp. 1326–1335. doi: 10.1038/ncb3632.

Curran, J. M., Chen, R. and Hunt, J. A. (2005) 'Controlling the phenotype and function of mesenchymal stem cells in vitro by adhesion to silane-modified clean glass surfaces', *Biomaterials*, 26(34), pp. 7057–7067. doi: 10.1016/j.biomaterials.2005.05.008.

Curran, J. M., Chen, R. and Hunt, J. A. (2006) 'The guidance of human mesenchymal stem cell differentiation in vitro by controlled modifications to the

cell substrate', *Biomaterials*, 27(27), pp. 4783–4793. doi: 10.1016/j.biomaterials.2006.05.001.

D'Ippolito, G. *et al.* (2006) 'Low oxygen tension inhibits osteogenic differentiation and enhances stemness of human MIAMI cells', *Bone*, 39(3), pp. 513–522. doi: 10.1016/j.bone.2006.02.061.

Dalby, M. J. *et al.* (2007) 'The control of human mesenchymal cell differentiation using nanoscale symmetry and disorder', *Nature Materials*, 6(12), pp. 997–1003. doi: 10.1038/nmat2013.

Dalby, M. J., Gadegaard, N. and Oreffo, R. O. C. (2014) 'Harnessing nanotopography and integrin-matrix interactions to influence stem cell fate.', *Nature materials*, 13(6), pp. 558–69. doi: 10.1038/nmat3980.

Decker, C. (1996) 'Photoinitiated crosslinking polymerisation', *Progress in Polymer Science*, 21(4), pp. 593–650. doi: 10.1016/0079-6700(95)00027-5.

Dellatore, S. M., Garcia, A. S. and Miller, W. M. (2008) 'Mimicking stem cell niches to increase stem cell expansion', *Current Opinion in Biotechnology*, 19(5), pp. 534–540. doi: 10.1016/j.copbio.2008.07.010.

Dexter, T. M. (1982) 'Stromal cell associated haemopoiesis', *Journal of Cellular Physiology*, 113(1 S), pp. 87–94. doi: 10.1002/jcp.1041130414.

DiGiusto, D. L. *et al.* (2010) 'RNA-based gene therapy for HIV with lentiviral vector-modified CD34 + cells in patients undergoing transplantation for AIDS-related lymphoma', *Science Translational Medicine*, 2(36). doi: 10.1126/scitranslmed.3000931.

Ding, L. *et al.* (2012) 'Endothelial and perivascular cells maintain haematopoietic stem cells.', *Nature*, 481(7382), pp. 457–62. doi: 10.1038/nature10783.

Ding, L. and Morrison, S. J. (2013) 'Haematopoietic stem cells and early lymphoid progenitors occupy distinct bone marrow niches', *Nature*. Nature

Publishing Group, 495(7440), pp. 231–235. doi: 10.1038/nature11885.

Discher, D. E., Janmey, P. and Wang, Y. L. (2005) ‘Tissue cells feel and respond to the stiffness of their substrate’, *Science*, 310(5751), pp. 1139–1143. doi: 10.1126/science.1116995.

Discher, D. E., Mooney, D. J. and Zandstra, P. W. (2009) ‘Growth factors, matrices, and forces combine and control stem cells’, *Science*, 324(5935), pp. 1673–1677. doi: 10.1126/science.1171643.

Domingues, M. J. *et al.* (2017) ‘Niche Extracellular Matrix Components and Their Influence on HSC’, *Journal of Cellular Biochemistry*, 118(8), pp. 1984–1993. doi: 10.1002/jcb.25905.

Dominici, M. *et al.* (2006) ‘Minimal criteria for defining multipotent mesenchymal stromal cells. The International Society for Cellular Therapy position statement.’, *Cytotherapy*, 8(4), pp. 315–7. doi: 10.1080/14653240600855905.

Donnelly, H. *et al.* (2018) ‘Current approaches for modulation of the nanoscale interface in the regulation of cell behavior’, *Nanomedicine: Nanotechnology, Biology, and Medicine*. The Authors, 14(7), pp. 2455–2464. doi: 10.1016/j.nano.2017.03.020.

Donnelly, H. (2020) ‘Mechanistic and Metabolic Insights into Bioengineering the Bone Marrow Niche In Vitro’.

Doyle, A. D. *et al.* (2015) ‘Local 3D matrix microenvironment regulates cell migration through spatiotemporal dynamics of contractility-dependent adhesions’, *Nature Communications*. Nature Publishing Group, 6. doi: 10.1038/ncomms9720.

Draper, E. R. *et al.* (2015) ‘Hydrogels formed from Fmoc amino acids’, *CrystEngComm*. Royal Society of Chemistry, 17(42), pp. 8047–8057. doi: 10.1039/c5ce00801h.

Driessen, R. L., Johnston, H. M. and Nilsson, S. K. (2003) 'Membrane-bound stem cell factor is a key regulator in the initial lodgment of stem cells within the endosteal marrow region', *Experimental Hematology*, 31(12), pp. 1284–1291. doi: 10.1016/j.exphem.2003.08.015.

Eble, J. and Niland, S. (2009) 'The Extracellular Matrix of Blood Vessels', *Current Pharmaceutical Design*, 15(12), pp. 1385–1400. doi: 10.2174/138161209787846757.

El-Ghannam, A., Starr, L. and Jones, J. (1998) 'Laminin-5 coating enhances epithelial cell attachment, spreading, and hemidesmosome assembly on Ti-6A1-4V implant material in vitro', *Journal of Biomedical Materials Research*, 41(1), pp. 30–40. doi: 10.1002/(SICI)1097-4636(199807)41:1<30::AID-JBM4>3.0.CO;2-R.

El-Rashidy, A. A. *et al.* (2017) 'Regenerating bone with bioactive glass scaffolds: A review of in vivo studies in bone defect models', *Acta Biomaterialia*. Acta Materialia Inc., 62, pp. 1–28. doi: 10.1016/j.actbio.2017.08.030.

Ema, H. *et al.* (2000) 'In vitro self-renewal division of hematopoietic stem cells', *Journal of Experimental Medicine*, 192(9), pp. 1281–1288. doi: 10.1084/jem.192.9.1281.

Engel, E. *et al.* (2008) 'Nanotechnology in regenerative medicine: the materials side', *Trends in Biotechnology*, 26(1), pp. 39–47. doi: 10.1016/j.tibtech.2007.10.005.

Escuder, B., LLusar, M. and Miravet, J. F. (2006) 'Insight on the NMR study of supramolecular gels and its application to monitor molecular recognition on self-assembled fibers', *Journal of Organic Chemistry*, 71(20), pp. 7747–7752. doi: 10.1021/jo0612731.

Fehrer, C. *et al.* (2007) 'Reduced oxygen tension attenuates differentiation capacity of human mesenchymal stem cells and prolongs their lifespan', *Aging Cell*, 6(6), pp. 745–757. doi: 10.1111/j.1474-9726.2007.00336.x.

Feng, Q. *et al.* (2006) 'Expansion of engrafting human hematopoietic

stem/progenitor cells in three-dimensional scaffolds with surface-immobilized fibronectin', 78(4), pp. 781–791. doi: 10.1007/s11103-011-9767-z.Plastid.

Ferraro, F., Celso, C. Lo and Scadden, D. (2010) 'Adult Stem Cels and Their Niches', in *Advances in Experimental Medicine and Biology*, pp. 155–168. doi: 10.1007/978-1-4419-7037-4_11.

Fossiez, F. *et al.* (1996) 'T cell interleukin-17 induces stromal cells to produce proinflammatory and hematopoietic cytokines', *Journal of Experimental Medicine*, 183(6), pp. 2593–2603. doi: 10.1084/jem.183.6.2593.

Foster, M. P., McElroy, C. A. and Amero, C. D. (2007) 'Solution NMR of large molecules and assemblies', *Biochemistry*, 46(2), pp. 331–340. doi: 10.1021/bi0621314.

Frantz, C., Stewart, K. M. and Weaver, V. M. (2010) 'The extracellular matrix at a glance', *Journal of Cell Science*, 123(24), pp. 4195–4200. doi: 10.1242/jcs.023820.

Frenette, P. S. *et al.* (2013) *Mesenchymal Stem Cell: Keystone of the Hematopoietic Stem Cell Niche and a Stepping-Stone for Regenerative Medicine*, *Annual Review of Immunology*. doi: 10.1146/annurev-immunol-032712-095919.

Friedman, W. (2012) *Growth Factors*. Eighth Edi, *Basic Neurochemistry*. Eighth Edi. Elsevier Inc. doi: 10.1016/B978-0-12-374947-5.00029-8.

Fu, Y. and Kao, W. J. (2011) 'In situ forming poly(ethylene glycol)-based hydrogels via thiol-maleimide Michael-type addition', *Journal of Biomedical Materials Research Part A*. Wiley Subscription Services, Inc., A Wiley Company, 98A(2), pp. 201–211. doi: 10.1002/jbm.a.33106.

Gagnoux-Palacios, L. *et al.* (2001) 'The short arm of the laminin γ2 chain plays a pivotal role in the incorporation of laminin 5 into the extracellular matrix and in cell adhesion', *Journal of Cell Biology*, 153(4), pp. 835–849. doi: 10.1083/jcb.153.4.835.

Gattazzo, F., Urciuolo, A. and Bonaldo, P. (2014) 'Extracellular matrix: A dynamic microenvironment for stem cell niche', *Biochimica et Biophysica Acta - General Subjects*. Elsevier B.V., 1840(8), pp. 2506–2519. doi: 10.1016/j.bbagen.2014.01.010.

Geckil, H. *et al.* (2010) 'Engineering hydrogels as extracellular matrix mimics.Geckil, H., Xu, F., Zhang, X., Moon, S., & Demirci, U. (2010). Engineering hydrogels as extracellular matrix mimics. Nanomedicine (London, England), 5(3), 469–84. http://doi.org/10.2217/nnm.10.12', *Nanomedicine (London, England)*, 5(3), pp. 469–84. doi: 10.2217/nnm.10.12.

Geiger, B., Spatz, J. P. and Bershadsky, A. D. (2009) 'Environmental sensing through focal adhesions', *Nature Reviews Molecular Cell Biology*, 10(1), pp. 21–33. doi: 10.1038/nrm2593.

Greenbaum, A., Hsu, Y. M. S., *et al.* (2013) 'CXCL12 in early mesenchymal progenitors is required for haematopoietic stem-cell maintenance', *Nature*. Nature Publishing Group, 495(7440), pp. 227–230. doi: 10.1038/nature11926.

Greenbaum, A., Hsu, Y.-M. S., *et al.* (2013) 'CXCL12 Production by Early Mesenchymal Progenitors is Required for Hematopoietic Stem Cell Maintenance', *Nature*, 495(7440), pp. 227–230. doi: 10.1038/nature11926.CXCL12.

Gubareva, E. A. *et al.* (2016) 'Orthotopic transplantation of a tissue engineered diaphragm in rats', *Biomaterials*, 77, pp. 320–335. doi: 10.1016/j.biomaterials.2015.11.020.

Guerrouahen, B. S., Al-Hijji, I. and Tabrizi, A. R. (2011) 'Osteoblastic and vascular endothelial niches, their control on normal hematopoietic stem cells, and their consequences on the development of leukemia', *Stem Cells International*, 2011. doi: 10.4061/2011/375857.

Guilak, F. *et al.* (2009) 'Control of Stem Cell Fate by Physical Interactions with the Extracellular Matrix', *Cell Stem Cell*. Elsevier Inc., 5(1), pp. 17–26. doi: 10.1016/j.stem.2009.06.016.

Guvendiren, M. and Burdick, J. A. (2013) 'Engineering synthetic hydrogel microenvironments to instruct stem cells', *Current Opinion in Biotechnology*. Elsevier Ltd, 24(5), pp. 841–846. doi: 10.1016/j.copbio.2013.03.009.

Han, D. and Gouma, P. I. (2006) 'Electrospun bioscaffolds that mimic the topology of extracellular matrix', *Nanomedicine: Nanotechnology, Biology, and Medicine*, 2(1), pp. 37–41. doi: 10.1016/j.nano.2006.01.002.

Hanley, P. J. *et al.* (2013) 'Manufacturing mesenchymal stromal cells for phase I clinical trials', *Cytotherapy*, 15(4), pp. 416–422. doi: 10.1016/j.jcyt.2012.09.007.

He, X., Ma, J. and Jabbari, E. (2008) 'Effect of grafting RGD and BMP-2 protein-derived peptides to a hydrogel substrate on osteogenic differentiation of marrow stromal cells', *Langmuir*, 24(21), pp. 12508–12516. doi: 10.1021/la802447v.

Her, G. J. *et al.* (2013) 'Control of three-dimensional substrate stiffness to manipulate mesenchymal stem cell fate toward neuronal or glial lineages', *Acta Biomaterialia*. Acta Materialia Inc., 9(2), pp. 5170–5180. doi: 10.1016/j.actbio.2012.10.012.

Hirst, A. R. *et al.* (2008) 'Low-molecular-weight gelators: Elucidating the principles of gelation based on gelator solubility and a cooperative self-assembly model', *Journal of the American Chemical Society*, 130(28), pp. 9113–9121. doi: 10.1021/ja801804c.

Hoffman, A. S. (2012) 'Hydrogels for biomedical applications', *Advanced Drug Delivery Reviews*, 64, pp. 18–23. doi: 10.1016/j.addr.2012.09.010.

Huang, S. and Ingber, D. E. (2005) 'Cell tension, matrix mechanics, and cancer development', *Cancer Cell*, 8(3), pp. 175–176. doi: 10.1016/j.ccr.2005.08.009.

Huebsch, N. *et al.* (2010) 'Harnessing traction-mediated manipulation of the cell/matrix interface to control stem-cell fate', *Nature Materials*. Nature Publishing Group, 9(6), pp. 518–526. doi: 10.1038/nmat2732.

Hynes, R. O. (1999) ‘The dynamic dialogue between cells and matrices: Implications of fibronectin’s elasticity’, *Proceedings of the National Academy of Sciences of the United States of America*, 96(6), pp. 2588–2590. doi: 10.1073/pnas.96.6.2588.

Hynes, R. O. (2002) ‘Integrins’, *Cell*. Elsevier, 110(6), pp. 673–687. doi: 10.1016/S0092-8674(02)00971-6.

Hynes, R. O. (2009) ‘The extracellular matrix: Not just pretty fibrils’, *Science*, 326(5957), pp. 1216–1219. doi: 10.1126/science.1176009.

Jana, S., Cooper, A. and Zhang, M. (2013) ‘Chitosan scaffolds with unidirectional microtubular pores for large skeletal myotube generation’, *Advanced Healthcare Materials*, 2(4), pp. 557–561. doi: 10.1002/adhm.201200177.

Jansen, L. E. *et al.* (2015) ‘Mechanics of intact bone marrow’, *Journal of the Mechanical Behavior of Biomedical Materials*, 50(5), pp. 299–307. doi: 10.1016/j.jmbbm.2015.06.023.

Jeyaprakash, J. D. *et al.* (2002) ‘Polymer brushes via ATRP: Role of activator and deactivator in the surface-initiated ATRP of styrene on planar substrates’, *Macromolecular Rapid Communications*, 23(4), pp. 277–281. doi: 10.1002/1521-3927(20020301)23:4<277::AID-MARC277>3.0.CO;2-U.

Jha, A. K. *et al.* (2016) ‘Matrix metalloproteinase-13 mediated degradation of hyaluronic acid-based matrices orchestrates stem cell engraftment through vascular integration’, *Biomaterials*. Elsevier Ltd, 89, pp. 136–147. doi: 10.1016/j.biomaterials.2016.02.023.

Jimi, E. *et al.* (2012) ‘The current and future therapies of bone regeneration to repair bone defects’, *International Journal of Dentistry*, 2012, pp. 1–8. doi: 10.1155/2012/148261.

Jing, D. *et al.* (2010) ‘Hematopoietic stem cells in co-culture with mesenchymal stromal cells - modeling the niche compartments in vitro’, *Haematologica*, 95(4), pp. 542–550. doi: 10.3324/haematol.2009.010736.

Kasemo, B. (1983) ‘Biocompatibility of titanium implants: Surface science aspects’, *The Journal of Prosthetic Dentistry*, 49(6), pp. 832–837. doi: 10.1016/0022-3913(83)90359-1.

Kern, S. *et al.* (2006) ‘Comparative Analysis of Mesenchymal Stem Cells from Bone Marrow, Umbilical Cord Blood, or Adipose Tissue’, *Stem Cells*, 24(5), pp. 1294–1301. doi: 10.1634/stemcells.2005-0342.

Khalili, A. A. and Ahmad, M. R. (2015) ‘A Review of cell adhesion studies for biomedical and biological applications’, *International Journal of Molecular Sciences*, 16(8), pp. 18149–18184. doi: 10.3390/ijms160818149.

Khan, F., Tanaka, M. and Ahmad, S. R. (2015) ‘Fabrication of polymeric biomaterials: a strategy for tissue engineering and medical devices’, *Journal of Materials Chemistry B*. Royal Society of Chemistry, 3(42), pp. 8224–8249. doi: 10.1039/c5tb01370d.

Khandare, J. and Minko, T. (2006) ‘Polymer-drug conjugates: Progress in polymeric prodrugs’, *Progress in Polymer Science (Oxford)*, 31(4), pp. 359–397. doi: 10.1016/j.progpolymsci.2005.09.004.

Khetan, S. and Burdick, J. (2009) ‘Cellular encapsulation in 3D hydrogels for tissue engineering’, *Journal of Visualized Experiments*, (32), pp. 2–5. doi: 10.3791/1590.

Kiel, M. J. *et al.* (2005) ‘Spatial differences in hematopoiesis but not in stem cells indicate a lack of regional patterning in definitive hematopoietic stem cells’, *Developmental Biology*, 283(1), pp. 29–39. doi: 10.1016/j.ydbio.2005.03.037.

Klamer, S. and Voermans, C. (2014) ‘The role of novel and known extracellular matrix and adhesion molecules in the homeostatic and regenerative bone marrow microenvironment http://www.tandfonline.com/doi/pdf/10.4161/19336918.2014.968501’, *Cell Adhesion and Migration*, 8(6), pp. 563–577. doi: 10.4161/19336918.2014.968501.

Knippenberg, M. *et al.* (2006) 'Osteogenesis versus chondrogenesis by BMP-2 and BMP-7 in adipose stem cells', *Biochemical and Biophysical Research Communications*, 342(3), pp. 902–908. doi: 10.1016/j.bbrc.2006.02.052.

Kolf, C. M., Cho, E. and Tuan, R. S. (2007) 'Mesenchymal stromal cells. Biology of adult mesenchymal stem cells: Regulation of niche, self-renewal and differentiation', *Arthritis Research and Therapy*, 9(1), pp. 1–10. doi: 10.1186/ar2116.

Kopp, H. G. *et al.* (2005) 'The bone marrow vascular niche: Home of HSC differentiation and mobilization', *Physiology*, 20(5), pp. 349–356. doi: 10.1152/physiol.00025.2005.

Kraus, K. H. and Kirker-Head, C. (2006) 'Mesenchymal stem cells and bone regeneration', *Veterinary Surgery*, 35(3), pp. 232–242. doi: 10.1111/j.1532-950X.2006.00142.x.

Krause, D. S. *et al.* (2001) 'Multi-organ, multi-lineage engraftment by a single bone marrow-derived stem cell', *Cell*, 105(3), pp. 369–377. doi: 10.1016/S0092-8674(01)00328-2.

Kretlow, J. D. and Mikos, A. G. (2007) 'Review: Mineralization of synthetic polymer scaffolds for bone tissue engineering', *Tissue Engineering*, 13(5), pp. 927–938. doi: 10.1089/ten.2006.0394.

Krosl, J. *et al.* (2003) 'In vitro expansion of hematopoietic stem cells by recombinant TAT-HOXB4 protein', *Nature Medicine*, 9(11), pp. 1428–1432. doi: 10.1038/nm951.

Krsko, P. and Libera, M. (2005) 'Biointeractive hydrogels', *Materials Today*. Elsevier Ltd, 8(12), pp. 36–44. doi: 10.1016/S1369-7021(05)71223-2.

Kuhl, P. R. and Griffith-Cima, L. G. (1996) 'Tethered epidermal growth factor as a paradigm for growth factor–induced stimulation', *Nature Medicine*, 2(9), pp. 1022–1027. doi: 10.1038/nm1196-1211.

Kumar, A. *et al.* (2016) 'Ternary hybrid polymeric nanocomposites through grafting of polystyrene on graphene oxide-TiO2 by surface initiated atom transfer radical polymerization (SI-ATRP)', *Materials Chemistry and Physics*. Elsevier B.V, 172, pp. 189–196. doi: 10.1016/j.matchemphys.2016.01.064.

Kunisaki, Y., Bruns, I., Scheiermann, C., Ahmed, J., Pinho, S., Zhang, D., Mizoguchi, T., Wei, Q., Lucas, D., Ito, K., Mar, Jessica C, *et al.* (2013) 'Arteriolar niches maintain haematopoietic stem cell quiescence', *Nature*, 502(7473), pp. 637–643. doi: 10.1038/nature12612.

Kunisaki, Y., Bruns, I., Scheiermann, C., Ahmed, J., Pinho, S., Zhang, D., Mizoguchi, T., Wei, Q., Lucas, D., Ito, K., Mar, Jessica C., *et al.* (2013) 'Arteriolar niches maintain haematopoietic stem cell quiescence', *Nature*. Nature Publishing Group, 502(7473), pp. 637–643. doi: 10.1038/nature12612.

Kyburz, K. A. and Anseth, K. S. (2015) 'Synthetic Mimics of the Extracellular Matrix: How Simple is Complex Enough?', *Annals of Biomedical Engineering*, 43(3), pp. 489–500. doi: 10.1007/s10439-015-1297-4.

Langer, R. and Tirrell, D. A. (2004) 'Designing materials for biology and medicine', *Nature*, 428(6982), pp. 487–492. doi: 10.1038/nature02388.

Lau, T. L. *et al.* (2009) 'The structure of the integrin αIIbB3 transmembrane complex explains integrin transmembrane signalling', *EMBO Journal*, 28(9), pp. 1351–1361. doi: 10.1038/emboj.2009.63.

Lee, D., Zhang, H. and Ryu, S. (2018) 'Elastic Modulus Measurement of Hydrogels', in Mondal, M. I. H. (ed.) *Cellulose-Based Superabsorbent Hydrogels*. Cham: Springer International Publishing, pp. 1–21. doi: 10.1007/978-3-319-76573-0_60-1.

Leisten, I. *et al.* (2012) '3D co-culture of hematopoietic stem and progenitor cells and mesenchymal stem cells in collagen scaffolds as a model of the hematopoietic niche', *Biomaterials*, 33(6), pp. 1736–1747. doi: 10.1016/j.biomaterials.2011.11.034.

Lerman, M. J. *et al.* (2018) 'The Evolution of Polystyrene as a Cell Culture Material', *Tissue Engineering - Part B: Reviews*, 24(5), pp. 359–372. doi: 10.1089/ten.teb.2018.0056.

Lesný, P. *et al.* (2002) 'Polymer hydrogels usable for nervous tissue repair', *Journal of Chemical Neuroanatomy*, 23(4), pp. 243–247. doi: 10.1016/S0891-0618(02)00011-X.

Lévesque, J. P., Helwani, F. M. and Winkler, I. G. (2010) 'The endosteal osteoblastic niche and its role in hematopoietic stem cell homing and mobilization', *Leukemia*, 24(12), pp. 1979–1992. doi: 10.1038/leu.2010.214.

Lin, C. C. and Anseth, K. S. (2009) 'Glucagon-like peptide-1 functionalized PEG hydrogels promote survival and function of encapsulated pancreatic ß-cells', *Biomacromolecules*, 10(9), pp. 2460–2467. doi: 10.1021/bm900420f.

Lin, F. *et al.* (2011) 'Fibronectin growth factor-binding domains are required for fibroblast survival', *Journal of Investigative Dermatology*. Elsevier Masson SAS, 131(1), pp. 84–98. doi: 10.1038/jid.2010.253.

Lindahl, U. *et al.* (2017) *Proteoglycans and Sulfated Glycosamionglycans*. 3rd edn, *Essentials of Glycobiology*. 3rd edn. Cold Spring Harour Laboratory Press.

Llopis-Hernández, V. *et al.* (2013) 'Role of Material-Driven Fibronectin Fibrillogenesis in Protein Remodeling', *BioResearch Open Access*, 2(5), pp. 364–373. doi: 10.1089/biores.2013.0017.

Llopis-Hernández, V. *et al.* (2015) 'Material-based strategies to engineer fibronectin matrices for regenerative medicine', *International Materials Reviews*, 60(5), pp. 245–264. doi: 10.1179/1743280414Y.0000000049.

Llopis-Hernández, V. *et al.* (2016) 'Material-driven fibronectin assembly for high-efficiency presentation of growth factors.', *Science advances*, 2(8), p. e1600188. doi: 10.1126/sciadv.1600188.

Lozano Picazo, P. *et al.* (2015) 'New semi-biodegradable materials from semi-

interpenetrated networks of poly(ε-caprolactone) and poly(ethyl acrylate)', *Macromolecular Bioscience*, 15(2), pp. 229–240. doi: 10.1002/mabi.201400331.

Lucas, D. *et al.* (2011) 'Bone Marrow Neuropathy Prevents Hematopoietic Regeneration', *Blood*, 118(21), pp. 139–139. doi: 10.1182/blood.V118.21.139.139.

Luster, A. D. (1998) 'Chemokines — Chemotactic Cytokines That Mediate Inflammation', *New England Journal of Medicine*. Edited by F. H. Epstein, 338(7), pp. 436–445. doi: 10.1056/NEJM199802123380706.

Lutolf, M. P. and Hubbell, J. A. (2005) 'Synthetic biomaterials as instructive extracellular microenvironments for morphogenesis in tissue engineering', *Nature Biotechnology*, 23(1), pp. 47–55. doi: 10.1038/nbt1055.

Lyman, S. D. and Jacobsen, S. E. W. (1998) 'c-kit Ligand and Flt3 Ligand: Stem/Progenitor Cell Factors With Overlapping Yet Distinct Activities', *Blood*, 91(4), pp. 1101–1134. doi: 10.1182/blood.V91.4.1101.

Madl, C. M. *et al.* (2017) 'Maintenance of neural progenitor cell stemness in 3D hydrogels requires matrix remodelling', *Nature Materials*, 16(12), pp. 1233–1242. doi: 10.1038/nmat5020.

Mao, A. S., Shin, J. and Mooney, D. J. (2016) 'Biomaterials Effects of substrate stiffness and cell-cell contact on mesenchymal stem cell differentiation', *Biomaterials*. Elsevier Ltd, 98, pp. 184–191. doi: 10.1016/j.biomaterials.2016.05.004.

Martino, M. M. and Hubbell, J. A. (2010) 'The 12th–14th type III repeats of fibronectin function as a highly promiscuous growth factor-binding domain', *The FASEB Journal*, 24(12), pp. 4711–4721. doi: 10.1096/fj.09-151282.

Mason, B. N. *et al.* (2013) 'Tuning three-dimensional collagen matrix stiffness independently of collagen concentration modulates endothelial cell behavior', *Acta Biomaterialia*. Acta Materialia Inc., 9(1), pp. 4635–4644. doi: 10.1016/j.actbio.2012.08.007.

Mason, B. N., Califano, J. P. and Reinhart-King, C. A. (2012) 'Matrix Stiffness: A Regulator of Cellular Behavior and Tissue Formation', in Bhatia, S. K. (ed.) *Engineering Biomaterials for Regenerative Medicine*. New York, NY: Springer New York, pp. 19–37. doi: 10.1007/978-1-4614-1080-5_2.

Mather, R. R. (2009) 'Surface modification of textiles by plasma treatments', in *Surface Modification of Textiles*. Elsevier, pp. 296–317. doi: 10.1533/9781845696689.296.

Matyjaszewski, K. *et al.* (2007) 'Grafting from Surfaces for "Everyone": ARGET ATRP in the Presence of Air', *Langmuir*, 23(8), pp. 4528–4531. doi: 10.1021/la063402e.

Matyjaszewski, K. and Xia, J. (2001) 'Atom transfer radical polymerization', *Chemical Reviews*, 101(9), pp. 2921–2990. doi: 10.1021/cr940534g.

Mellott, M. B., Searcy, K. and Pishko, M. V. (2001) 'Release of protein from highly cross-linked hydrogels of poly(ethylene glycol) diacrylate fabricated by UV polymerization', *Biomaterials*, 22(9), pp. 929–941. doi: 10.1016/S0142-9612(00)00258-1.

Méndez-Ferrer, S., Michurina, T. V, *et al.* (2010) 'Mesenchymal and haematopoietic stem cells form a unique bone marrow niche.', *Nature*, 466(7308), pp. 829–34. doi: 10.1038/nature09262.

Méndez-Ferrer, S., Michurina, T. V., *et al.* (2010) 'Mesenchymal and haematopoietic stem cells form a unique bone marrow niche', *Nature*, 466(7308), pp. 829–834. doi: 10.1038/nature09262.

Metzger, T. A. *et al.* (2014) 'Rheological behavior of fresh bone marrow and the effects of storage', *Journal of the Mechanical Behavior of Biomedical Materials*. Elsevier, 40, pp. 307–313. doi: 10.1016/j.jmbbm.2014.09.008.

Mitragotri, S. and Lahann, J. (2009) 'Physical approaches to biomaterial design', *Nature Materials*, 8(1), pp. 15–23. doi: 10.1038/nmat2344.

Mohammadi, M., Olsen, S. K. and Goetz, R. (2005) 'A protein canyon in the FGF-FGF receptor dimer selects from an à la carte menu of heparan sulfate motifs', *Current Opinion in Structural Biology*, 15(5), pp. 506–516. doi: 10.1016/j.sbi.2005.09.002.

Mohyeldin, A., Garzón-Muvdi, T. and Quiñones-Hinojosa, A. (2010) 'Oxygen in Stem Cell Biology: A Critical Component of the Stem Cell Niche', *Cell Stem Cell*, 7(2), pp. 150–161. doi: 10.1016/j.stem.2010.07.007.

Morandi, G., Heath, L. and Thielemans, W. (2009) 'Cellulose nanocrystals grafted with polystyrene chains through Surface-Initiated Atom Transfer Radical Polymerization (SI-ATRP)', *Langmuir*, 25(14), pp. 8280–8286. doi: 10.1021/la900452a.

Morrison, S. J. and Scadden, D. T. (2014) 'The bone marrow niche for haematopoietic stem cells.', *Nature*, 505(7483), pp. 327–34. doi: 10.1038/nature12984.

Moulisová, V. *et al.* (2017) 'Engineered microenvironments for synergistic VEGF – Integrin signalling during vascularization', *Biomaterials*, 126, pp. 61–74. doi: 10.1016/j.biomaterials.2017.02.024.

Mouw, J. K., Ou, G. and Weaver, V. M. (2014) 'Extracellular matrix assembly: A multiscale deconstruction', *Nature Reviews Molecular Cell Biology*. Nature Publishing Group, 15(12), pp. 771–785. doi: 10.1038/nrm3902.

Mpoyi, E. N. *et al.* (2016) 'Protein Adsorption as a Key Mediator in the Nanotopographical Control of Cell Behavior'. doi: 10.1021/acsnano.6b01649.

Murphy, W. L., McDevitt, T. C. and Engler, A. J. (2014) 'Materials as stem cell regulators', *Nature Materials*, 13(6), pp. 547–557. doi: 10.1038/nmat3937.

Nair, D. P. *et al.* (2014) 'The Thiol-Michael addition click reaction: A powerful and widely used tool in materials chemistry', *Chemistry of Materials*, 26(1), pp. 724–744. doi: 10.1021/cm402180t.

Nakamura, Y. *et al.* (2010) 'Isolation and characterization of endosteal niche cell populations that regulate hematopoietic stem cells', *Blood*, 116(9), pp. 1422–1432. doi: 10.1182/blood-2009-08-239194.

Nakatsu, M. N. *et al.* (2003) 'Angiogenic sprouting and capillary lumen formation modeled by human umbilical vein endothelial cells (HUVEC) in fibrin gels: The role of fibroblasts and Angiopoietin-1', *Microvascular Research*, 66(2), pp. 102–112. doi: 10.1016/S0026-2862(03)00045-1.

Nelea, V. and Kaartinen, M. T. (2010) 'Periodic beaded-filament assembly of fibronectin on negatively charged surface', *Journal of Structural Biology*. Elsevier Inc., 170(1), pp. 50–59. doi: 10.1016/j.jsb.2010.01.009.

Nuttelman, C. R. *et al.* (2001) 'Attachment of fibronectin to poly(vinyl alcohol) hydrogels promotes NIH3T3 cell adhesion, proliferation, and migration', *Journal of Biomedical Materials Research*, 57(2), pp. 217–223. doi: 10.1002/1097-4636(200111)57:2<217::AID-JBM1161>3.0.CO;2-I.

O'Brien, F. J. (2011) 'Biomaterials & scaffolds for tissue engineering', *Materials Today*. Elsevier Ltd, 14(3), pp. 88–95. doi: 10.1016/S1369-7021(11)70058-X.

Omatsu, Y. *et al.* (2010) 'The Essential Functions of Adipo-osteogenic Progenitors as the Hematopoietic Stem and Progenitor Cell Niche', *Immunity*. Elsevier Inc., 33(3), pp. 387–399. doi: 10.1016/j.immuni.2010.08.017.

Orkin, S. H. and Zon, L. I. (2008) 'Hematopoiesis: An Evolving Paradigm for Stem Cell Biology', *Cell*, 132(4), pp. 631–644. doi: 10.1016/j.cell.2008.01.025.

Ott, H. C. *et al.* (2008) 'Perfusion-decellularized matrix: Using nature's platform to engineer a bioartificial heart', *Nature Medicine*, 14(2), pp. 213–221. doi: 10.1038/nm1684.

Page-McCaw, A., Ewald, A. J. and Werb, Z. (2007) 'Matrix metalloproteinases and the regulation of tissue remodelling', *Nature Reviews Molecular Cell Biology*, 8(3), pp. 221–233. doi: 10.1038/nrm2125.

Pankov, R. and Yamada, K. M. (2002) 'Fibronectin at a glance', *Journal of Cell Science*, 115(20), pp. 3861–3863. doi: 10.1242/jcs.00059.

Park, S. and Park, K. M. (2016) 'Engineered polymeric hydrogels for 3D tissue models', *Polymers*, 8(1). doi: 10.3390/polym8010023.

Pelletier, A. J. *et al.* (2000) 'Presentation of chemokine SDF-1α by fibronectin mediates directed migration of T cells', *Blood*, 96(8), pp. 2682–2690. doi: 10.1182/blood.v96.8.2682.h8002682_2682_2690.

Peppas, N. A. and Langer, R. (1994) 'New challenges in biomaterials', *Science*, 263(5154), pp. 1715–1720. doi: 10.1126/science.8134835.

Petrini, C. (2010) 'Umbilical cord blood collection, storage and use: Ethical issues', *Blood Transfusion*, 8(3), pp. 139–148. doi: 10.2450/2010.0152-09.

Pfister, D. and Morbidelli, M. (2014) 'Process for protein PEGylation', *Journal of Controlled Release*, 180(1), pp. 134–149. doi: 10.1016/j.jconrel.2014.02.002.

Phelps, E. A. *et al.* (2012) 'Maleimide cross-linked bioactive PEG hydrogel exhibits improved reaction kinetics and cross-linking for cell encapsulation and in situ delivery', *Advanced Materials*, 24(1), pp. 64–70. doi: 10.1002/adma.201103574.

Phillips, J. E. *et al.* (2010) 'Human mesenchymal stem cell differentiation on self-assembled monolayers presenting different surface chemistries', *Acta Biomaterialia*. Acta Materialia Inc., 6(1), pp. 12–20. doi: 10.1016/j.actbio.2009.07.023.

Pinho, S. *et al.* (2013) 'PDGFRα and CD51 mark human Nestin+ sphere-forming mesenchymal stem cells capable of hematopoietic progenitor cell expansion', *Journal of Experimental Medicine*, 210(7), pp. 1351–1367. doi: 10.1084/jem.20122252.

Pinho, S. and Frenette, P. S. (2019) 'Haematopoietic stem cell activity and interactions with the niche', *Nature Reviews Molecular Cell Biology*, 20(5), pp.

303–320. doi: 10.1038/s41580-019-0103-9.

Platt, M. O. *et al.* (2009) 'Sustained epidermal growth factor receptor levels and activation by tethered ligand binding enhances osteogenic differentiation of multi-potent marrow stromal cells', *Journal of Cellular Physiology*, 221(2), pp. 306–317. doi: 10.1002/jcp.21854.

Plodinec, M. *et al.* (2012) 'The nanomechanical signature of breast cancer', *Nature Nanotechnology*. Nature Publishing Group, 7(11), pp. 757–765. doi: 10.1038/nnano.2012.167.

Plow, E. F. *et al.* (2000) 'Ligand binding to integrins', *Journal of Biological Chemistry*, 275(29), pp. 21785–21788. doi: 10.1074/jbc.R000003200.

Pobloth, A.-M. *et al.* (2018) 'Mechanobiologically optimized 3D titanium-mesh scaffolds enhance bone regeneration in critical segmental defects in sheep', *Science Translational Medicine*, 10(423), p. eaam8828. doi: 10.1126/scitranslmed.aam8828.

Powers, C. J., McLeskey, S. W. and Wellstein, A. (2000) 'Fibroblast growth factors, their receptors and signaling', *Endocrine-Related Cancer*, 7(3), pp. 165–197. doi: 10.1677/erc.0.0070165.

Pradhan, S. *et al.* (2016) 'Polymeric biomaterials for in vitro cancer tissue engineering and drug testing applications', *Tissue Engineering - Part B: Reviews*, 22(6), pp. 470–484. doi: 10.1089/ten.teb.2015.0567.

Psaltis, P. J. *et al.* (2010) 'Enrichment for STRO-1 expression enhances the cardiovascular paracrine activity of human bone marrow-derived mesenchymal cell populations', *Journal of Cellular Physiology*, 223(2), pp. 530–540. doi: 10.1002/jcp.22081.

Qian, H. *et al.* (2007) 'Critical Role of Thrombopoietin in Maintaining Adult Quiescent Hematopoietic Stem Cells', *Cell Stem Cell*, 1(6), pp. 671–684. doi: 10.1016/j.stem.2007.10.008.

Qian, Y. *et al.* (2018) 'An integrated multi-layer 3D-fabrication of PDA/RGD coated graphene loaded PCL nanoscaffold for peripheral nerve restoration', *Nature Communications*. Springer US, 9(1). doi: 10.1038/s41467-017-02598-7.

Quint, C. *et al.* (2011) 'Decellularized tissue-engineered blood vessel as an arterial conduit', *Proceedings of the National Academy of Sciences of the United States of America*, 108(22), pp. 9214–9219. doi: 10.1073/pnas.1019506108.

Raeber, G. P., Lutolf, M. P. and Hubbell, J. A. (2005) 'Molecularly Engineered PEG Hydrogels: A Novel Model System for Proteolytically Mediated Cell Migration', *Biophysical Journal*, 89(2), pp. 1374–1388. doi: 10.1529/biophysj.104.050682.

Raghavan, S. R. *et al.* (1996) 'Rheological study of crosslinking and gelation in chlorobutyl elastomer systems', *Polymer*, 37(26), pp. 5869–5875. doi: 10.1016/S0032-3861(96)00446-6.

Ramsey, W. S. *et al.* (1984) 'Surface treatments and cell attachment', *In Vitro*, 20(10), pp. 802–808. doi: 10.1007/BF02618296.

Redick, S. D. *et al.* (2000) 'Defining Fibronectin's cell adhesion synergy site by site-directed mutagenesis', *Journal of Cell Biology*, 149(2), pp. 521–527. doi: 10.1083/jcb.149.2.521.

Rho, J. Y., Kuhn-Spearing, L. and Zioupos, P. (1998) 'Mechanical properties and the hierarchical structure of bone', *Medical Engineering and Physics*, 20(2), pp. 92–102. doi: 10.1016/S1350-4533(98)00007-1.

Rhodes, J. M. and Simons, M. (2007) 'The extracellular matrix and blood vessel formation: Not just a scaffold: Angiogenesis Review Series', *Journal of Cellular and Molecular Medicine*, 11(2), pp. 176–205. doi: 10.1111/j.1582-4934.2007.00031.x.

Rizzi, S. C. *et al.* (2006) 'Recombinant protein-co-PEG networks as cell-adhesive and proteolytically degradable hydrogel matrixes. Part II: Biofunctional characteristics', *Biomacromolecules*, 7(11), pp. 3019–3029. doi:

10.1021/bm060504a.

Rizzi, S. C. and Hubbell, J. A. (2005) ‘Recombinant protein-co-PEG networks as cell-adhesive and proteolytically degradable hydrogel matrixes. Part I: Development and physicochemical characteristics’, *Biomacromolecules*, 6(3), pp. 1226–1238. doi: 10.1021/bm049614c.

Roberts, J. J. and Bryant, S. J. (2013) ‘Comparison of photopolymerizable thiol-ene PEG and acrylate-based PEG hydrogels for cartilage development’, *Biomaterials*. Elsevier Ltd, 34(38), pp. 9969–9979. doi: 10.1016/j.biomaterials.2013.09.020.

Rodrigues, M. *et al.* (2013) ‘Surface tethered epidermal growth factor protects proliferating and differentiating multipotential stromal cells from FasL-induced apoptosis’, *Stem Cells*, 31(1), pp. 104–116. doi: 10.1002/stem.1215.

Rodriguez-Fraticelli, A. E. *et al.* (2018) ‘Clonal analysis of lineage fate in native haematopoiesis’, *Nature*. Nature Publishing Group, 553(7687), pp. 212–216. doi: 10.1038/nature25168.

Romano, N. H. *et al.* (2011) ‘Protein-engineered biomaterials: Nanoscale mimics of the extracellular matrix’, *Biochimica et Biophysica Acta - General Subjects*. Elsevier B.V., 1810(3), pp. 339–349. doi: 10.1016/j.bbagen.2010.07.005.

Rose, J. C. *et al.* (2017) ‘Nerve Cells Decide to Orient inside an Injectable Hydrogel with Minimal Structural Guidance’, *Nano Letters*, 17(6), pp. 3782–3791. doi: 10.1021/acs.nanolett.7b01123.

Rowley, J. A. and Mooney, D. J. (2002) ‘Alginate type and RGD density control myoblast phenotype’, *Journal of Biomedical Materials Research*, 60(2), pp. 217–223. doi: 10.1002/jbm.1287.

Sakai, K., Fujii, T. and Hayashi, T. (1994) ‘Cell-Free Formation of Disulfide-Bonded Multimer from Isolated Plasma Fibronectin in the Presence of a Low Concentration of SH Reagent under a Physiological Condition’, *The Journal of Biochemistry*, 115(3), pp. 415–421. doi:

10.1093/oxfordjournals.jbchem.a124353.

Salinas, C. N. and Anseth, K. S. (2008) 'The influence of the RGD peptide motif and its contextual presentation in PEG gels on human mesenchymal stem cell viability', *Journal of Tissue Engineering and Regenerative Medicine*, 2(5), pp. 296–304. doi: 10.1002/term.95.

Salmerón-Sánchez, M. *et al.* (2011) 'Role of material-driven fibronectin fibrillogenesis in cell differentiation', *Biomaterials*. Elsevier Ltd, 32(8), pp. 2099–2105. doi: 10.1016/j.biomaterials.2010.11.057.

Schedin, P. *et al.* (2004) 'Mammary ECM Composition and function are altered by reproductive state', *Molecular Carcinogenesis*, 41(4), pp. 207–220. doi: 10.1002/mc.20058.

Schneider, R. K. *et al.* (2010) 'The osteogenic differentiation of adult bone marrow and perinatal umbilical mesenchymal stem cells and matrix remodelling in three-dimensional collagen scaffolds', *Biomaterials*, 31(3), pp. 467–480. doi: 10.1016/j.biomaterials.2009.09.059.

Schwalm, R. (2007) 'Introduction to Coatings Technology', in *UV Coatings*. Elsevier, pp. 1–18. doi: 10.1016/B978-044452979-4/50001-9.

Schwartz, M. A. (2010) 'Integrins and Extracellular Matrix in Mechanotransduction', *Cold Spring Harbor Perspectives in Biology*, 2(12), pp. a005066–a005066. doi: 10.1101/cshperspect.a005066.

Sharma, M. B., Limaye, L. S. and Kale, V. P. (2012) 'Mimicking the functional hematopoietic stem cell niche in vitro: Recapitulation of marrow physiology by hydrogel-based three-dimensional cultures of mesenchymal stromal cells', *Haematologica*, 97(5), pp. 651–660. doi: 10.3324/haematol.2011.050500.

Shi, S. and Gronthos, S. (2003) 'Perivascular Niche of Postnatal Mesenchymal Stem Cells in Human Bone Marrow and Dental Pulp', *Journal of Bone and Mineral Research*, 18(4), pp. 696–704. doi: 10.1359/jbmr.2003.18.4.696.

Sieburg, H. B. *et al.* (2006) 'The hematopoietic stem compartment consists of a limited number of discrete stem cell subsets', *Blood*, 107(6), pp. 2311–2316. doi: 10.1182/blood-2005-07-2970.

Siegwart, D. J., Oh, J. K. and Matyjaszewski, K. (2012) 'ATRP in the design of functional materials for biomedical applications', *Progress in Polymer Science (Oxford)*. Elsevier Ltd, 37(1), pp. 18–37. doi: 10.1016/j.progpolymsci.2011.08.001.

Singh, V. K. *et al.* (2016) 'Describing the stem cell potency: The various methods of functional assessment and in silico diagnostics', *Frontiers in Cell and Developmental Biology*, 4(NOV). doi: 10.3389/fcell.2016.00134.

Sodunke, T. R. *et al.* (2007) 'Micropatterns of Matrigel for three-dimensional epithelial cultures', *Biomaterials*, 28(27), pp. 4006–4016. doi: 10.1016/j.biomaterials.2007.05.021.

Spinelli, V., Guillot, P. V. and De Coppi, P. (2014) *Principles of Stem Cell Biology, Regenerative Medicine Applications in Organ Transplantation*. Elsevier Inc. doi: 10.1016/B978-0-12-398523-1.00004-5.

Sprott, M. R. *et al.* (2019) 'Functionalization of PLLA with Polymer Brushes to Trigger the Assembly of Fibronectin into Nanonetworks', *Advanced Healthcare Materials*. Wiley-VCH Verlag, 8(3). doi: 10.1002/adhm.201801469.

Stier, S. *et al.* (2005) 'Osteopontin is a hematopoietic stem cell niche component that negatively regulates stem cell pool size', *Journal of Experimental Medicine*, 201(11), pp. 1781–1791. doi: 10.1084/jem.20041992.

Stratesteffen, H. *et al.* (2017) 'GelMA-collagen blends enable drop-on-demand 3D printablility and promote angiogenesis', *Biofabrication*. IOP Publishing, 9(4). doi: 10.1088/1758-5090/aa857c.

Sugimura, R. *et al.* (2017) 'Haematopoietic stem and progenitor cells from human pluripotent stem cells', *Nature*. Nature Publishing Group, 545(7655), pp. 432–438. doi: 10.1038/nature22370.

Sweeten, P. (2019) ‘Modelling an in vitro haematopoietic stem cell niche using poly (ethyl acrylate) surfaces’.

Taichman, R. S., Reilly, M. J. and Emerson, S. G. (1996) ‘Human osteoblasts support human hematopoietic progenitor cells in in vitro bone marrow cultures’, *Blood*, 87(2), pp. 518–524. doi: 10.1182/blood.v87.2.518.bloodjournal872518.

Takagi, J. and Springer, T. A. (2002) ‘Integrin activation and structural rearrangement’, *Immunological Reviews*, 186, pp. 141–163. doi: 10.1034/j.1600-065X.2002.18613.x.

Takagi, S. *et al.* (2012) ‘Membrane-bound human SCF/KL promotes in vivo human hematopoietic engraftment and myeloid differentiation.’, *Blood*, 119(12), pp. 2768–2777. doi: 10.1182/blood-2011-05-353201.

Tibbitt, M. W. and Anseth, K. S. (2009) ‘Hydrogels as extracellular matrix mimics for 3D cell culture’, *Biotechnology and Bioengineering*. doi: 10.1002/bit.22361.

Trappmann, B. *et al.* (2012) ‘Extracellular-matrix tethering regulates stem-cell fate’, *Nature Materials*. Nature Publishing Group, 11(7), pp. 642–649. doi: 10.1038/nmat3339.

Trujillo, S. *et al.* (2019) ‘Engineered full-length Fibronectin-based hydrogels sequester and present growth factors to promote regenerative responses in vitro and in vivo’, *bioRxiv*, p. 687244. doi: 10.1101/687244.

Trujillo, S. *et al.* (2020) ‘Engineered 3D hydrogels with full-length fibronectin that sequester and present growth factors’, *Biomaterials*. Elsevier, 252(November 2019), p. 120104. doi: 10.1016/j.biomaterials.2020.120104.

Tsai, M. S. *et al.* (2004) ‘Isolation of human multipotent mesenchymal stem cells from second-trimester amniotic fluid using a novel two-stage culture protocol’, *Human Reproduction*, 19(6), pp. 1450–1456. doi: 10.1093/humrep/deh279.

Tsapogas, P. *et al.* (2017) ‘The cytokine Flt3-ligand in normal and malignant hematopoiesis’, *International Journal of Molecular Sciences*, 18(6). doi:

10.3390/ijms18061115.

Tse, J. R. and Engler, A. J. (2010) ‘Preparation of Hydrogel Substrates with Tunable Mechanical Properties’, *Current Protocols in Cell Biology*, 47(1), pp. 10.16.1-10.16.16. doi: 10.1002/0471143030.cb1016s47.

Tsimbouri, P. *et al.* (2014) ‘Nanotopographical effects on mesenchymal stem cell morphology and phenotype’, *Journal of Cellular Biochemistry*, 115(2), pp. 380–390. doi: 10.1002/jcb.24673.

Turner, L.-A. and Dalby, M. J. (2014) ‘Nanotopography – potential relevance in the stem cell niche’, *The Royal Society of Chemistry*, 2, pp. 154–194. doi: 10.1039/c4bm00155a.

De Ugarte, D. A. *et al.* (2003) ‘Differential expression of stem cell mobilization-associated molecules on multi-lineage cells from adipose tissue and bone marrow’, *Immunology Letters*, 89(2–3), pp. 267–270. doi: 10.1016/S0165-2478(03)00108-1.

Ulmer, J., Geiger, B. and Spatz, J. P. (2008) ‘Force-induced fibronectin fibrillogenesis in vitro’, *Soft Matter*, 4(10), pp. 1998–2007. doi: 10.1039/b808020h.

Vandenburgh’, H. H., Karlisch, P. and Farr, L. (1988) ‘MAINTENANCE OF HIGHLY CONTRACTILE TISSUE-CULTURED AVIAN SKELETAL MYOTUBES IN COLLAGEN GEL’, *IN VITRO CELLULAR ~t DEVELOPMENTAL BIOLOGY*, 24(3), pp. 166–174.

Vanterpool, F. A. *et al.* (2014) ‘A Material-Based Platform to Modulate Fibronectin’, 3(6), pp. 286–296. doi: 10.1089/biores.2014.0033.

Vartio, T. (1986) ‘Disulfide-bonded polymerization of plasma fibronectin in the presence of metal ions’, *Journal of Biological Chemistry*, 261(20), pp. 9433–9437.

Walasek, M. A., van Os, R. and de Haan, G. (2012) ‘Hematopoietic stem cell expansion: Challenges and opportunities’, *Annals of the New York Academy of*

Sciences, 1266(1), pp. 138–150. doi: 10.1111/j.1749-6632.2012.06549.x.

Wang, H.-S. *et al.* (2004) 'Mesenchymal Stem Cells in the Wharton's Jelly of the Human Umbilical Cord', *Stem Cells*, 22(7), pp. 1330–1337. doi: 10.1634/stemcells.2004-0013.

Wang, L. D. and Wagers, A. J. (2011) 'Dynamic niches in the origination and differentiation of haematopoietic stem cells', *Nature Reviews Molecular Cell Biology*, 12(10), pp. 643–655. doi: 10.1038/nrm3184.

Watt, F. M. and Hogan, B. L. M. (2000) 'Out of eden: Stem cells and their niches', *Science*, 287(5457), pp. 1427–1430. doi: 10.1126/science.287.5457.1427.

Weaver, J. D. *et al.* (2018) 'Design of a vascularized synthetic poly(ethylene glycol) macroencapsulation device for islet transplantation', *Biomaterials*, 172, pp. 54–65. doi: 10.1016/j.biomaterials.2018.04.047.

Weber, L. M. *et al.* (2007) 'The effects of cell-matrix interactions on encapsulated ß-cell function within hydrogels functionalized with matrix-derived adhesive peptides', *Biomaterials*, 28(19), pp. 3004–3011. doi: 10.1016/j.biomaterials.2007.03.005.

Weiss, M. L. and Troyer, D. L. (2006) 'Stem cells in the umbilical cord', *Stem Cell Reviews*, 2(2), pp. 155–162. doi: 10.1385/SCR:2:2:155.

Wijelath, E. S. *et al.* (2006) 'Heparin-II domain of fibronectin is a vascular endothelial growth factor-binding domain: Enhancement of VEGF biological activity by a singular growth factor/matrix protein synergism', *Circulation Research*, 99(8), pp. 853–860. doi: 10.1161/01.RES.0000246849.17887.66.

Williams, E. C. *et al.* (1983) 'Fibronectin. Effect of disulfide bond reduction on its physical and functional properties', *Journal of Biological Chemistry*, 258(9), pp. 5911–5914.

Woon Park, C. *et al.* (2009) 'Cytokine Secretion Profiling of Human Mesenchymal Stem Cells by Antibody Array', *International Journal of Stem Cells*, 2(1), pp. 59–

68. Available at: https://www.ncbi.nlm.nih.gov/pmc/articles/PMC4021795/pdf/ijsc-02-058.pdf.

Xiong, J.-P. *et al.* (2001) 'Crystal Structure of the Extracellular Segment of Integrin alpha Vbeta 3', *Science*, 294(5541), pp. 339–345. doi: 10.1126/science.1064535.

Yan, C. and Pochan, D. J. (2010) 'Rheological properties of peptide-based hydrogels for biomedical and other applications', *Chemical Society Reviews*, 39(9), p. 3528. doi: 10.1039/b919449p.

Yang, J. *et al.* (2014) 'Nanotopographical induction of osteogenesis through adhesion, bone morphogenic protein cosignaling, and regulation of microRNAs', *ACS Nano*, 8(10), pp. 9941–9953. doi: 10.1021/nn504767g.

Yin, T. and Li, L. (2006) 'The stem cell niches in bone', *Journal of Clinical Investigation*, pp. 1195–1201. doi: 10.1172/JCI28568.

Yoshihara, H. *et al.* (2007) 'Thrombopoietin/MPL Signaling Regulates Hematopoietic Stem Cell Quiescence and Interaction with the Osteoblastic Niche', *Cell Stem Cell*, 1(6), pp. 685–697. doi: 10.1016/j.stem.2007.10.020.

Yu, Y. *et al.* (2016) 'Decellularized scaffolds in regenerative medicine', *Oncotarget*, 7(36). Available at: www.impactjournals.com/oncotarget/.

Yuan, T. *et al.* (2014) 'Collagen hydrogel as an immunomodulatory scaffold in cartilage tissue engineering', *Journal of Biomedical Materials Research - Part B Applied Biomaterials*, 102(2), pp. 337–344. doi: 10.1002/jbm.b.33011.

Zhang, C. C. *et al.* (2006) 'Angiopoietin-like proteins stimulate ex vivo expansion of hematopoietic stem cells', *Nature Medicine*, 12(2), pp. 240–245. doi: 10.1038/nm1342.

Zhang, C. C. and Lodish, H. F. (2008) 'Cytokines regulating hematopoietic stem cell function', *Current Opinion in Hematology*, 15(4), pp. 307–311. doi: 10.1097/MOH.0b013e3283007db5.

Zhang, G. (2012) ‘Biomimicry in biomedical research’, *Organogenesis*, 8(4), pp. 101–102. doi: 10.4161/org.23395.

Zhang, J.-M. and An, J. (2009) ‘Cytokines, Inflammation and Pain’, *Int Anesthesiol Clin.*, 69(2), pp. 482–489. doi: 10.1097/AIA.0b013e318034194e.Cytokines.

Zhang, J. *et al.* (2003) ‘Identification of the haematopoietic stem cell niche and control of the niche size’, *Nature*, 425(6960), pp. 836–841. doi: 10.1038/nature02041.

Zhao, W. *et al.* (2014) ‘Effects of substrate stiffness on adipogenic and osteogenic differentiation of human mesenchymal stem cells’, *Materials Science and Engineering C*. Elsevier B.V., 40, pp. 316–323. doi: 10.1016/j.msec.2014.03.048.

Zhong, C. *et al.* (1998) ‘Rho-mediated contractility exposes a cryptic site in fibronectin and induces fibronectin matrix assembly’, *Journal of Cell Biology*, 141(2), pp. 539–551. doi: 10.1083/jcb.141.2.539.

Zhu, J. *et al.* (2009) ‘Design and synthesis of biomimetic hydrogel scaffolds with controlled organization of cyclic RGD peptides’, *Bioconjugate Chemistry*, 20(2), pp. 333–339. doi: 10.1021/bc800441v.

Zhu, J. (2010) ‘Bioactive modification of poly(ethylene glycol) hydrogels for tissue engineering’, *Biomaterials*. Elsevier Ltd, 31(17), pp. 4639–4656. doi: 10.1016/j.biomaterials.2010.02.044.

Zhu, J. and Clark, R. A. F. (2014) ‘Fibronectin at select sites binds multiple growth factors and enhances their activity: Expansion of the collaborative ECM-GF paradigm’, *Journal of Investigative Dermatology*. Elsevier Masson SAS, 134(4), pp. 895–901. doi: 10.1038/jid.2013.484.

Zia, K. *et al.* (2019) ‘Nuclear Magnetic Resonance Spectroscopy for Medical and Dental Applications: A Comprehensive Review’, *European Journal of Dentistry*, 13(1), pp. 124–128. doi: 10.1055/s-0039-1688654.

Zollinger, A. J. and Smith, M. L. (2017) ‘Fibronectin, the extracellular glue’, *Matrix Biology*. Elsevier B.V., 60–61, pp. 27–37. doi: 10.1016/j.matbio.2016.07.011.